

AD-A220 643

TACTICAL WEAPON
GACIAC
GUIDANCE & CONTROL
INFORMATION ANALYSIS CENTER

GACIAC PR-89-07

**PROCEEDINGS OF THE DIGITAL/ELECTRONIC
TERRAIN BOARD SYMPOSIUM**

5-6 OCTOBER 1989

Conducted at Boeing Military Airplane Company
Wichita, Kansas



Jointly sponsored by: U.S. Army CECOM Center for Night Vision
and Electro-Optics in conjunction with the
23rd Meeting of the Automatic Target
Recognizer Working Group

APPROVED FOR PUBLIC RELEASE:
DISTRIBUTION UNLIMITED

Published by GACIAC
IIT Research Institute
10 West 35th Street
Chicago, Illinois 60616-3799



90 01 11 051

NOTICES

Proceedings. This proceedings has been published by the Tactical Weapon Guidance and Control Information Analysis Center (GACIAC) as a service to the defense community. GACIAC is a DoD Information Analysis Center, administered by the Defense Technical Information Center, operated by IIT Research Institute under Contract No. DLA900-86-C-0022. GACIAC is funded by DTIC, DARPA, and U.S. Army, U.S. Navy, and U.S. Air Force Laboratories/Controlling Activities having an interest in tactical weapon guidance and control. The Director of GACIAC is Dr. Robert J. Heaston. The Contracting Officer is Mrs. S. Williams, DESC, Dayton, Ohio. The Contracting Officer's Technical Representative is Mr. Chalmer D. George, and the Alternate Representative is Mr. H. C. Race, AMC Smart Weapons Management Office, ATTN: AMSMI-SW, Redstone Arsenal, Alabama 35898-5222.

Reproduction. Permission to reproduce any material contained in this document must be requested and approved in writing by the AMC Smart Weapons Management Office, AMSMI-SW, Redstone Arsenal, Alabama 35898-5222. This document is only available from GACIAC, IIT Research Institute, 10 West 35th Street, Chicago, Illinois 60616-3799. Copies are available to Conference attendees, Government agencies, and GACIAC industrial subscribers.

UNCLASSIFIED

SECURITY CLASSIFICATION OF THIS PAGE

REPORT DOCUMENTATION PAGE				Form Approved OMB No. 0704-0188	
1a. REPORT SECURITY CLASSIFICATION UNCLASSIFIED/UNLIMITED			1b. RESTRICTIVE MARKINGS		
2a. SECURITY CLASSIFICATION AUTHORITY			3. DISTRIBUTION / AVAILABILITY OF REPORT Approved for Public Release Distribution Unlimited		
2b. DECLASSIFICATION / DOWNGRADING SCHEDULE			5. MONITORING ORGANIZATION REPORT NUMBER(S)		
4. PERFORMING ORGANIZATION REPORT NUMBER(S) GACIAC PR-89-07			7a. NAME OF MONITORING ORGANIZATION Commander U.S. Army Missile Command		
6a. NAME OF PERFORMING ORGANIZATION IIT Research Institute/GACIAC		6b. OFFICE SYMBOL (if applicable)	7b. ADDRESS (City, State, and ZIP Code) ATTN: AMSMI-SW Redstone Arsenal, AL 35898-5222		
6c. ADDRESS (City, State, and ZIP Code) 10 West 35th Street Chicago, IL 60616-3799		9. PROCUREMENT INSTRUMENT IDENTIFICATION NUMBER			
8a. NAME OF FUNDING / SPONSORING ORGANIZATION U.S. Army CECOM CTR for NV and Electro-Optics		8b. OFFICE SYMBOL (if applicable)	10. SOURCE OF FUNDING NUMBERS		
8c. ADDRESS (City, State, and ZIP Code) Ft. Belvoir, VA 22060-5677		PROGRAM ELEMENT NO. 65802 S	PROJECT NO. 1.0	TASK NO.	WORK UNIT ACCESSION NO.
11. TITLE (Include Security Classification) Proceedings of The Digital/Electronic Terrain Board Symposium. U/U					
12. PERSONAL AUTHOR(S) Various; Carl W. Hoover, Jr., Symposium Chairman ,et;al					
13a. TYPE OF REPORT Proceedings		13b. TIME COVERED FROM Oct 89 TO Feb 90		14. DATE OF REPORT (Year, Month, Day) February 1990	
15. PAGE COUNT 312					
16. SUPPLEMENTARY NOTATION This document available only from IIT Research Institute/GACIAC, 10 West 35th Street, Chicago, IL 60616-3799. (410948) \$100.00					
17. COSATI CODES			18. SUBJECT TERMS (Continue on reverse if necessary and identify by block number)		
FIELD	GROUP	SUB-GROUP	Target recognition, Automatic target recognition, Image generation, Multiple sensors, Fusion, Radar (SEE REVERSE) ←		
17	11				
08	02				
19. ABSTRACT (Continue on reverse if necessary and identify by block number) The Digital/Electronic Terrain Board Symposium was organized for the objective of providing an opportunity for those working in the field to discuss and demonstrate their state-of-the-art and to uncover areas of duplication and gaps in these efforts. The symposium was held 5-6 October 1989 at Boeing Military Airplane Co., Wichita Kansas, in conjunction with the 23rd meeting of the Automatic Target Recognizer Working Group. The Proceedings contain 23 papers which address various aspects of D/ETB technology including algorithm development, image generation, scene modeling, multi-sensor fusion and simulation. Acoustic, infrared, 3-D radar and laser radar imagery were the topics of several papers. The effects of atmospheric turbulence and smart weapons applications were also discussed.					
20. DISTRIBUTION / AVAILABILITY OF ABSTRACT <input type="checkbox"/> UNCLASSIFIED/UNLIMITED <input checked="" type="checkbox"/> SAME AS RPT. <input type="checkbox"/> DTIC USERS			21. ABSTRACT SECURITY CLASSIFICATION Unclassified		
22a. NAME OF RESPONSIBLE INDIVIDUAL Chalmer D. George			22b. TELEPHONE (Include Area Code) (205) 876-3788		22c. OFFICE SYMBOL AMSMI-SW

18. SUBJECT TERMS (cont)

Laser radar, Images, Infrared images, Thermal images, Mathematical models, Simulation, Acoustics, Symposia, Terrain, Terrain modeling, Digital techniques.

Accession For	
NTIS GRA&I	<input checked="" type="checkbox"/>
DTIC TAB	<input type="checkbox"/>
Unannounced	<input type="checkbox"/>
Just location	
By <i>HC \$100.00</i>	
Distribution/	
Availability Codes	
Dist	Avail and/or Special
<i>A-1</i>	<i>21</i>



PROCEEDINGS OF THE DIGITAL/ELECTRONIC TERRAIN BOARD SYMPOSIUM

5-6 OCTOBER 1989

**Conducted at the
Boeing Military Airplane Company
Wichita, Kansas**

Jointly sponsored by:

**U.S. Army CECOM Center for Night Vision and Electro-Optics
Held in conjunction with the 23rd Meeting of the
Automatic Target Recognizer Working Group**

**Distribution: Unclassified/Unlimited
and Cleared for Public Release**

**Published by GACIAC
IIT Research Institute
10 West 35th Street
Chicago, Illinois 60616-3799**

***GACIAC -- A DoD Information Analysis Center
Operated by IIT Research Institute, 10 West 35th Street, Chicago, IL 60616-3799
DoD Technical Sponsor - Joint Service Guidance and Control Committee
Members from OSD, Army, Navy, Air Force, and DARPA***

THIS PAGE IS INTENTIONALLY BLANK

FOREWORD

Several years ago, the US Army CECOM Center for Night Vision and Electro-Optics (C2NVEO) was faced with the problem of evaluating the performance of Automatic Target Recognizers (ATR) before going out to conduct expensive field tests. We used a TV camera to simulate infrared inputs on a physical terrain board so that we could control conditions and thus have a known, repeatable input to enable a statistically valid test. However, there are some drawbacks to a physical terrain board, such as a lack of dynamics, limited number of scenes, single spectrum, single sensor, etc. In order to advance the evaluation technology and include human performance as well as multisensor processors and algorithms, the use of a digital/electronic terrain board (D/ETB) is required.

A D/ETB is conceptually analogous to a physical terrain board in that it is expected to be a computer resident, three- or more dimensional simulation of the real world that simultaneously represents the scene in all useful spectrums including acoustic, radar, laser radar, thermal, visible, etc. Additionally, the D/ETB should be capable of simulating various atmospheric and active sensor effects, as well as moving targets and sensor platforms.

The Digital/Electronic Terrain Board Symposium was organized for the objectives of providing an opportunity for those working in the field to discuss and demonstrate their state-of-the-art to peers; and to uncover areas of duplication and, more importantly, gaps in these efforts. I believe that both objectives were met, thanks to the excellent work provided by the authors and speakers. These Proceedings are a permanent record of their work, which will allow others in the industry to share in their knowledge and understanding, and lead to an operational Digital/Electronic Terrain Board in the future.

Every successful endeavor depends upon the support and efforts provided by many people, so I would like to thank the following for assistance in helping us conduct the first Digital/Electronic Terrain Board Symposium.

Boeing Military Airplane Company, for use of their facilities to hold the Symposium; and especially Dr. Shelly Eucker for hosting the co-sponsored ATRWG Meeting and Symposium.

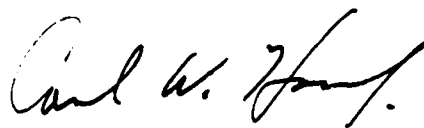
The Automatic Target Recognition Working Group (ATRWG), particularly Lloyd Clark and Bonita Moutoux, for organizing the co-sponsored ATRWG Meeting and Symposium.

The IIT Research Institute, and Andrew Zembower, for organizing publication of the Symposium Proceedings.

The speakers who presented papers at the Symposium: Scott Brandt, Honeywell; William Cameron, Boeing Aerospace & Electronics; Syama Chaudhuri, Sensor Data Integration Inc.; Geoffrey Gardner, Grumman Data Systems; Jeffrey Gillberg, Honeywell; Laslo Greczy, US Army Environmental Topographic Laboratory; Conrad Hoeppe, AAI Corporation; Michael Lander, US Army CECOM Center for Night Vision & Electro-Optics; Jerry Lent, Image Data Corporation; Charles Lindahl, Texas Instruments; Maximo Lorenzo, US Army CECOM Center for Night Vision & Electro-Optics; Dennis Lui, US Army CECOM Center for Electronic Warfare, Reconnaissance, Surveillance and Target Acquisition; Jay Mendelsohn, Grumman Corporate Research Center; Richard Ramroth, Northrop Electronics System Division; Dale Robison, US Naval Weapons Center; Timothy Rogne, OptiMetrics Inc.; Richard Shirkey, US Army Atmospheric Sciences Laboratory; Lori Scarlatos, Grumman Data Systems; and Craig Yandow, Hughes Aircraft Company.

The Symposium guest speakers: Dr. Kimball Kramer, Defense Advanced Research Project Agency; and Dr. Rudolf G. Buser, Director, US Army CECOM Center for Night Vision and Electro-Optics.

Most importantly, to Jill Bloxam for her assistance and untiring efforts in organizing the Symposium.



CARL W. HOOVER, JR.
CHIEF, LABORATORY EVALUATION
VISIONICS DIVISION, C2NVEO

THIS PAGE IS INTENTIONALLY BLANK

Digital/Electronic Terrain Board Symposium
5-6 October 1989

AGENDA

Thursday, October 5

- 1430-1440 Introduction by Carl Hoover, Symposium Chairman
- 1440-1500 Speech by Dr. Rudolf Buser, Acting Director, C2NVEO
- 1500-1530 "Major Areas of Application - Algorithm Development Test and Evaluation"
Featured Guest Speaker: Mr. Kimball Kramer, Defense Advanced Research Project Agency
- 1530-1550 "C2NVEO Digital Terrain Board (DTB) Concept"
Max Lorenzo, US Army C2NVEO
- 1550-1610 "Synthetic Image Generation for Multi-Sensor Fusion"
J.V. Geago, Northrop Research and Technology Center
- 1610-1630 "Digital Generation of Synthetic Multi-Sensor Imagery"
Charles Lindahl, Alan Cockcroft, John Sigler and Mark Yablonski, Texas Instruments
- 1630-1650 "Efficient Scene Modeling for Digital/Electronic Terrain Boards"
Geoffrey Gardner, Grumman Data Systems
- 1650-1710 "Synthetic Image Generation Model and Its Interface with the Digital/Electronic Terrain Board"
Gertrude Kornfeld, US Army C2NVEO
- 1715 **Conclude first day of Symposium**

Friday, October 6

- 0830-0850 "Computer Image Generation of IR Scenes and Sequences"
David Englund, Alex Peck and Jay Mendelsohn, Grumman Data Systems and David Thomas, US Army TACOM
- 0850-0910 "US Army TACOM Thermal Image Model (TTIM)"
Timothy Rogne, OptiMetrics Inc.
- 0910-0930 "Performance Simulations of Acoustics and Location Systems for Vehicles"
Frederick Smith, OptiMetrics, Inc.
- 0930-0950 "Automatic Target Recognition of Sub Pixelar Targets"
Conrad Hoeppner, AAI Corporation

0950-1010 "3D Radar Scatterer Model Derived From Dual Mode Data"
Dr. William Cameron, Boeing Aerospace and Electronics

1010-1030 **Break**

1030-1050 "Synthetic Laser Radar Image Generation"
Jeffrey Gillberg, R. Johnston and J.T. Lee, Honeywell, and R. Peters, D. Nguyen, Multi Sensor ATR Algorithm Development Team

1050-1110 "Effect of Atmospheric Turbulence on Electro-Optical Systems"
Dr. Walter Miller, US Army Atmospheric Sciences Lab

1110-1130 "Adaptive Terrain Models for Real-Time Simulation"
Lori Scarlatos, Grumman Data Systems

1130-1150 "Terrain Visualization"
George Simcox, US Army Engineering Topographic Lab

1150-1310 **Lunch Break**

1310-1330 "Multitarget Multisensor Data Fusion: Radar, ESM, RWR, IFF, and JEM Applications"
Sam P. Chaudhuri, Sensor Data Integration, Inc.

1330-1350 "Multidisplay Multifunction Cockpit Interface for the Silicon Graphics IRIS Environment"
Dale Robison, US Naval Weapons Center

1350-1410 "Sandtable, an Electronic Battlefield Simulator"
Thomas Newson, US Army CECOM, Center for EW/RSTA

1410-1430 "Terrain and Target Signature Simulation"
Dr. John Lewis, Hughes Aircraft Company

1430-1450 "Image Generation"
Scott Brandt, Honeywell

1450-1510 **Break**

1510-1530 "Smart Weapons Operability Enhancement Demonstration"
Pat Welch, US Army CRREL

1530-1550 "From Data Base Creation to Perspective Scene Generation in a Single Parallel Platform"
Michael Battaglia, Image Data Corporation

1550-1600 **Symposium Wrap Up**

Digital Electronic Terrain Board Symposium
5-6 October 1989

TABLE OF CONTENTS

"Major Areas of Application - Algorithm Development"	1
Test and Evaluation" K. Kramer	
"C2NVEO Digital Terrain Board (DTB) Concept"	9
M. Lorenzo, S. Der, D. Walthall and J.R. Moulton, Jr.	
"Synthetic Image Generation for Multisensor Fusion"	23
J.V. Geaga, R.R. Ramroth and J.W. Bair	
"Digital Generation of Synthetic, Multi-Sensor Imagery"	35
C. Lindahl, A. Cockcroft, J. Sigler and M. Yablonski	
"Efficient Scene Modeling for Digital/Electronic Terrain Boards"	43
G.Y. Gardner	
"Synthetic Image Generation Model and its Interface with The Digital Electronic Terrain Board"	55
G. Kornfeld, J. Penn, M. Lander, H. Nguyen, J. Ho and T. Steck	
"Computer Image Generation of IR Scenes and Sequences"	89
D. Englund, A. Peck, J. Mendelsohn and D. Thomas	
"U.S. Army Tank-Automotive Command (TACOM) Thermal Image Model (TTIM)" ...	101
T.J. Rogne, F.G. Smith, G.R. Gerhart and D.J. Thomas	
"Performance Simulation of Acoustic Detection and Location Systems Vehicles"	115
F.G. Smith and J.L. Manning	
"Automatic Target Recognition of Sub Pixelar Targets"	125
C.H. Hoepfner	
"3D Radar Scatterer Model Derived From Dual Mode Data"	167
W.L. Cameron	
"Synthetic Laser Radar Image Generation"	183
J.M. Gillberg, R. Johnston, J.T. Lee, R. Peters and D. Nguyen	
"Effect of Atmospheric Turbulence on Electro-Optical Systems"	193
W.B. Miller, J.C. Ricklin and D.H. Marlin	
"Adaptive Terrain Models for Real-Time Simulation"	219
L.L. Scarlatos	

TABLE OF CONTENTS (Contd.)

"Terrain Visualization"	233
L. Greczy	
"Multitarget Multisensor Data Fusion: Radar, ESM, RWR, IFF, and JEM Applications"	239
S.P. Chaudjuri	
"Multidisplay Multifunction Cockpit Interface for The Silicon Graphics IRIS Environment"	261
D. Robison	
"Sandtable, A Display of the Electronic Battlefield"	275
D. Lui	
"Terrain and Target Signature Simulation"	279
J.H. Lewis	
"Image Generation - VICAM"	281
S. Brandt, M. Miller and C. Graf	
"Smart Weapons Operability Enhancements Program"	283
P. Welsh	
"From Data Base Creation to Perspective Scene Generation in a Single Parallel Platform"	285
M.P. Battaglia	
Attendance List	293

Digital/Electronic Terrain Board



MAJOR AREAS OF APPLICATION

ALGORITHM DEVELOPMENT
TEST and EVALUATION

DARPA-TTO - Kimball Kramer - 694-7996

9/28/89-3

Digital/Electronic Terrain Board



PROBLEMS

- REAL-TIME OPERATION
- HIGH DEVELOPMENT COSTS
 - MODERATE INITIAL COSTS
- PERCEPTION OF LACK OF FIDELITY
- VERIFICATION (NON-VISIBLE SPECTRUM)
 - FIDELITY THRU FEEDBACK
- PERCEPTION OF THE IMPOSSIBILITY OF REPLACING CAPTIVE FLIGHT TESTS
 - ALL vs. 1st n

DARPA-TTO - Kimball Kramer - 694-7996

9/28/89-4



ADVANTAGES (1)

- **VERY LOW CONTINUING COSTS
COMPARED TO THE COSTS OF
CAPTIVE FLIGHT TESTS
(CA. \$100,000/WEEK- FULL COST)**



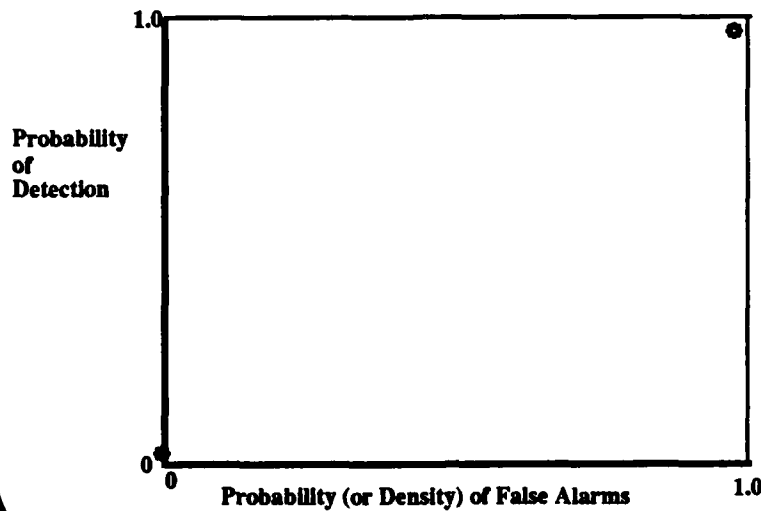
ADVANTAGES (2)

- **FLEXIBILITY NECESSARY TO HELP
SOLVE THE PROBLEMS OF
ESTABLISHING METRICS AND
OF MEASURING PERFORMANCE**

Digital/Electronic Terrain Board



PERFORMANCE METRICS PROBLEM (1)



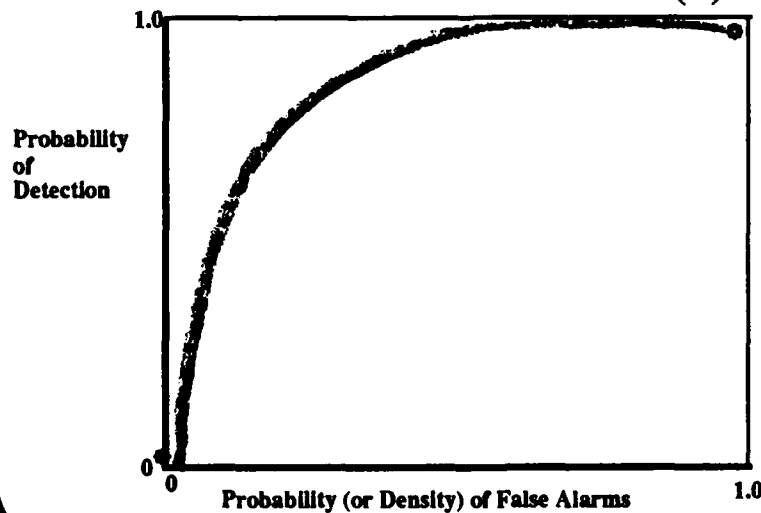
DARPA-TTO - Kimball Kramer - 694-7006

9/28/89-7

Digital/Electronic Terrain Board



PERFORMANCE METRICS PROBLEM (2)



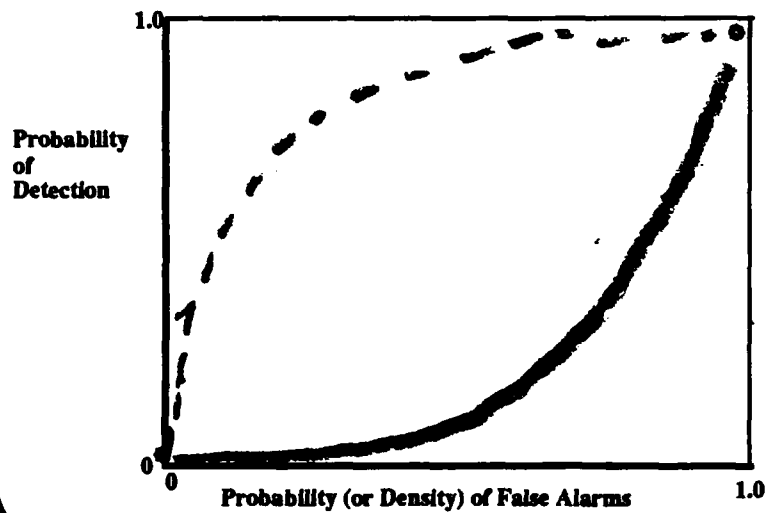
DARPA-TTO - Kimball Kramer - 694-7006

9/28/89-8

Digital/Electronic Terrain Board



PERFORMANCE METRICS PROBLEM (3)



DARPA-TTO - Kimball Kramer - 894-7996

9/28/89-9

Digital/Electronic Terrain Board



SCENE METRICS PROBLEM (1)

W. Texas

INCREASING CLUTTER

Beruit

DARPA-TTO - Kimball Kramer - 894-7996

9/28/89-10



SCENE METRICS PROBLEM (2)

INCREASING
ADVERSE
WEATHER

W. Texas

INCREASING CLUTTER

Beruit



SCENE METRICS PROBLEM (3)

INCREASING
COUNTER-
MEASURES

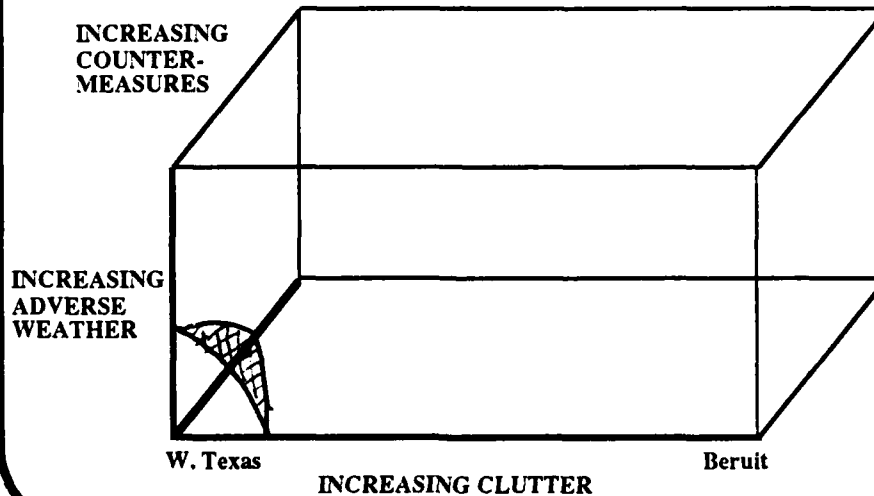
INCREASING
ADVERSE
WEATHER

W. Texas

INCREASING CLUTTER

Beruit

INCREASING COUNTER-MEASURES



DARPA-TTO - Kimball Kramer - 694-7998

9/28/89-13

PERFORMANCE SPECIFICATIONS

[illegible]

A MEASURE OF THE CURRENT STATE-OF-THE-ART
A MEASURE OF WHEN TO FIELD
THE RELATION BETWEEN THE TWO

[illegible]

We must not let PERCEIVED INADEQUACIES of systems in development and ANTICIPATED IMPROVEMENTS in these systems keep us from fielding working systems which are significantly better than what we have in the field now.

❖ ❖ ❖ ❖ ❖ ❖ ❖ ❖ ❖ ❖ ❖ ❖

DARPA-TTO - Kimball Kramer - 694-7998

9/28/89-14



ADVANTAGES (3)

- EXPAND THE VALUE OF SIMNET



THE CHALLENGE

- THE TERRAIN BOARD MUST BE BASED ON SELECTED REAL WORLD DATA ("STANDARD" AREAS)
- IT MUST ACCOMMODATE MULTI-SENSOR SIMULATIONS
- NEW SENSORS AND NEW SENSOR MODES AND PARAMETERS ARE CONTINUALLY APPEARING
- THERE MUST BE A FLEXIBLE "LAYERED" ARCHITECTURE TO ACCOMMODATE THESE AUGMENTATIONS WITH MINIMUM RE-WRITING OF SOFTWARE



LONG-RANGE GOAL

**A DoD STANDARD
DIGITAL/ELECTRONIC TERRAIN BOARD
TEST SET
for EACH ALGORITHM TYPE**

Presented at the
DIGITAL/ELECTRONIC TERRAIN BOARD SYMPOSIUM
5-6 October 1989 GACIAC PR 89-07

C2NVEO Digital Terrain Board (DTB) Concept

Maximo Lorenzo, Sandor Der
US Army CECOM Center for Night Vision & Electro-Optics
Attn: AMSEL-RD-NV-V
Fort Belvoir, Virginia 22060-5677

David Walthall, J. R. Moulton, Jr.
E/OIR Measurements Inc.
P. O. Box 3348 College Station
Fredericksburg, Virginia 22402

ABSTRACT

The US Army CECOM Center for Night Vision and Electro-Optics (C2NVEO) has recognized the need for computer generated synthetic sensor output for the testing and development of automatic target recognizers/cuers and for human observer testing. This capability should include simulations of real world terrain, vegetation, atmospherics and objects as well as simulations of various sensors, including FLIR, TV, laser radar, millimeter wave radar, and vibration sensors.

1. INTRODUCTION

Current testing and development of automatic target recognizers (ATR) and cuers rely on data generated from field testing and from physical terrain boards. Field data collection efforts implement the use of actual sensors on actual terrain with actual targets, which ensure validity of the data used, however the data suffers from several disadvantages. Terrain variety is limited to the immediate location of the test, which is usually a small portion of a military base. Target variety is limited to whatever targets are on hand and available, which often means that important threat vehicles are absent. The lack of environmental control over field data puts severe constraints on the data collected. ATR

problems that could be discovered in a controlled environment often are masked by the unpredictability of the environment. For example, if a range sensitivity test was conducted by recording imagery with targets at set intervals, it is undeterminable whether the changes in ATR performance were caused by changes in range, target temperature, atmospheric turbulence, or some other factor. Also, field testing is very expensive, which means that only a very limited set of data is collected.

The C2NVEO physical terrain board uses a TV camera as the sensor. FLIR imagery is simulated by inverting the TV image. The targets placed on the board are painted various shades of gray to simulate their temperature; the hotter the target, the darker the paint. Thus, when the image is inverted, the target appears white hot. The physical terrain board allows great control over target signatures and environmental conditions, and is much less expensive than field testing; but it can serve only as a first step toward evaluating an ATR. A physical terrain board test allows the ATR contractor to debug hardware and software problems before a field test, and gives evaluators some measure of contrast required for detection, and a measure of false alarm rate. The physical terrain board cannot simulate laser radar, millimeter wave radar, or vibration sensors; the only target signatures it can use are those that are painted onto a model, which is difficult, time consuming, and limits the variety of available target signatures. The physical terrain board has a limited number of available backgrounds. Creating new backgrounds, new vegetation types, or new

environmental conditions is expensive because all work must be done manually. For these reasons, the physical terrain board serves better as a stationary benchmark than as a robust model.

A Digital Terrain Board (DTB) would have the advantages of low cost data collection and environmental control, and would have the capability to simulate a much wider variety of environmental conditions than the physical terrain board. DTB imagery would simulate sensor observables and noise directly, presumably resulting in more realistic imagery with wider usage than the physical terrain board imagery. Images could be generated of any terrain for which a digital map exists, and any targets for which models exist could be included at will. The low cost would allow a wide variety of data to be collected, and its flexibility would allow new data to be collected as needs arise. This data could be used for ATR algorithm development as well as testing. Currently, ATR algorithm development is hindered by a lack of training data. It is not anticipated that the DTB would completely replace field or physical terrain board testing; both forms of testing still are needed as a control and to test the DTB itself. The issue of image validation is discussed in more detail at the end of this paper.

Current ATR algorithm development efforts suffer from a lack of data for the training of algorithms. The data sets provided usually cover a very limited set of environmental conditions and targets. Due to the low cost and ease with which DTB imagery could

be generated, an algorithm developer could be provided with a rich set of data, and easily could request additional data as needs arise.

The DTB, envisioned by C2NVEO, is driven by different requirements than most existing DTBs which are used for mission planning purposes. Mission planning requires real time or near real time generation of images which only serve to give humans some idea of the appearance of visible features in a scene. Real time generation is unnecessary for our data collection, but the images generated must be adequate for the testing of ATRs as well as humans. ATRs use various image metrics to arrive at a target recognition decision, and it is important that the synthetic images have metrics similar to the real world. Different ATRs use very different metrics, and the metrics that future ATRs will use cannot be predicted; thus, the authors believe that the best approach is to model real world observables directly, rather than attempt to force specific image metrics in the synthetic images to be the similar to real world values. It is believed that adequate modeling will provide realistic image metric values for currently used metrics as well as future ones, while forcing of specific metrics may cause the DTB to be useless for the development and testing of ATRs which use other metrics.

Abundant computer facilities and relaxation of the real time requirement will allow the use of computationally intensive algorithms. This will allow us to concentrate on using the most

realistic algorithms available, while temporarily overlooking time constraints. Attention will be given to speeding up the algorithms only after a given synthetic scene generator is performing acceptably.

One of the biggest problems common to field and physical terrain board data collection is the lack of flexibility in choosing the data. Consequently, a great deal of attention will be given to maintaining flexibility in the design of the DTB, which, along with fidelity, are the driving requirements behind this project.

The synthetic scene generators will take input from a common set of files to ensure uniformity and reduce duplication of effort. These consist of dynamic files which are specified by the event control module, and stationary files which have data that is fixed for every scenario. The dynamic files contain the vehicle activity, sensor activity, and meteorological activity file. The stationary files contain the vehicle, object, vegetation, and background data files. Each of these files are described in more detail below. It should be noted that these files are subject to change as work on the DTB progresses.

2. The Event Control Module

The event control module will serve as the interface between the user and the entire DTB system. The user will use this interface to completely define the scenario. Thus, all dynamic input to the DTB system will be chosen in this module. Dynamic

input is all information that is specific to a given scenario, such as target sets, flight paths, real world location of vehicles and sensors, and weather conditions. This information is contained in the vehicle activity, meteorological activity, and sensor activity files, which are described in more detail below. It is envisioned that the user will be able to create new files or use existing ones.

3. Vehicle Activity File

The vehicle activity file will specify all the activities of all vehicles included in the scenario which are relevant to any of the sensors being simulated. A few of these are stated here, but it is not intended that this list be all inclusive. It is expected that as the synthetic scene generation programs are being developed, the relevance of other actions to a targets' signature will be realized, and these actions will be included in the file. It should be kept in mind that while not all of these will be implemented from the outset, including them here will ensure that they are not forgotten.

The first group of activities in the file actually will be a history of operations before the scenario started, including those activities that occur at a time $t < 0$ that effect the signature at $t = 0$. Examples would include: firing of the main gun, running of the engine, movement of the vehicle, and miscellaneous items such as running the heater. The effect of the first three on the

thermal signature of the vehicle is obvious, and the fourth may have relevance. It would be incumbent upon the designers of the synthetic thermal signature generator to make that determination.

The file also needs to include the activities of the vehicle during the scenario being run which are relevant to the signature for any sensor. These activities are dynamic in the sense that it is necessary to know them through the duration of the scenario, thus all of these activities will be expressed as a function of time. This would include vehicle location on the terrain board, vehicle facing, the facing of the turret if applicable, whether the engine is running, whether the weapons on the vehicle are being fired, and whether a stationary vehicle is dug in, in defilade, or using camouflage. These, too, are considered dynamic because they could change within the time period of a scenario.

4. Sensor Activity File

The sensor activity file will specify the location, attitude, and settings of all the relevant sensors for each time period in the duration of the scenario, and will specify the sensor platform in use. This would direct the synthetic scene generator to a platform file, which would specify the vibration inherent in the platform, as well as information on the gimbal, such as gimbal vibration and speed.

5. Meteorological Data File

This file will include relevant weather information during the scenario as well as for some as yet unspecified time before the beginning of the scenario. Meteorological effects on signatures are not well understood, so it is quite likely that the factors specified here will prove to be incomplete. The factors listed and the rationale behind their inclusion may serve as a guide to the thoughts of the authors on the complexity of the DTB problem.

Solar loading both during and prior to the scenario is one of the more obvious meteorological effects on object and background observables for the TV and FLIR sensors. The history of solar loading is particularly essential for estimating infrared observables. Wind information is necessary to estimate object and background temperature, to simulate the movement of wind movable objects, and to account for atmospheric turbulence effects on laser radar (Ladar) output. Precipitation and humidity alter the atmospheric transmission of both infrared and light waves. Clouds selectively mitigate the effects of solar loading, and often will appear in the far background of an image. Air temperature history is required to estimate the temperature of ground objects. Ground moisture changes the thermal conductivity as well as reflectivity of the earth surface. Other relevant items would, of course, be included.

6. Background Data File

This file only contains information on the surface of the DTB. It specifies the elevation of each point, the surface properties of the point, and indicates what objects, if any, reside on that point.

The surface properties of each point will be specified in the file. These would include surface texture, consistency, and other properties. Consistency would specify the surface type, i.e., grass, sand, rock. Heat conductance and spectral properties, such as reflectivity and emissivity, also would be included.

The object indicator would be a pointer to a specific stationary object or piece of stationary object, or vegetation that resides on that point. Examples are given in the object and vegetation files.

7. Object Data Files

This will be a set of files that contain information on a specific object. The location of any objects would be specified in the background data file. Objects, as defined in this paper, include any man made structures that might affect the output of a sensor. Both geometric and spectral characteristics will be included in this file.

It is envisioned that object files would be generated as needed and thus the collection would grow slowly. Object files initially would take a lower priority than vehicle files. Some of

the more necessary files would describe buildings, fences, rail road tracks, or power lines. Note that there is a need for many different building or fence files, but these could be generated only when needed and then saved for later use.

8. Vegetation Data Files

The vegetation models, mostly trees, probably will be generated using fractal methods. Different tree types could use different fractal models or the same models with different input parameters. Due to the computation-intensive nature of fractal images, it is hoped that a set of trees of various types could be stored in a data base and recalled randomly. This will require a large set of trees and an adequate method of storing the output. It should be noted that storage of fractal images could be a non-trivial problem.

The vegetation models should include spectral and geometric characteristics in order for the signature models to estimate the vegetation observables.

9. Vehicle Structure Files

The vehicle structure files will contain all static information about a given vehicle. This would include detailed vehicle geometry, texture of outside surfaces, reflectivity of outside surfaces, heat conductance and emissivity of vehicle parts, and

miscellaneous information such as internal heat sources or fluid circulation which effects vehicle observables. More information can be added as its relevance becomes apparent.

It is anticipated that the US Army Ballistic Research Laboratory (BRL) target models, which contain detailed external and internal geometric information, may be used as the starting point for preparing the vehicle structure files. If needed information were added to these BRL models, they could serve as vehicle structure files for the DTB.

10. Synthetic Scene Generators

The designers of a synthetic scene generator for a given sensor would use the above files to create the sensor output. The approach taken would be determined by the designer, but there are certain characteristics which would be encouraged for inclusion in the DTB.

A modular approach should be used whenever possible, which would facilitate making changes in the system, as well as allow mixing and matching of parts. For example, it might be desirable to use one developer's atmospheric model while using another sensor model. In order to make integration of any component easier, it is desirable that ongoing discussion take place between a designer and those integrating their components into the DTB.

It is also desirable to make each component as flexible as possible. For example, a module that can handle both common module and focal plane array FLIRs would be preferable to a more limited system. This flexibility would make comparison of the two systems easier.

11. Image Validation Issues

A key factor in determining the usefulness of the DTB will be the realism of the synthetic sensor outputs. Synthetic images should not be used to develop or test ATRs or to train humans if they are not realistic. The authors believe that methods for evaluation and validation of synthetic images should be prepared prior to testing or training in order to facilitate attaining a consensus on the validity of specific synthetic images. The issue of image validation is controversial, therefore, not all the methods suggested here necessarily will be used.

The first method of examination would be a review of the sensor output by human experts. The experts would look at the signatures of man-made and natural objects in the scene and make a subjective evaluation of realism.

For synthetic FLIR images only, a large set of images could be generated representing several backgrounds with targets at a number of different ranges and temperature levels. A similar set of images could be generated on the physical terrain board, and both sets would be used as input to a set of ATRs. The scored output of

the ATRs should be statistically equivalent for physical terrain board and synthetic images. The same method could be used to compare ATR performance on field and synthetic data, using FLIR input, TV, Ladar, millimeter wave radar, or other sensors, in single or multi-sensor mode.

Other approaches have been suggested. The previous method could be applied to human observers, instead of ATRs, for low contrast targets. For non-imaging systems, such as millimeter wave radar, a target signature correlation comparison probably would be useful. For very high quality synthetic images, human observers could be asked to determine which images, from a set, are synthetic and which are real. Image metrics could be computed on synthetic and real images, and a comparison made. The issue of image validation will continue to be controversial, but it demands greater attention if a useful DTB is to be realized.

THIS PAGE INTENTIONALLY BLANK

SYNTHETIC IMAGE GENERATION FOR* MULTISENSOR FUSION

J. V. Geaga
Northrop Research and Technology
Palos Verdes, California

R. R. Ramroth, and J.W. Bair
Northrop Electronics Systems
Anaheim, California

ABSTRACT

Synthetic image generation is essential for the development of robust Automatic Target Recognition (ATR) systems. Although it does not eliminate the need for real data collection, it offers flexibility and supports traceability, parametric analysis, and ATR performance optimization. This paper describes the synthetic image generation tools that we have built and implemented to support the development of ATR's and Multisensor Fusion (MSF) algorithms. The suite of simulated sensors includes laser radar, millimeter wave radar, infrared, and synthetic aperture radar. These tools were designed to simulate both target and background, and are based on geometric facet models. With the facet model, objects are assumed to be solid and are represented with triangular panels defining only the outer surface. Such a modeling approach conveniently supports the requirement for concurrent and colocated image generation of several sensors.

To simulate laser radar imagery, target and background facets are binned into the appropriate angle-angle and range bins. Speckle, noise, and sensor response functions are modeled in the simulator. Millimeter wave turntable image simulation is similar to laser radar simulation with the exception that two-dimensional binning is done in azimuth and range.

Infrared images are generated using the same target geometric model and assigning thermal grey-scale values to the facets. Thermal assignments are based on empirical data derived from real imagery and can be made by both manual and automatic techniques. Atmospheric, battlefield, and sensor effects are added using the Tacom Thermal Image Model.

These synthetic image tools have been used to support the development of multisensor fusion for automatic target recognition and search algorithms. This capability provides a cost-effective means of generating a sufficient number of samples for statistics-based algorithms, and the synthetic targets inherently lend themselves to the development of model-based algorithms as well.

* The work reported in this paper was performed under Northrop Corporation Independent Research and Development (IR&D) funding.

1.0 Introduction

The collection of real data is very expensive and time consuming. Although the use of synthetic data does not eliminate the need for real data, sensor and target signature models have a niche in the development of statistics-based, model-based, and Multisensor Fusion (MSF) Automatic Target Recognizer (ATR) algorithms. In the following paragraphs we establish the needs for multisensor modeling for ATR algorithm development and performance evaluation.

1.1 Statistical Pattern Recognition

Many existing ATR's use statistics-based algorithms to detect and classify targets found in Forward Looking Infrared (FLIR) imagery. Feature vectors, assigned to potential targets, form a feature vector space that is separated into regions, and each region is assigned a probability based on whether or not a feature vector (object) within that region is a target. Since measured features are susceptible to noise, statistical trends over a large number of images are more meaningful than a few measurements made from a limited number of images. The large data base requirements of this approach can be fulfilled by the augmentation of real imagery with synthetic imagery.

1.2 Model-Based Target Recognition

The current trend in ATR development is toward the use of model-based algorithms. The inherent nature of synthetic targets makes them the cornerstone of a model-based technique. At the very least, "ideal" (uncorrupted) synthetic target signatures act as the reference model to which sensed target signatures are aligned and compared. Additional synthetic target signatures can be corrupted and convolved with point spread functions and used as the input or sensed image to the model-based algorithm.

1.3 Development of Multiple Sensor Algorithms

The limited availability of multisensor data can hinder the development of algorithms for sensor suites. Without a sufficient data base, algorithms are sometimes limited in performance by the inability to test and refine development. Data generated from different sensor models provide registered imagery on which even pixel-level fusion can be investigated. Additionally, with the use of a multisensor data base, studies can be conducted to determine the best combinations of sensor types for directed mission and scenario requirements.

1.4 Performance Evaluation

To adequately assess the performance of a single sensor or multisensor ATR, exhaustive parametric studies are needed. To this end, some parameters within the images are fixed while performance is measured under various conditions of other parameters. For instance, performance of an algorithm can be measured with respect to changes in target orientation or inaccuracies in range estimations. It is important to be able to fix specific parameters within a data base while testing algorithms' robustness with respect to other parameters. Images generated from a synthetic sensor modeling system are easy to "ground truth" and provide a large number of target signatures at any specified orientation and thermal state.

2.0 Techniques for Multisensor Modeling Sensor Modeling

Using a triangular facet model as a basis, we have developed and integrated a system that models CO₂ laser radar, Millimeter Wave (MMW) Radar, Synthetic Aperture Radar (SAR), and Infrared target signatures.

2.1 CO₂ Laser Radar Model

The imaging model used is the point projection model [1] that approximates the transformation performed by our eye and many imaging devices on a visual scene. The

imaging process consists of passing the scene through a pinhole (focus) and projecting the image onto an image plane. This is depicted for the triangular panel in Figure 1. The origin "o" is the location of the focus.

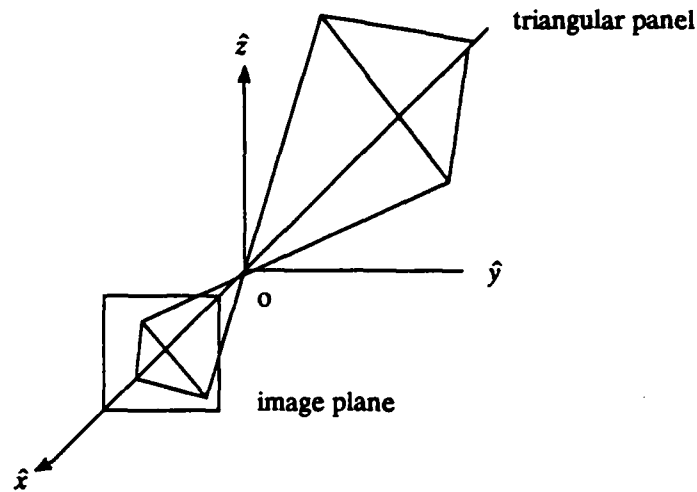


Figure 1: Projection Geometry

The object represented is assumed to be solid with the triangular panels defining only the outer surface. These triangular panels therefore have intersections only at their edges. We have adopted a convention for facet representation whereby the information stored for each triangular facet consists of the three-dimensional coordinates of the three corner points. These points are ordered in a counterclockwise direction corresponding to a condition where the "outer" surface normal of the facet has a positive component in the direction of the viewer as shown in Figure 2 (the normal will be pointed directly at the viewer if such component of the unit normal is 1). The "outer" unit normal vector is then determined by:

$$\begin{aligned}\vec{N} = & \{ [(y_2 - y_1)(z_3 - z_2) - (z_2 - z_1)(y_3 - y_2)] \hat{i} \\ & + [(z_2 - z_1)(x_3 - x_2) - (x_2 - x_1)(z_3 - z_2)] \hat{j} \\ & + [(x_2 - x_1)(y_3 - y_2) - (y_2 - y_1)(x_3 - x_2)] \hat{k}\end{aligned}\quad (1)$$

$$\hat{n} = \vec{N} / |\vec{N}| \quad (2)$$

$$\hat{n} = n_x \hat{i} + n_y \hat{j} + n_z \hat{k} \quad (3)$$

where (x_i, y_i, z_i) are the coordinates of the triangle's corners. N is the cross product of sides a and b as shown in Figure 2.

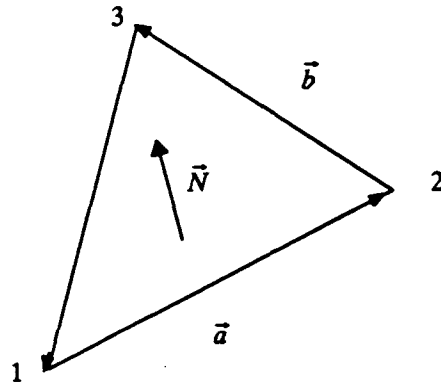


Figure 2: Panel Normal

Shadowing of the facets is determined analytically [2]. Simulation of a laser radar image then proceeds by binning facets or sections of facets visible to the sensor in the appropriate angle-angle and range bins [3]. Speckle, noise, and the sensor response function are modeled by the simulator (Figure 3).

A simulated 2-D angle-angle (no-range) laser radar image of a T-62 tank with resolution of 6 inches at viewing angles of 30 degrees in elevation and 120 degrees in azimuth is shown in Figure 4. The facet data, acquired from the U. S. Air Force Armament Technology Laboratory at Eglin Air Force Base, consists of about 1,100 facets defining the outer surface

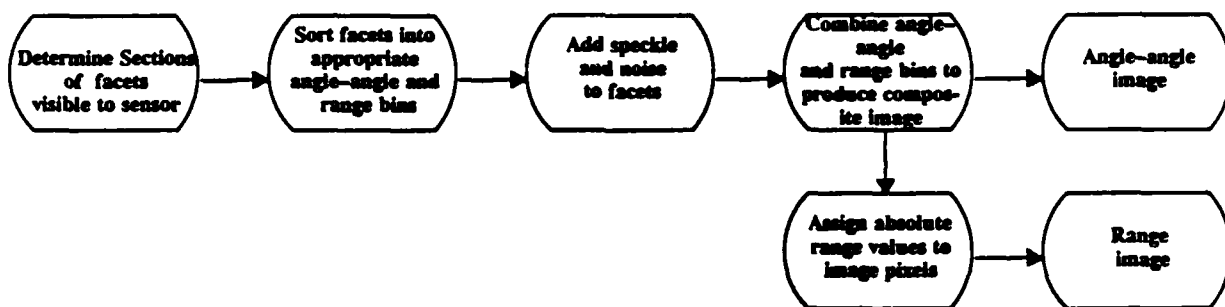


Figure 3. Laser Radar Target Signature Generation Procedure

of the T-62 tank. A color-coded simulated range-angle image at the same viewing angles is shown in Figure 5.

The 3-D information (angle-angle-range) can be rotated to provide a planar view of the target as shown in Figure 6. The shadowing caused by the turret at this aspect angle is clearly visible.

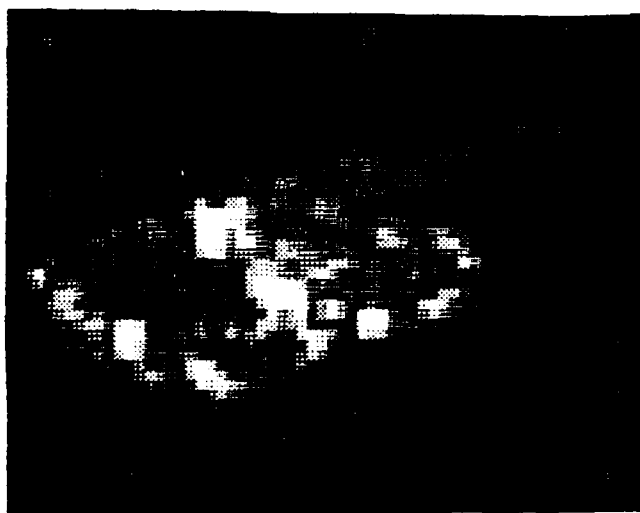


Figure 4. Angle-Angle Image, T-62, Soviet Tank



Figure 5. Range-Angle Image, T-62 Soviet Tank

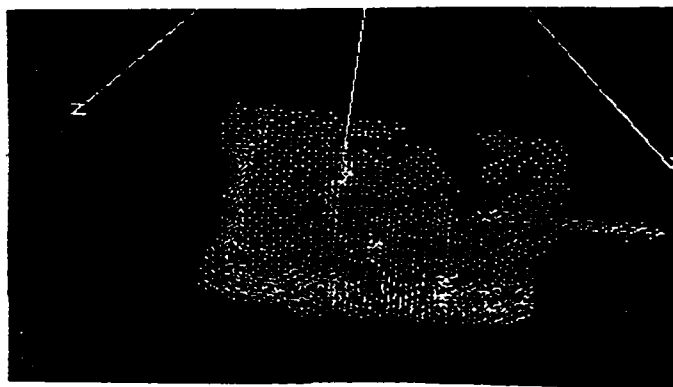


Figure 6. Rotated Image T-62 Soviet Tank

2.2 MMW Sensor Model

The modeling of MMW sensor imagery consists of binning facets or parts of facets into the appropriate angle-range bins (Figure 7). The cross section is then calculated for each bin. Physical optics and edge diffraction are currently modeled in the algorithm for calculating cross section. Polarization signatures can be modeled for each bin, given appropriate modeling tools for calculating the polarization response of a collection of facets in a bin. The facet representation and shadowing techniques are described in the laser radar model section. A comparison of MMW Imaging SAR (ISAR) simulations with MMW turntable data on a T-62 tank is shown in Figure 8.

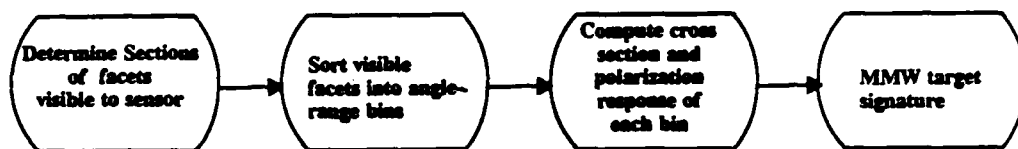


Figure 7. MMW Target Generation Procedure

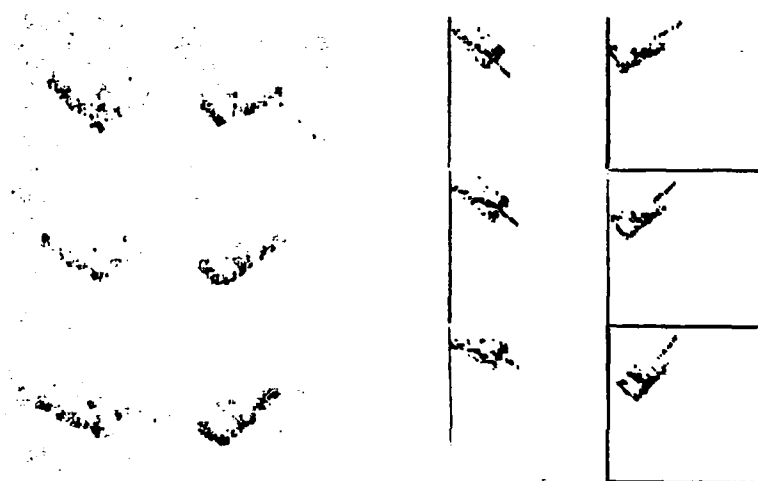


Figure 8. MMW Turntable Data vs. Simulation, T-62, Soviet Tank

2.3 SAR Model

We have developed a combined target and background signature simulator to support development of SAR ATR algorithms [3]. The calculation of the SAR image of a target, depicted in Figure 9 proceeds as follows: (1) The three-dimensional surface boundary of a target is represented by facets as described in paragraph 2.1; (2) the facets or portions of facets are binned into their appropriate SAR image bins; (3) shadowed facets or parts of facets are determined and eliminated; and (4) the electromagnetic field scattered by each facet in an image is calculated using the formalism of physical optics and diffraction as documented in

[4]. Shown in Figure 10 is a comparison of measured SAR data of a B52 airplane and simulated imagery.

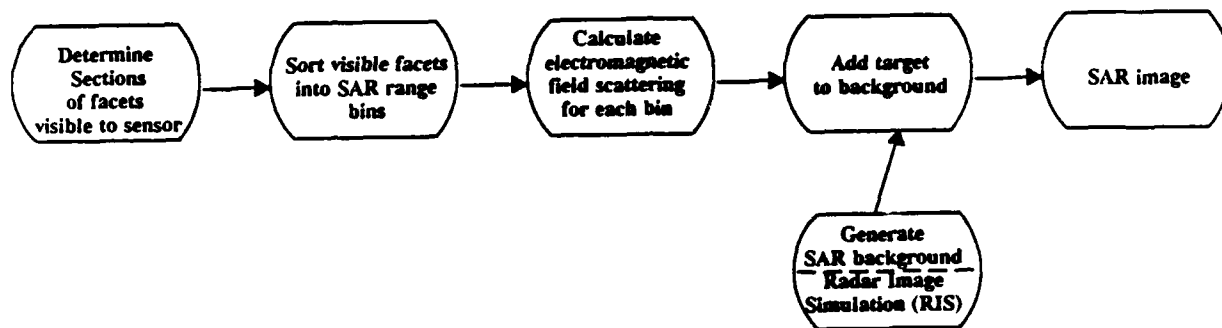


Figure 9. SAR Image Generation Procedure

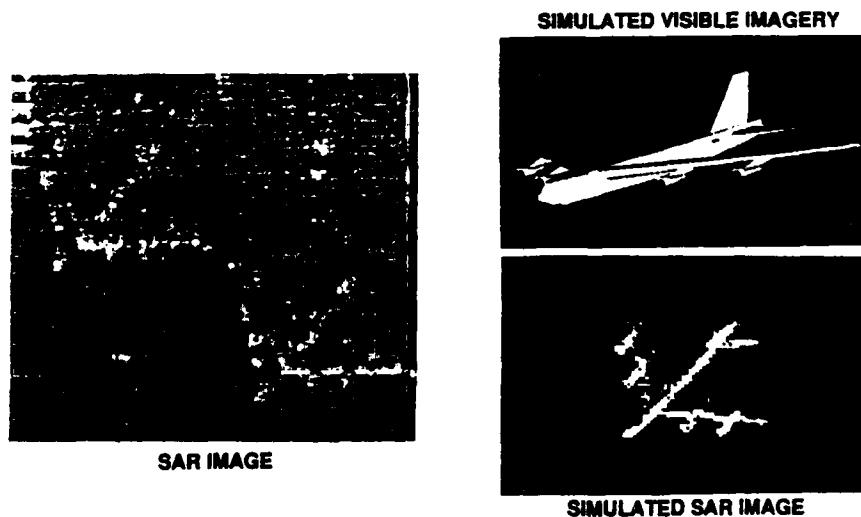


Figure 10. Measured and Simulated B52 SAR Images

The background signature simulation used in our simulator is based on the Radar Image Simulation (RIS) software developed by the Remote Sensing Laboratory at the University of Kansas, Lawrence. Input to the simulator consists of terrain elevation maps, lands use maps, and texture maps. A final SAR target and background image is generated by embedding the target into the background image and applying system noise. Shown in Figure 11 is a simulated image showing military vehicles positioned in a clearing.

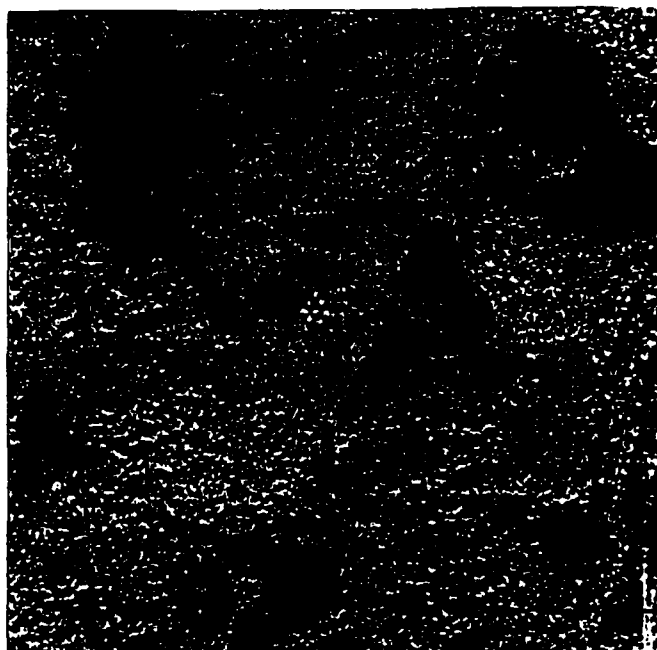


Figure 11. Simulated Image of Targets Embedded in Terrain

2.4 IR Model

The current implementation of the synthetic infrared model places an infrared target in either a real or synthetic background. Grey-level values are assigned to the projections of the three-dimensional target facets onto the two-dimensional image plane. Various approaches can be employed to assign thermal states to the target facets. The current implementation (shown in Figure 12) assigns pixel values by examining pixel values in real imagery and assigning those values to the projected facets of a model target of similar

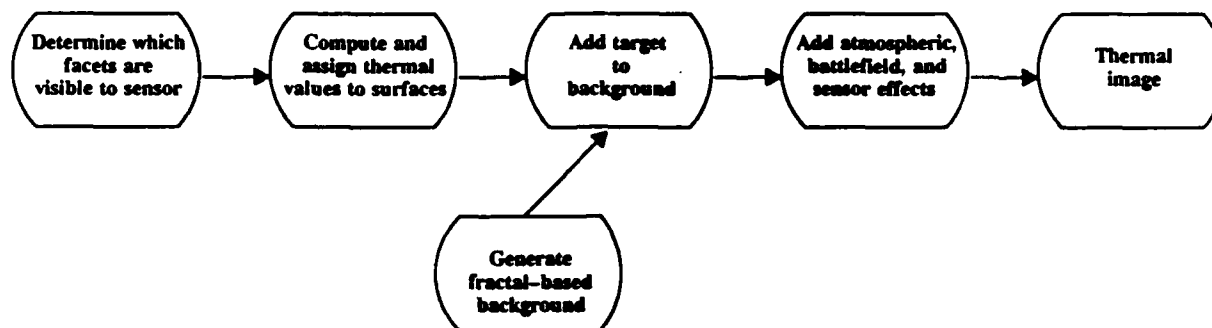


Figure 12. Thermal Image Generation Procedure

orientation. In algorithm development, the contrast between a target and background is often the most important feature of the infrared target signature. With this in mind, pixel values are also assigned to the target model such that the relative grey values of the synthetic image closely match those of a real image under the same set of conditions.

The modeled thermal signature of the target is placed in a real or synthetic background and a point spread function is convolved over the final image to mimic sensor effects. Also, the final image can be used by the TACOM Thermal Imaging Model (TTIM—OptiMetrics, Inc.) to model atmospheric and battlefield effects.

3.0 Conclusions and Recommendations

Synthetic image generation is essential for the development of statistics-based and model-based ATR algorithms. The target descriptions used by synthetic image systems should be designed to support target signature modeling of multiple sensors. This provides a basis for the generation of registered synthetic imagery from multiple sensors and allows an algorithm developer to perform a well-defined parametric analysis of ATR performance. The effects of image and sensor degradation as well as deviations from predicted mission scenarios can be studied and quantified using synthetic imagery.

There are several different modules for creating synthetic image data, but an overall, user-friendly system or environment needs to be developed to fully utilize the individual packages. Coordination between government and industry would help accomplish this and would reduce duplication of effort. Government-defined mission and validation requirements will allow industry to develop synthetic sensor model and terrain data that will boost ATR technology and benefit the entire community.

References

1. [1] D. H. Ballard and C. M. Brown, Computer Vision, Prentice-Hall, Inc. (1982), p. 19.
2. [2] J. V. Geaga, "Shadowing Between Flat Triangular Panels," Northrop Research and Technology Center Report No. TP-704 (1986).
3. [3] J. V. Geaga, "Synthetic Aperture Radar Target and Terrain Simulator," Northrop Research and Technology Center Report No. 86-4R (1985).
4. [4] H. B. Tran and T.J. Kim, "Monostatic and Bistatic Radar Cross Section Analysis," Volume 1, The High Frequency Electromagnetic Scattering Theory, Northrop Corporation Report NOR-820215 (1982).

Presented at the
DIGITAL/ELECTRONIC TERRAIN BOARD SYMPOSIUM
5-6 October 1989 GACIAC PR 89-07

DIGITAL GENERATION OF SYNTHETIC, MULTI-SENSOR IMAGERY

Charles Lindahl, Alan Cockcroft,
John Sigler, and Mark Yablonski
Texas Instruments Incorporated
Image Processing Laboratory
P.O. Box 660246 MS-3603
Dallas, Texas 75266

ABSTRACT

The advantages of using a synthetic database for the development, testing, and evaluation of Automatic Target Recognition algorithms are well recognized. Real multi-sensor scene combinations reflecting operational requirements, missions, and targets are unavailable and economically difficult, if not impossible to obtain. This paper describes Texas Instruments (TI's) Synthetic Multi-Sensor (IR, TV, Laser Radar) Image Generation System which has been developed to address this database problem. The system described has the capability of generating single image frames or image sequences based upon scenarios derived directly from DMA digital map data. The major components of the system include scene rendering, sensor, atmospheric environment, and user interface modules. The generation of synthetic backgrounds (trees) utilizing fractal techniques is also considered.

1. INTRODUCTION

The development of robust automatic target recognition (ATR) algorithms depends critically on an adequate database for testing them. At the present time there is a significant lack of real, boresighted, multi-sensor imagery available for this purpose. Furthermore, the acquisition of such data is difficult and expensive in the variety of environmental and target conditions that are needed. In 1988 Texas Instruments completed the development and validation of a multi-sensor hybrid image generation system to extend existing real databases by inserting synthetic targets in real image backgrounds. It was an extension of the Defense Advanced Projects Agency (DARPA) Characterization of Algorithms for Passive Infrared (CAPIR) program¹. This system has the capability of modeling various sensors and controlling image parameters of importance to ATR algorithms such as signal-to-noise ratio, target-to-background contrast ratio, target detail (variance of target intensities), and clutter content (IR and TV) in image backgrounds. However, this hybrid system is not adequate to support autonomous, ATR system smart search and end-to-end, mission simulations. Hence, a synthetic, multi-sensor(IR,

¹ Cockcroft, Alan, Krebaum, Ken, Thomson, Chris J., "Final Report, Characterization of Algorithms for Passive Infrared (CAPIR)," Report No. U2-85301-F, Center for Night Vision & Electro-Optics, Advanced Concepts Division, Fort Belvoir, VA 22060; 31 January 1988.

TV, Laser Radar) image generation system utilizing Defense Mapping Agency data with modeling of scene backgrounds, sensors, and environmental effects was created. Particular emphasis has been placed on those features necessary to support ATR algorithm development.

2. SYNTHETIC SCENE RENDERING

The synthetic image generation system has been developed to produce single image frames or image sequences of IR, TV, and/or laser radar images as shown in Figure 1. The terrain elevation and background cultural data are derived from Defense Mapping Agency (DMA) Digital Terrain Elevation Data (DTED) and Digital Feature Analysis Data (DFAD).

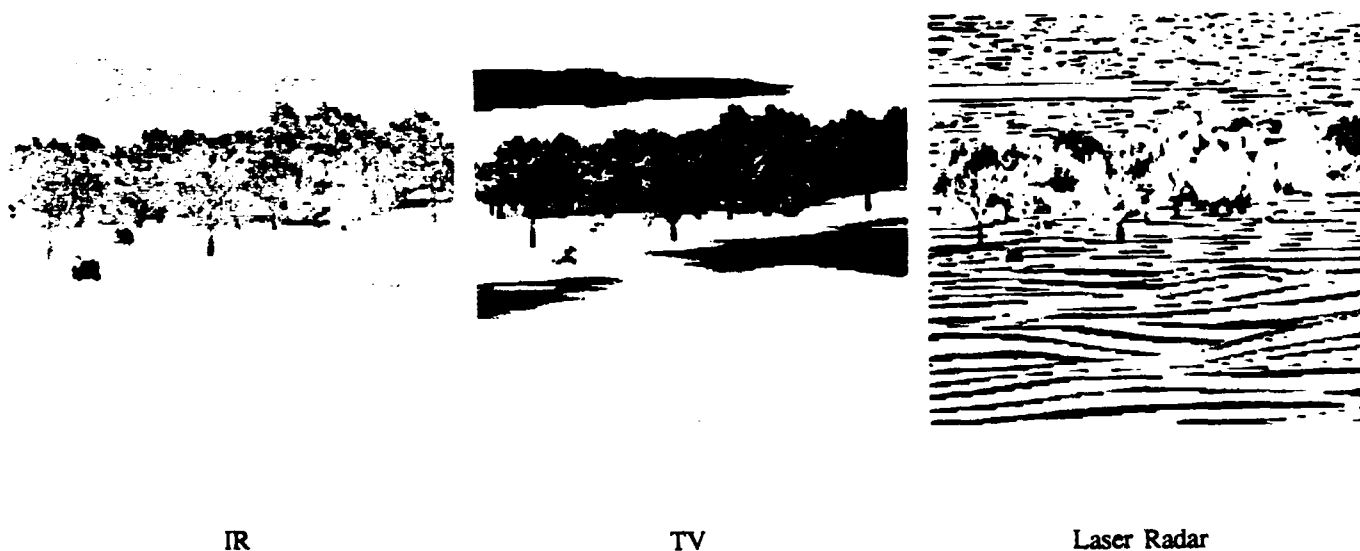
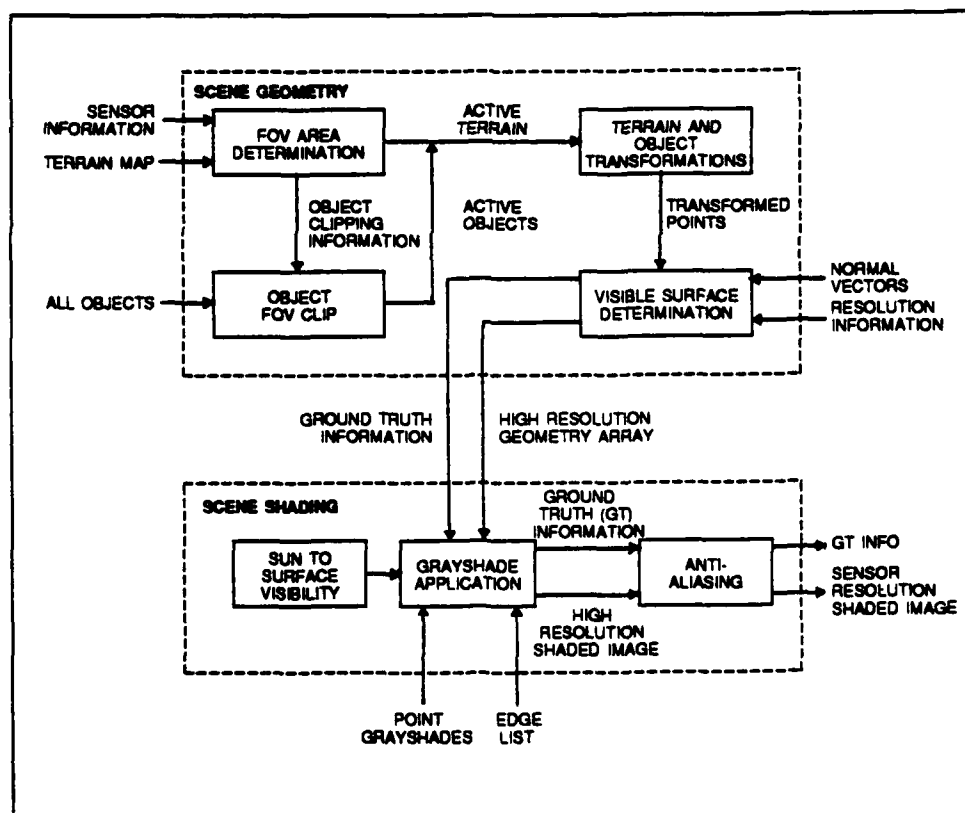


Figure 1. Synthetic Imagery

The DMA elevation data are interpolated using a fractal interpolation technique to achieve a realistic appearing terrain at the resolution of the sensors being simulated. Fractal techniques have also been used to create individual background trees of various types and forested regions. Figure 2 presents a block diagram of the synthetic image generation system currently in operation.

Three types of data are utilized: terrain data at a base resolution determined by the DMA elevation data used; class map data containing material type data derived from DMA feature analysis data, registered with the terrain data, and stored in quad-tree form; and object/target data stored as facet and point lists. In general, a large portion of the scenario is not within a sensor's field-of-view (FOV) during a single snapshot. Hence, terrain data are initially clipped to a subset of the overall terrain area to reduce the amount of data to be processed. Exact terrain points within the projected sensor

All objects specified within a sensor's field-of-view are translated, rotated, and scaled to the desired location and orientation in world coordinates. A transformation from the world coordinate system to the sensor viewpoint is performed and a perspective transformation maps the object and terrain data into a two-dimensional sensor image plane view. A Z-buffer hidden surface algorithm is then used to calculate which surfaces are blocked from view by other surfaces. The output contains the visible surfaces as they would appear to the sensor with a geometric sampling resolution sufficient for the application of subsequent antialiasing processing.



Greyscale is now applied to the two-dimensional sensor image. The shading of the IR sensor imagery currently depends upon user determined shades with solar effects not implemented (future work will incorporate thermal modeling

from first principles). Attached to each object or terrain model point is a property which can be used as a greyscale or related to a greyscale (i.e., material type from the class map data). The area between these points is shaded using Gouraud (intensity interpolated) shading. Greyscaling for TV sensor simulation consists of ambient and diffuse components (specular shading is not currently implemented) with coefficient lookup tables used for different material types.

Laser radar sensor simulation is obtained by generating a range image at the required sensor pixel resolution and applying the necessary sensor effects to simulate a particular laser radar sensor.

Subpixel areas are finally averaged to reduce antialiasing artifacts and to obtain the final sensor imagery.

The scene rendering system described has a wide variety of configurations available to the user for multi-sensor image generation. The sensor type (TV, IR, and Laser Radar), sensor parameters (FOV and resolution), and location/orientation (latitude, longitude, altitude, heading, depression angle, and roll) are all user selectable. Also, multiple sensors (sensor types, wide/narrow FOV's, etc) may be included in a sequence with any sensor capable of being selected for a particular frame. Objects may be shaded with unique greyscales in a sensor's FOV (e.g., an M-60 can be shaded with a single greyscale, each type of tree with its own different greyscale, and various material types of the terrain with still different greyscales). This can be useful for determining ground truth for the testing of ATR segmentation algorithms.

3. SYNTHETIC BACKGROUND GENERATION

Synthetic background generation methods utilizing fractal techniques have been developed to increase scene detail with emphasis on the generation of individual tree types, tree lines, and forests. These methods have been severely constrained because of the requirement to generate synthetic scenes as fast as is practically possible.

Two types of individual trees (deciduous and coniferous) have been modeled as well as individual trees without leaves. For trees without leaves a recursive procedure is used with a tree node defined as a branch (stem) with one or more tree nodes attached and with each tree node generated by means of a 3x3 linear transformation. The generation process is terminated once the branches (stems) are small enough. The variable parameters of the algorithm are: stem diameter at base of the tree, initial stem length, minimum stem length, and number of branches per branching point. The branches and stems are modeled as elongated three-sided pyramids. Additional details can be found in the paper² referenced below.

Trees with leaves are generated using a fractal initiator/generator technique. This is accomplished in three steps. The first step is to use fractal techniques to generate the outline of the tree object as viewed from uniformly spaced directions

² Oppenheimer, Peter E., "Real Time Design and Animation of Fractal Plants and Trees," SIGGRAPH '86 Conference Proceedings, Vol. 20, No. 4, August 1986; pg. 55-64.

around it. The number of such viewing directions is an algorithm input. This set of two-dimensional half-planes essentially consists of tree side views as seen from appropriate directions. The second step is to orient each half-plane in three-dimensional object space at the appropriate rotation angle about the tree axis. Finally the vertices of the straight lines making up each half-plane tree outline are connected together to form point and facet lists defining the tree model which can then be rendered by the scene rendering software after having been transformed from object to world coordinate space. Examples of the results obtained are shown in Figure 3.

Since tree lines define the edges of forests where partially obscured or totally obscured target objects may be located, scene realism is an important issue for the development and testing of advanced ATR algorithms which are being designed to locate targets in these regions. The fractal technique used to model individual trees with leaves as described above has been applied to large groups of trees. Tree lines have been simulated by randomly placing individual trees along the defined tree lines. Forest regions have been modeled by randomly placing high-detailed trees along its edge (tree lines) and filling these regions with low-detailed trees which only have their top halves modeled. This is possible since only those approximating facets within a line of sight are visible.



Figure 3. Synthetic Tree Imagery

4. SENSOR AND ATMOSPHERIC ENVIRONMENT MODELING

Sensor models for IR, TV, and laser radar sensors were developed for use with the Synthetic Multi-Sensor Image Generation System. They have been specially designed for speed of execution and hence have been simplified from those that were developed for the hybrid image generation system mentioned in the introductory section of this paper. A two-dimensional Gaussian point-spread function is used to approximate the effects of optical diffraction and blur, detector and

LED spatial response, and stabilization jitter for both the IR and TV sensors. The use of a Gaussian point-spread function greatly simplifies both the computational process as well as the modeling process, since the effort in determining all the possible distortions and their parameters is replaced by the simple determination of the variance of the Gaussian estimate of the system response. The final output images of the IR and TV sensors are obtained by multiplying the spatial MTF of each sensor type (IR and TV) by the FFT of the pre-MTF IR or TV image, adding colored noise appropriately matched to the sensor's noise characteristics, and calculating the inverse FFT for the IR and TV images. The range image which is also obtained as an output from the scene generation system is currently processed to simulate signal dropouts and then divided into range bands or used as an absolute range image depending upon the laser radar sensor being simulated.

In general, meteorological conditions affect the atmospheric transmission of infrared energy from background, target, and object scene elements to a given sensor. Knowing relevant weather information, one can predict the atmospheric transmission using the LOWTRAN-7 model. This atmospheric transmission is specified in units of transmission per kilometer. This factor in conjunction with the range value associated with each image pixel is used to take into account atmospheric effects.

5. USER INTERFACE

The development of an operator/user interface which allows an operator or user to control easily the operation of the synthetic image generation system and to create, modify and control an associated synthetic scene scenario is of utmost importance in achieving a successful capability to generate synthetic imagery. The creation of scene scenarios is extremely labor intensive unless adequate scenario creation and editing facilities are available. Figure 4 shows the VAX computer interface menu that has been developed. The right-hand portion of the menu corresponds to the VT-100 keypad with the individual keypad display areas highlighted when the associated key has been activated. Appropriate responses are requested in the *Information Area* on the left-hand area of the display. An error message line is utilized on the bottom of the display when errors occur. The following operator functions have been implemented: the specification of scenario flight paths and sensor parameters; the addition, deletion, or replacement of targets and objects; and the graphical display of the scenario map at various scales with an indication of the location and type of cultural features and objects in the scenario. The interface also allows the specification of the simulated rate of image frame generation for each sensor and displays an indication of a sensor's field-of-view along the specified flight path. In addition, an AutoCad 10, PC-based software system is used to develop target and object models for the synthetic image generation system. This system also allows target and object models to be imported through the use of industry standard graphics interchange formats.

In this manner the large number of various synthetic targets and objects needed to support the development of advanced ATR algorithms is cost effectively provided.

Synthetic Image Generation				
Information Area	START NEW SESSION	RESTORE OLD SESSION	SAVE CURRENT SESSION	EXIT
	DEFINE FLIGHT PATH	MODIFY FLIGHT PATH	ADD OBJECTS	MODIFY OBJECTS
	SHOW MAP INFO	SHOW TERRAIN HEIGHT	SHOW FLIGHT PATH	SHOW OBJECT INFO
	ZOOM	DEZOOM	PAN	GENERATE SCENE
	SHOW/ALTER MATERIAL CHARACTERISTICS			
ERROR MESSAGE LINE				

Figure 4. User Interface Menu

6. CONCLUSIONS AND COMMENTS

The Synthetic, Multi-Sensor Image Generation System developed by Texas Instruments for the development, testing, and evaluation of ATR algorithms has been described. It is envisioned that this system will be most useful for supporting the smart search and end-to-end, mission simulations of autonomous, advanced ATR algorithms. At this point in time, it is clear that synthetically generated multi-sensor imagery will not replace real imagery, but it is believed that use of the system described in this paper will provide valuable insights not otherwise obtainable during the advanced ATR algorithm development process.

THIS PAGE INTENTIONALLY BLANK

Presented at the
DIGITAL/ELECTRONIC TERRAIN BOARD SYMPOSIUM
5-6 October 1989 GACIAC PR 89-07

Efficient Scene Modeling for Digital/Electronic Terrain Boards

by
Geoffrey Y. Gardner, PhD
Grumman Data Systems

ABSTRACT

The complexity of real-world scenes makes faithful digital simulation computationally expensive unless efficient modeling and image generation techniques are applied. The large volumes of data required to represent terrain and natural surface features make storage, access, and processing costly. Simplifying the data to alleviate computation or merely overlaying an image onto terrain data will not provide the 3-D clutter and obscuration necessary to test target recognition fully.

Grumman Data Systems has developed efficient digital technology to simulate complex and realistic 3-D scenes into which specific targets can be inserted. The background scenes, including terrain, trees and clouds, can be generated entirely from mathematical functions or can include real terrain and feature data enhanced by such functions. Terrain is modeled by polygons fitted to a mesh of elevation values. Trees are modeled by textured quadric surfaces positioned on the terrain procedurally. A dynamic cloud model simulates cumulus cloud development as well as smoke screens by manipulating ellipsoids and controlling textural translucence. Convincing tree and cloud shadows are simulated efficiently, enhancing the realism of background clutter and obscuration.

Levels of detail dependent on the view point are generated automatically for the terrain, trees, and clouds. This tailors the image content to the viewer's perception, alleviating image computation by greatly reducing the amount of geometric data required to model distant scene features. In addition, detail on terrain, trees, and clouds is simulated by texture to provide natural complexity without adding to the geometric data base.

1. INTRODUCTION

The digital/electronic terrain board (DETB) will be a useful tool for a variety of applications which include acquiring or recognizing targets in cluttered backgrounds. The control provided by computer simulation offers far greater flexibility than physical model boards, allowing changes in targets and environments with relative ease compared to physical models. Unfortunately, the real world is extremely complex and includes a wide variety of natural detail difficult to simulate with traditional computer graphics techniques. Valid simulation of natural environments must include a representation of this natural clutter and obscuration.

Computer graphics technology has made impressive advances toward realistic simulation of natural scenes. Two techniques in particular have been very successful. Fractal surfaces [2,5] allow representation of terrain with a high level of three-dimensional detail. But the standard implementation of fractals entails the creation of a terrain model composed of hundreds of thousands of polygons or elevation points, necessitating a large geometric data base that requires heavy computation loads for rendering. The second innovative technique is the overlaying of high resolution imagery on lower resolution terrain data. This technique provides photographic realism at high altitude views, but fails to provide three-dimensional structure at low altitudes.

Grumman Data Systems (GDS) has taken a different approach to the simulation of natural scenes to provide realistic target backgrounds economically. Our approach is to minimize the geometric data base and represent natural detail with

texturing. Our technique extends research initiated at the Grumman Corporate Research Center (CRC)[3]. This initial work used quadric surfaces to model scene features and added detail by means of a texturing function which modulated surface shading intensity and object translucence. At GDS we have extended the technique of functional texturing to a more comprehensive technique of functional modeling by using the "texturing" function to define large scale natural structure. This greatly facilitates the construction of arbitrary natural scenes covering large areas. It also provides a greater degree of realism because of the natural quality produced by the functions. We have also incorporated the function into a dynamic cloud model to enhance the scene model with time-varying obscuration from atmospheric clouds and smoke screens.

A second extension we have made to the original CRC research is the use of hierarchical data structures, to reduce data volume by matching resolution to view range.

2. A FUNCTIONAL MODEL FOR NATURAL SCENES

Our functional scene model is currently designed to provide three elements critical for target backgrounds:

1. Terrain model
2. Clutter
3. Obscuration

The scene model is generated using spectral functions, i.e. functions defined by

their frequency content. Our basic spectral function is composed of sums of cosines with increasing frequency [4]. Our 2-D function uses two sums of cosines. The cosines of the first sum are variables of the south-to-north ground coordinate; and the cosines of the second sum are functions of the west-to-east ground coordinate. Our 3-D function includes a third sum of cosines dependent on the vertical coordinate.

By appropriate definition of the frequency content of the functions, we are able to model large scale structure using no more than 7 cosines per sum. We can add natural detail using functions with the same number of cosines but of higher frequency.

2.1 Terrain

We generate our terrain model by defining a horizontal grid with specified grid spacing. We select parameters for our spectral function to define the desired terrain characteristics. A wide spectral bandwidth will produce rugged terrain, while attenuating high frequencies produces smooth terrain. We compute the function at each grid point and define the elevation at that point to be the resulting function value. We then triangulate each quadrilateral to produce a geometric terrain data base of triangular polygons.

This low-frequency geometric terrain data is enhanced by adding natural detail with functions having higher frequency content. Color variations are added by modulating the basic terrain color, and topographical detail is added by modulating the surface normals [1]. The resulting imagery is comparable to that produced

by fractal surfaces modeled with 10 to 100 times more polygons. Because the functional detail is applied in 2-D image space, it requires significantly less computation than geometric (polygon) detail which must be processed in 3-D scene space.

2.2 Clutter

The most prevalent source of clutter in natural scenes is vegetation, particularly trees. To avoid the geometric complexity normally associated with trees, we model such features with simple curved surfaces, ellipsoids. To facilitate generation of large clusters of trees, we use our 2-D function computed on a fine grid on the terrain's surface. Applying a threshold to the function values isolates regions where tree clusters exist. At each tree grid point within such a region, we place a tree ellipsoid with small random variations in position, size and color. To assure consistency in the scene when viewed from different eye points, the random variations are keyed to the tree grid position.

We add natural detail to each tree ellipsoid by manipulating its surface shading intensity and translucence using our 3-D spectral function with high frequencies. A natural foliage look is achieved by increasing the translucence at the ellipsoid silhouette.

A secondary source of clutter prevalent in natural scenes is the contrast produced by shadows. Shadows have traditionally been an expensive feature to add to computer-generated images. Our functional model approximates shadows economically by projecting the tree cluster regions onto the terrain under the trees and darkening the terrain surface.

2.3 Obscuration

In addition to trees, meteorological clouds and man-made smoke screens produce obscuration which can adversely effect military operations.

We model clouds in a manner very similar to that in which we model trees, using ellipsoids with functional texturing which modulates both shading intensity and translucence. There are two significant differences, however. First, we cluster trees two-dimensionally on the terrain surface, while we cluster clouds three-dimensionally above the terrain. Second, our cloud model is dynamic, allowing the visualization of time-variations and their effect on obscuration. A dynamic model also allows rerunning a simulation quickly with changes in initial parameters to study a variety of "what if" situations effecting decision sensitivity or system reliability.

Our dynamic cloud model simulates the "parcel" theory of cloud formation, which describes cloud formation due to heated bubbles of air expanding and rising into cooler atmospheric regions forcing condensation of moisture. We implement this theory by computing our 2-D spectral function at each point in a specified cloud grid defined at a specified altitude (the altitude of condensation). The function simulates heat energy and expands the cloud ellipsoids and decreases translucence to represent condensation.

We add cloud shadows in a cost-effective manner by projecting the cloud function along the light vector and darkening tree and terrain surfaces in regions where clouds are functionally defined.

2.4 Variable Resolution

Despite the economy of our model, natural scenes can be so complex that computation can be unacceptable and buffers can overflow unless efficient data management techniques are applied. Our overall approach is based on tailoring the data base to the viewers perception. Thus we use 2-D texturing when it is indistinguishable from 3-D geometric detail.

We have extended this strategy by applying hierarchical data structures, specifically quadtrees, to represent scene features in varying levels of detail dependent on viewing distance. Quadtrees provide a controlled means of reducing data volume without loss of significant information. We apply quadtrees to terrain, tree, and cloud data independently. For each set of data, we define a minimum viewing size for an object (a triangular polygon for terrain and an ellipsoid for trees and clouds). The minimum size is used to compute radial sectors within the scene for a given eye point, with the sectors centered at the eye point.

Terrain data is reduced by maintaining the original grid spacing for the closest terrain sector and successively doubling the spacing for each distant sector. Because doubling the spacing decreases sampling resolution, a weighted average is used to filter the data. Continuity is maintained by subdividing a small percentage of the nearest polygons in each distant sector to match the farthest polygons in the preceding sector.

Tree and cloud data are reduced by a similar doubling of grid spacing accompanied by a doubling of ellipsoid width. This is equivalent to replacing trees in

the foreground with groves and forests in the distance.

This technique is very effective in compressing large data volumes because for each successive resolution sector, four polygons or ellipsoids are replaced by one. This is important not only for computation savings but also because it allows the modeling of large, complex scenes with limited memory buffers. Without such a variable-resolution data management scheme, scene models would be limited to either small regions of high resolution or large regions of low resolution. Defining resolution as a function of view point tailors the imagery to perception, so that no important information is lost. Finally, we have implemented parametric control (minimum viewing size) to allow selection of an appropriate tradeoff between detail and computation for a given application.

Figure 1 shows an example of a 3-D scene model generated entirely from functions. The use of texture and variable-resolution geometric data allow a realistic representation of natural complexity and clutter necessary for an effective DETB.

2.4 Enhancement of Real Data

A great deal of flexibility is provided by the capability to generate an entire scene background under functional control. For certain applications, however, it will be desirable or necessary to replicate an actual geographic region. In such cases, real data can be used and enhanced by functional modeling. Figure 2 shows a model of the Fulda Gap in Germany using real terrain elevation data and real feature data specifying treed regions. Functions were used to add terrain detail and color variations and to insert 3-D trees within the specified treed regions. Figure 3

shows the same model enhanced with clouds and cloud shadows to provide a more realistic simulation of natural clutter and obscuration. This 512-by-640 pixel image took under 10 minutes to generate on a Silicon Graphics Personal Iris workstation.

3. CONCLUSIONS

Functional modeling combined with variable-resolution management is a cost-effective means of providing realistic simulation of complex natural background scenes for Digital/Electronic Terrain Boards. The technique provides great flexibility for generating and changing scenes which include realistic clutter and obscuration. The dynamic cloud model can be used to simulate varying degrees of obscuration due to cloud cover and smoke screens, as shown in figures 4 and 5.

4. REFERENCES

1. Blinn, J. F., Computer display of curved surfaces. PhD Thesis, Computer Science Department, U. of Utah (Dec 1978).
2. Fournier, A., Fussell, D., and Carpenter, L., Computer rendering of stochastic models. Comm. ACM 25,6 (June 1982), 371-384.
3. Gardner, G. Y., Simulation of natural scenes using textured quadric surfaces. Computer Graphics 18,3 (July 1984), 11-20.
4. Gardner, G. Y., Functional Modeling of Natural Scenes. Course 28, Functional-Based Modeling, SIGGRAPH '88 (August 1988), 44-93.

5. Mandelbrot, B. B., Fractals: Form, Chance and Dimension. Freeman, San Fransisco, (1977).



Figure 1. Functional Scene Model



Figure 2. Functional Enhancement of Real Data



Figure 3. Functional Enhancement of Real Data with Clouds Added



Figure 4. Simulation of Obscuration by Cloud Cover



Figure 5. Simulation of Obscuration by Smoke Screen

Presented at the
DIGITAL/ELECTRONIC TERRAIN BOARD SYMPOSIUM
5-6 October 1989 GACIAC PR 89-07

**Synthetic Image Generation Model and its Interface With the
Digital Electronic Terrain Board**

Gertrude Kornfeld, Joseph Penn, Michael Lander,
Hung Nguyen, John Ho, and Thomas Steck
US Army Communications-Electronics Command
Center for Night Vision and Electro-Optics
Attn: AMSEL-RD-NV-V
Fort Belvoir, Virginia 22060-5677

ABSTRACT

The US Army Communications-Electronics Command (CECOM) Center for Night Vision and Electro-Optics (C2NVEO) has originated a facility for Computer-generation of Realistic Environments with Atmospheres for Thermal Imagery with Optics and Noise (CREATION). This is essentially a model which allows the user to synthesize and analyze infrared images of target and backgrounds with atmospheric and sensor degradations. Realistic electro-optical sensor effects can be applied selectively to both synthetic and high quality Forward Looking Infrared (FLIR) imagery.

The versatility of CREATION is a valuable tool for several applications, such as generation of imagery for human search, systems analysis and the visualization of important image properties that are pertinent to Automatic Target Recognizer (ATR) performance. Enhancements to CREATION are planned in the areas of incorporating fully three dimensional targets and backgrounds, and in improving the ability to add textures.

INTRODUCTION

The important differences between human and machine visual performance must be considered when imagery is chosen. In general, machine vision of higher resolution than human vision is within the present state of the art. The greater repeatability and absence of fatigue are also important assets of machine vision. Unfortunately, simple perception tasks that humans perform instinctively are

beyond present machine vision capability, and image artifacts that are disregarded easily by humans can seriously affect ATR performance.

A digital electronic terrain board is being established at C2NVEO. The CREATION Facility will be used for the production of synthetic imagery that does not have the unavoidable artifacts of real time (30 frames/second) dynamic sequence programming. The trade-off will be precision at the expense of computation time. This report outlines C2NVEO plans to pursue using CREATION capabilities for producing sets of imagery for human observers and ATR performance tests on first and second generation FLIR imagery. Necessary amendments for its interface with the terrain board are explored.

The CREATION facility currently is comprised of a Hewlett-Packard (HP) series 900 model 320C workstation that supports only two-dimensional graphics and has only 7.5 megabytes of Random Access Memory (RAM). A new Silicon Graphics workstation that performs 3D operations in hardware, and has the software for sophisticated texture merging, is being procured for inclusion in the Facility. Sample imagery is being generated on the existing HP configuration. Mass production of synthetic imagery has been postponed to a date when the new equipment will be available.

I. THE CREATION CAPABILITY

A. Geometry.

The version of CREATION currently being used at C2NVEO has insufficient RAM for implementing readily available rigorous three-dimensional software. Other government agencies have procured geometric target files and digitized landscapes of particular geographic locations that we plan to interface with CREATION later. Currently specialized RAM economical routines that were developed in-house are being implemented. For the particular case of an observation point with limited horizontal motion these specialized routines transform perceived shortcomings into advantages.

1. **Landscape.** To investigate search strategies, a wide horizontal panoramic view and narrow vertical field are required. Image distortions are minimized over the area of interest¹ when a polar coordinate geometry, depicted on Simulation 1, is chosen.

A stationary viewer, at the center of the coordinate system, has a 360-degree search field. This arrangement is also advantageous for helicopters that rise for a short time over tree lines. Motion is simulated by shifting rings of equal viewer-to-object distance (range) relative to each other². Simulation 2 shows a horizontal projection of Simulation 1. This landscape has generic features that would not occur in such close proximity in nature.

Simulation 3a shows gray shades and Simulation 3b is a range integer picture. Each pixel has a one-byte materials parameter that is converted to a shade of gray in a signature prediction model, and a one-byte range integer that is a look-up table address to the range in kilometers. The trees in Simulation 3 have the same range integer as the location where the bottom of the trunk was inserted.

2. Preparation for Insertions.

a. Natural Objects. The bottom half of the image in Simulation 2 shows natural objects that have been constructed by a semi-artistic method. A large branch structure, drawn by hand with a digitizer pen, was reduced and distorted to form a set of variations on the input shape that are pieced together later to form the complex trees. This method avoids repeated manual drawings and allows selective improvements; desirable combinations of features are stored, and poor choices are discarded. The final results are retouched, if necessary, prior to scaling and application of distortions.

Ground textures may be drawn with the digitizer pen, extracted from a thermogram, or derived analytically. In later sections, the realism of our textures will be demonstrated, and limitations of the flat planes approach used will be analyzed. Specialized distortion algorithms³ are used to make a set of different trees out of a single master, and a gradual change in distortion gives a two-dimensionally constructed tree remarkable plasticity in planned approach sequences.

b. Targets. Rigorous three-dimensional targets were tested in CREATION, but inputs were cumbersome and execution was slow when what were known to be sufficient facets were input. In parallel, a simple target geometry (2 1/2D) was implemented where textured planes are shifted relative to each other. Viewing angles can be changed only to a certain degree, but the targets do not have the typical artifacts nor the cartoon-like character of Computer Aided Design (CAD) constructions which contain an insufficient number of facets.

A. Modeling and its Digital Simulation Implementation.

1. **Thermal Signatures.** Simulation set 4 shows the fidelity of synthetic imagery by means of comparing a FLIR image to a synthetic image originated with CREATION using thermal signatures predictions generated by d'Agostino's SPACE model⁴. This model is available from the Xontech Corporation. Simulation set 5 illustrates the signature changes over a diurnal cycle⁵. The SPACE model would require excessive RAM if implemented concurrently with CREATION on the existing HP configuration; therefore, predictions were performed on an IBM PC/AT, and data files ported to the HP 9000.

The limited number of facets used in the validation exercise, illustrated on Simulations set 4 and 5, would have been objectionably cartoon-like in the absence of texture merging and/or systems degradation simulations. Successful texture merging was achieved by a distribution of materials integers that are assigned

to the same output from the SPACE model. The SPACE model predicts the mean radiant power. Superimposed are the fluctuations that are either drawn with a digitizer pen or derived analytically. The standard deviation of the gray shades of the grass blades on Simulation 4b are an input that can be compared to fluctuations on grass areas of FLIR imagery.

2. **Atmospheres.** A simplified LOWTRAN 7⁶ equivalent atmospheric attenuation routine, called LTR⁷, was originated by G. Kornfeld in FORTRAN on the IBM 4341. It explicitly uses equilibrium thermodynamics, described in standard textbooks^{8,9} to eliminate LOWTRAN 6 look-up tables. Comparison tests performed with LOWTRAN 6 show less than 1% of difference for all cases where identical results are desirable (comparable agreement with LOWTRAN 7 is anticipated). Some step discontinuities in LOWTRAN are removed intentionally.

A specialized regression algorithm is used for very large calculation sets. LOWTRAN or LTR is used to calculate atmospheric transmissions at several ranges. These pairs are inputs to the regression algorithm whose output are two parameters that are ported to the HP. More details are given in a later section where range and altitude dependence is discussed.

3. **Sensors.** The Sensor Degradation Digital Simulation Module of CREATION is probably the most sophisticated one of its type currently available. The reason is that, unlike most other

similar efforts, our module is based on methods of sensor specifications that include nonlinearities, asymmetry of spread functions and off axis resolution.

Efforts, by other agencies of which we are aware, use Fourier Transformation methods that are advantageous for sensor performance predictions based on a matched filter signal to noise ratio, because multiple convolutions can be replaced by products. Excellent fast Fourier Transformation software is readily available, but it lacks the versatility of the shift variant convolution method used in CREATION. Previous publications by G. Kornfeld^{1,3,5} illustrate several sensor effects that would be prohibitively difficult to calculate by the Fourier Transform method. The use of CREATION routines for visual experimentation and the on-going interaction with systems analysis efforts will be the subject of a later section.

II. APPLICATIONS

Two human observer tasks will be compared to typical ATR simulations. Important differences that must be considered are as follows.

a. The human observer can distinguish, at most, one hundred shades of gray; therefore, results of a thermal signature prediction model over a diurnal cycle cannot be displayed with a unique normalization, but the dynamic range of 12 bits (4096 shades of gray) of the new C2NVEO 2-color FLIR is used to enable uniform

scaling of radiant powers over a diurnal cycle. The input to the ATR is a matrix that cannot be visualized by humans, but normalization can be consistent.

b. In dynamic sequences, the human observer integrates over several frames, but the ATR views frames individually. The ATR is bothered by artifacts within a single frame that human observers can learn to disregard, but inconsistencies between frames that cause sudden jumps in the imagery do not affect ATR performance, yet can be very bothersome to human observers.

c. Machine vision can be performed from a digitization at the focal plane of the sensor after preamplification, but prior to display degradation. Digital simulations of sensor degradation at the focal plane will be compared to the display that is viewed by the human observer.

A. Imagery for Enhancement of Current Sensor Performance Predictions.

The C2NVEO¹⁰ Static Performance Model, used for the prediction of Thermal Sensors, and the Image Intensifier model currently are undergoing extensive revisions. These consist of model unification and conceptional changes to include impacts of new inventions and computer code revisions.

The use of CREATION sensor degradation routines play a major role is a visual experimental series performed by J. Howe and coworkers¹¹. Military targets were extracted from close-up FLIR

imagery, and selective sensor degradation routines were applied to these FLIR images with negligible initial degradation.

Visual experiments that currently are being performed address the impacts of sampling schemes and white Gaussian noise addition. Some problems that may arise during further developments of the experimental series are outlined here.

1. **Assembly Difficulties.** Current visual experiments analyze the impact of target degradations against a bland background, but future insertions into FLIR imagery will be required that were not necessarily recorded under identical conditions. Objectionable artifacts caused by mismatches are minimized if extreme close ups are assembled, then extensive size reduction is performed.

Synthetic Imagery Assembly. Figure 1 illustrates an unavoidable assembly difficulty that is absent in the synthetic imagery of CREATION, but present in the specialized application where FLIR images are assembled. The dashed arc depicts the boundary between a target of gray shade G_T and background of gray shade G_B . In digital simulations, boundary pixels are assigned the gray shade G_T and a weight, w , that is the fraction of the pixel area that belongs to the target. The computer generated targets and background clutter objects, shown on the bottom half of Simulation 2, were inserted in a preliminary background of gray shades zero to allow further scaling. Averaging is performed over non-zero gray shades and the pixels of gray shade zero are used to establish the new weights.

FLIR Image and/or Hybrid Assembly. The extractions of targets from FLIR images were performed by the Systems Analysis team. Boundary pixels had to be assigned either to the target or background; reconstruction would be prohibitively labor intensive. The heavy outline on Figure 1 depicts the approximation to the dashed arc. Pixels of weight that exceed 0.5 are assigned to the target, but their shade of gray have target and background contributions. The extracted targets are inserted into preliminary backgrounds of gray shade zero so that scaling can be performed by methods described in the previous paragraph, but the result is less precise because a contribution of the previous background has bled in.

In current visual experiments, targets are inserted into a bland background that has gray shade of target mean, but for later experiments, insertions into realistic backgrounds will be required. Merging will be performed according to weights, but the inherent imprecision of the extraction method can nevertheless cause objectionable halos. Two assembly method compromises are submitted:

a) Do not extract the precise target, but surround it with part of the previous background. The mismatch is shifted from the region of importance around the target circumference to some irregular shape that cannot be confused with a logical boundary.

b) Use weighted insertions similar to the CREATION method and minimize the error by a proper choice of background.

2. Non-White Noise Character. Figure 2 shows a typical noise spectrum and Simulations set 6 shows the impact of white and $1/f$ noise. There is an electronic filter that consists of a low frequency cut-off with 3 dB point of frequency f_C and a high frequency roll-off of 3 dB point f_R . At a knee frequency, f_K , white and $1/f$ noises have the same power.

Simulations 6 a,b demonstrate the C2NVEO serial scan calibrated FLIR where 32 detectors are time delay integrated (TDI); a digitized single frame is compared to frame averaging over 9 frames. Non-uniformities do not exist in serial scans, thus the streaks are caused by $1/f$ noise. This effect is apparent on the FLIR monitor, but was lost in the reproduction, thus instead digital simulation is shown.

Two distinct noise effects are present. White noise is applied to individual pixels; and $1/f$ noise, caused by infrequently occurring strong voltage spikes, is smeared over the entire picture, thus acting like a slowly varying non-uniformity that is reduced by frame averaging. A non-uniformity caused by different detector characteristics would become more, not less, apparent after frame averaging.

In the Static Performance Model¹⁰, the noise bandwidth, Δf_n , is calculated by combining the two contributions, although FLIR image 1a clearly shows the different noise characters. The problem is solved by the separation:

$$\Delta f_n = \Delta f_w + \Delta f_{(1/f)} \quad (1)$$

where Δf_w can be evaluated numerically, but

$$\Delta f_{(1/f)} = f_K \ln \{ f_R / f_c \} \quad (2)$$

is a rigorous closed form solution. An important difficulty found in the numerical solutions of the static performance model is the approach of 1/f noise to infinity when f approaches zero. The meaning of the physics involved is improved and computational methods are simplified by the individual treatment of the noise sources.

CREATION accepts the two noise sources as equivalent temperature differences that would causes the same voltage difference as standard deviations of the noises. White noise can be positive or negative and is applied to all individual pixels; 1/f noise consists of positive and definite strong voltage spikes that are smeared over entire lines by the detector motion.

The 256 shades of gray that can be displayed on the monitor are correlated to the scene maximum and minimum temperatures that are used to scale the noise standard deviations. Visual experiments then can establish their impact on performance.

B. Search Experiments.

This program is being promoted by Mr. W. Hollis, Deputy Undersecretary of the Army for Operations Research.

A cooperative effort is planned between the US Army Human Engineering Laboratory (HEL), the Institute for Defense Analysis (IDA) and C2NVEO for the investigation of search strategies. C2NVEO furnishes undegraded imagery with controlled clutter variation; IDA and HEL perform visual experiment and test metrics for clutter description.

Simulation set 1 shows the plan for the panoramic views in polar coordinates that was used to originate four landscapes that simulate different geographic locations. One of these was chosen to apply controlled increases in clutter. Simulation set 7 illustrates six of the fifteen clutter steps that were furnished to HEL. Similar controlled clutter increases also will be applied to the other landscapes shown on Simulation set 8.

The controlled clutter increase was performed in a single day because CREATION has very efficient scaling and distortion algorithms and performs automatic blending, as described in a 1988 SPIE presentation⁵. The telltale halo is absent because each tree pixel has its shade of gray and a weight $0 < w < 1$ that emerges from nonuniform scaling. The assembled image has pixel replacements where the fraction, w , is the insertion gray shade and the fraction $(1-w)$ is the gray shade of the background. All pixels where $w > 0.5$ receive the range integer of the insertion point; range integers where the weight of the insertion $w < 0.5$ remain unaltered.

C. Digital Simulations for ATR Tests.

Two important considerations that impact ATR performance will be outlined here.

1. Properties of the Digitized Focal Plane Image. The human observers view a display, but the ATR is furnished with a digitized image from the focal plane, after preamplification but prior to display degradations. Theoretically, a linear response from the detectors can be anticipated. Digitization that is finer than the noise standard deviation would be counterproductive, but if 12 bits/pixel (4096 distinct radiant power steps) are very useful for diurnal cycle analyses, although they cannot be expressed on single frames.

2. Artifacts of the Scanning System. A salient feature of CREATION is the capability to precisely simulate the properties of different scanning strategies and their impact on the imagery as seen on the different stages of the sensor¹.

Simulation set 9 illustrates artifacts caused by scanning strategies that the human observer can disregard, but might seriously hamper ATR performance. Unfortunately we were faced with making the choice between gross exaggerations that seem unnatural or simulation of effects that are clearly noticeable on the HP monitor, but lost in the reproduction.

a. The False Shadow is caused by a rotating mirror parallel scan system. Simulation 9a shows the impact of the spread function asymmetry with unidirectional scan that gives images

plasticity. The false shadow is advantageous to the human eye, but this is not necessarily true for the ATR.

b. The Zig-Zag is caused by a very scan efficient bidirectional scan. Scan efficiency is optimized by the bidirectional scan with mirror motion that causes alternate pixel strings to be read from left to right and right to left. Resolution is optimized with a fixed number of detectors on a parallel scan system when the image is formed by interlacing the pixel strings. This optimization neglects the asymmetry of the spread function that prevents perfect registration of the interlaced scan lines. Vertical boundaries appear to have sawtoothed characteristics. The ATR algorithms that compare straight and jagged edges will encounter problems due to these artifacts.

c. Recapitulation. The false shadow is helpful for human perception; the zig-zag is not significantly bothersome to humans, but was the cause for rejection of the bidirectional interlaced scan for ATR systems. Noninterlaced bidirectional scan might cause objectionable flicker and/or widening of the apparent spread function that adversely affects human perception. The ATR analyzed single frames, thus bidirectional noninterlaced scan appears as successive unidirectional scan in opposite directions.

Decisions on systems design must be based on a compromise between human and ATR requirements, where the difference between valid requests and "wishful thinking" by the ATR manufacturers must be recognized. Simulations performed with the specialized CREATION

routines that address artifacts not considered in Sensor Performance prediction programs facilitate these decisions. An example where CREATION simulations could have been helpful is the choice of an interlaced bidirectional scan for the common module FLIR based on a scan efficiency optimization. The systems analysis program does not consider the stabilization effect of rotating mirrors or the spread function asymmetry.

III. DIGITAL ELECTRONIC TERRAIN BOARD IMPLEMENTATION

The software will be ported from the HP 9000 to the Silicon Graphics workstation. In parallel, implementations on the C2NVEO Autospec super-minicomputer will be investigated. There will be no severe RAM limitations, therefore, methods are now feasible that were previously discarded. The individual parts in the CREATION will be reexamined.

A. Geometry.

1. **The Landscape.** The digital electronic terrain board must have the capability to process DMA data and accept correlations of feature and elevation maps performed by Faust at the Georgia Institute of Technology¹². For precise scenes, enhancements of the feature maps that give logical positions for natural objects will be performed in-house. For dynamic sequences, simplifications proposed by Boeing will be analyzed.

Cartesian and polar coordinate implementations. Intuitively, it may seem that the standard three-dimensional transformations of DMA data are less prone to distortions than the shifting

of the rings of equal viewer distance used in CREATION. In reality, bad distortions and objectionable artifacts can and do occur when limitations of the standard methods are misunderstood, and rigorous 3D polar coordinates will also be implemented.

Ms. Lori Scarlatos¹³ explained the correction of distortions of mountain crest lines caused by sampling instead of integration of input DMA data. A different correction is used in the high quality flight simulators by Evans and Sutherland. Under certain conditions the proposed polar coordinates are a prevention of distortions. (Prevention is preferable to correction.)

Each method has its advantages and disadvantages. For stationary observers, or observers with limited horizontal motion, prohibitively dense data sets would be required to approach the undistorted detailed foreground representation of CREATION. Cartesian coordinates should be chosen for flight simulators and/or the view from a moving vehicle.

Requiring artistic ability for users to generate realistic landscapes must be avoided. With the RAM and disk space available on the new system, this will be achieved by pre-storage of texture planes and/or the program steps that create them. In addition to fractals, the simpler texture merging used in the flight simulator, procured by the US Army Environmental Topographic Laboratory (ETL) from Boeing, will be investigated.

Standard b splines are part of the Silicon Graphics software. They will be compared to the distortion algorithms

created in-house that were used to achieve the variety of the shapes of natural objects demonstrated in this report. The versatility and automatization of the C2NVEO distortion algorithms was improved and only RAM limitations prevent current implementations. Examples are as follows.

a. Instead of range integers $0 < I_R < 256$, floating point ranges are planned. This improvement will allow us to show fine distance differences, within the structure of three dimensional trees, that are important for radar simulations.

b. The set of distortion parameters was increased.

c. In addition to shade of gray and range information, altitude and a material parameter will be stored for each pixel. This capability enhancement will allow fully automatic merging of many trees with placement and scaling governed by a random number generator. The range dictates scaling, occlusions, altitude, radiative temperature; and the material parameter defines whether the position is a logical insertion position.

2. Preparation for Insertions. Simple three dimensional transformations use the same preparations as for insertion of objects in the Cartesian and polar coordinate geometry. The important consideration is the quality of the computer generation of the objects that must be inserted.

a. Natural Objects. The trees, assembled from parts drawn with the digitizer pen, can be regarded as a construction

from deterministic fractals that are more human labor intensive, but less computationally intensive than the standard Mandelbrot or Carpenter fractals. It is a misconception that the latter require less artistic ability than the origination of the ones for CREATION because random number operators are used whose results then are evaluated by the user for their structural and artistic appropriateness.

Fractals are based on the shape repetition in nature that is very apparent, for instance, in the structure of a cauliflower, which is built out of progressively smaller dome shapes. Similarly, coast lines of Sweden's fjords, the little canyons that form the Grand Canyon, little falls on the sides of the Niagara Falls, or cloud formations show the fractal nature that is computationally expressed by breaking up shapes until the pixel structure is the limiting factor. They apply to some, but not all tree structures. Also the manner of breaking up of shapes and the scaling of the random numbers require considerable insight into the structure formations as well as artistic ability.

b. Targets. For Computer Aided Design (CAD), a Cartesian coordinate system with the origin inside the target is advantageous. Targets are built out of facets or primitive solids. Shading algorithms, which are readily available, apply to reflected, not emitted, radiation. The US Army Ballistic Research Laboratory (BRL), in cooperation with the University of Utah, has originated a very sophisticated geometric model. P. Dietz¹⁴ points out that an interface attempt with the PRISM signature prediction

model, originated by the Keweenaw Research Institute, is planned. In parallel, C2NVEO is investigating an interface between the SPACE model and BRL CAD that would not require some of the approximations necessary for the PRISM interface, but are detrimental to BRL CAD realism.

C2NVEO is aware of other agencies who have constructed images of vehicles using rigorous three-dimensional CAD software without shading algorithms. These might be readily interfaced with signature prediction models, but the images tend to be cartoon-like.

B. Modeling.

1. **Thermal Signatures.** An interface of BRL targets with the PRISM model, originated by the Keweenaw Research Center, is funded by the US Army Tank-Automotive Command (TACOM). This interface could be very cost effective because BRL already has invested many years into the construction of the geometry of many targets.

C2NVEO has procured the three-dimensional target signature prediction model from the Georgia Institute of Technology, called GTSIG¹⁵, that interfaces with their geometric model. It is less sophisticated than the BRL CAD geometry, but the interface is currently operational, not a future plan.

The SPACE model must also be implemented in parallel. It is simple and user friendly, and after some limited verifications it compared favorably with the more complicated signature predic-

tion models. It also uses primitive shapes not only facets thus might not require the facetization of BRL CAD. For radar models that would be detrimentally affected by false corners, facetized target files might be inappropriate. The interface of the original BRL CAD with SPACE model predictions might have the distinct advantage of unifying IR and radar synthetic imagery creation methods.

2. **Atmospheres.** A salient feature of LTR is its simplicity that allows transmission calculations to individual pixels because a specialized curve fit algorithm can be used to establish parameters for a range and altitude dependent simple equation.

$$\tau_{p,A} = \exp\left\{-\left(\bar{\sigma}\rho\right) / \left[1 + \left(b\bar{\sigma}\rho\right)^{\left(1-E_p\right)}\right]\right\} \quad (3)$$

ρ = number of attenuators in a slant path

$\bar{\sigma}$ = average attenuation cross section calculated from
HIGHTRAN or Frauenhofer lines

b, E_p are empirical outputs from the regression algorithm

This range, R, and altitude, A, dependent transmission expression is simple enough to allow calculations to individual pixels using:

$$P_{out}(I_x, I_y) = P_{AIR} + \tau_{p,A} \left\{ P_{in}(I_x, I_y) - P_{AIR} \right\} \quad (4)$$

Here, P_{out} and P_{in} are output and input radiant powers from the I_x, I_y location on the picture plane, P_{air} is the power emitted from the ensemble of air molecules on the path that the beam traverses.

The RAM limitations of the HP 9000 model 320C forced us to calculate the parameters of Equation (3) separately on either the IBM 4341 or IBM PC/AT. Moreover, transmission is only important when a long range approximation is justified.

$$\tau_R \approx \exp\{-(\sigma_N R)^{E_R}\} \text{ when } \sigma_N R \gg 1 \quad (5)$$

The approximation $\rho \propto R$ was made because RAM limitations forced us to neglect the altitude information. Using Equation (5) instead of Equation (3) cuts down the number of adjustable parameters from 3 to 2, but has the disadvantage that σ_N is empirical, but $\bar{\sigma}$ theoretical. Broad band transmission calculations that do not make the Beer's law approximation of exponential decay are made with only two input parameters that are easily ported to the HP. (The normalization of σ_N was achieved by including $b(E_p^{-1})$ and a conversion from ρ to R , in addition to the units conversion.)

With sufficient RAM at our disposal, the same specialized curve fit algorithms also can be applied to LOWTRAN 7 results. There are some theoretically advantageous properties to Equation (3) because $\bar{\sigma}$ is very well established, and temperature and pressure dependencies of b and E_p can be investigated.

3. **Sensors.** No drastic changes in the sensor model are anticipated. This module will be an ongoing evolution where properties of new sensors will be added.

A user-friendly interface that was developed for three different audiences is already operational on the HP 9000 and will be ported to the new facility.

a. The general users are able to access sample atmospheric and/or sensor degradation options via a code number.

b. The systems analysts are able to input the same systems parameters as for the Static Performance Model. In addition, they have the option to access the specialized routines that make CREATION unique.

c. Software developers will have the option to interface new CREATION processes in a modularized manner without corrupting the main CREATION architecture. This method already has been used by the CREATION developers for several projects, but to date it is not yet user friendly.

IV. CONCLUSIONS

CREATION has proven its usefulness for realistic digital simulations of unusual geometries that could not have been developed with readily available software. Its usefulness was demonstrated for realistic digital simulations where the observation point is either stationary or essentially moves vertically.

The polar coordinate geometry can be regarded as a "distortion prevention" on an area of importance where targets are neither trivially detectable nor too far away for acquisition. The presentations on corrections of distortions that were attended indicate the attractive features of prevention instead of correction.

Imagery for human observer performance tests was produced. CREATION's versatility in controlled clutter positioning and automatic scaling/distortions enabled the production of imagery for search strategy tests. Precise variations of sensor effects also helped evaluate the impact of sensor properties on human observer performance.

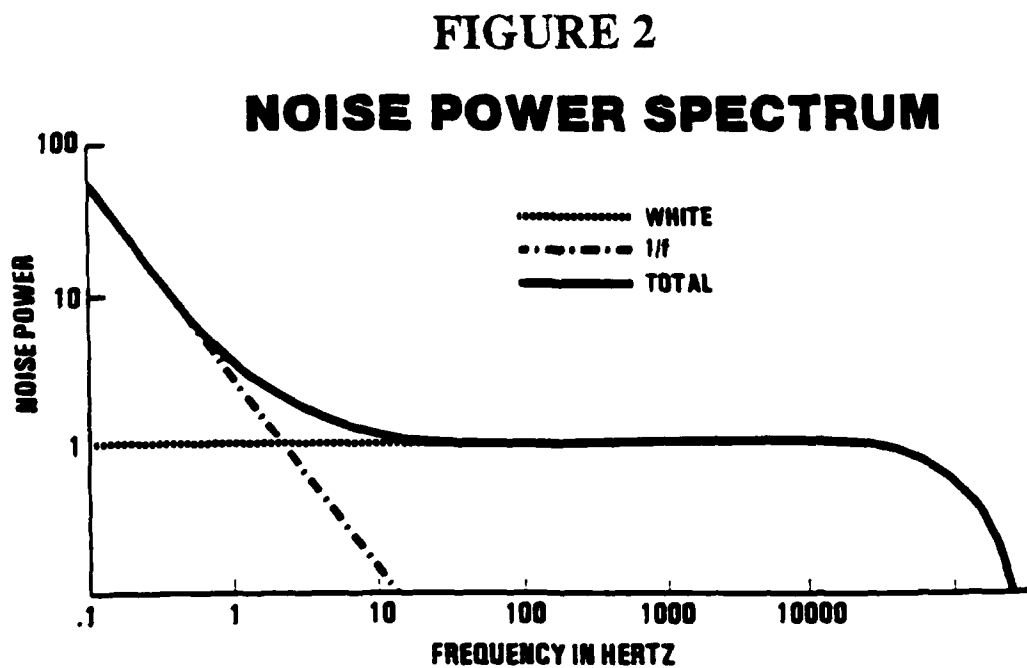
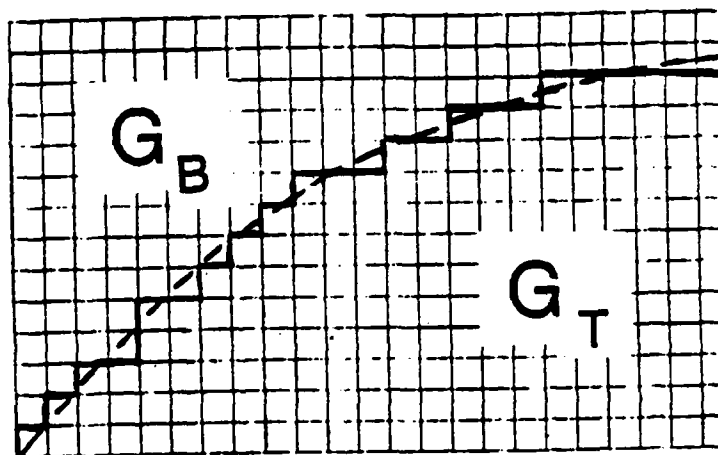
The important differences between human observers who view a display and the ATR that receives a digitized image from the focal plane of a sensor prior to display degradation were analyzed.

CREATION will become a vital part of the digital electronic terrain board, enabling us to push the capability of this state of the art facility to its productive limits. The advantages of the specialized methods discussed in this report, achievements of other government agencies and readily available visualization methods

will be combined. The 2 1/2-D geometry that currently is implemented on the HP is dictated by RAM limitations. Rigorous 3D algorithms that minimize distortions according to task dependent rules are already solved on paper. Hardware implementations will be used whenever possible to increase speed; but for specialized purposes, rigorous 3D algorithms that have advantages over the generally available facetized method will be implemented in software.

FIGURE 1

**UNAVOIDABLE BORDER
IMPRECISIONS OF EXTRACTIONS
FROM FLIR IMAGERY**



CAN 1/f NOISE BE TREATED LIKE A NON UNIFORMITY

SIMULATION 1

**AERIAL VIEW, WITH
POLAR COORDINATES PLAN**



SIMULATION 2

**PANORAMIC VIEW WITH
OBJECTS FOR INSERTIONS**

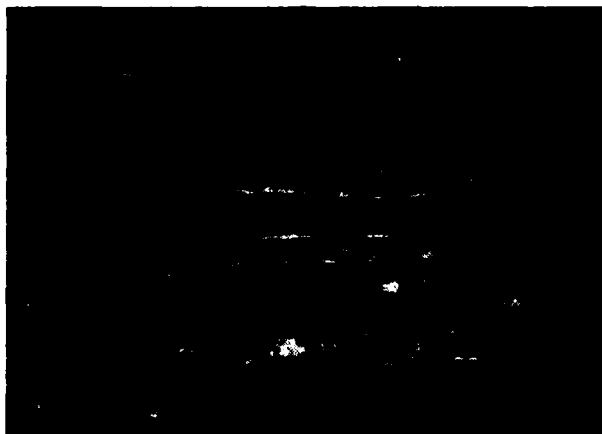


SIMULATION 3

HUNTER-LIGGETT DESERT AREA

SHADES OF GREY

a



RANGE INTEGERS

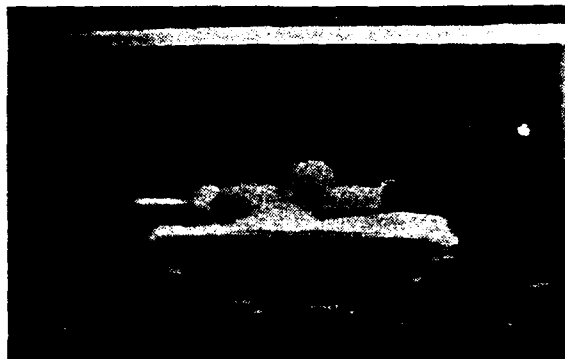
b



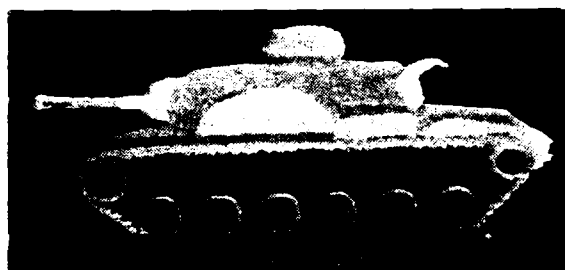
SIMULATION 4

SPACE MODEL VALIDATION

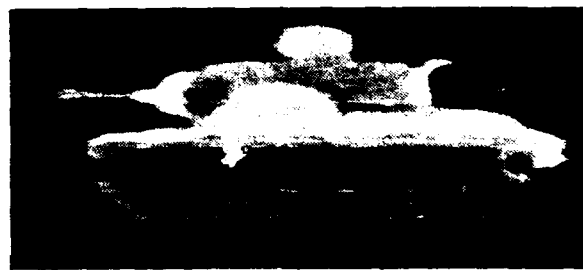
FLIR IMAGE



SYNTHETIC



UNDEGRADED



SENSOR DEGRADATION

SIMULATION 5

DIURNAL CYCLE

0700



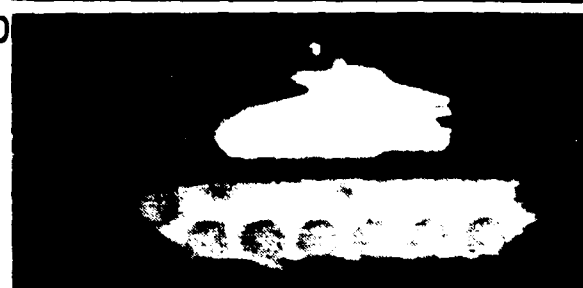
1200



1700



2200

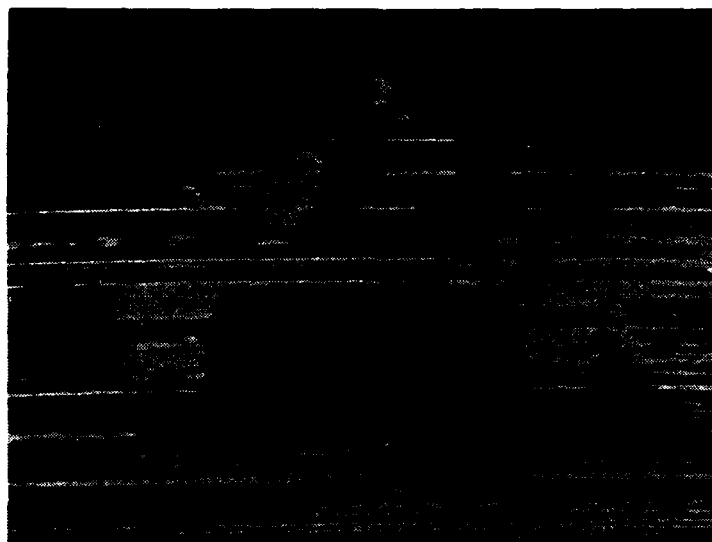


SIMULATION 6

CALIBRATED FLIR

WITH DIFFERENT FRAME INTEGRATIONS

a



SINGLE FRAME

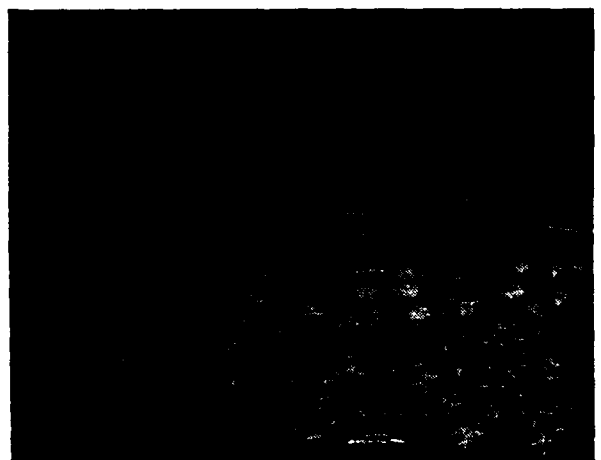
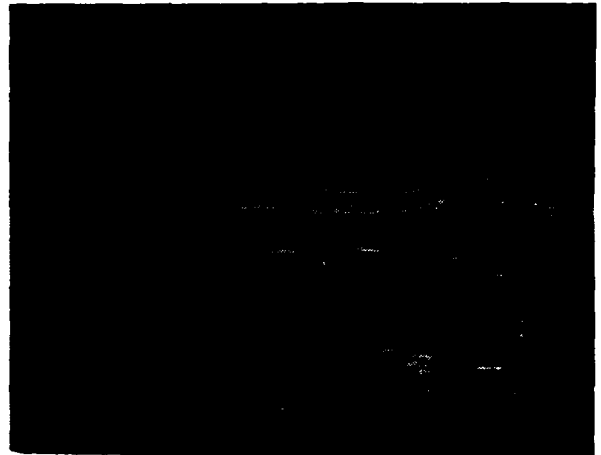
b



9 FRAMES

SIMULATION 7

CONTROLLED CLUTTER INCREASE



SIMULATION 8

DIFFERENT LANDSCAPES FOR SEARCH EXPERIMENT

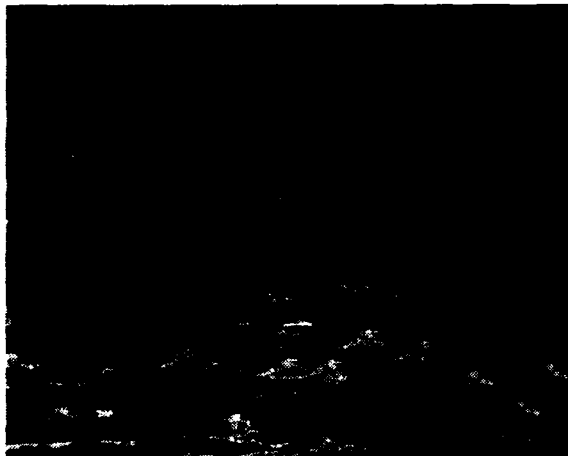
a



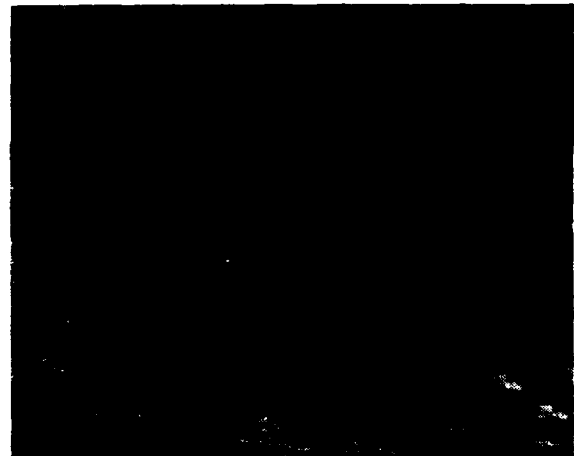
b



c



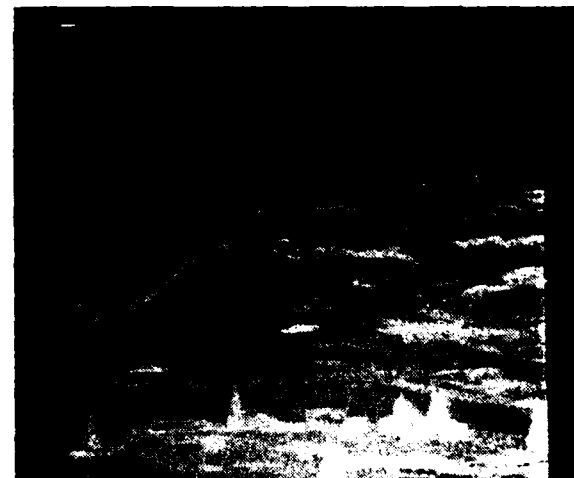
d



e



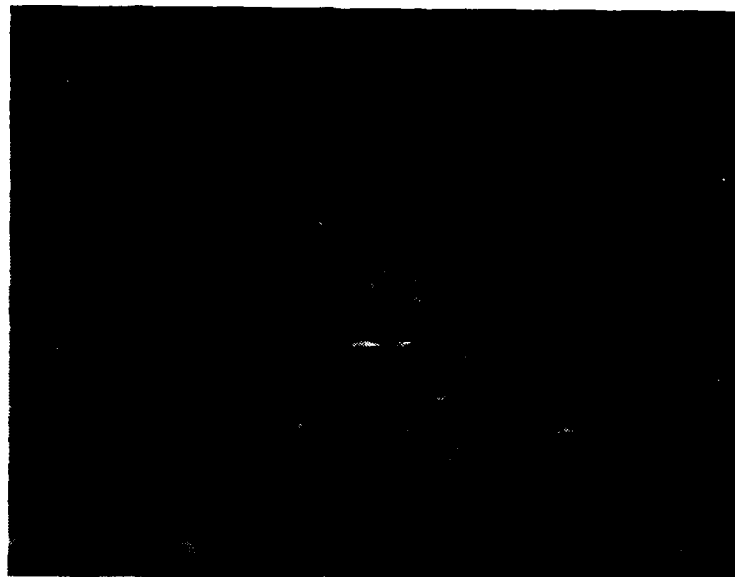
f



SIMULATION 9

ARTIFACTS CAUSED BY SCANNING

a



UNI-DIRECTIONAL SCAN

b



BI-DIRECTIONAL SCAN

V. REFERENCES

1. Kornfeld, G. H., Computer Generated Imagery for Model Testing, Proceedings of the SPIE Optical Science Conference, Orlando, FL, 1989.
2. Kornfeld, G. H., Computer Generation of Infrared Imagery, Applied Optics, Vol. 24, No. 24, pp. 4534-42, December 15, 1985.
3. Kornfeld, G.H., Synthetic Imagery Data Set for the PAIRSTECH Program, Proceedings of the Ninth Annual KRC Symposium on Ground Vehicles Infrared Signatures, Keweenaw Research Center, Michigan Technological University, Houghton, MI, 1987.
4. D'Agostino, J.A., The SPACE Thermal Model: Principles and Applications, Proceedings of the SPIE Optical Science Conference, Orlando, FL, 1987.
5. Kornfeld, G.H., Diurnal Cycle Digital Simulations Using the SIGTAD Model, Proceedings of the SPIE Optical Science Conference, Orlando, FL, 1988.
6. Kneizys, R. Z., Shteele, E. P., Gallery, W. O., Chetwynd, Jr., J.H., Abrem, L. W., Selby, J. E. A., Clough, S. A., Penn, R.W., Atmospheric Transmittance/Radiance: Computer Code LOWTRAN 7, Air Force Geophysics Laboratory Project 7670, Hanscom AFB, MA.
7. Kornfeld, G.H., Theoretical and Experimental Justification for a Simplified LOWTRAN 6 Equivalent Model, Proceedings of the Seventh EO-SAEL Meeting, December, 1986.
8. Fowler, R., Guggenheim, E. A., Statistical Thermodynamics, Cambridge University Press, 1960.
9. Zemansky, M.W., Heat and Thermodynamics, McGraw Hill Book Company, 1951.
10. Ratches, J. A., Lawson, W. R., Obert, L. P., Bergemann, R. J., Cassidy, T.W., Night Vision Laboratory Static Performance Model for Thermal Viewing Systems, Technical Report ECOM 7043, April, 1975.
11. Howe, J.D., Scott, L.B., Pletzt, P., Horger, J.D., Mark, J.S., Thermal Model Improvement Through Perception Tests, Proceedings of the IRIS Meeting, March, 1989.

12. Horst, M. M., N. L. Faust, and A. D. Sheffer, GTSPECS - Multi-spectral Sensor Simulation, Proceedings of Second National Symposium of Sensors and Sensor Fusion, Orlando, FL, 27-31 March, 1989.
13. Scarlatos, Lori L., Adaptive Terrain Models for Real-Time Simulation, Presented at the Digital/Electronic Terrain Board Symposium, Wichita, KS, 5-6 October, 1989.
14. Dietz, P.H., Item Level Weapons Modeling Predictive Signatures, Army Research Development & Acquisition Bulletin, July-August, 1989.
15. Johnson, K. R., and W. R. Owens, TCM2 - A New Medium Resolution Thermal Contrast Model, Report AFWAL-TR-87-105A, July, 1987.

Presented at the
DIGITAL/ELECTRONIC TERRAIN BOARD SYMPOSIUM
5-6 October 1989 GACIAC PR 89-07

COMPUTER IMAGE GENERATION OF IR SCENES AND SEQUENCES

David Englund
Alex Peck
Jay Mendelsohn

Grumman Corporation
Corporate Research Center

David Thomas
U.S.Army Tank and Automotive Command

ABSTRACT

This paper describes a method for the computer generation of visual and infrared scenes and sequences. The principal use of this program has been for Automatic Target Recognition and ground vehicle vulnerability studies carried out at the Grumman Corporate Research Center and at TACOM. The program is capable of generating realistic visual and infrared scenes and sequences based on a variety of sources including topographic maps, DMA maps, and photographs. In particular, we have developed an accurate computer model of the Keweenaw Research Center's standard scene for which extensive IR measured values are available. If specific real places are not desired then the user can create fictitious scenes using natural objects such as trees, roads, clouds and ground vehicles with relative ease. The program gives the user complete control of aspect, orientation, lighting and viewing input, and the trajectories of all moving objects in the scene and of the sensor viewing the scene. Environmental conditions such as rain, snow and fog are included as well as seasonal effects in both the IR and visual scenes. Effects of atmospheric transmission is also included using a late version of LOWTRAN. The program has great generality in that it considers both faceted and quadric objects as geometric primitives and therefore can use the available data bases of faceted targets as well as efficiently generate natural objects using quadric primitives. Targets are simply considered as objects in the scene and generated together with the background. This avoids the problem of matching targets to background in scale and intensity which arises when the target is "stuffed" into a computer generated scene. The IR model used is the Infrared Modeling and Analysis (IRMA) model developed for the USAF by Grumman.

The paper will discuss the continuing development of this program (under the partial sponsorship of TACOM), strengths and limitations, future development plans and applications of the program. Extensive examples of the programs capabilities will be given via videotapes.

INTRODUCTION

The use of synthetic imagery is finding a widening acceptance as a tool for analysis in many tactical systems studies. Automatic Target Recognition, signature identification and the inverse problem of signature suppression, tactical decision aids, and the design of new concept vehicles are all areas where synthetic imagery can be used to an advantage.

For the past several years, the Grumman Corporate Research Center has been engaged in a research program to develop computer software which will produce scenes and sequences of tactical imagery which are both visually and numerically correct. Our initial efforts in the area of Computer Image Generation (CIG) were concerned with modeling natural phenomena such as trees and clouds in a computationally efficient and visually realistic manner. This was achieved by using quadrics as the basic modeling primitives (Ref. 1). However, as the use of synthetic imagery grew in the military community, it became obvious that polygons (faceted models) were the favored primitives especially with respect to the modelling of targets. In order to make the growing data base of targets available to us, we included the possibility of mixing both polygons and quadrics. This further gave us the ability to match shapes of terrain objects which was somewhat difficult to do with quadrics alone. Geometrically, the program now contains both polygons and quadric primitives and each is used to the best possible advantage in the generation of an arbitrary scene.

Our initial concentration on visual scenes has now shifted to infrared. In conjunction with the Keweenaw Research Center (KRC), we initially constructed a visual model of Standard Scene # 1 in Houghton. Then, using measured data collected at Standard Scene #1 by KRC, we "painted" the visual scene with the measured data. Each object in the scene was given gray level so that the mean and standard deviation of the gray levels over that object was in agreement with the mean and standard deviation of KRC's measurements. Using this procedure, a sequence of visual and IR scenes was constructed showing a generic tank moving across the Houghton scene (Ref. 2). The sequence of viewpoints was representative of the views which might be obtained from a missile seeker while the target was under attack. This effort demonstrated the general usefulness of the synthetic imagery and specifically how it might be applied in a target recognition problem.

While using measured data certainly gives authenticity to the IR scene generation program, it also severely limits its applicability since it only applies to those cases in which the measurements are available. In order to gain the full benefits of using synthetic imagery, among them the possibility of examining scenes under arbitrary environmental conditions, a phenomenology modeling approach seemed necessary. Consistent with this goal, we added an IR modeling capability to the program. The model we chose was one developed by Grumman for the Air Force. The Infrared Modelling and Analysis program (IRMA) is a theoretical model which uses empirically extracted thermodynamic properties for prediction of both terrain and target radiances as a function of weather, time and atmosphere and allows for the generation of IR sequences under a wide number of input conditions. We also included in the program the latest version of LOWTRAN to account for the effects of atmospheric transmittance. We then used the updated program to produce a IR sequence similar to the one described above as well as many single IR scenes which showed the effects of weather conditions, time of day and a variety of other environmental conditions (Ref. 3).

We have continued to gain experience in the use and usefulness of the synthetic scene generator program and this paper includes our most recent improvements and thoughts about the directions which we intend to take in the future. Some of this thinking is influenced by the fact that under the sponsorship of TACOM we have delivered a version of the program for use on their recently acquired CRAY. Much of our thinking about ways in which the program can be improved and new features to be included in updates to the program is and will be influenced by the experience of the TACOM users. Thus, we are moving the program from what had been a research tool to what will be a user tool.

The topics relative to new features and new directions which are discussed in detail in the body of this paper are:

We are interested in extending the scene generation capability from a specific location (Houghton) to arbitrary location and therefore have been included the capability to generate terrain data from DMA data and from topographic maps. The latter appears to have greater applicability to tactical image generation

We have developed a terrain following technique so that ground vehicles following specific trajectories in the scene will follow the terrain profiles along those trajectories.

Because of the widespread use of the PRISM model in the user community and because of certain limitations of the IRMA model, we have begun discussions with KRC on including PRISM as an option for generating the IR radiances for the scenes. We are also considering including the updated version of the IRMA model now under development at Eglin Air Force Base.

Development of a user interface which will allow inexperienced users to develop scenes and sequences in which various objects (terrain and natural features as well as targets), their locations and motion, and the associated viewing parameters can be arrived at by the viewer in a "natural way", is receiving a great deal of emphasis. This interface is the most significant step in increasing the value of the program to the users.

Terrain Modeling

Previously, quadric surfaces were the main modeling primitive in the CIG program. These surfaces provide great flexibility in the modeling of natural objects such as trees and clouds which have some inherent 'fuzziness' to their structure. They are not, however, as well suited for accurate modeling of well-defined objects. Representing specific terrain features such as a hill with a second order surface presents some problems. Given measured elevation data, one must calculate some sort of 'best fit' of a quadric surface to that data. On some global scale, this approach may be acceptable, but locally the real world irregularities of the terrain are lost in the smoothness of the approximating quadric. Some of these irregularities may be of importance in that they are identifiable features for that specific terrain.

With the use of polygonal modeling primitives, terrain can be modeled to the accuracy of the measured elevation data. Any irregularities present in the data will be present in the model. The resolution of the measured data thus becomes a factor in the accurate modelling of specific geographic regions. Fig. 1 shows an image that was modeled from DMA elevation data at 30 meter postings. The grid of DMA elevations was triangularized to obtain a polygonal model that could be viewed in three dimensions. While this figure shows the global irregularities of the region, any features that have dimensions of less than 30 meters may fall in the gaps of the measured data and will not appear in the model.

In order to model local features, it is necessary to obtain elevation data at a resolution in accordance with the features of interest. Topographic maps can provide this data, such as the one in Fig. 2 showing a region in Houghton, Michigan. Fig. 3 shows that same region where elevation increases as the image goes from black to white. Fig. 4 depicts a three dimensional view of the polygonal model of the hill in the region. This model was obtained by digitizing the contour lines from the topographic map and then fitting triangular polygons to those contours. The topographic maps used to model this area also contained information about tree

lines, individual shrubs, fences, and roads. After separately modeling these types of objects, the map can be used to position them accurately with respect to the polygonal terrain model. The inclusion of these types of objects greatly adds to the realism and 'recognizability' of specific locations.

Terrain Following

Terrain following allows an animator to describe a dynamic object's position and orientation over a terrain surface by simply entering the 2-D path the object should follow.

An object's position and orientation in the 3 dimensional database is described by 6 parameters; X,Y,Z,ROLL,PITCH,YAW. These parameters must be specified for each frame in which a dynamic object is present. If an animator is interested in sending an earth-bound vehicle (car,truck,tank,etc.) over a three dimensional object, terrain following calculates these parameters for each frame using only the vehicle's trajectory start and end points and velocity.

To produce a terrain following movie, one must have an object to move, a path for the object to follow, and, of course, terrain. Terrain data is acquired in a variety of ways. It can be hand digitized from an elevation map (see Fig. 2), taken directly from Defense Mapping Agency (DMA) data, or created with an object generation program. Any object compatible with the renderer can be sent over this terrain. All that is needed is a text file defining the path the object should take. Currently, this file consists of a starting position (X, Y) and a number of positions toward which the object should move, along with the velocity it should travel (X, Y, VELOCITY).

Once the terrain follower has the required information, it looks at the first trajectory and calculates the number of frames it must produce, as well as the X and Y deviations (DELTA X, DELTA Y) for each frame. Additionally, YAW is computed at this time. For each frame above, the terrain follower then searches the terrain database to find the terrain triangle beneath the moving objects center of gravity. The object's elevation, roll, and pitch are then calculated from the three dimensional coordinates of the triangles vertices. Time spent searching the terrain database is reduced by keeping track of both the current terrain triangle and a list of it's neighbors. If the new object position is not encompassed by the current terrain triangle, the neighbors list is examined. If the correct triangle is not found, a new neighbors list is constructed by rapidly searching the terrain database. This process is repeated for each path data point.

New Versions

The current program runs in the Grumman Corporate Research Center on a Data General MV10000 under AOS/VS and a CRAY XMP under COS. It has also been transported to TACOM to run on a CRAY 2 under UNICOS and on an IRIS 4D under UNIX.. TACOM has also run a VAX version under VMS. This version, while not as fast as any of the above, will make the program available to a much larger group of users.

For the most part, the FORTRAN 77 source code is easily transportable from machine to machine. I/O and file handling are the major areas of trouble. There were a few problems in this area in that the format used at Grumman for storing image data was not the same as that used by TACOM. The user now has access to generic file handling routines that when linked with the program allow a user to define his own format for image storage.

"Old" code such as IRMA and LOWTRAN written in FORTRAN IV are not guaranteed to move as easily between machines. While no problems have yet been encountered with the IRMA code, LOWTRAN uses some constants that are too large for the VAX to handle. For this reason, the VAX version at this point does not include LOWTRAN for atmospheric effects. Future concentration will be on the "workstation" versions possibly including a MAC II with Transputers which will allow parallelism and therefore significant running time reduction.

User Interface

The synthetic scenes which we consider generating are complex with respect to the number and kinds of objects that make up the scene. In order to use the generated scenes for analyzing the adequacy of a target detection algorithm or to measure the IR characteristics of a concept vehicle, the scene model must include vehicles and backgrounds which are realistic in terms of clutter, and features both natural and man-made. Various objects within the scene must be made to move in a realistic manner if complete sequences are to be examined. The first component of the user interface is a tool that will facilitate the creation of such scenes, producing the databases required by the program to calculate three dimensional views. The second component of the interface will help the user specify object motions throughout a sequence as well as the motion of the hypothetical lens through which the entire sequence is to be viewed.

Scene building is the term we use for the first component of the user interface. In order for a user to readily put together a scene, various tools must be available that will simplify the process. These tools are being designed with some sort of graphics capabilities to enable the user to visualize various aspects of the scene as it is developed.

The first part of building a scene would be to describe the terrain. It is necessary that this happen first so that objects, such as trees, defined later on can be positioned on the terrain (at the correct elevation). The terrain could be described in several forms. Files containing regular (gridwork) elevation maps could be referenced directly whether from DMA data or user supplied. A more powerful tool for creating terrain models would be to input topographic contour lines from which the interface could generate a polygonal description.

After describing the terrain, the user would specify the remaining contents of the scene. In addition to allowing the user (if they so desire) to specify the exact parameters of the low-level polygon and quadric modeling primitives, generic objects are being defined that will enable the user to specify at a high level the components of his scene. These generic objects will have various parameters that the user can modify to obtain the actual object(s) he desires.

An example of this type of generic object might be a tree line. Rather than having the user locate each individual tree, he can input parameters that would shape a generic tree line to the scene he is modeling. Some parameters that may be used would be the coordinates of the tree line as well as the average tree size,

shape, and color. These parameters, when combined with randomizing factors, would produce a tree line along the user specified path.

One more example of a generic object may be a road. The parameters involved here would be a description of the centerline of the road and an associated width. Other possible generic objects may be clouds, lakes, rivers, and individual trees and shrubs.

Animation of the objects and eyepoint to produce a sequence of images is the second component of the user interface. In the case where the motions are predefined by some real world event, the user will simply need to put the motions in the format required by the CIG program. An example of this would be the simulation of a sensor mounted on some dynamic platform such as a missile or an aircraft throughout some predefined flight. The dynamics of the platform will provide the appropriate eyepoints for the generation of the sequence. When the user has to specify the trajectories of objects and eyepoints, once again some tools are required.

The most straightforward of the trajectory types that the user will have to define is that of a vehicle whose motion is constrained to follow the terrain. In this case the user must provide a description of the trajectory for only two spatial dimensions. This can be accomplished using key points and interpolating splines and can be readily visualized in a two dimensional plot of the region of interest.

For objects whose motions are not constrained to follow terrain, the elevation of the object over the terrain must also be specified. While splines in three dimensions can be used to solve this problem, it is difficult to provide the user with any quick three dimensional visual feedback. The use of an additional 2-D plot of elevation versus the 2-D spline parameter could be used efficiently to display the 3-D trajectory to the user.

While the ideal interface for animating sequence would make use of real time frame generation, we must do the best we can given the limitations of hardware and software. Trajectories defined by the user can be tested by low resolution sequences (both spatially and temporally) where each frame contains enough content to check the validity of the defined motion. When a low resolution test of a sequence has shown the motion to be what the user wants, a final high resolution version of the sequence can be generated.

User Defined Textures

Within the SSG program, objects are textured according to texture models. In the generation of visual images, these texture models are used to vary the intensity of color across an object's surface. For IR imagery, the texture models are actually used to distinguish between different IR object classes (trees, road, grass, etc.). A texture model is the instantiation of a texture type or texture function with some set of parameters. Several texture models based upon the same texture type/function can be defined at the same time.

A texture type is the algorithmic means by which an object in the scene is textured. This is usually a mathematical function of scene coordinates that returns a value used to texture (i.e. modulate intensity) of some object. There are currently three predefined texture types which the user has available. Two of these are based on summations of sines used for the texturing of natural objects like trees and ground, while the third type varies intensity with elevation for use in generating relief map images of terrain. User defined texture types are now supported by the SSG program. By following a simple interface for the passing of parameters, the user can provide code for the definition of any texture types they may have developed.

Another extension of the SSG program in order to provide the user with a more flexible tool is the concept of texture functions. Like a texture type, a texture function is a function of scene coordinates. Rather than returning a value to be

used directly in applying texture, a texture function returns a number that identifies a texture model. The texture model referenced by this number is then used to texture the object. User defined texture types and functions can be instantiated as models in the same way as the predefined types. An example will help explain the differences between texture types, models, and functions.

Suppose we have a texture type that generates a regular pattern of circles. The parameters to this texture type might specify the radius of circle used and the pattern spacing. Two distinct texture models can be defined as instantiations of this texture type. Figures 1 & 2 shows the patterns generated using these models. A texture function can then be written that is based upon a checkerboard tiling. This function will return a one or a two depending upon the location within the checkerboard. A third texture model (Fig. 3) can be defined based upon this texture function by supplying specific parameters for the checkerboard tile size. When this model is referenced to texture the ground at some (X,Y,Z) coordinate, the SSG program recognizes it to be based on a texture function. The result of that texture function is either a one or a two. The SSG program uses texture model 1 or 2 accordingly to apply the correct circular pattern at the original (X,Y,Z) position. Figure 4 shows the resulting pattern generated upon the ground. Figures 5 and 6 illustrate the use of these capabilities using more realistic textures.

It should be noted that a model number returned by a texture function could reference yet another texture function and so on. This allows the ambitious user to generate extremely complex textures.

PROGRAM REVISIONS

Over the past year, some attention has been given to the improvement of the scene and sequence generator's imaging capabilities. Previously, antialiasing (the removal of sampling error artifacts) was done as a post process to the calculation of the visible image. However, in the generation of IR imagery, aliasing artifacts were reintroduced. The conversion from visual to IR required taking statistics over image segments and then modulating those segments to match the predicted statistics. The segments here represented object classes of different IR characteristics. Since each pixel in the image could belong to only a single segment, this segmentation process introduced further spatial aliasing. Furthermore, since the modulation from visual to IR was based upon statistics gathered on a scene by scene basis, temporal aliasing could occur during animations.

The current approach to antialiasing is to allow pixels to contain information from more than one object. The partial contribution of an object to a pixel is represented as a pixel fragment with attributes such as color, fragment area, and opacity. When all the fragments for a pixel have been determined, they can be blended together to produce a final pixel color. This method produces visual images that are correctly antialiased.

The aliasing within the IR imagery (both spatial and temporal) was a result of the post processing which assigned each pixel in the image to a segment in order to obtain statistical information for the object class represented by that segment. This aliasing can be avoided if the statistics for that segment within the visual image are known a priori. The modulation from visual to IR can then be done at a pixel fragment level and the blending of those fragments will produce antialiased IR imagery. Since the intensity variation within an object class is due only to the texturing applied by the SSG program, knowing the statistical nature of each texture model is sufficient. Thus the current SSG program requires that the mean and standard deviation of each texture model be specified along with the usual parameters. This method eliminates the need to calculate the object class statistics

as a post process thus saving the SSG program some computational overhead in the generation of IR imagery.

Data Generation

We have invested a portion of our time in extending the Houghton scene in various ways. Most of the geometric modelling was done on a Symbolics 3675 using a software package called SGeometry™. This program enabled us to extend the terrain database to encompass a wider area. We were then able to model additional objects for placement within this area. We designed some components for an airport consisting of a tower, runway, hangars, buildings, and a light plane. A car and bridge were also modeled for inclusion in the scene. Eventually, scenes containing objects such as these can be useful in high value target recognition studies. Figure 7 shows a view of the plane while figure 8 displays the bridge. After these objects were constructed on the Symbolics, the associated data files were passed to our host Data General MV10000 system where they were reformatted for use by the SSG program. It should be stressed that this modeling is geometrical only. It is our intention to model these objects for IR simulation in the near future. The capability to quickly model geometric objects has played an important part in our extension of the Houghton scene.

We have also developed a program that allows a user to generate and examine positional data that may be required by the SSG program. This program runs on the MV10000 using a Gould IP8500 for image and graphics display. After displaying a map of the terrain as an image on the Gould and identifying the mapping from image to world coordinates, the user can employ graphic overlays to interactively define various types of positional data.

The first of these data types is called a region. When a user is given a terrain database, there may be some sort of accompanying feature database. Features that may be indicated are forest, swamp, field, pond, etc. Working with this feature information, the user can define polygonal boundaries for regions representing specific features. The polygonal boundaries of these regions can be output in world coordinates for use later with a separate program that will split the original terrain database into separate pieces, each representing a single region. These separate pieces can then be textured and colored appropriately for the feature represented. For features like forests however, the user isn't concerned about the region as a solid area. It is possible instead to have the program attempt to fill the region to a specified density with randomly positioned discs of a user supplied radius. The positions of these discs can then be output for use in placing trees upon the terrain.

The other type of positional data generated by the program is used to describe two dimensional trajectories. The user first specifies control points to define a cubic interpolating spline. These control points can then be edited (moved, deleted, etc.) to obtain the desired trajectory over the terrain map. Associated with each control point are parameters to provide local control of the tension, continuity, and bias of the spline (Ref. 5). When the user is satisfied with the defined trajectory, the (X,Z) positions (Y is elevation in the SSG system) along the spline can be output. These positions can then be used to define trajectories for animation of objects or eyepoints within a sequence.

Terrain-Object Handling

Given the position data as generated by the program discussed above, the user might want to place a tree at all the positions that filled a region, or calculate the location and orientation of a vehicle as it moved along some trajectory.

Originally there existed a program for each of these tasks, one to place trees and one to determine vehicle motion. Rather than stamping out carbon copies of some predefined tree, the tree placing program had some randomness for parameters such as height, width, and color. This produced a forest of trees distributed around some generic tree model. This approach works well until one wishes to place something other than trees on the terrain. Making a copy of the code and patching it to produce the new object didn't seem to be a very practical solution since that leads to N programs to place N different objects on terrain where the bulk of those programs is identical.

Our solution was to develop a single program that placed objects on terrain using user defined object templates. The program takes as input a polygonal terrain, a list of positions, and an object template. For each (X,Z) position it calculates Y, the elevation of the terrain as well as the attitude of the underlying polygon at that point. These values are used to generate an instance of the object template at the current position. Early on in the development of this program it was seen that the user would need access from within an object template to some of the variables calculated internally by the program. At the very least, the user would need to refer to the (X,Y,Z) position. Elementary arithmetic capabilities as well as some means of specifying randomness were also needed. These concerns indicated that a parser should be written in order to interpret the object template. During the output phase of the program, the parser would substitute values of the program's internal variables for symbols within the object template and perform any arithmetic necessary.

Once it was determined that a full-fledged parser needed to be written, we were able to provide the user with capabilities above and beyond the ones mentioned above. All of the standard arithmetic operations are supported (*,*,/,+,-). Parentheses can be used to change the order of operations within an expression. The user now has access to the random functions N(x₁,x₂) and U(min,max) for generating normal and uniform distributed values. Intrinsic functions such as MIN, MAX and ABS also exist. Along with the set of predefined symbols (X,Y,Z,ROLL,PITCH,YAW,etc.) that define the state of the terrain at the current position, the user can also define his own symbols. As the program and parser were used, it became apparent that file access and conditional output would be useful. The parser was then extended to include basic file handling routines and an IF-THEN-ELSE capability.

An example object template for the definition of a tree is shown in Fig 9. It can be used to generate quadric objects to represent trees whose color is normally distributed about the RGB value (50,180,90). The radii of the quadrics are also normally distributed. The Y radius is assigned to the symbol HT for later use in positioning the center of the quadrics above the terrain. This example demonstrates the initial use of templates to produce a data file containing quadric descriptions representing trees placed on terrain. We have also used this template approach to produce data files describing the motion of a vehicle as it follows a trajectory across the terrain as well as eyepoint motions along another trajectory while tracking that vehicle. Thus the simple object placing program has developed into a powerful tool for handling terrain and objects.

```

Comment: RGB color
N(50,5)  N(180,15)  N(90,7)
Comment: Quadric Radii
N(8,1)  HT=N(60,5)  N(8,1)
Comment: Position of center of quadric
X  Y+U(0,0.3)*HT  Z

```

Conclusions

We have discussed and demonstrated some of the newly developed capabilities of the Grumman visual and IR scene generation program. We believe that these changes, some of which have already been made and some of which are anticipated, will make our program a more useful tool in the analysis of many tactical situations. Further, we hope that some of these changes will eventually make the program available to a larger number of users and that their experiences will in turn feedback to us in a way that will cause the program to be improved and made more useful.

Acknowledgements

The authors would like to acknowledge the sponsorship of TACOM over the past years. It has provided some of the resources necessary to carry out the work described here. We are especially grateful to Grant Gerhart and to Dave Thomas who provided valuable "user" feedback to us. Terry Gonda and Gary Martin also were helpful in providing suggestions and insights. We would also like to thank Bill Reynolds of KRC for his constant support of this effort.

REFERENCES

1. Kim, J. et al, "Computer Image Generation of IR Scenes and Sequences, Part I," *Proceedings of the Eighth Annual Symposium on Ground Vehicle Signatures*, August 1986.
2. Gearhart, J. et al, "Computer Image Generation of IR Scenes and Sequences, Part II," *Proceedings of the Ninth Annual Symposium on Ground Vehicle Signatures*, August 1987.
3. Englund, D. et al, "Computer Image Generation of IR Scenes and Sequences, Part III," *Proceedings of the Tenth Annual Symposium on Ground Vehicle Signatures*, August 1988.
4. Gardner, G., "Simulation of Natural Scenes Using Textured Quadric Surfaces," *Siggraph '84 Conference Proceedings*, July 1984.
5. Kochanek, D., and Bartels, R. "Interpolating Splines with Local Tension, Continuity, and Bias Control," *Siggraph '84 Conference Proceedings*, July 1984.

THIS PAGE INTENTIONALLY BLANK

U.S. Army Tank-Automotive Command (TACOM)
Thermal Image Model (TTIM)

Timothy J. Rogne
Frederick G. Smith
OptiMetrics, Inc.
2008 Hogback Road, Suite 6
Ann Arbor, Michigan 48105

Grant R. Gerhart
David J. Thomas
U.S. Army Tank-Automotive Command
Attn: AMSTA-RSA
Warren, Michigan 48397-5000

ABSTRACT

The TACOM Thermal Image Model (TTIM) is an interactive computer code which simulates the performance of IR imaging sensors operating in realistic battlefield environments. Its ability to produce simulated imagery has proven useful in applications including sensor and tracking algorithm simulations, obscurant model development, and vehicle design evaluations.

This paper reviews the development and current functionality of TTIM, concentrating on descriptions of the most recent distribution version (3.0) and two new modules which treat staring Focal Plane Array (FPA) and Image Intensifier sensors, respectively.

1.0 INTRODUCTION AND BACKGROUND

The TACOM Thermal Image Model (TTIM) development was initiated to address the problem of evaluating the infrared signature vulnerability (probability of detection) for individual concept vehicle designs. Standard analytic methods¹ evaluate target probability of detection on the basis of average signature and target size. While this approach provides a very convenient way to translate imaging sensor capabilities into detection range performance measures, it provides no sensitivity to specific vehicle shapes and signature patterns which may form cue features increasing the probability of detection and recognition.

The TTIM approach to the problem is to start with target imagery, impose natural and battlefield atmospheric effects, treat the degradation caused by thermal imaging sensors, and provide imagery for evaluation by techniques including

1. J.A. Ratches et al., Night Vision Laboratory Static Performance Model for Thermal Viewing Systems, ECOM-7043, U.S. Army Night Vision and Electro-Optics Laboratory, April 1975.

human interpretation, statistical analysis, and tracking algorithms. In this way, all of the target infrared signature characteristics important for any particular application are inherently considered.

Development of TTIM was started in 1984; a version including the LOWTRAN6 natural atmospheric model, the AMGREN/ACT II smoke model, and a scanning array IR sensor model was delivered to TACOM late that year. By 1987, the model had matured considerably and it was decided that TTIM might be of interest to the modeling community at large. In October 1987, the first TACOM Thermal Image Model users meeting was held to release version 2.3 of the model to the DoD community. In April 1988, a second meeting was held to release the model contractors. Version 3.0 was released to users in March 1989. As of this writing there are 28 registered TTIM users.

There are a number of references (including^{2,3,4,5}) which describe prior TTIM developments. The reader is encouraged to refer to those for details concerning the basic modeling techniques. Our goals in this paper are to describe the modeling philosophy behind the latest TTIM release (version 3.0), present two new sensor models which are undergoing validation and preparation for release later this year, and provide an example illustrating simulation experiments encouraged by the TTIM approach.

2.0 TTIM VERSION 3.0

The structure of the latest TTIM version is depicted in Figure 1. The capabilities emphasized in the current release include a more generalized vertical structure, more formalized definitions of module interfaces for improved horizontal

2. B.K. Matise et al., "Simulating the Performance of Imaging Sensors for Use in Realistic Tactical Environments", Proc. SPIE, Vol. 550, Sensor Design Using Computer Tools II, April 1985.
3. B.K. Matise et al., "TACOM Imaging Sensor Simulation Model for Vehicle Signature Vulnerability Evaluation", Proc. of the Sixth Annual KRC Symposium on Ground Vehicle Signatures, August 1984.
4. T.J. Rogne et al., Development of an Imaging Sensor Simulation Model, OMI-118(I), OptiMetrics, Inc., November 1984.
5. C.S. Hall et al., TACOM Thermal Image Model Technical Reference and User's Guide, OMI-183, OptiMetrics, Inc., December 1986.

interchangeability, and the definition of a core set of parameters which allow modules to more easily share a common situation reference.

The vertical structure divides the model into eight functional areas representing the components of most engagement modeling problems. Summarizing each area, target and sensor geometries are defined by a scenario. The engagement takes place in the context of a scene representing the appropriate target and background signatures viewed from the proper sensor perspective. Natural and battlefield effects modify how the scene appears to the sensor. The sensor measures apparent scene properties limited by its design capabilities. The sensor output may be processed before it is displayed or acted upon. Finally, the auto-sequence function is a generic name for the functions required when a simulation is dynamic. For example, in a missile tracker simulation, the auto-sequence function could include a flight dynamics model allowing closed-loop flight simulations.

The full benefit of a general vertical structure is not achieved without a modular approach to implementing each function. The advantages include a common structure that can be applied to most engagement problems, only requiring changes in modules specific to the application. Through consistent application, a library of modules is envisioned that can be mixed and matched to meet specific needs. The two smoke modules are a relevant example. The AMGREN/ACT II model treats aspects of the smoke transport and radiative transfer problems in fine detail at great computational expense; it is general enough to undertake completely arbitrary smoke system design. In some applications, the detail was not needed or desired; a fast running but accurate model capable of representing typical inventory smoke systems was required. This resulted in the development of a version of EO-SAEL COMBIC⁶ as a TTIM module. Now, both modules are available to support future applications at the discretion of the analyst.

6. D.W. Hoock et al., Combined Obscuration Model for Battlefield-Induced Contaminants COMBIC, TR-0221-11, U.S. Army Laboratory Command Atmospheric Sciences Laboratory, October 1987.

Modularity also protects the future utility of the code. The state-of-the-art in several simulation functional areas such as scene modeling is constantly changing. It is intended that TTIM provide a framework to combine the best and most appropriate functional models at any given time to form a complete through-the-sensor simulation package.

The final major refinement in version 3.0 is the concept of core simulation variables. There is an obvious need in simulation to make sure that all models are working from common assumptions. For example, the weather conditions used by one model to predict signatures ought to match the conditions used to predict smoke transport and atmospheric transmittance. To date, this has been the responsibility of the analyst. Now, there is a mechanism to ensure this automatically.

TTIM version 3.0 was distributed to users during March 1989. It should be mentioned that version 3.0 has removed all known extensions to FORTRAN 77 used in prior versions. Along with a new, flexible display driver, this will facilitate transport of the code to workstation environments. The image intensifier and FPA sensor models discussed in the next sections are planned for release later this year.

3.0 IMAGE INTENSIFIER MODEL

Although TTIM was originally developed for use in the infrared spectral region, the atmospheric models retain their capability to operate in the visible and near-IR bands. In 1987, the development of an image intensifier sensor model was initiated by TACOM resulting in a stand-alone model⁷. With the completion of TTIM version 3.0, the image intensifier model is currently being validated and prepared as a module for release to users later this year.

The structure of the image intensifier model is shown as Figure 2. Its current form maps into three TTIM modules representing scene model, sensor model, and display functions. The sensor model uses a completely linear system

7. T.J. Rogne, An Image Intensifier Simulation Model - Program IIMODEL, OMI-209, OptiMetrics, Inc., June 1987.

representation for image intensifier or direct view optics devices. The model includes three noise sources (representing background, tube, and eye sensitivity limits) and three classes of transfer functions (representing resolution limits of optics, tube, and the observer's eye). For convenience, all of the transfer functions are applied in the frequency domain. The order for application of noise sources and transfer functions is shown in the figure.

The model calculations begin with computation of the mean tube signal current produced by each scene pixel:

$$I = \frac{\pi f^2 \tau_o PH PW}{4F_{\#}^2} \frac{\rho}{\pi} \int_{\Delta\lambda} I(\lambda) R_T(\lambda) d\lambda \times 10^{-13}$$

where	I	=	pixel photocurrent (A)
	f	=	objective focal length (cm)
	F _#	=	objective f/#
	τ _o	=	objective transmittance
	PH	=	scene pixel height (mrad)
	PW	=	scene pixel width (mrad)
	ρ	=	scene pixel diffuse reflectance
	I(λ)	=	source spectral illumination (W/m ² -μm)
	R _T (λ)	=	tube responsivity (mA/W)

The model includes illumination spectra for sun, moon, and clear night sky conditions, as well as artificial illumination as provided by a 2870K standard tungsten lamp. The signal current is converted to the number of photo-electrons produced during one eye integration time by the expression:

$$N_e = \frac{I t_e}{e}$$

where N_e = # photoelectrons/pixel/eye integration time
 t_e = eye integration time(s)
 e = electron charge (C)

Noise in the tube signal and dark current are governed by Poisson statistics so that for each component, the noise variance is equal to the mean electron flux. An empirical eye sensitivity model^{8,9} expressed as a noise source is included. The model represents the fact that at low light levels, the eye sensitivity can be limited by photon rate statistics, but that at higher light levels the sensitivity reaches a limit defined by contrast.

Transfer functions used in the model are shown in Table 1. Generic functional forms are available for the optics and eye [8,9]; tabular input must be used to define the tube resolution.

Sample imagery produced by the model is shown in Figure 3 based on a night goggle specification provided in Table 2 and a scene reflectance map (original image) derived from visible imagery. The images illustrate the influence of light level on this postulated sensor's ability to represent the original scene. The reader should be cautioned that since the original scene reflectance map was derived from visible imagery, it does not accurately represent the specific near-IR reflectance of each scene component (particularly the vegetation). Thus, no specific performance conclusions should be drawn. Nevertheless, the example demonstrates the model capability.

8. J.E. Rice, Documentation and Technical User's Guide for the Night Vision Laboratory Image Intensifier Computer Code, OMI-82-024, OptiMetrics, Inc., December 1982.
9. Robert J.L. Corriveau, The Image Intensifier Model, Unpublished report of work at the U.S. Army Night Vision and Electro-Optics Laboratory, June 1978.

4.0 FOCAL PLANE ARRAY SENSOR MODEL

As part of development of the Missile Enhanced TACOM Thermal Image Model (MET-TIM)^{10,11}, a version of the original scanning IR sensor model was modified to treat Focal Plane Array (FPA) sensors with specific emphasis on PtSi detectors. Major changes to create the FPA model included the addition of a responsivity model, a simulation of fixed pattern noise, the addition of new transfer functions representing CCD effects, and the addition of new noise terms.

The responsivity model for Schottkey barrier type detectors predicts the spectral response as a function of emission factor and Schottkey barrier height:

$$R(\lambda) = C_1 \left(1 - \frac{\lambda \Phi_b}{hc} \right)^2$$

where Φ_b = Schottkey barrier height (eV)
 λ = wavelength in microns
 C_1 = emission factor (eV⁻¹)

For a PtSi detector, representative values for the the barrier height and emission factors are 0.23 eV and 0.33 eV⁻¹, respectively.

A spatial-domain sampling model and a fixed pattern noise simulation were derived to treat fill factor and uniformity problems associated with FPAs. The sampling model explicitly represents active detector areas in the array pattern. The model is necessary to account for energy loss and aliasing effects in present arrays which have fill factors varying from 10 to 100%.

10. R. Freeling et al., Missile-Enhanced TACOM Thermal Image Model (METTIM): Addendum to TACOM Thermal Image Model Technical Reference and User's Guide, OMI-302, OptiMetrics, Inc., September 1988.
11. R. Freeling et al., "Update on Recent Improvements to the TACOM Thermal Image Model (TTIM)", Proc. of the Tenth Annual Symposium on Ground Vehicle Signatures, August 1988.

At the present time, fixed pattern noise is represented as a random variation in responsivity across the array, uncorrelated from detector to detector. The variation is input as a standard deviation based on experimental data. That standard deviation can represent the inherent variability for an uncorrected system, or the residual variations that remain after application of a correction algorithm. It is recognized that pattern noise is frequently a limiting factor in the practical operation of FPA sensors. Due to its importance, this area is receiving further attention through the development of 1-point and 2-point correction algorithm simulations under the direction of Eustace Dereniak at the University of Arizona Optical Sciences Center. Results of this effort will be incorporated when the FPA module is distributed.

As is the case in earlier TTIM sensor models, linear transfer functions applied in the frequency domain are used to treat degradations caused by optics, electronics, and so forth. Two new effects treated in the FPA model are charge transfer efficiency and correlated double sampling. The transfer functions which approximate these effects are given below:

$$MTF_{CTE} = \exp \left[-m(1 - \epsilon) \left(1 - \cos \frac{2\pi f}{f_{HC}} \right) \right]$$

where

MTF_{CTE}	=	MTF for charge transfer efficiency
ϵ	=	CCD charge transfer efficiency
m	=	number of charge transfers from detector to output amplifier
f_{HC}	=	horizontal spatial frequency cutoff of the array (mrad^{-1})

$$MTF_{CDS} = \left[\frac{1 - \cos(2\pi f t)}{1 + (2\pi f T_D)^2} \right]^{1/2}$$

where

MTFCDS	=	MTF for correlated double sampling
f	=	frequency (Hz)
t	=	clamp-to-sample time(s)
T _D	=	CDS dominant time constant(s)

Finally, additional noise models have been added to treat mechanisms found in CCD structures. The CCD noise sources represented are trapping state, pixel reset, charge transfer, output amplifier, and dark current noise. For a well designed sensor viewing terrestrial scenes, all of these noise sources should be small compared with the photon shot noise; nevertheless, they are treated in the model to allow consideration of low background scenes.

The FPA model is currently in use for the MET-TIM application. Validation exercises are planned following the incorporation of the new fixed pattern noise correction model. Distribution of the model as a TTIM module is planned for later this year.

5.0 IMAGING SEEKER SIMULATION EXAMPLE

The image sequence shown as Figure 4 illustrates the type of simulations made possible using TTIM. In this case, TTIM is mated with the Infrared Modeling and Analysis (IRMA) scene generator¹² which produces the required target and background imagery. TTIM introduces the atmospheric effects, models a PtSi FPA imaging seeker and simulates the operation of a simple gated video tracker. The six frames show samples of the tracker behavior during the flight. The simulation actually considered tracking updates at the full 30 Hz frame rate of the postulated sensor.

¹². D.H. Goldstein, Infrared Modeling and Analysis (IRMA) Computer Program User's Manual, AFATL-TR-85-44, U.S. Air Force Armament Laboratory, June 1985.

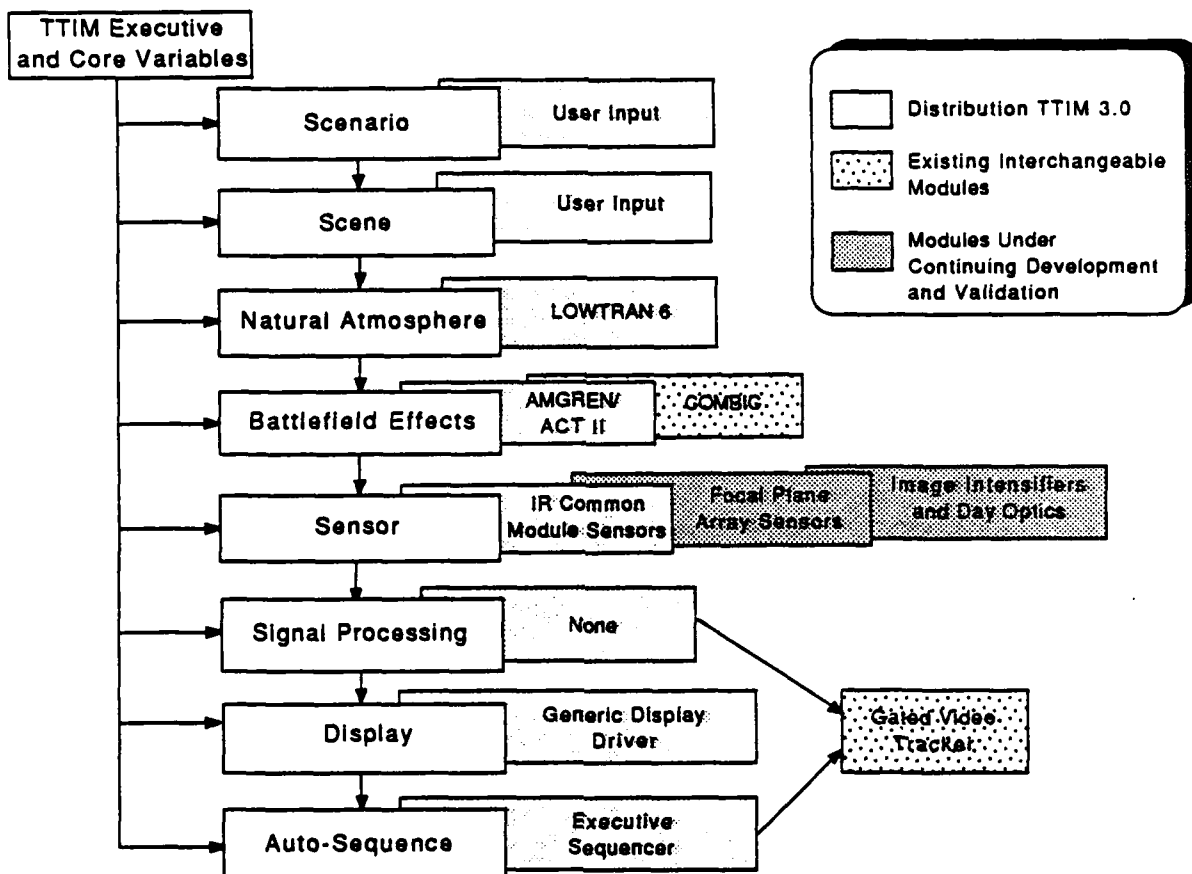


Figure 1. TTIM 3.0 vertical structure and module summary.

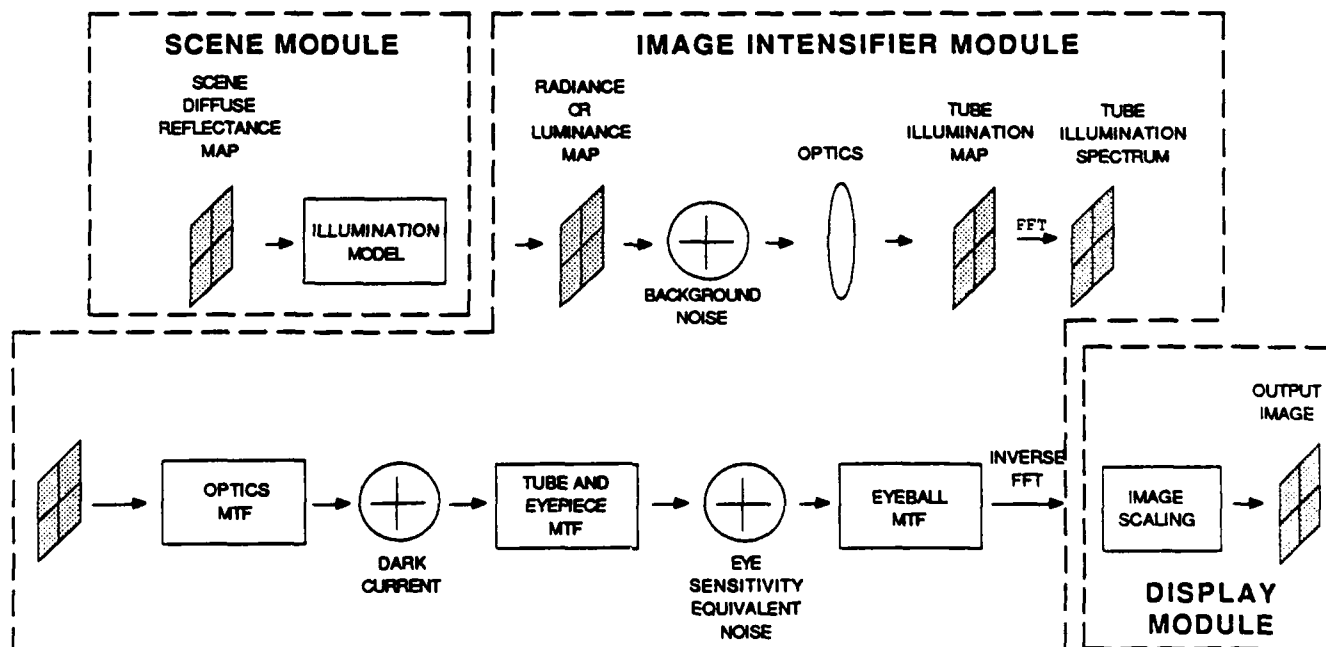
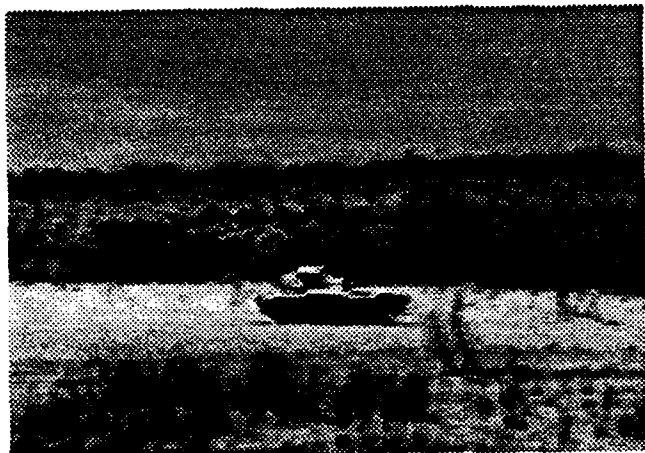


Figure 2. Schematic representation of the image intensifier model.



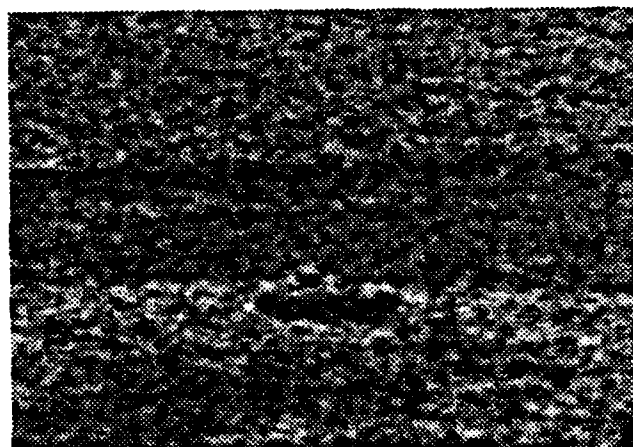
ORIGINAL IMAGE



TWILIGHT

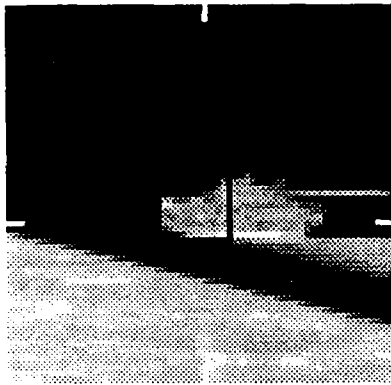


QUARTER MOON

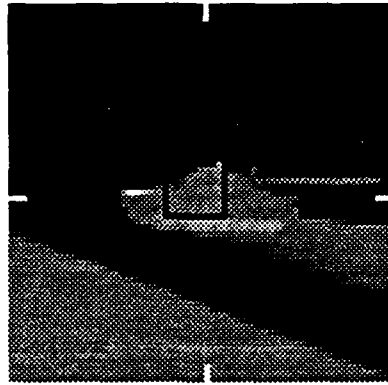


CLEAR NIGHT

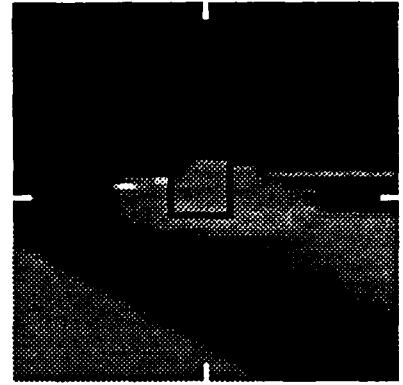
Figure 3. Sample simulated imagery at three light levels for prototype night goggles viewing a winter scene.



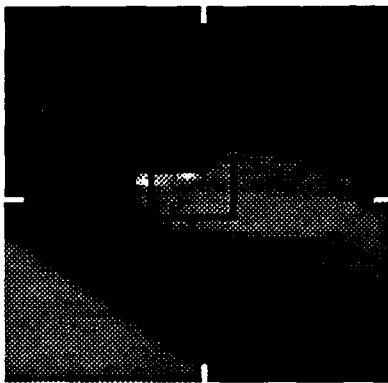
414.3 m



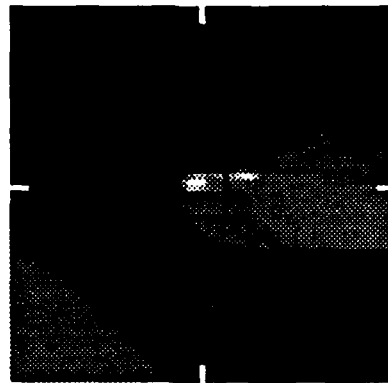
383.7 m



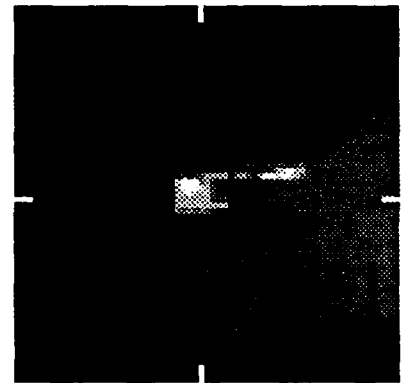
344.8 m



310.2 m



258.0 m



146.2 m

Figure 4. Closing sequence simulation for a postulated imaging seeker and tracker. The tracking gate is indicated on each image and range to target is given below each image.

Table 1. Image Intensifier Subsystem Transfer Function Definitions

1. Optics - Diffraction	
$H(k_x, k_y)$	$= 2/\pi [\cos^{-1}(A) - A(1-A^2)^{1/2}]$
A	$= \lambda_D F_\# (k_x^2 + k_y^2)^{1/2} / f$
λ_D	$=$ diffraction wavelength (microns)
$F_\#$	$=$ objective f/#
k_x, k_y	$=$ image spatial frequency components (mrad ⁻¹)
f	$=$ objective focal length (mm)
2. Optics - Blur	
$H(k_x, k_y)$	$= e^{-\pi^2 w^2 (k_x^2 + k_y^2)}$
w	$= e^{-1}$ half-width of the optical system point spread function (mrad)
3. Optics	- User input table describing an arbitrary optical system MTF.
4. Tube	- User input table describing an arbitrary tube MTF.
5. Eyeball 1	
$H(k_x, k_y)$	$= e^{(-2\pi k_{xy} \gamma / M)} e^{(-6\pi k_{xy} \gamma / M)}$
k_{xy}	$= (k_x^2 + k_y^2)^{1/2}$
M	$=$ system magnification
γ	$=$ eyeball resolution parameter
6. Eyeball 2	
$H(k_x, k_y)$	$= e^{(-2\pi k_{xy} \gamma / M)}$

Table 2. Prototype Night Goggles Specification

Parameter	Specification
Objective Lens Focal Length	2.6 cm
T/Number of Lens	1.5
Eyepiece Transmission	0.8
Magnification	1.0
Luminous Gain of Image Intensifier	20,000
Maximum Brightness of Image Intensifier	2.0 fL
Photocathode	S-20ER
Type of Image Intensifier	2nd Generation Proximity Focused
Tube Resolution	300 Cycles/cm Typical
Equivalent Brightness Input (EBI)	About 2×10^{-11} lm/cm ²
Filter	None

THIS PAGE INTENTIONALLY BLANK

PERFORMANCE SIMULATION OF ACOUSTIC
DETECTION AND LOCATION SYSTEMS VEHICLES

Frederick G. Smith and Joseph L. Manning
OptiMetrics, Inc.
2008 Hogback Road, Suite 6
Ann Arbor, Michigan 48105-9748

ABSTRACT

The Multi-Mission Area Sensor (MMAS) Study is to provide improved target acquisition information to the Brigade Commander. This improved information will be derived through the use of new types of sensors and by the fusion of data from existing brigade sensors. This study is considering electro-optical, infrared, radar, acoustic and signal intelligence sources. The simulation of the performance of acoustic sensors is an important part of the MMAS program

For the MMAS Study, multi-location acoustic sensor systems are being simulated. These systems consist of two or three acoustic receivers each of which can measure the intensity, spectral signature and approximate bearing of an acoustic target. The spectral signatures are used to infer target type. The bearing information obtained from two or three receivers is combined to triangulate the apparent location of the acoustic source. Performance modeling for these systems has been separated into four components:

- 1) modeling the detectability of each target at each receiver location;
- 2) modeling the bearing tracking function for each target at each location;
- 3) modeling the fusion of data from multiple receiver locations to triangulate the apparent target positions; and
- 4) correcting for the acoustic propagation time delays to estimate the current target locations.

As part of the MMAS program, OptiMetrics has developed a simulation model which includes the above functions.

The paper discusses simulation methodologies used in the acoustic system performance prediction model. Algorithms are presented which are used for smoothing and correlating the acoustic reports from the various sensor locations. Results are shown which predict the performance of the acoustic sensor suite in a sample scenario.

The acoustic performance simulation model described in the paper is applicable to the Digital/Electronic Terrain Board (DETB) simulation. Various model enhancements could be performed to improve the flexibility of the model in the DETB application.

1.0 INTRODUCTION AND BACKGROUND

Early this year S³TO was designated to lead the Multi-Mission Area Sensor (MMAS) Study to provide improved target acquisition information to the Brigade Commander. This improved information is to be provided by the use of

additional sensors and by the fusion of data from all brigade sensors. Two sensor classes are to be addressed: those presently in 6.3 or above, Advanced Development, for deployment between 1996 and 2000 and those presently in 6.2, Advanced Research, for deployment from 2000 to 2006.

This Study is to consider electro-optical, infrared, radar, acoustic and signal intelligence sources. A key component of the Study is the development and application of a sensor performance and data fusion model to evaluate performance trade-offs. One key aspect of that model is the development of a module for acoustic sensors and the fusion of data from such sensors with other types of target acquisition information.

For the simulation part of the MMAS Study, it was decided to use an enhanced version of the Intelligence and Electronic Warfare (IEW) Model developed by TRAC-WSMR and its contractors¹. That model was originally developed to predict the performance of Signal Intelligence sensors for a Corps area of the battlefield. In 1986, OptiMetrics Inc. was funded by TRAC-WSMR to add the capability to address electro-optical and infrared sensors with in that model². For the MMAS Study, additional sensor models and fusion models have had to be added to the IEW Model.

In reality, the "IEW Model" is not one model but a series of models which can be used in concert to address a particular battlefield scenario. For the MMAS Study additional sensor modules had to be added to predict the performance of air defense radars, moving target indicator (MTI) ground surveillance radars, and acoustic sensors. In addition, enhancements were made to the EO/IR sensor models to better model the time-lines for target detection and to improve the countermeasure modeling capabilities. Simulation models for data fusion were also added. A schematic representation of the model, as it is being used for the MMAS Study, is shown in Figure 1. In the present paper, we will discuss only the acoustic portions of the model.

2.0 ACOUSTIC SENSOR SIMULATION

For the MMAS Study, a multi-location acoustic sensor system is to be simulated. This multi-location system consists of two or three acoustic receivers each of which can measure the intensity, spectral signature and approximate bearing of an acoustic target. The spectral signatures are used to infer target type. The bearing information obtained from

¹ K. C. Trott, F. K. Frantz and D. A. Barnes, "Intelligence and Electronic Warfare Movement Simulator," TRASANA-TR-2-1986, PAR Government System Corp, July 1985.

² J. W. Petraska, N. Hadwick, T. J. Rogne, "Intelligence and Electronic Warfare Model Electro-Optical Sensor Simulation Package -- User's Guide," OMI-204, April 1987.

two or three receivers is combined to triangulate the apparent location of the acoustic source. The modeling of the performance of this system was separated into four components:

- 1) modeling the detectability of each target at each receiver location;
- 2) modeling the bearing tracking function for each target at each location;
- 3) modeling the fusion of data from multiple receiver locations to triangulate the apparent target positions; and
- 4) correcting for the acoustic propagation time delays to estimate the current target locations.

3.0 ACOUSTIC DETECTION RANGE PREDICTIONS

For the MMAS Study, it was decided to use the TACOM Acoustic Detection Range Prediction Model (ADRPM) off-line as a component of the acoustic sensor performance predictions. TACOM supplied representative ground vehicle signatures in the 1/3 octave format required by ADRPM. ADRPM could then be used in the standard manner to perform range prediction calculations.

ARDEC supplied representative helicopter signature data which was processed to the ADRPM format by OptiMetrics. However, because ADRPM assumes a relatively wide, 1/3 octave, spectral bands, if used in the normal manner ADRPM would not correctly predict the range performance for the narrow, 1 hertz, bandwidth helicopter signature lines. As a expedient method to correct for this, the background intensity was decreased by the square root of the bandwidth ratio in those spectral bands. A companion paper presents examples of the target signatures and the range predictions developed for the study.

The standard ADRPM model only provides a measure of the range where the target is just at the detection threshold. For the present study it was required that some measure be provided of the ranges at which targets can be identified and accurately tracked by a directional acoustic sensor. Relations have been developed by others for the accuracy of bearing determination verses the sensor S/N ratio³. This relationship, called the Cramer-Rao bound, is shown in Figure 2. Using that curve we have computed three functional ranges for use in the model: detection, identification with 6 degree bearing accuracy and identification with 3 degree bearing accuracy. The S/N ratio corresponding to each of those ranges is 3 dB, 9 dB and 13 dB, respectively. These functional ranges were then computed with ADRPM for each target and condition.

³ Private Communication, W. Donnally, ARDEC, January 1989.

When the MMAS acoustic simulation is run, the distance is determined between each target and receiver pair. It is then determined if the target is detectable given the precomputed range results from ADRPM. If the target is detectable, it is then determined if it is identifiable and the approximate angular accuracy with which it can be tracked. A Gaussian random error is then added to the target bearing and an acoustic detection report (bearing and identification) is generated for later use with the fusion model.

4.0 ACOUSTIC BEARING TRACKING ALGORITHMS

The initial algorithms for acoustic tracking were proposed by John Allen as part of a fusion study for S³TO⁴. The algorithms were modified during the model development process by OptiMetrics' personnel. The bearing track algorithms are intended to correlate and smooth bearing reports resulting from a single target. If two sequential bearing reports fall within predefined angular velocity and angular acceleration gates, then they are used to create a new bearing track file. Subsequent observations will be added to a track file when they fall within an acceptance bound of the extrapolated position of an existing track. After three or more observations are associated with a track, then a least square polynomial fit is used to smooth and extrapolate the bearing observations in time.

5.0 ACOUSTIC POSITION TRACKING ALGORITHMS

The purpose of the position tracking algorithms are to associate bearing tracks from the same target observed from different sensor locations to obtain a triangulated position fix on each target. The algorithm for the position determination uses the assumptions that the S/N ratio is inversely proportional to range and a knowledge of the velocity of sound to develop a time coincidence equation between two bearing reports. Once that has been accomplished, the target position is found by simple triangulation. This simple sounding process is complicated by the facts that all of the data includes random errors and that a single bearing track from one receiver may associate with multiple bearing tracks from another receiver. The random errors can cause missed position tracks or incorrect associations, while the multiple associations cause ghost tracks.

The position tracks formed are also smoothed by fitting to polynomials. The polynomials are used to establish gates for the next expected locations of the targets. Because acoustic signals have finite propagation delays, the measured

⁴ Private Communication, J. Allen, LICA Systems Inc., March 1989.

tracks represent past positions of the targets; hence the polynomials are also used estimate the target locations at the present instant.

6.0 SAMPLE RESULTS OF ACOUSTIC FUSION

The acoustic fusion algorithms have been demonstrated by running against a small scenario illustrated in Figure 3. In that view, two acoustic receiver locations are seen at the left end of the terrain grid. These sensors are attempting to track four ground targets and three helicopters moving over trajectories as shown. The ground vehicles are moving on the terrain and the helicopters are assumed to be flying at 50 meters above the local terrain. The ground vehicles are generally visible to the sensors; however line-of-sight to the helicopters is often restricted by the terrain.

The apparent positions determine by the acoustic position tracking algorithms is shown in Figures 4 and 5. It can be seen from this plan view, that the model shows that both the ground vehicles and the helicopters are tracked over most of their trajectories by the acoustic sensors. Where the targets are not tracked, it is mostly due to range and terrain obscuration which lowers the target signal levels below the background noise level. It is also apparent from the figures that there are a number of position tracks where there are no targets. These are ghost tracks resulting from incorrect associations between bearing tracks from the two acoustic receivers. It is believed that many of those tracks can be eliminated through correlations with true tracks and through the use of realistic velocity gates; however, those algorithms have not yet been implemented in the model.

7.0 ADDITIONAL FUSION LEVELS

The fusion of the multi-location acoustic data is only the first level of fusion envisioned in the MMAS Study. In addition, fusion of multiple types of sensor data is to be accomplished. Figure 6. shows the fusion structure being implemented in the MMAS program. The overall structure was developed by a contractor team headed by LICA Systems Inc. for S³TO ⁵. That structure represents a three level approach, with the first level being the fusion of bearing only sensors to get position data. The bearing only sensors include the acoustic sensors and signal intelligence sensors. The next level of fusion will correlate reports from the sensors assigned within a single battlefield functional area. The battlefield functional areas (BFA's) addressed include: air defense, fire support, maneuver control and IEW. The air defense

⁵ J. Allen, G. Wittenberg, G. Fox, et. al., "Functional Architecture Description of the Force Level Integration Segment for the Multi-Mission Area Sensor Study," LICA Systems, Inc., SAIC, TRW Federal Systems Group, Draft Report prepared for S³TO, Harry Diamond Laboratories, January 1989.

node represents the most challenging for fusion, because the time lines are short and the targets may be observed with multiple sensors. It is proposed that a multi-hypothesis tracking algorithm will be used for BFA fusion at the air defense node.

For the other BFA nodes and at the Brigade level (Functional Level Integration) spatial and temporal correlation will be used for data fusion. Basically, target reports at those levels will be associated when they meet correlation gates which imply they are the same target, even though they have been reported by various types of sensors. Track files will be obtained and updated for such reports in a manner similar to the method described for the position reports from the acoustic sensors.

8.0 MEASURES OF EFFECTIVENESS

A new module has been developed to calculate measures of effectiveness for the MMAS Study. The measures of effectiveness are calculated for one-on-one, one-on-many and many-on-many sensor and target combinations. The measures of effectiveness calculated include:

- maximum detection, recognition and identification ranges for each type of target;

- accuracy of location;

- range at which location accuracy of a defined level is obtained;

- percentage of time a target is detected within a critical area;

- time to report a target; and

- time that target report leads or lags target's entry into a critical area.

Various options are also available for averaging those statistics over classes of targets and sensors. One difficulty with the MMAS Study is how to measure the effectiveness of the fusion algorithms. The fusion algorithms do not generally lead to the detection of more targets, but rather improve the quality of information about those targets which are detected and minimize confusion generated by multiple detections of the same target. Hence it is anticipated that additional measures of effectiveness will be developed to quantify those factors.

9.0 STATUS AND FUTURE PLANS

The MMAS sensor models and the fusion model are operational on OptiMetrics' Micro-VAX II computer. The models will soon be adapted to the Silicon Graphics 4/D computer workstation. Predictions have been completed for the

MMAS Demonstration Experiment which is presently planned for June of 1990. The model is presently being used to predict MMAS system performance in a Brigade area scenario set in Europe in 1995. Plans are underway to add cross-sensor cuing to the model.

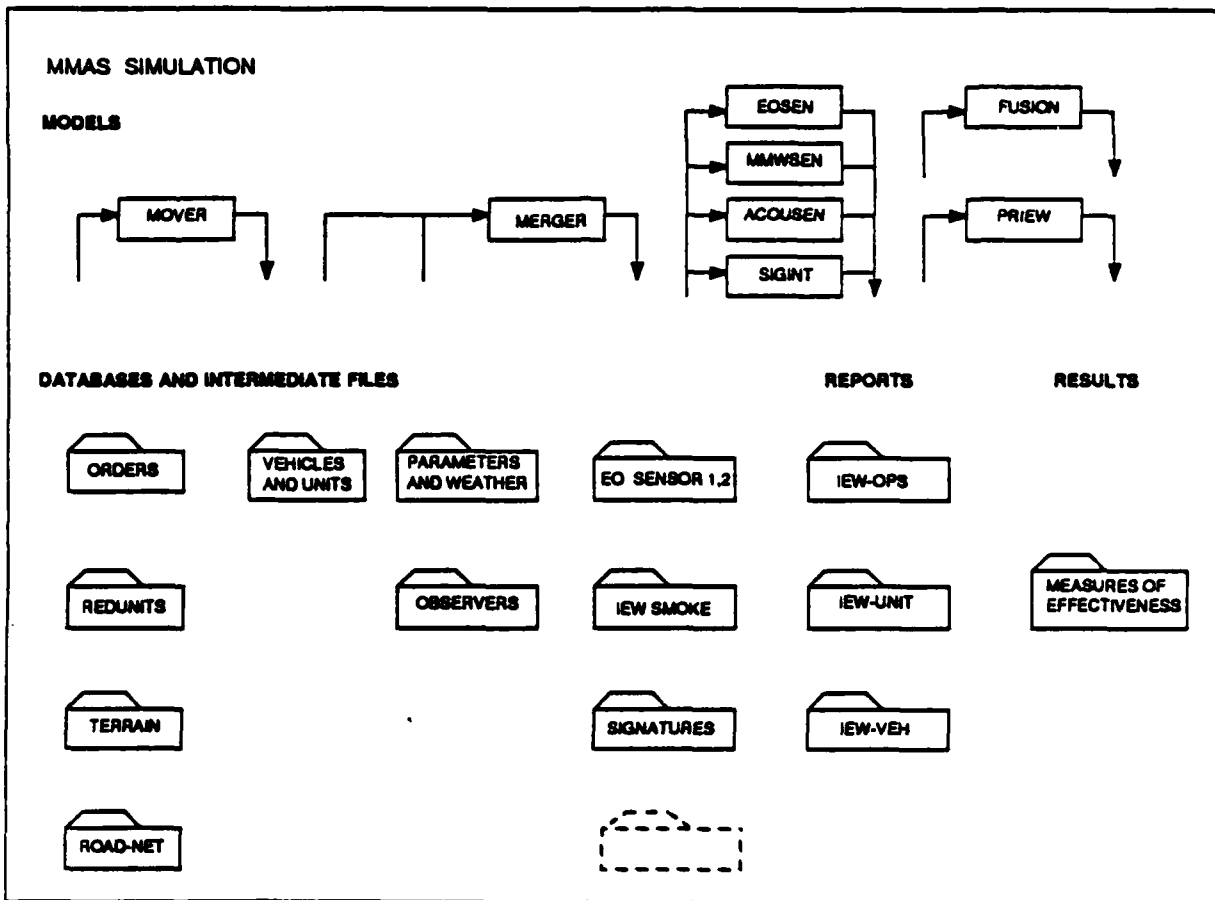


Figure 1. MMAS simulation (improved IEW) model simplified program flow.

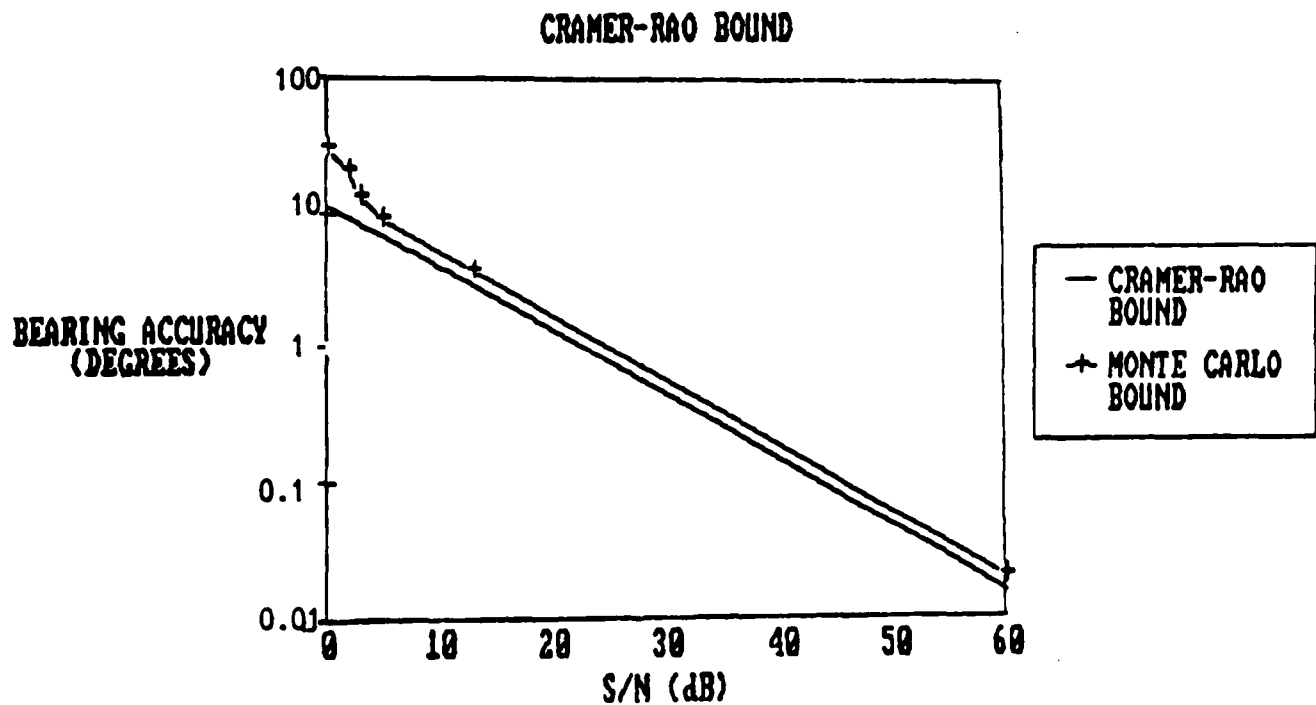


Figure 2. Bearing accuracy as related to S/N for acoustic sensor.

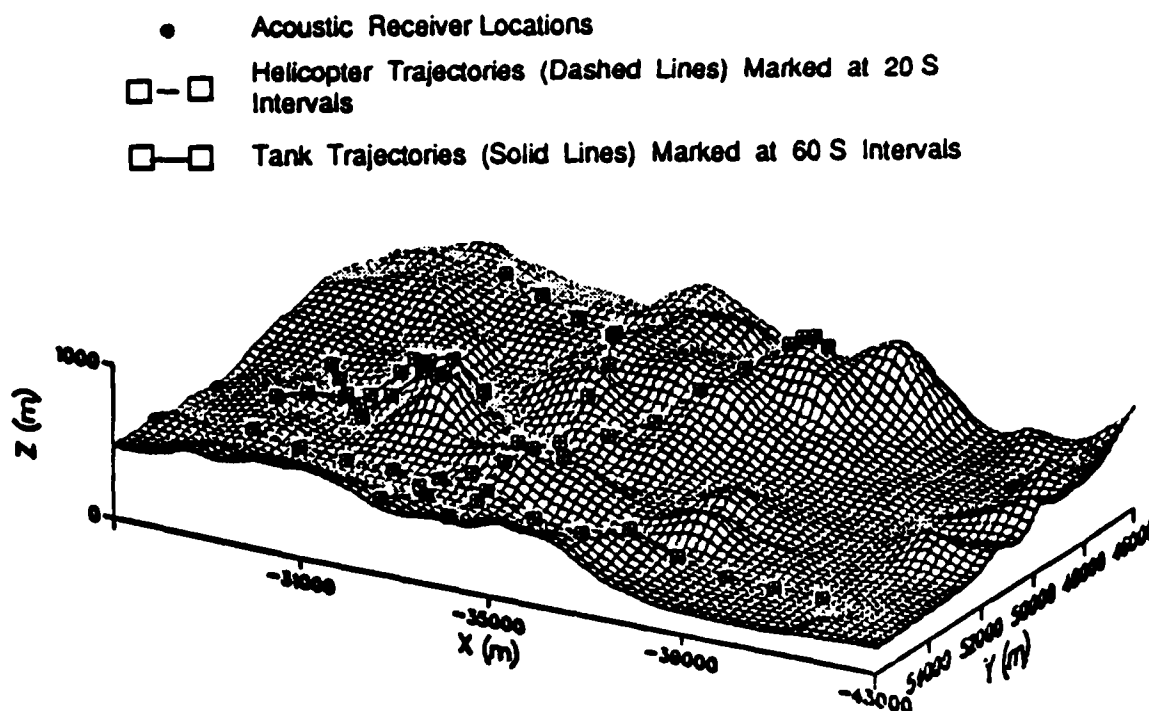


Figure 3. Sample scenario used to demonstrate the acoustic position tracking simulation.

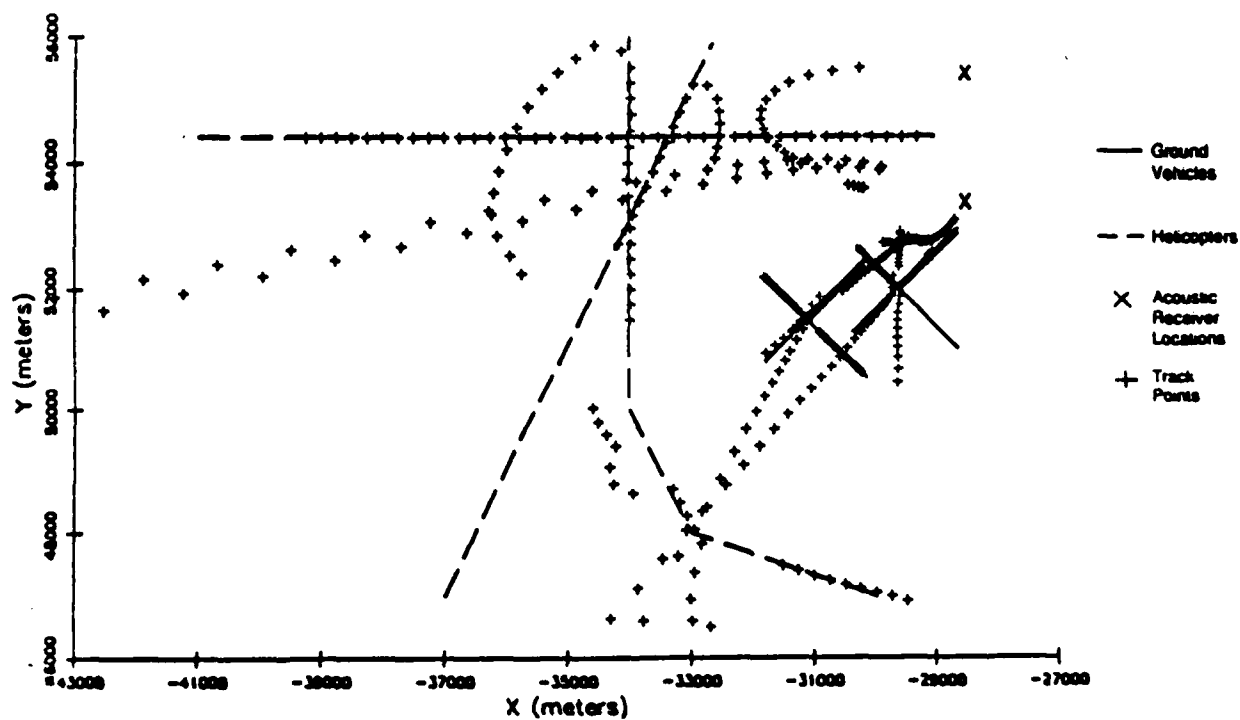


Figure 4. Model target from sample scenario (zero errors assumed for bearing accuracy).

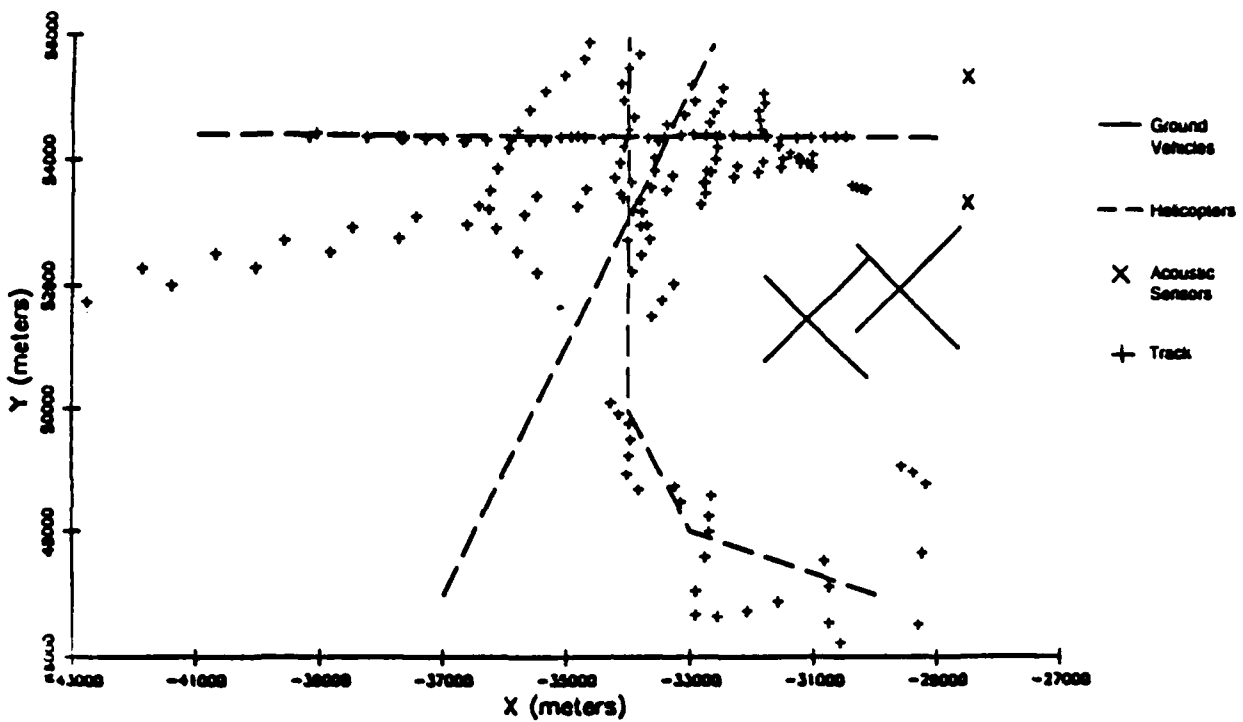


Figure 5. Modeled helicopter tracking from sample scenario (realistic errors assumed for bearing accuracy).

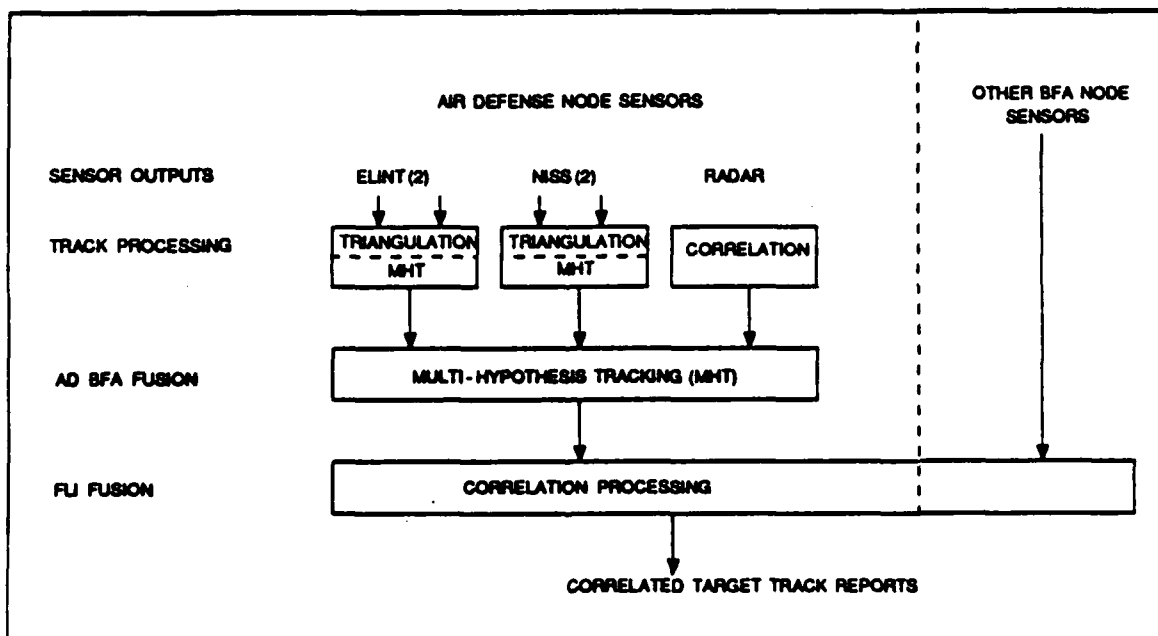


Figure 6. Multi-level fusion architecture for the MMAS program.

AUTOMATIC TARGET RECOGNITION OF SUB PIXELLAR TARGETS

Conrad H. Hoepfner
AAI Corporation

The detection, recognition and classification of objects which are potential targets by means of non-imaging techniques, which are completely passive, represents a new field with a tremendous potential. AAI Corporation has pioneered in this field classifying objects based on their modulated exitance. Exitance is the term used to denote the radiation of energy from an object by virtue of its temperature being above absolute zero. Its units are watts per square centimeter per micrometer of bandwidth. This is the familiar blackbody radiation but reduced by the surface emissivity. The object does not "cool off" as a result of this energy emission because surrounding objects radiate energy to it. Nonetheless, the object is radiating energy which can be detected at great distances. If this exitance is changed in some manner, either statically or dynamically, by means peculiar to the radiating object, such that it is different than the exitance from the surrounding terrain, the object can be detected, recognized and classified. An example, in the visible spectrum is the digital color temperature thermometer. Another example, with reflected radiation again in the visible spectrum, an object may be recognized if painted red while the background is green. This same principle holds true for the cooler objects radiating in the far infrared. They may be recognized by the selective emissions of their exitance.

AAI has constructed equipment and conducted tests in the far infrared region (7-14 microns) detecting and recognizing road vehicles of various kinds. Low cost pyroelectric room temperature sensors were used in conjunction with first surface Cassegrain optics for wide band energy reception. AAI's location is extremely favorable for these tests, being next to a rock quarry and crushing operation where various vehicles are moving in a confined space, foliage is in place for penetration tests and a foreground consisting of an AAI parking lot makes it possible to run tests on vehicles in AAI inventory such as tanks and armored personnel carriers without leaving the protected area of AAI property. Consequently, the tests were made in this area; some tests through foliage, some with unrestricted vision and some in fog and rock dust in which the objects could not be discerned visibly. The wide band optics of the first surface Cassegrain telescope was employed for these tests. The system may be described as follows.

The system utilizes a unique technique for locating and identifying armored vehicles, including tanks, in the modern battlefield. Using analysis techniques adapted from anti-submarine warfare, the approach differentiates a tank from its surroundings by detecting its emission and reflections and the modulation of those emissions and reflections caused by movement (vibration) of the tank parts and surfaces. These vibrational target characteristics are used to locate and classify the target with great accuracy.

The basic approach is to examine the modulation spectrum of the infrared (IR) energy from the target vehicle by exploring the vibrations of the tank exterior and/or the motion of the exterior parts with either active or passive vibration/motion detectors. While these two methods are complementary, it is expected that the active method would not be used when it is desired to remain covert. Both methods (active and passive) utilize analysis techniques employed in anti-submarine warfare detection and identification, rather than optical type pattern recognition.

The same system is applicable to the detection and classification of aircraft and ships.

Contemporary Automatic Target Recognition (ATR) is largely directed toward geometric pattern recognition using models, matched filters, neural networks, etc. All are spatially oriented and all require multiple pixels (50 to 100) to inspect the target. The range of operation is, therefore, limited by a combination of pixel size and target size. It is also necessary that there be thermal contrast between target and background to determine the geometric pattern of the target.

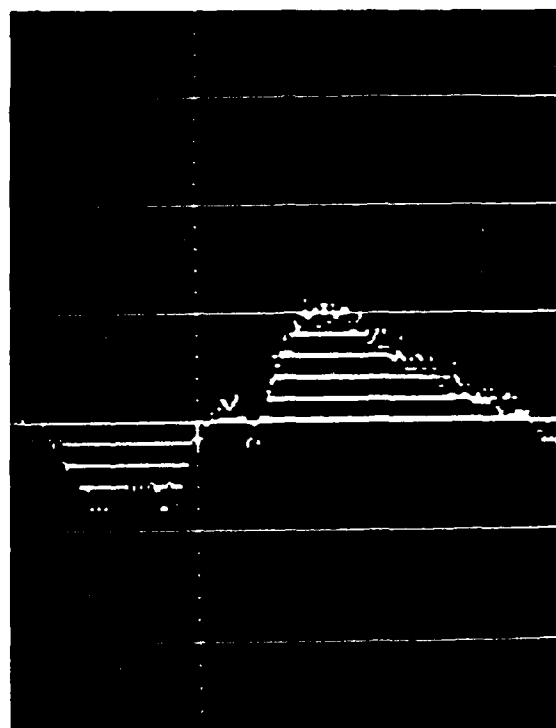
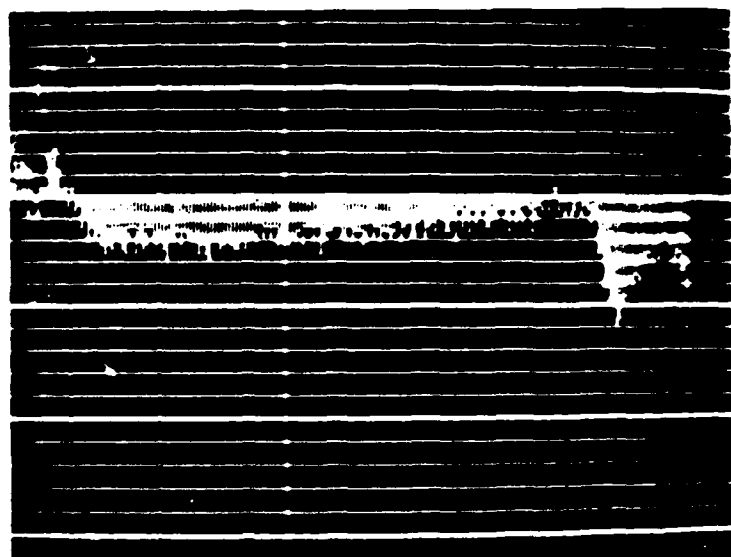
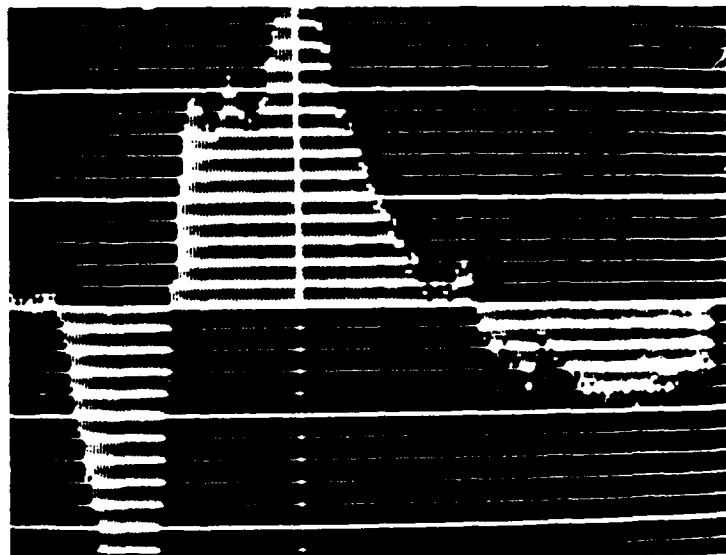
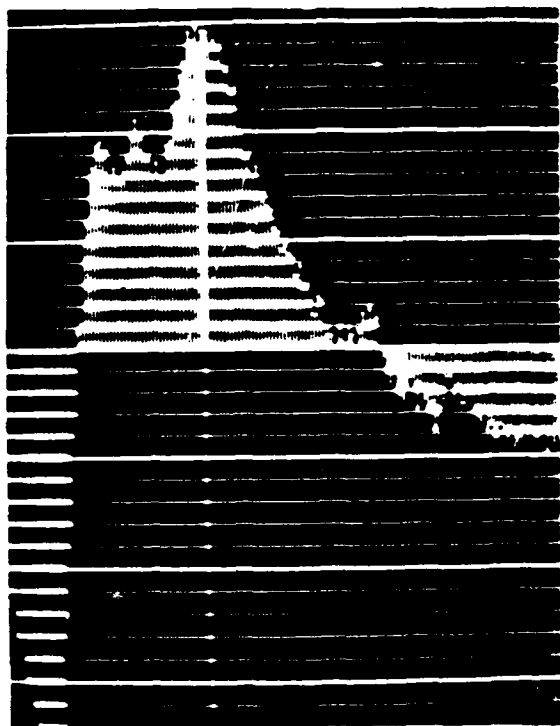
Other methods of detecting, recognizing, identifying and classifying targets are available and should be considered in the ATR system. Techniques are presented here which extend the effectiveness of ATR and at the same time simplify the process. These techniques are temporal rather than spatial and use ATR techniques to get a "signature" much as is done in sonar, geophysical prospecting and speech recognition. The movement of the target into, within and emerging from a pixel is characterized by both the shape of the target and its motion. Motion may include linear translation, rotation, linear vibration or angular vibration. With narrow bandwidth filters and parallel processing, the signal to noise ratio may be greatly improved over that obtained by scanning with starrang arrays. This makes possible ATR with targets occupying only a small part of a pixel. When the target is not in motion, equivalent relative movement may be produced by a mini scan of the optics (less than one pixel up to two pixels in amplitude), producing effect similar to target motion. Under many circumstances, distance to target and target velocity may also be obtained. Also, under many conditions, thermal contract between target and background is not required.

The task of gathering background data for geometrical target pattern recognition, now just beginning, is a monumental one. Both targets and background (clutter) must be catalogued. For temporal signatures, the complexity is reduced by several orders of magnitude. Most background clutter does not move or vibrate.

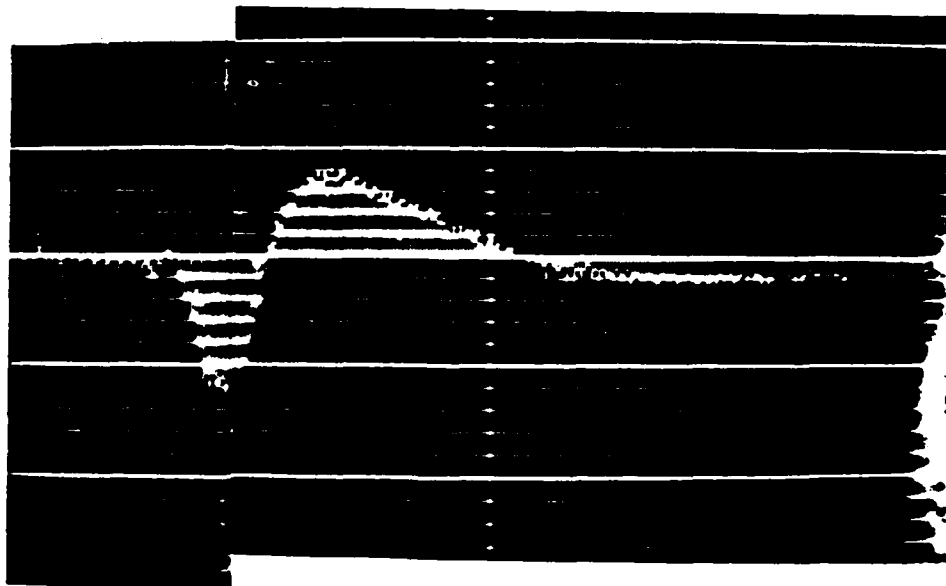
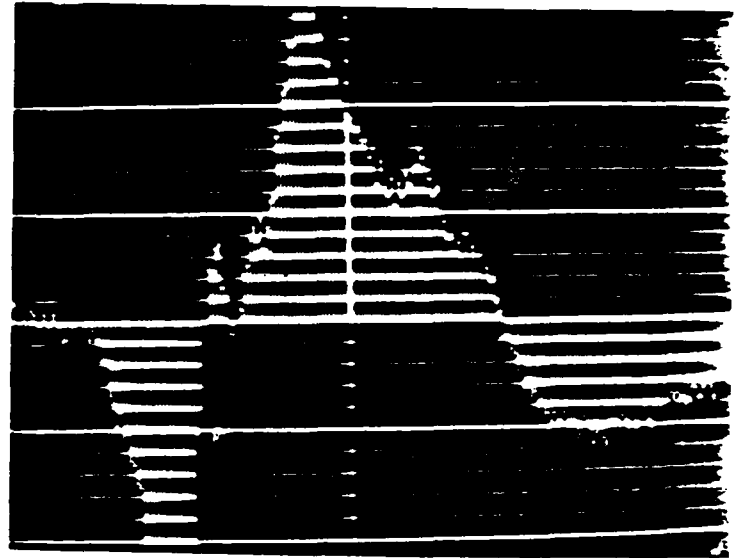
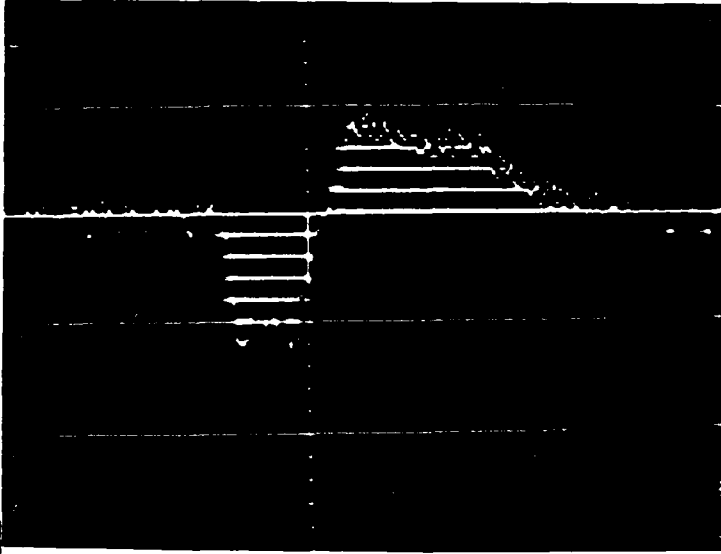
The ability of the sub-pixellar system to penetrate foliage is phenomenal. Shown in Figure 1 is a photograph of the area being inspected. Figure 2 and Figure 3 show signal analyzer records of automobiles and trucks which passed on the far side of the foliage. Figures 8 through 31 are detector output voltages obtained from various targets at ranges to 2.8 Km.

Dynamic Targets in the Digital/Electronic Terrain Board

Targets with characteristic translation, rotation and reciprocal translation-rotation should be included in the terrain board. Developing technology portends far more economical and definitive target recognition and classification methods than does the presently pursued geometric pattern recognition. These new methods, however, require that the target be moving or vibrating in many cases.



BRUEL & KJAER HIGH RESOLUTION ANALYZER TYPE 2033
EXPONENTIAL AVERAGING DYNAMIC RANGE: 80dB
FIGURE 2



**BRUEL & KJAER HIGH RESOLUTION ANALYZER TYPE 2033
EXPONENTIAL AVERAGING DYNAMIC RANGE: 80dB
FIGURE 3**

However, they should not be limited to "stand alone" use but may be combined with imaging systems. The methods of performing automatic target recognition by means of vibration analysis are often simple and direct. They can be employed with either optical or radio frequency systems and may operate in an active, semi-active or passive manner. The system described herein is a passive optical system utilizing first surface Cassegrain optics, an 8 - 12 micrometer band pass filter and two pyroelectric detectors. The data, displayed in graphic form as shown here, has been taken using this system.

Another important consideration is that typical targets will be camouflaged and hidden, making geometric pattern recognition quite useless.

Vibration Signatures May be Obtained from a Small Spot of the Target

Refer again to Figure 1. In the two foot square opening in the leaves, a portion of the rear end of an automobile will be noted. It was through this aperture that much of the data was taken. This is another feature to be included in the terrain board.

IFF is still another feature to be considered. Methods of modulating exitance with the "code of the day" are simple and inexpensive.

One example of the IFF unit is an electronic shutter which alternately transmits and diffuses the exitance from a portion of the vehicle. The chopping code may be vary extensive and precise to allow correlation deep into noise. another example is the use of two shutters, each used in conjunction with a polarizer. At one shutter, the exitance would be polarized vertically and at the other horizontally. Switching them alternately maintains the total exitance at a constant level but permits a dual polarized detector to differentiate and receive the identification code. These units may be controlled electrically to be silent or active at the discretion of the vehicle operator.

Target detection and recognition may be considered at three levels:

1. The target is larger than the pixels and many pixels may scan the target. This is the case used for geometric image analysis.
2. The target and pixel are approximately the same size.
3. The target is smaller than each pixel and may be lost between pixels.

The first case is well known. Target motion and vibration signatures may be obtained in much the same way as in geometric image analysis and obtained in addition to it.

The second case represents an extension of the capabilities of the system to classify targets which previously could not be classified by the image analysis system. An example of how the technique is used is shown in Figures 4 and 5.

In the third case, when the target may be lost between pixels because of its small size, it may still be detected and classified if it moves through one or more pixels. Only if it is stationary or moving radially with respect to the detector will it not be detected. For this situation, the pixel pattern may be translated or rotated.

The multi-microbeam telescope described later can be converted very simply into a mini-scan system by moving either the secondary or tertiary mirrors. They may be moved in a vibratory manner or in discrete steps, but in either event, the entire volume of the beam of the telescope is inspected. It is only necessary to have the target penetrate a single pixel to obtain a temporal signature.

The effects which produce exitance signatures are numerous and varied. The salient requirement is that the signature be above the noise level of the detector. This noise level may be considered in two parts: that inherent in the detector (Johnson noise) and that produced by the atmosphere modulating the exitance. In the latter noise contribution, the atmosphere may modulate exitance from the background or change the modulated exitance from the target. They are expected to be of low frequency (0-5 Hz) and will be removed by the narrow band filters. Some of the effects which produce signatures are listed in Table 1. It should be noted that most do not require that there be contrast between target and background--a requirement in geometrical imaging.

When it is desired to find a target in clutter, any or all of the modes may be exploited. It is not necessary that the target have a net translation with respect to the background to be detected. It may be a reciprocal linear motion, a reciprocal rotational motion or a continuous rotational motion. In this respect, the technique described is different from the moving target indicating (MTI) radar which requires that the target change its location with respect to the background. Net translational motion may also be detected by the system and differentiated from the reciprocal motion or vibration. The multi-microbeam and mini-scan, multi-microbeam telescopes perform this function.

It should be noted that the two functions requiring contrast with the background may have limitations in some circumstances, but in other circumstances, these may be overcome. For example, if it is desired to measure the vertical vibrations of a nearby vehicle against a distant background, then a band pass filter is chosen for the optical system at a wavelength at which there is atmospheric attenuation. The contrast is then greatly enhanced by the atmospheric absorption difference between the short path and the long path. The detector is sensitive at all wavelengths and the band pass filter imposes limits on its reception of energy. If the vibration measurement is being made with the sky as a background, then far infrared is chosen in which there is essentially no sky radiation.

In the category for which no optical contrast with the background is required, a very powerful means of target detection and identification is obtained. The great linear dynamic range of the sensors (LiTaO_3 is 10^{12} to 1) permits nearly any degree of steady energy to fall upon the sensor without producing an output and without affecting its sensitivity to changing (or vibrating) energy. The low frequency response can be made to cut off at any chosen frequency. Also, the sensors are used in pairs connected with opposing polarity such that any general or unfocused energy which falls on both sensors cancels. Thus, a large area may be inspected and only if there is a vibrating object present will there be output from the detecting system. Multiple vibrating objects may be detected in a single area and then differentiated by analysis of their vibration "signatures".

Targets may be identified by the shape of the detector output as the target enters and leaves a pixel. This is shown in Figures 4 and 5.

Background Contrast With Target Required

Moving into and out of beam

Moving forward and backward

No Background Contrast With Target Required

Doppler shift caused by vibration

Polarization caused by vibration

(a) Change of surface angle

(b) Stretching and compressing

Heating and cooling caused by stretching and compressing

Emissivity change caused by stretching and compressing

Interferometer

Target tilting or turning to expose new surfaces at different temperatures

TABLE 1

THE MODULATION OF EXITANCE

The projected area, which is related to shape, of a target moving into a pixel produces a temporal signature as shown in Figure 4.

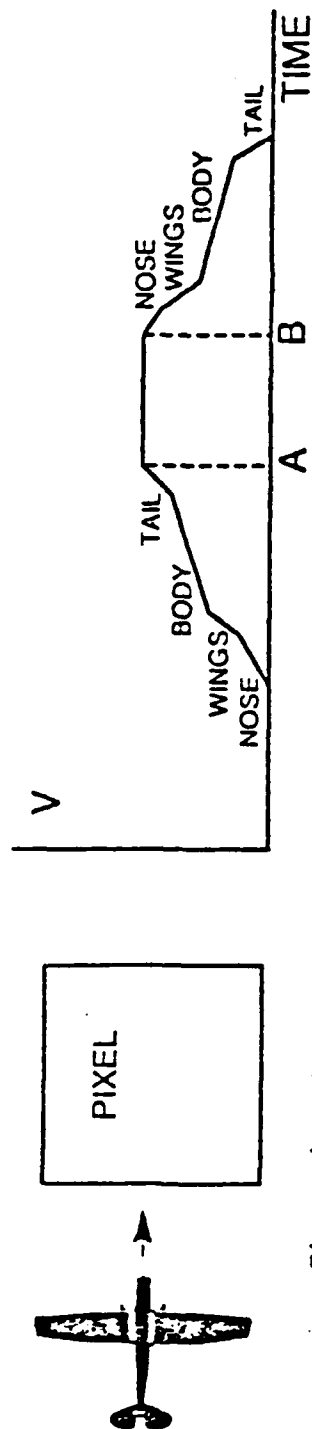


Figure 4. Temporal Signature Produced by a Plane Entering a Pixel

During period A-B the plane is completely in the pixel.

If the target is vibrating at the same time it is translating the signature may be as shown in Figure 5.

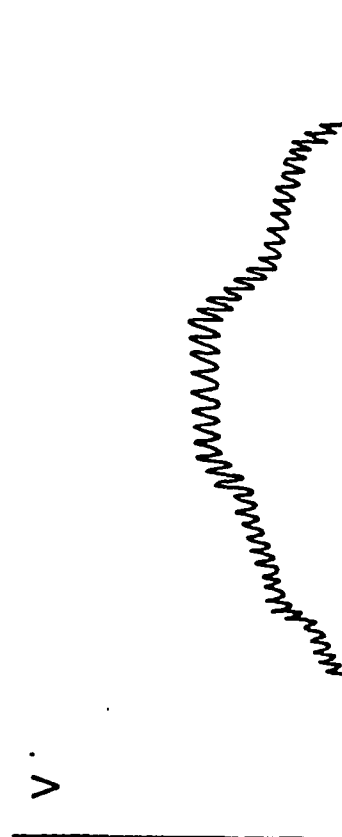


Figure 5. Temporal Signature of a Vibrating and Translating Target

TECHNICAL DISCUSSION

Characterization by Modulated Exitance

Targets such as tanks, transports and aircraft will be found to possess characteristic structural and vibrational modes containing distinctive temporal frequencies which affect the emitted infrared radiation field; this is the case just as ships and submarines emit distinctive sonar frequencies and tactical land vehicles and air vehicles emit unique combinations of sound frequencies. Infrared signatures of vehicles of interest can be obtained either by direct measurement (empirically) or by analysis. Such signatures could be developed for all targets both with and without specific payloads.

Exitance is merely the self emittance of an IR source arising from its absolute temperature. Modulated exitance, in the context of the AAI concept, refers to the changes in the radiated pattern due to structural, motional and thermal changes in the object being considered.

The basic approach for modulated exitance detection is to examine the modulation spectrum of the emitted infrared (IR) energy. Amplitude modulation of an IR signal from a tactical target is produced by moving parts when they present different surfaces or surface temperature changes to the direction of the sensor. Other amplitude modulation sources may be exhaust gases, reflected radiation from other sources (such as the sun), changing of aspect angles of any parts and so forth. These are relatively large variations that are readily detectable and which may be used to characterize and identify the source.

If the contrast between the target and the background is significant, motion of the surface of the target with respect to the field-of-view (FOV) of an individual detector is sufficient to modulate the detected signal. This motion may be either vibration induced variation of the surface area viewed by a detector or by similarly induced motion forward and backward between the emitting surface and the aperture of the detector's optical system.

Little or no background contrast is needed to detect certain kinds of exitance modulation. These include:

- . Doppler shift of the emitted radiation caused by vibration induced relative motion
- . Polarization of the emitted radiation caused by changes in the angle of the surface or by changes in the state of stress on the surface
- . Heating and cooling caused by straining and relieving the surface
- . Changes in the emissivity of the surface caused by stretching and compressing
- . Interferometry effects

Target facet rotation exposing surfaces at different temperatures.

Each of these mechanisms can be related to vibration and causes the received steady state signal to be altered by the addition of some transient component. These transient signal components consist of the spectral attributes (frequencies) that characterize the source.

Characterization Using an Active Optical System

Enhanced detection of certain kinds of vehicle modal and vibration response is achievable using an active system based on solid state laser technology. Gallium-aluminum-arsenide (GaAlAs) lasers may be modulated into the gigahertz region. Detectors with matching response capabilities are similarly available. Thus, it is possible to probe specific small areas within a large target using a collimated beam to determine the frequencies and displacements of selected structural elements to extreme precision. The wavelengths involved would be outside the visible band, around 850 nm, so some degree of covertness is available.

Other types of processes related to optical schemes are also potentially useful: thermographic and photographic techniques.

Modulated Exitance Detection System

AAI is developing a novel passive IR detection concept which is adaptable to a variety of missions including detection and tracking of tactical targets and evaluation and characterization of structures (including vehicles).

The basic approach is to examine the modulation spectrum of the infrared (IR) energy from the target vehicle by examining the vibrations of the vehicle's exterior parts with passive vibration/motion detectors. This passive method of detecting the modulations in IR signatures has the advantages of being covert and simple; in addition, it has promise of being low cost, small, and lightweight.

The radiated power from a blackbody source is not small; a 10 square meter surface at ambient temperature emits about 2,000 watts. Thus, even though the amplitude of the modulated thermal emission may represent a small fraction of the total signal, it may nevertheless still be sensed by an IR detector system.

Two factors produce modulation of the received radiation: the vibration of the object and the motion of the object through the detection beam pattern of a multi-microbeam receiving antenna. The antenna does not scan but is held stationary against the background in the field of view. The vibrations of the object are detected by motion in a microbeam using frequency selective filters; while its cross range speed, for example, is determined by the rate at which it crosses the microbeams. There are several mechanisms that produce the modulation detectable by a microbeam sensor pattern. Each of these effects is potentially detectable using the passive multibeam method conceived by AAI. A key aspect that greatly enhances the detection of these emissions is that they are transient or temporally variable so that sensitive frequency based detection methods may be used.

AAI Prototype System

The detection of a vehicle using this technique may be accomplished with a Fast Fourier Spectrum analysis of the sensor output signal for frequencies from nearly dc to 100 Hz. Any frequencies within the band constitutes a detection signal. Certain specific bands with ratios of the signals received constitutes recognition. A fine structure analysis of all frequencies constitutes identification. AAI has already developed and constructed such a recognition system. The frequencies of interest are shown on Table 2.

Using 0.1 seconds for analysis, the frequencies from 25 to 200 Hz will register on the signal analyzer and a detection occurs. To establish that the detected target is a vehicle (recognition), certain discrete frequencies are selected and the ratios of the signal levels within these subbands are analyzed. This process may take 0.5 to 1 seconds. The process of identifying the target as a particular vehicle may require an additional 5 seconds.

Measurements made at AAI show the feasibility of sensing far IR energy emitted from an object to determine the surface vibrations of that object. These tests used a passive IR sensor to measure the vibration of a 2 inch diameter thermal energy source. Vibrations from 8 to 30 Hz were detected and observed on an oscilloscope with a signal-to-noise ratio (SNR) of 20 to 30 dB. The thermal energy source used was the center dome of a conventional loud speaker, heated by a remote projector lamp. The passive sensor was a lithium tantalate pyroelectric sensor with a 7 to 14 bandpass filter. The sensor was used with a 7-inch diameter reflective telescope. The distance between the sensor and the heat source was 16 feet.

The speaker was driven by a signal generator at an amplitude of 0 to 0.1 inch peak-to-peak and a frequency of 8 to 30 Hz. No signal was received when the speaker vibrated while at ambient temperature. The projector lamp was used to heat the center dome of the speaker. Over a period of 45 seconds, the output of the sensor increased from zero to full scale, and then decreased again to zero over the same period when the lamp was turned off. The maximum temperature change was approximately 20 degrees, from 75°F to 95°F. Several additional tests confirmed these results.

At a constant frequency of 10 Hz, the amplitude of vibration was changed from 0 to 0.1 inches peak-to-peak. The signal was discernable at an amplitude of 0.0001 inch peak-to-peak. The bandwidth of the amplifier was 0 to 30 Hz.

At a constant amplitude and constant frequency, the modulation was changed from sinusoidal to square. The output signal changed from sinusoidal to triangular, reflecting the 30 Hz bandwidth of the amplifier.

At a constant amplitude, the frequency was changed from 8 to 30 Hz. A sine wave was preserved throughout, and the amplitude of the signal from the sensor decreased to one-half, also reflecting the 30 Hz bandwidth of the amplifier.

Figure 6 shows the micro-beam receiving telescope used in the tests. The oscilloscope pattern shown in this figure was stable before the photographer's flash. The voltage SNR was 100 to 1 (40 dB) with the wide band (0.5 to 50 Hz) receiver. The pyroelectric sensor is visible on the circuit board. It has a band pass filter that passes frequencies from 2.1×10^{13} to 4.3×10^{13} Hz (7 to 14 μ wavelength).

Selected Frequency Bands (Hertz)

2-3	9-11	24-27	53-58	91- 98	147-157
3-4	11-13	27-30	58-63	98-105	157-167
4-5	13-15	30-33	63-68	105-113	167-178
5-6	15-17	33-37	68-73	113-121	178-187
6-7	17-19	41-45	73-79	121-129	187-197
7-8	19-21	45-49	79-85	129-138	197-207
8-9	21-24	49-53	85-91	138-147	

TABLE 2
FREQUENCY BANDWIDTHS FOR VIBRATION ANALYSIS



FIGURE 6 MICROBEAM TELESCOPE

Figure 7 shows the vibrating heat source used with the micro-beam receiver. In the photograph the projector lamp is on, but when the receiving photograph was taken, the projector lamp was off. The speaker cone was heated approximately 5°F above ambient. The temperature of the spot returned to ambient in about forty-five seconds.

System Optical Implementation

Detection of modulated IR emissions is enhanced if the periodic changes in the radiated field couples the flux collected by the optical aperture to a pair of differentially connected detectors. Thus, one detector is illuminated during one half cycle of a periodic displacement and the other detector is illuminated during the other half cycle. In this arrangement, the signal appearing at the output of the detector-pair circuit contains the information about the motion of the emitting surface while any steady state, common mode component is easily rejected.

Several practical means are available to produce this arrangement. One method under study at AAI involves the multi-microbeam telescope. In this approach, a masking structure consisting of an array of apertures is located at the telescope focal plane. Radiation passing through this mask is later refocused onto a pair of detectors. When viewed from the detectors, the telescope FOV is subdivided into an array of small fields of view; a pair of detectors at the focal plane would each see a slightly different collection of pieces of the overall FOV. For example, the mask is constructed so that each detector sees radiation from alternating segments within the telescope FOV, like red or black squares on a checker board.

An extended source viewed (at relatively close range) with such a system would have its image subdivided so that the detectors would become very sensitive to local surface exitance effects produced by structural or mechanical vibration. These include changes in temperature, polarization or emissivity, or other changes such as aspect angle or similar effects. These effects could facilitate detection since the differentially connected detectors would produce a signal containing the same frequencies as the mechanical perturbations within the emitting structure.

Optical Detectors

Detection of IR radiation has been the subject of intense scientific development during the last 10 to 20 years. A variety of detector materials and types have evolved; typically each type is targeted at one of the atmospheric IR windows or at some related technology (the wavelengths of significant or important lasers, for example).

Pyroelectric detectors have undergone development as part of this general interest in IR technology. These detectors are of potential interest in the present case because they do not require cooling; and, in addition, they have essentially flat response throughout the IR band. Elimination of the cooling requirement is of special interest because of the resulting simplification and reduced size and cost. Pyroelectric detectors come with drawbacks compared to many other kinds of IR detectors. Except for very limited optical modulation or chopping temporal frequencies, the detectivity (D^*) of pyroelectrics, the principal figure of merit for IR detectors, cannot compare with that of cooled detectors.

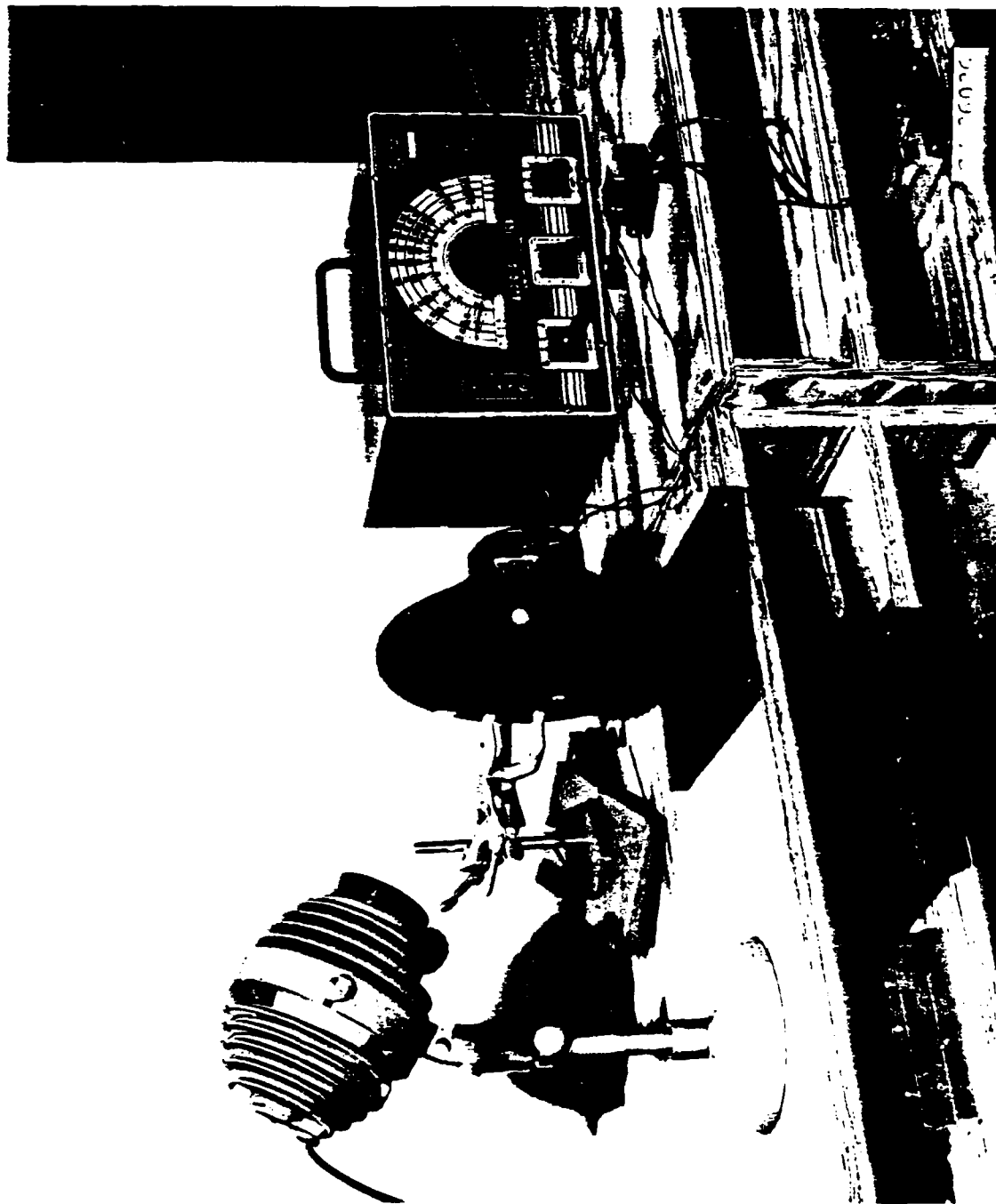


FIGURE 7 VIBRATING HEAT SOURCE

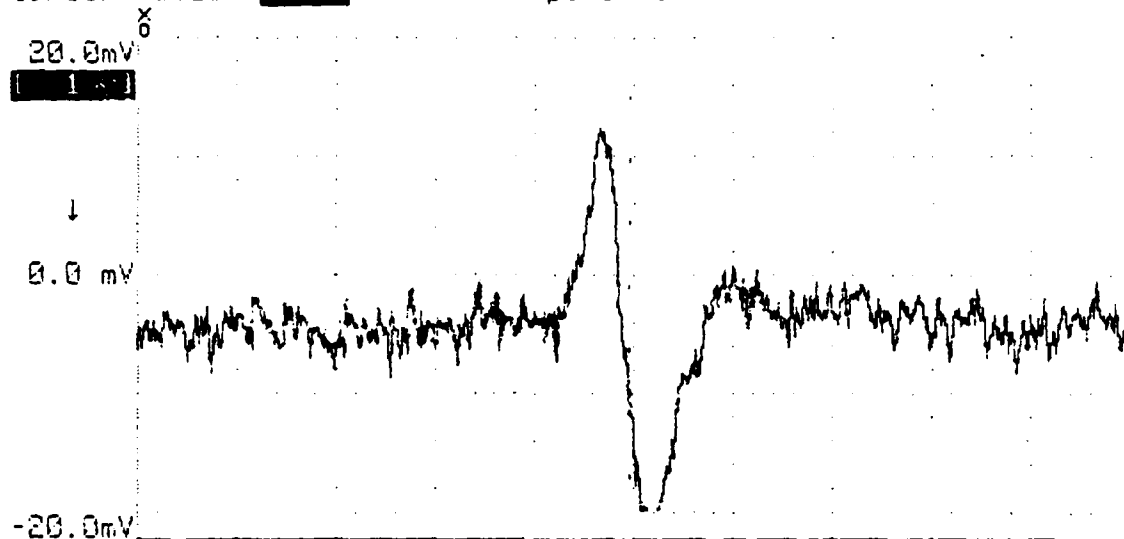
Pyroelectric detectors are competitive from near dc to around 1 kHz with optimum capability usually around 100 Hz. Fortunately this is precisely the frequency band of interest. For this reason, along with the inherent importance of not requiring cooling, pyroelectrics are potentially of major importance.

While being more costly, cooled detectors offer performance benefits that must be considered. There are several good choices for the present application: photoconductive HgCdTe operated at both LN₂ (77K) or TE (195K), photovoltaic HgCdTe operated at 77K, InSb (usually operated at 77K), and the lead salts (PbS and PbSe) that are available for use from ambient down to 77K. Each of these has a better D* than any pyroelectric device, and a much greater optical modulation bandwidth. Thermoelectric (TE) coolers require the least impact on the overall design and packaging; liquid nitrogen (LN₂) cooling, while achievable in closed cycle processes, could ultimately be difficult to accomplish covertly.

Another cooled detector technology of potential interest in this application is platinum silicide (PtSi). This technology is based on the formation of Schottky barrier diodes through the deposition of a thin film of metallic platinum on silicon Charge Coupled Device (CCD) or Charge Injection Device (CID) structures. This process forms a silicide layer only a couple of nanometers thick. The resultant IR detector devices are easily fabricated into large arrays based on well developed silicon electronics and solid state imager technology. PtSi detectors have inherently low quantum efficiencies; however, this drawback is usually more than offset by excellent fixed pattern noise characteristics. For applications where insufficient integration times are available (detection takes place through photo-electron charge accumulation), PtSi detectors can compete with other technologies. PtSi focal planes are operated at a temperature of 77°K to freeze out dark current.

Analog **Waveform Diagram**-----INSERT to add traces-----

Sample Period **10 ms** **Time 3**
Magnification **1X** 1.000 s/div
Magnify About **X 1** 10.00 ms/sample
Cursor Moves **X 1** 0.0 μ s 0 to X



Analog **Waveform Diagram**-----INSERT to add traces-----

Sample Period **10 ms** **Time 3**
Magnification **1X** 1.000 s/div
Magnify About **X 1** 10.00 ms/sample
Cursor Moves **X 1** 0.0 μ s 0 to X

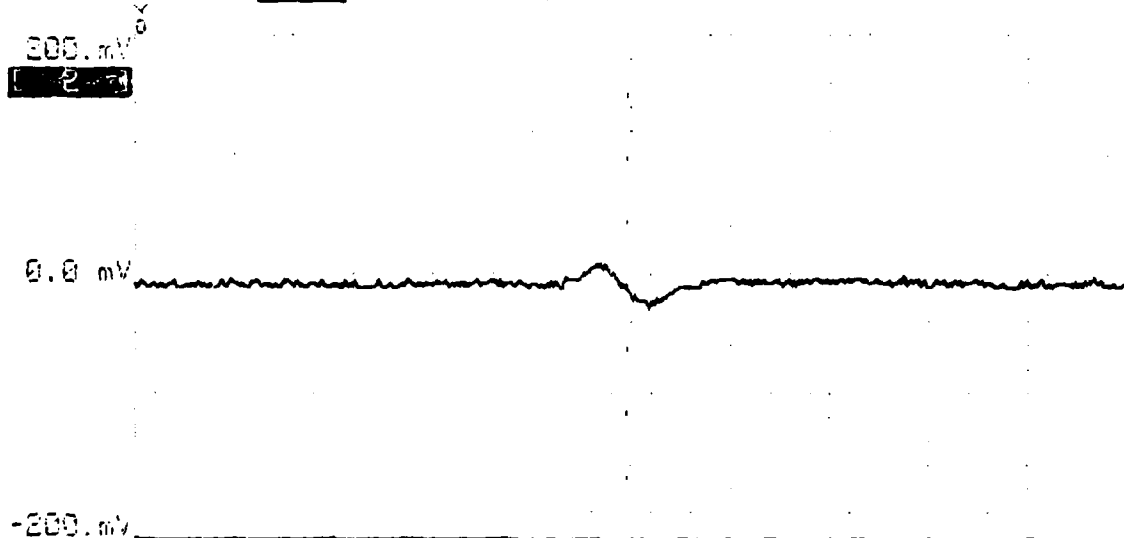


FIGURE 8

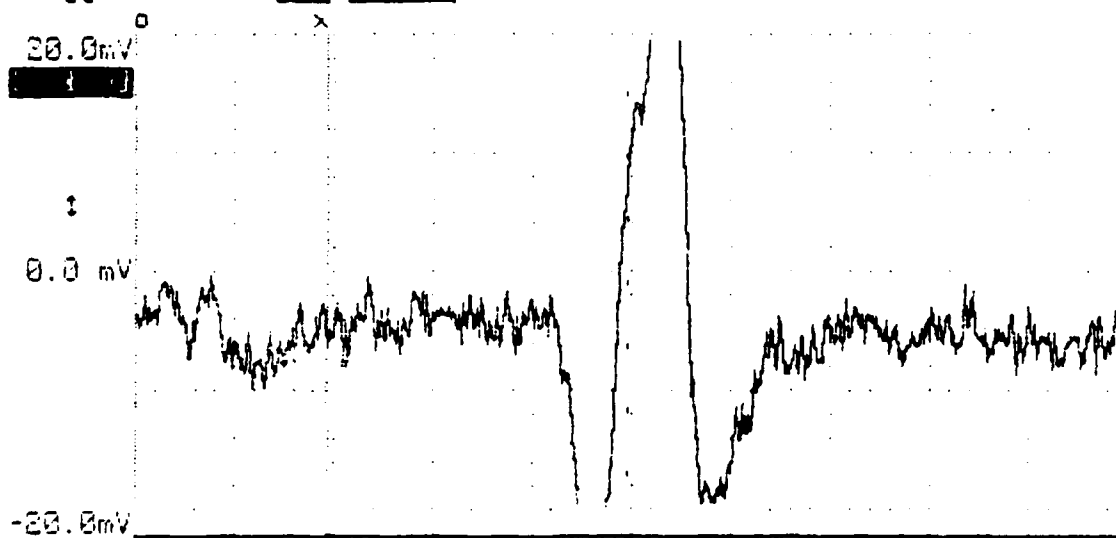
Analog ☐ ☐ -----INSERT to add traces-----

Sample Period ☐ 20 ms ☐ Single Trace Mode

☐ Center Trace ☐ 100 ms After Trigger

Trigger ☐ 1.0 V ☐ Rising

Trigger Level ☐ +1 0.010V



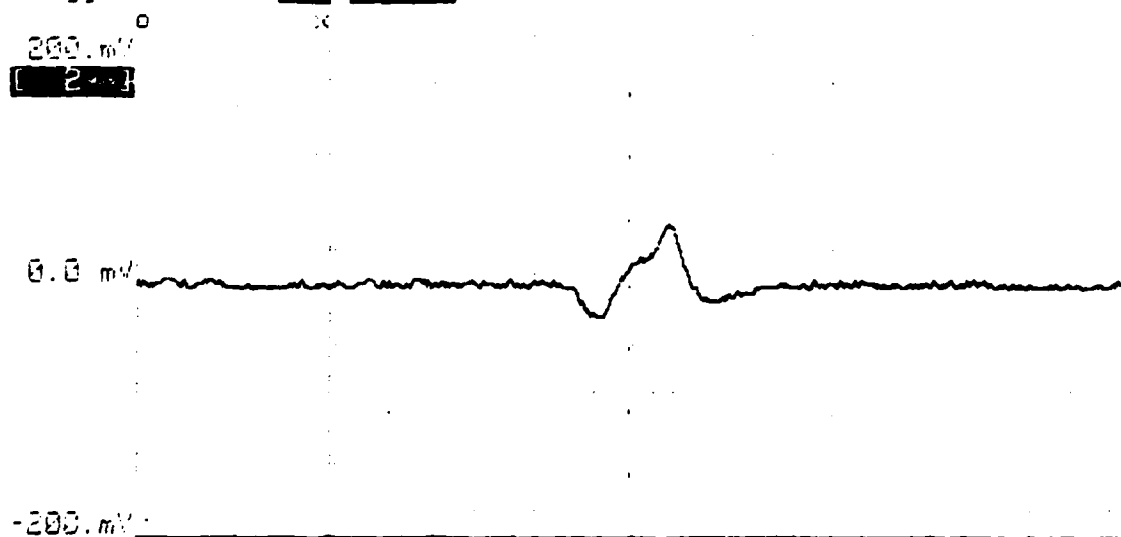
Analog ☐ ☐ -----INSERT to add traces-----

Sample Period ☐ 20 ms ☐ Single Trace Mode

☐ Center Trace ☐ 100 ms After Trigger

Trigger ☐ 1.0 V ☐ Rising

Trigger Level ☐ +1 0.010V



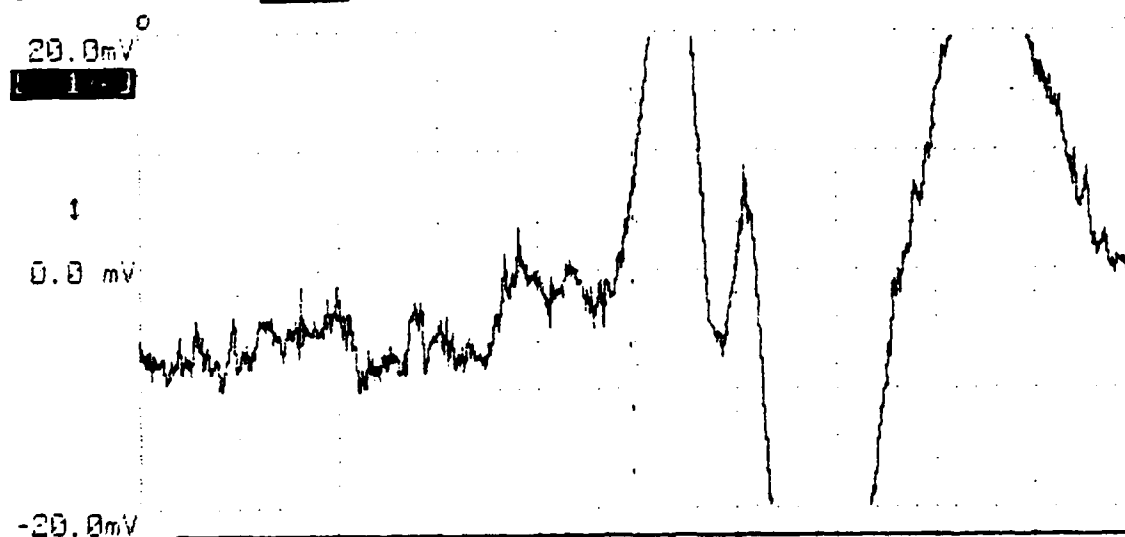
SOUTH BOUND
TRUCK TRAILER
SITE # 3

FIGURE 9



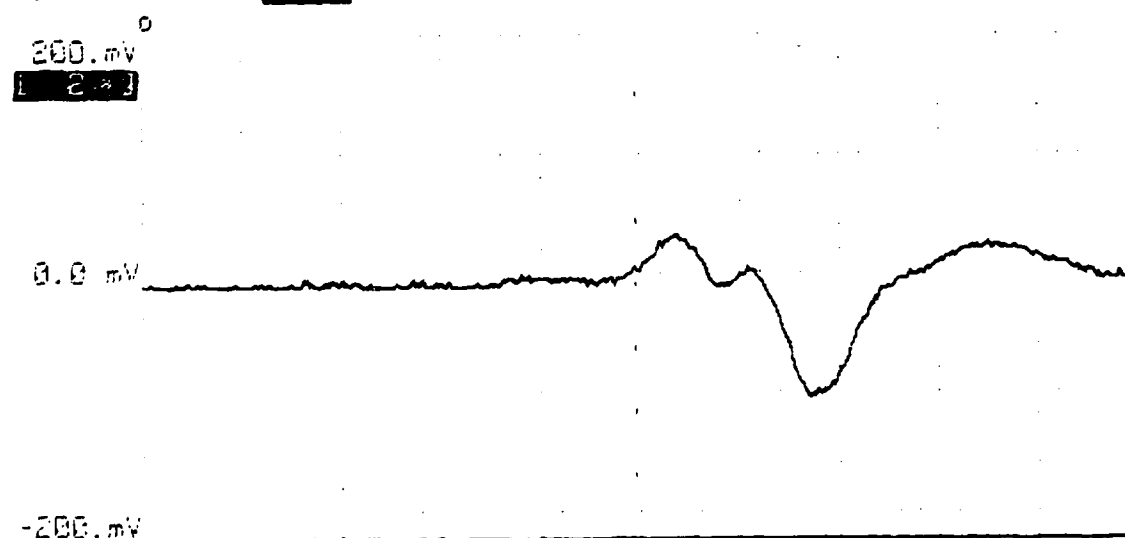
Analog XXXXXXXXXX-----INSERT to add traces-----

Sample Period [10 ms] [Time 3]
 Magnification [1X] 1.000 s/div
 Magnify About [X 1] 10.00 ms/sample
 Cursor Moves [X 3] 9.992 s o to x



Analog XXXXXXXXXX-----INSERT to add traces-----

Sample Period [10 ms] [Time 3]
 Magnification [1X] 1.000 s/div
 Magnify About [X 1] 10.00 ms/sample
 Cursor Moves [X 3] 9.992 s o to x



None Found ↙
 Case #2

FIGURE 10

12.00

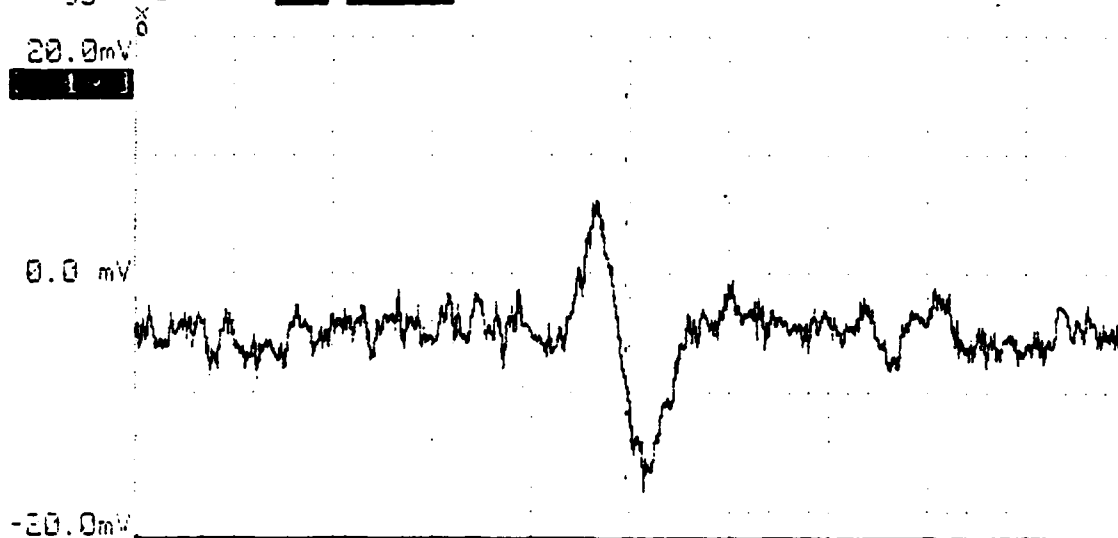
Analog ☐ Waveform ☐ Trace ☐ -----INSERT to add traces-----

Sample Period ☐ 10 ms ☐ Single ☐ Trace Mode

☐ Center ☐ Trace ☐ 0000 ☐ ns ☐ After Trigger 2500

Trigger ☐ 1 ☐ Rising

Trigger Level ☐ 1.010V



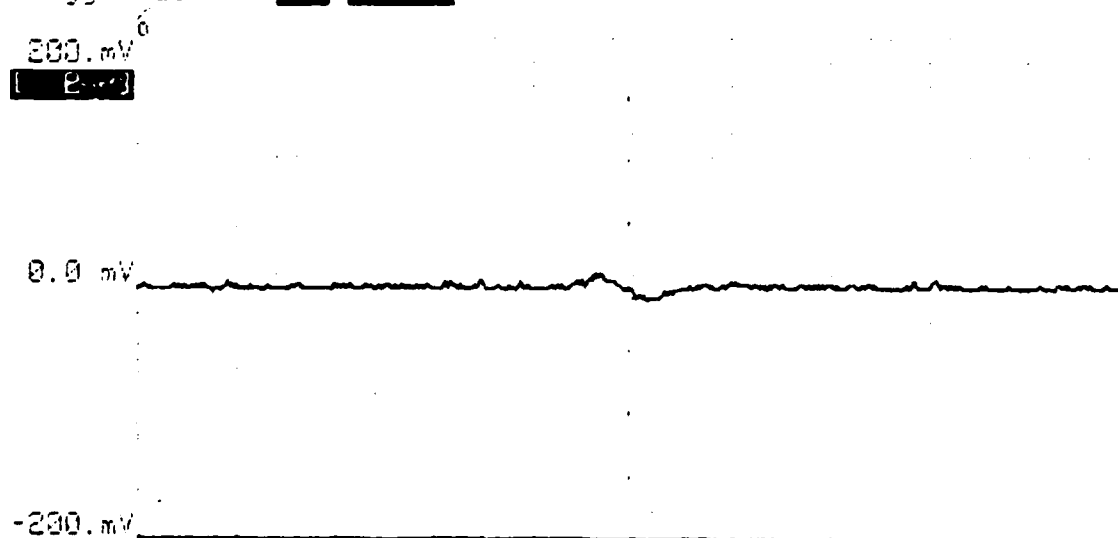
Analog ☐ Waveform ☐ Trace ☐ -----INSERT to add traces-----

Sample Period ☐ 10 ms ☐ Single ☐ Trace Mode

☐ Center ☐ Trace ☐ 0000 ☐ ns ☐ After Trigger 2500

Trigger ☐ 1 ☐ Rising

Trigger Level ☐ 1.010V



SN-P3

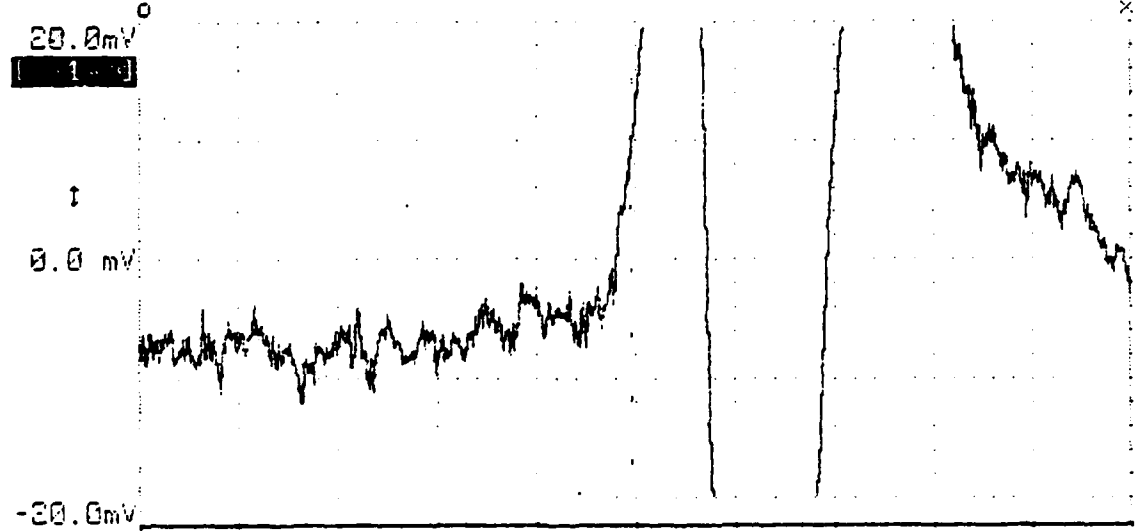
10.00 1.010V

FIGURE 11

7/25/74
A. C.

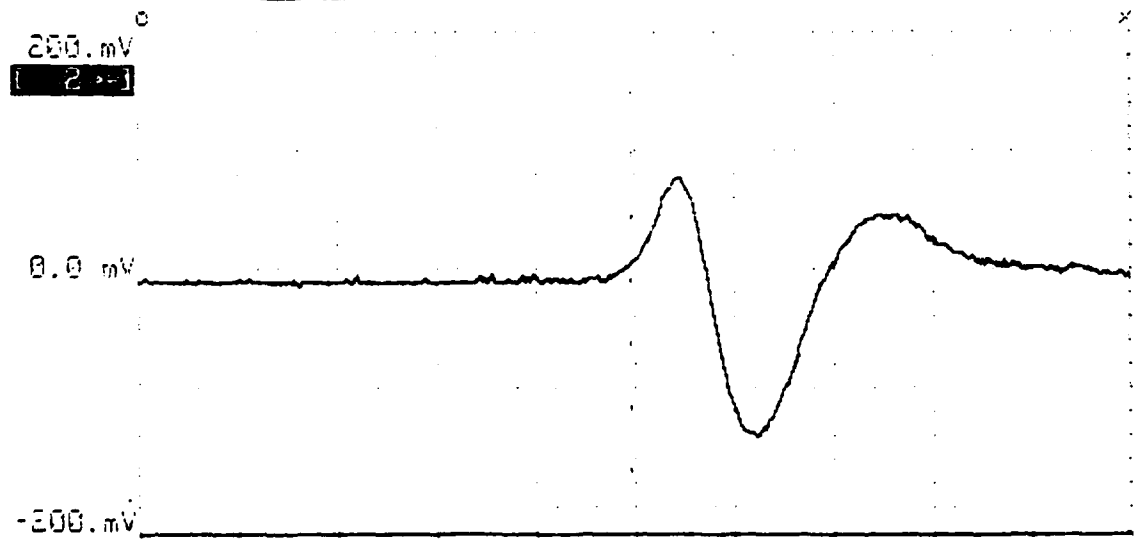
Analog **Waveform Diagram**-----INSERT to add traces-----

Sample Period **[10 ms]** **[Time]**
Magnification **[1X]** 1.000 s/div
Magnify About **[x]** 10.00 ms/sample
Cursor Moves **[x]** 9.992 s o to x



Analog **Waveform Diagram**-----INSERT to add traces-----

Sample Period **[10 ms]** **[Time]**
Magnification **[1X]** 1.000 s/div
Magnify About **[x]** 10.00 ms/sample
Cursor Moves **[x]** 9.992 s o to x

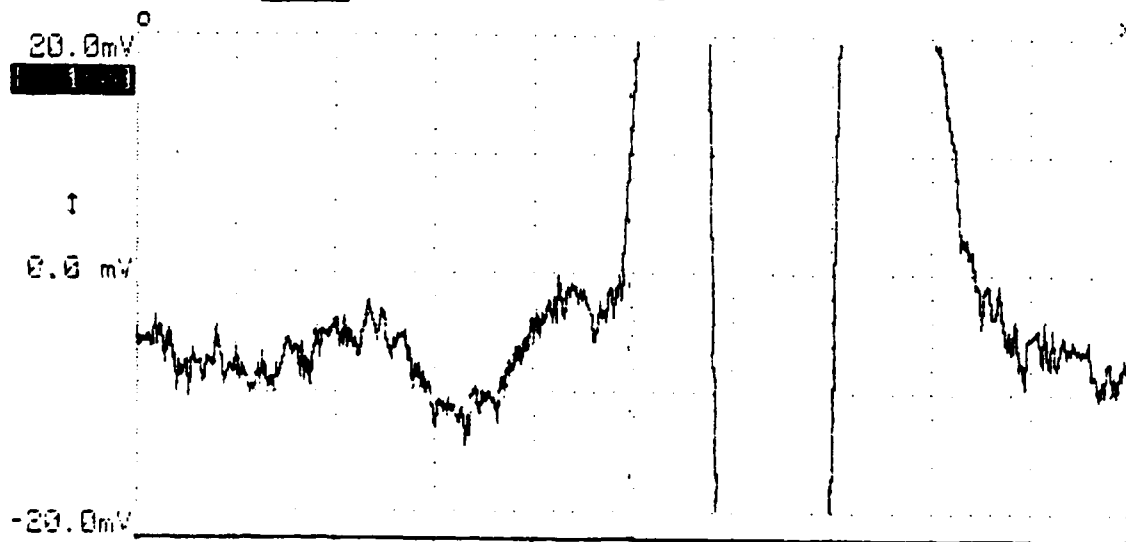


Not on Board Yoke
SL = 2

FIGURE 12

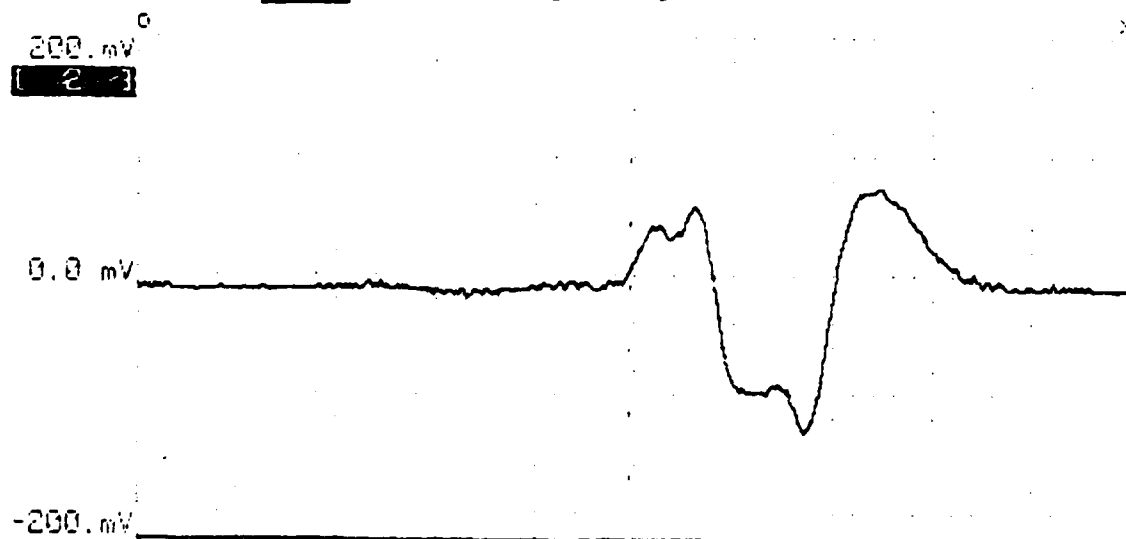
Analog [Waveform Diagram]-----INSERT to add traces-----

Sample Period [10 ms] [Time]
Magnification [1X] 1.000 s/div
Magnify About [x] 10.00 ms/sample
Cursor Moves [x] 9.992 s o to x



Analog [Waveform Diagram]-----INSERT to add traces-----

Sample Period [10 ms] [Time]
Magnification [1X] 1.000 s/div
Magnify About [x] 10.00 ms/sample
Cursor Moves [x] 9.992 s o to x

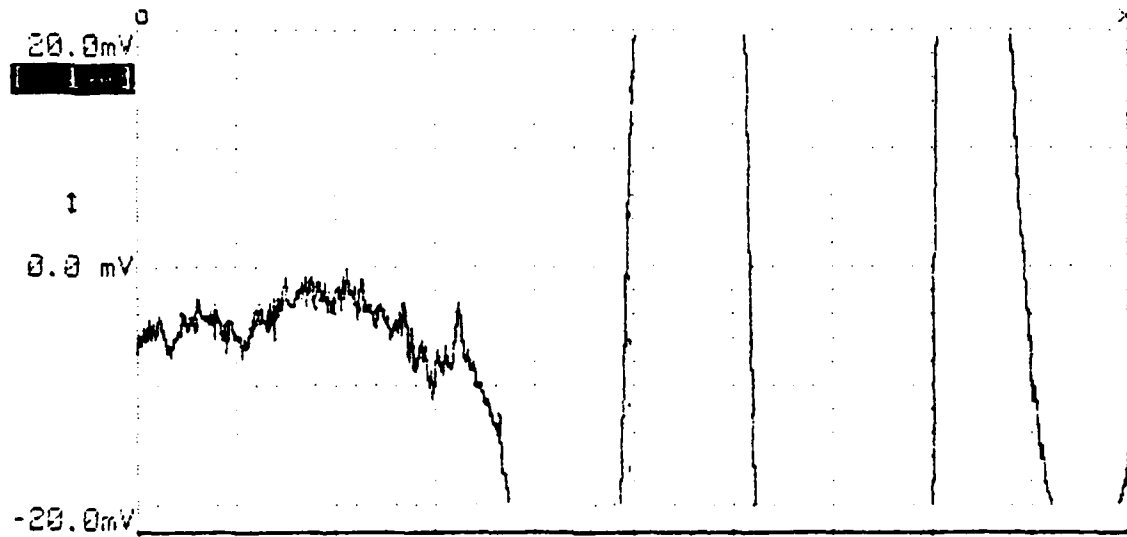


None 2x Dump Trk
S-2

FIGURE 13

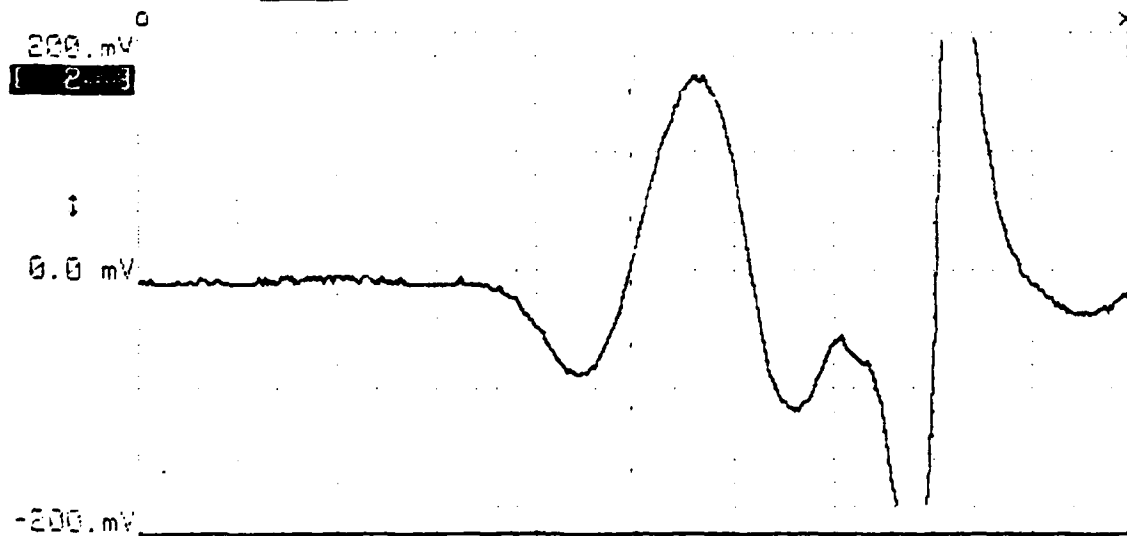
Analog ~~Waveform Display~~-----INSERT to add traces-----

Sample Period [10 ms] [Time]
Magnification [1X] 1.000 s/div
Magnify About [x] 10.00 ms/sample
Cursor Moves [x] 9.992 s o to x



Analog ~~Waveform Display~~-----INSERT to add traces-----

Sample Period [10 ms] [Time]
Magnification [1X] 1.000 s/div
Magnify About [x] 10.00 ms/sample
Cursor Moves [x] 9.992 s o to x



2 Sour Board Dump Tracks

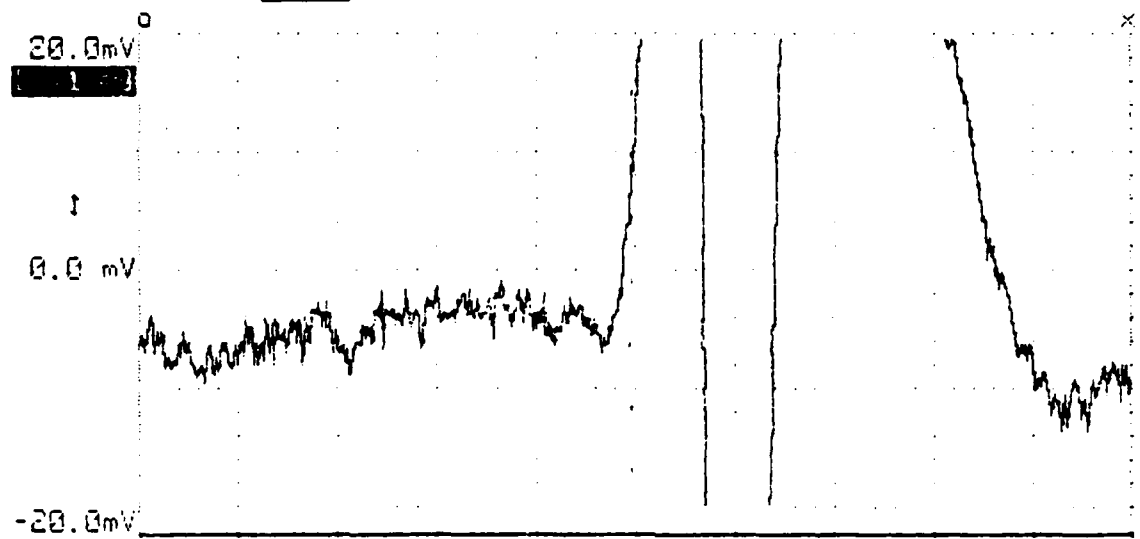
5 x 2

FIGURE 14

7/20/77
W. C. ...

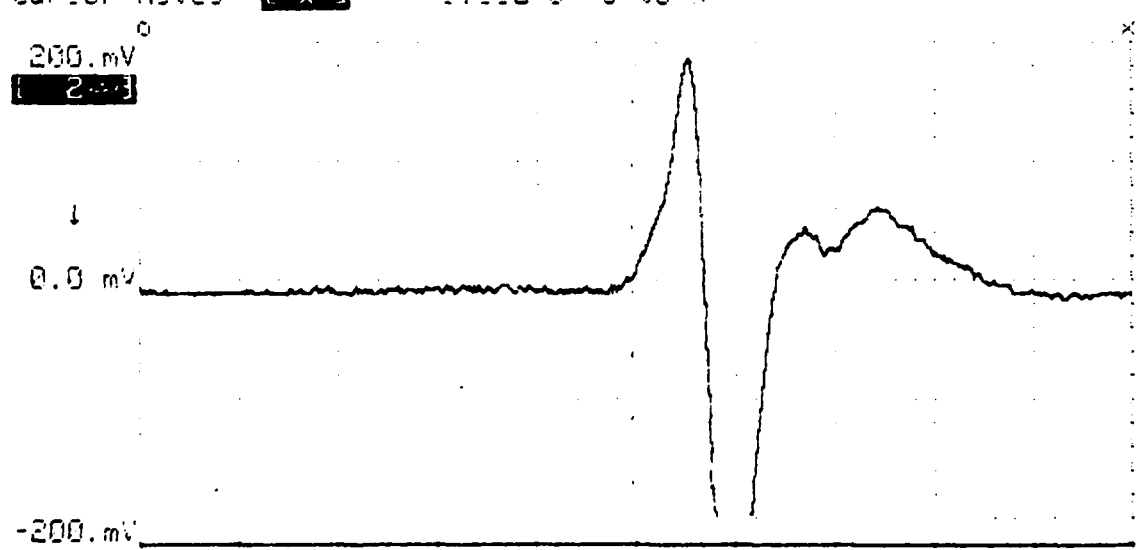
Analog [1] [10 ms] [Time] ----- INSERT to add traces -----

Sample Period [10 ms] [Time]
Magnification [1X] 1.000 s/div
Magnify About [x] 10.00 ms/sample
Cursor Moves [x] 9.992 s o to x



Analog [Waveform Diagram] ----- INSERT to add traces -----

Sample Period [10 ms] [Time]
Magnification [1X] 1.000 s/div
Magnify About [x] 10.00 ms/sample
Cursor Moves [x] 9.992 s o to x

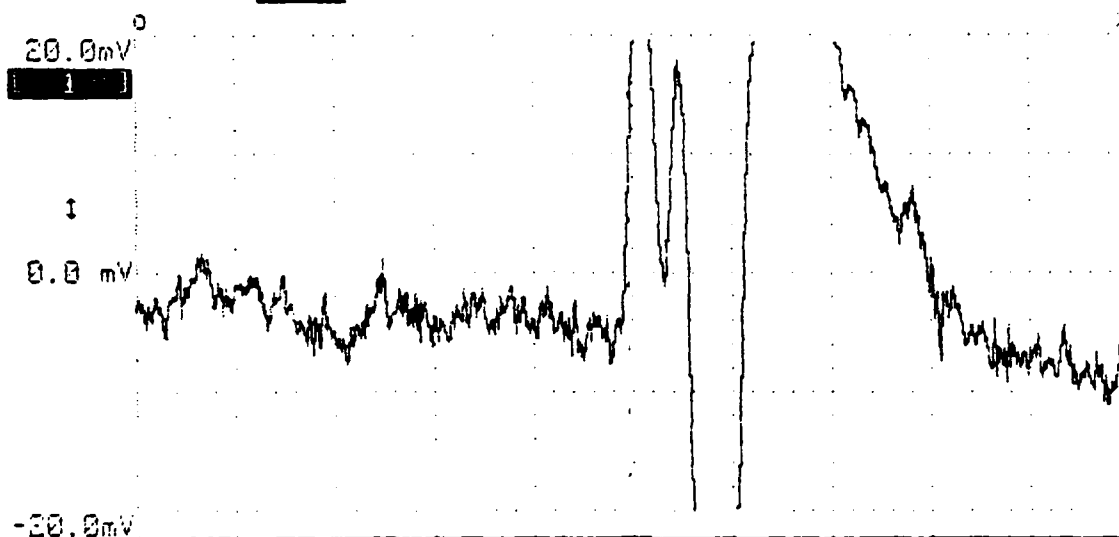


Non-Invasive
S. 4 + 2

FIGURE 15

Analog [REDACTED] -----INSERT to add traces-----

Sample Period [10 ms] [Time]
 Magnification [1X] 1.000 s /div
 Magnify About [x] 10.00 ms/sample
 Cursor Moves [x] 9.992 s 0 to x



Analog [REDACTED] -----INSERT to add traces-----

Sample Period [10 ms] [Time]
 Magnification [1X] 1.000 s /div
 Magnify About [x] 10.00 ms/sample
 Cursor Moves [x] 9.992 s 0 to x

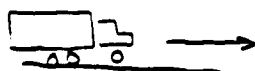
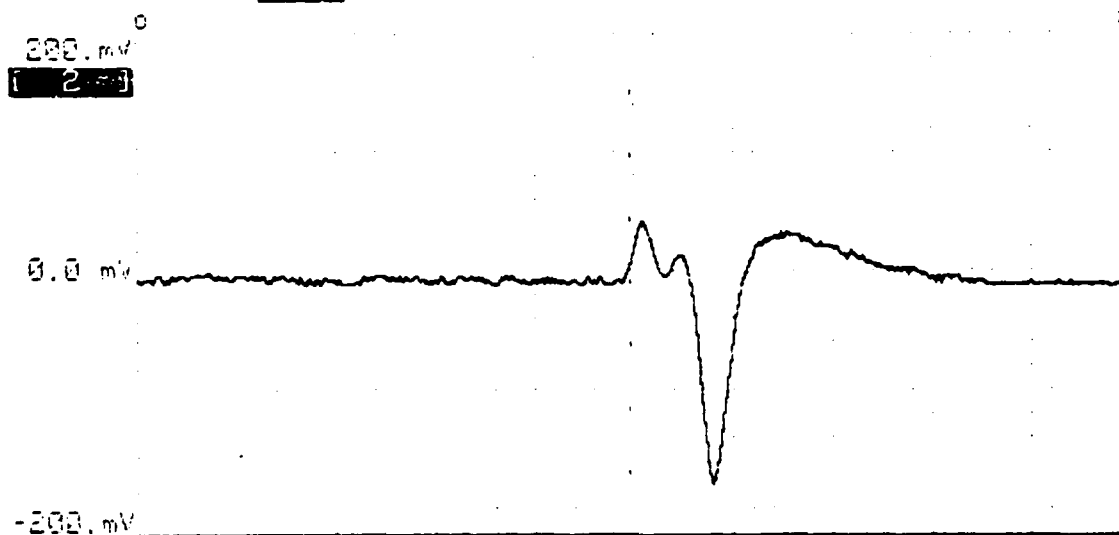


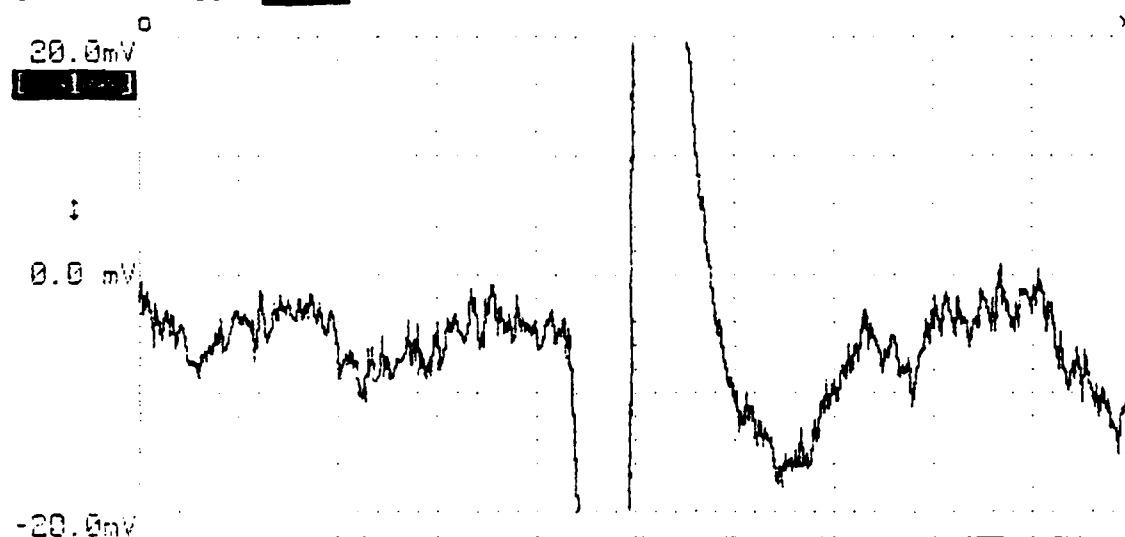
FIGURE 16

171-6-002 20MP-RUC
 2-2 = 2



Analog [Waveform Diagram]-----INSERT to add traces-----

Sample Period [10 ms] [Time]
Magnification [1X] 1.000 s/div
Magnify About [x] 10.00 ms/sample
Cursor Moves [x] 9.992 s o to x



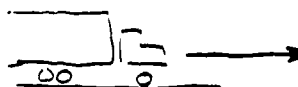
Analog [Waveform Diagram]-----INSERT to add traces-----

Sample Period [10 ms] [Time]
Magnification [1X] 1.000 s/div
Magnify About [x] 10.00 ms/sample
Cursor Moves [x] 9.992 s o to x



FIGURE 17

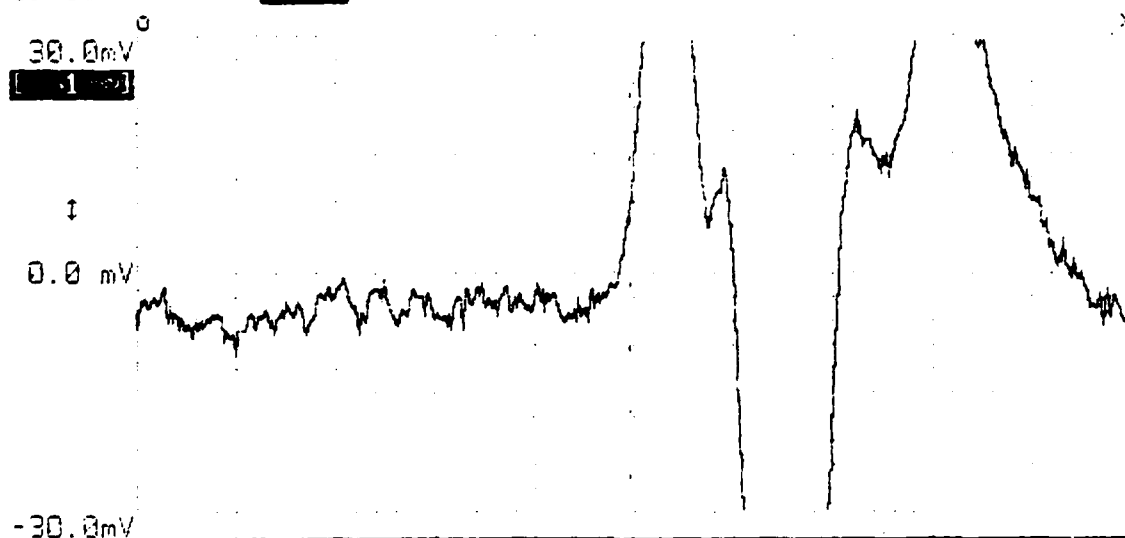
SWT - BOUND for - 7100
SITE #2



7/28/89
J. C. ...

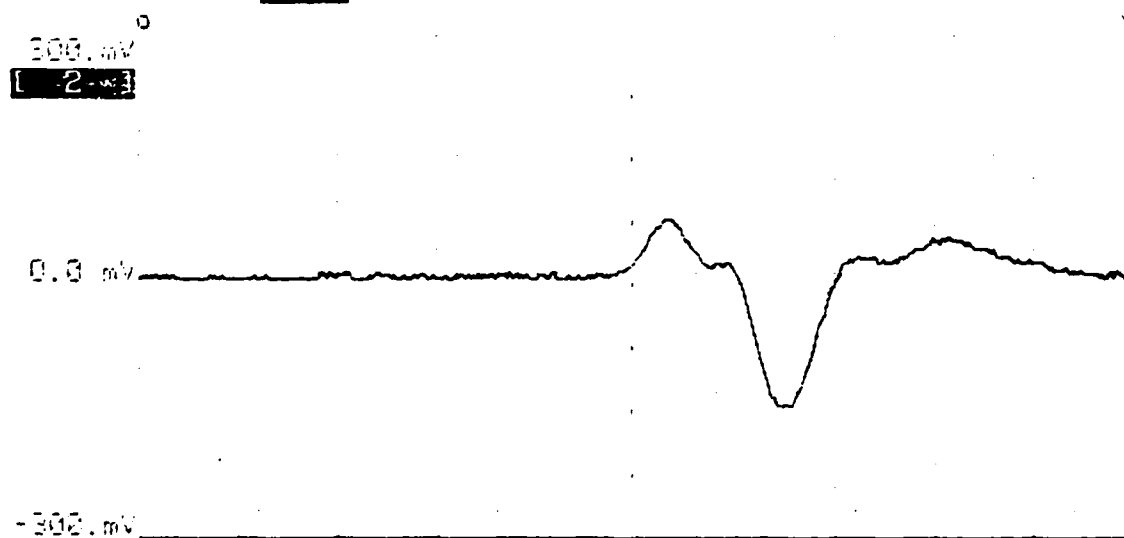
Analog [Waveform Diagram]-----INSERT to add traces-----

Sample Period [10 ms] [Time 1]
Magnification [1X] 1.000 s/div
Magnify About [x] 10.00 ms/sample
Cursor Moves [x] 9.992 s o to v



Analog [Waveform Diagram]-----INSERT to add traces-----

Sample Period [10 ms] [Time 3]
Magnification [1X] 1.000 s/div
Magnify About [x] 10.00 ms/sample
Cursor Moves [x] 9.992 s o to v

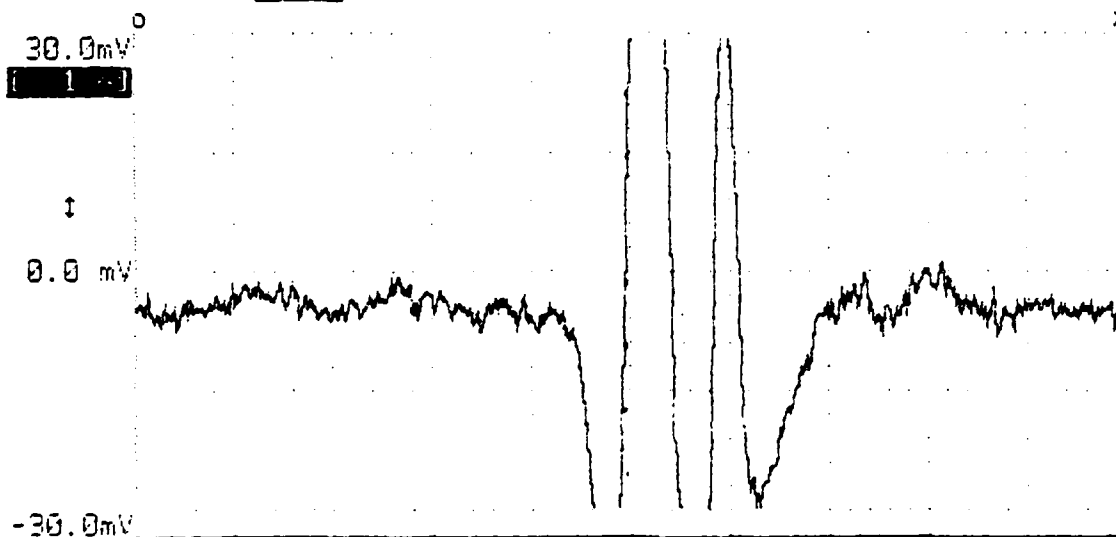


1. 3. 4. 5. 6. 7. 8. 9. 10. 11. 12. 13. 14. 15. 16. 17. 18. 19. 20. 21. 22. 23. 24. 25. 26. 27. 28. 29. 30. 31. 32. 33. 34. 35. 36. 37. 38. 39. 40. 41. 42. 43. 44. 45. 46. 47. 48. 49. 50. 51. 52. 53. 54. 55. 56. 57. 58. 59. 60. 61. 62. 63. 64. 65. 66. 67. 68. 69. 70. 71. 72. 73. 74. 75. 76. 77. 78. 79. 80. 81. 82. 83. 84. 85. 86. 87. 88. 89. 90. 91. 92. 93. 94. 95. 96. 97. 98. 99. 100. 101. 102. 103. 104. 105. 106. 107. 108. 109. 110. 111. 112. 113. 114. 115. 116. 117. 118. 119. 120. 121. 122. 123. 124. 125. 126. 127. 128. 129. 130. 131. 132. 133. 134. 135. 136. 137. 138. 139. 140. 141. 142. 143. 144. 145. 146. 147. 148. 149. 150. 151. 152. 153. 154. 155. 156. 157. 158. 159. 160. 161. 162. 163. 164. 165. 166. 167. 168. 169. 170. 171. 172. 173. 174. 175. 176. 177. 178. 179. 180. 181. 182. 183. 184. 185. 186. 187. 188. 189. 190. 191. 192. 193. 194. 195. 196. 197. 198. 199. 200. 201. 202. 203. 204. 205. 206. 207. 208. 209. 210. 211. 212. 213. 214. 215. 216. 217. 218. 219. 220. 221. 222. 223. 224. 225. 226. 227. 228. 229. 230. 231. 232. 233. 234. 235. 236. 237. 238. 239. 240. 241. 242. 243. 244. 245. 246. 247. 248. 249. 250. 251. 252. 253. 254. 255. 256. 257. 258. 259. 260. 261. 262. 263. 264. 265. 266. 267. 268. 269. 270. 271. 272. 273. 274. 275. 276. 277. 278. 279. 280. 281. 282. 283. 284. 285. 286. 287. 288. 289. 290. 291. 292. 293. 294. 295. 296. 297. 298. 299. 300. 301. 302. 303. 304. 305. 306. 307. 308. 309. 310. 311. 312. 313. 314. 315. 316. 317. 318. 319. 320. 321. 322. 323. 324. 325. 326. 327. 328. 329. 330. 331. 332. 333. 334. 335. 336. 337. 338. 339. 340. 341. 342. 343. 344. 345. 346. 347. 348. 349. 350. 351. 352. 353. 354. 355. 356. 357. 358. 359. 360. 361. 362. 363. 364. 365. 366. 367. 368. 369. 370. 371. 372. 373. 374. 375. 376. 377. 378. 379. 380. 381. 382. 383. 384. 385. 386. 387. 388. 389. 390. 391. 392. 393. 394. 395. 396. 397. 398. 399. 400. 401. 402. 403. 404. 405. 406. 407. 408. 409. 410. 411. 412. 413. 414. 415. 416. 417. 418. 419. 420. 421. 422. 423. 424. 425. 426. 427. 428. 429. 430. 431. 432. 433. 434. 435. 436. 437. 438. 439. 440. 441. 442. 443. 444. 445. 446. 447. 448. 449. 450. 451. 452. 453. 454. 455. 456. 457. 458. 459. 460. 461. 462. 463. 464. 465. 466. 467. 468. 469. 470. 471. 472. 473. 474. 475. 476. 477. 478. 479. 480. 481. 482. 483. 484. 485. 486. 487. 488. 489. 490. 491. 492. 493. 494. 495. 496. 497. 498. 499. 500. 501. 502. 503. 504. 505. 506. 507. 508. 509. 510. 511. 512. 513. 514. 515. 516. 517. 518. 519. 520. 521. 522. 523. 524. 525. 526. 527. 528. 529. 530. 531. 532. 533. 534. 535. 536. 537. 538. 539. 540. 541. 542. 543. 544. 545. 546. 547. 548. 549. 550. 551. 552. 553. 554. 555. 556. 557. 558. 559. 560. 561. 562. 563. 564. 565. 566. 567. 568. 569. 570. 571. 572. 573. 574. 575. 576. 577. 578. 579. 580. 581. 582. 583. 584. 585. 586. 587. 588. 589. 590. 591. 592. 593. 594. 595. 596. 597. 598. 599. 600. 601. 602. 603. 604. 605. 606. 607. 608. 609. 610. 611. 612. 613. 614. 615. 616. 617. 618. 619. 620. 621. 622. 623. 624. 625. 626. 627. 628. 629. 630. 631. 632. 633. 634. 635. 636. 637. 638. 639. 640. 641. 642. 643. 644. 645. 646. 647. 648. 649. 650. 651. 652. 653. 654. 655. 656. 657. 658. 659. 660. 661. 662. 663. 664. 665. 666. 667. 668. 669. 670. 671. 672. 673. 674. 675. 676. 677. 678. 679. 680. 681. 682. 683. 684. 685. 686. 687. 688. 689. 690. 691. 692. 693. 694. 695. 696. 697. 698. 699. 700. 701. 702. 703. 704. 705. 706. 707. 708. 709. 710. 711. 712. 713. 714. 715. 716. 717. 718. 719. 720. 721. 722. 723. 724. 725. 726. 727. 728. 729. 730. 731. 732. 733. 734. 735. 736. 737. 738. 739. 740. 741. 742. 743. 744. 745. 746. 747. 748. 749. 750. 751. 752. 753. 754. 755. 756. 757. 758. 759. 760. 761. 762. 763. 764. 765. 766. 767. 768. 769. 770. 771. 772. 773. 774. 775. 776. 777. 778. 779. 780. 781. 782. 783. 784. 785. 786. 787. 788. 789. 790. 791. 792. 793. 794. 795. 796. 797. 798. 799. 800. 801. 802. 803. 804. 805. 806. 807. 808. 809. 810. 811. 812. 813. 814. 815. 816. 817. 818. 819. 820. 821. 822. 823. 824. 825. 826. 827. 828. 829. 830. 831. 832. 833. 834. 835. 836. 837. 838. 839. 840. 841. 842. 843. 844. 845. 846. 847. 848. 849. 850. 851. 852. 853. 854. 855. 856. 857. 858. 859. 860. 861. 862. 863. 864. 865. 866. 867. 868. 869. 870. 871. 872. 873. 874. 875. 876. 877. 878. 879. 880. 881. 882. 883. 884. 885. 886. 887. 888. 889. 890. 891. 892. 893. 894. 895. 896. 897. 898. 899. 900. 901. 902. 903. 904. 905. 906. 907. 908. 909. 910. 911. 912. 913. 914. 915. 916. 917. 918. 919. 920. 921. 922. 923. 924. 925. 926. 927. 928. 929. 930. 931. 932. 933. 934. 935. 936. 937. 938. 939. 940. 941. 942. 943. 944. 945. 946. 947. 948. 949. 950. 951. 952. 953. 954. 955. 956. 957. 958. 959. 960. 961. 962. 963. 964. 965. 966. 967. 968. 969. 970. 971. 972. 973. 974. 975. 976. 977. 978. 979. 980. 981. 982. 983. 984. 985. 986. 987. 988. 989. 990. 991. 992. 993. 994. 995. 996. 997. 998. 999. 1000. 1001. 1002. 1003. 1004. 1005. 1006. 1007. 1008. 1009. 1010. 1011. 1012. 1013. 1014. 1015. 1016. 1017. 1018. 1019. 1020. 1021. 1022. 1023. 1024. 1025. 1026. 1027. 1028. 1029. 1030. 1031. 1032. 1033. 1034. 1035. 1036. 1037. 1038. 1039. 1040. 1041. 1042. 1043. 1044. 1045. 1046. 1047. 1048. 1049. 1050. 1051. 1052. 1053. 1054. 1055. 1056. 1057. 1058. 1059. 1060. 1061. 1062. 1063. 1064. 1065. 1066. 1067. 1068. 1069. 1070. 1071. 1072. 1073. 1074. 1075. 1076. 1077. 1078. 1079. 1080. 1081. 1082. 1083. 1084. 1085. 1086. 1087. 1088. 1089. 1090. 1091. 1092. 1093. 1094. 1095. 1096. 1097. 1098. 1099. 1100. 1101. 1102. 1103. 1104. 1105. 1106. 1107. 1108. 1109. 1110. 1111. 1112. 1113. 1114. 1115. 1116. 1117. 1118. 1119. 1120. 1121. 1122. 1123. 1124. 1125. 1126. 1127. 1128. 1129. 1130. 1131. 1132. 1133. 1134. 1135. 1136. 1137. 1138. 1139. 1140. 1141. 1142. 1143. 1144. 1145. 1146. 1147. 1148. 1149. 1150. 1151. 1152. 1153. 1154. 1155. 1156. 1157. 1158. 1159. 1160. 1161. 1162. 1163. 1164. 1165. 1166. 1167. 1168. 1169. 1170. 1171. 1172. 1173. 1174. 1175. 1176. 1177. 1178. 1179. 1180. 1181. 1182. 1183. 1184. 1185. 1186. 1187. 1188. 1189. 1190. 1191. 1192. 1193. 1194. 1195. 1196. 1197. 1198. 1199. 1200. 1201. 1202. 1203. 1204. 1205. 1206. 1207. 1208. 1209. 1210. 1211. 1212. 1213. 1214. 1215. 1216. 1217. 1218. 1219. 1220. 1221. 1222. 1223. 1224. 1225. 1226. 1227. 1228. 1229. 1230. 1231. 1232. 1233. 1234. 1235. 1236. 1237. 1238. 1239. 1240. 1241. 1242. 1243. 1244. 1245. 1246. 1247. 1248. 1249. 1250. 1251. 1252. 1253. 1254. 1255. 1256. 1257. 1258. 1259. 1260. 1261. 1262. 1263. 1264. 1265. 1266. 1267. 1268. 1269. 1270. 1271. 1272. 1273. 1274. 1275. 1276. 1277. 1278. 1279. 1280. 1281. 1282. 1283. 1284. 1285. 1286. 1287. 1288. 1289. 1290. 1291. 1292. 1293. 1294. 1295. 1296. 1297. 1298. 1299. 1300. 1301. 1302. 1303. 1304. 1305. 1306. 1307. 1308. 1309. 1310. 1311. 1312. 1313. 1314. 1315. 1316. 1317. 1318. 1319. 1320. 1321. 1322. 1323. 1324. 1325. 1326. 1327. 1328. 1329. 1330. 1331. 1332. 1333. 1334. 1335. 1336. 1337. 1338. 1339. 1340. 1341. 1342. 1343. 1344. 1345. 1346. 1347. 1348. 1349. 1350. 1351. 1352. 1353. 1354. 1355. 1356. 1357. 1358. 1359. 1360. 1361. 1362. 1363. 1364. 1365. 1366. 1367. 1368. 1369. 1370. 1371. 1372. 1373. 1374. 1375. 1376. 1377. 1378. 1379. 1380. 1381. 1382. 1383. 1384. 1385. 1386. 1387. 1388. 1389. 1390. 1391. 1392. 1393. 1394. 1395. 1396. 1397. 1398. 1399. 1400. 1401. 1402. 1403. 1404. 1405. 1406. 1407. 1408. 1409. 1410. 1411. 1412. 1413. 1414. 1415. 1416. 1417. 1418. 1419. 1420. 1421. 1422. 1423. 1424. 1425. 1426. 1427. 1428. 1429. 1430. 1431. 1432. 1433. 1434. 1435. 1436. 1437. 1438. 1439. 1440. 1441. 1442. 1443. 1444. 1445. 1446. 1447. 1448. 1449. 1450. 1451. 1452. 1453. 1454. 1455. 1456. 1457. 1458. 1459. 1460. 1461. 1462. 1463. 1464. 1465. 1466. 1467. 1468. 1469. 1470. 1471. 1472. 1473. 1474. 1475. 1476. 1477. 1478. 1479. 1480. 1481. 1482. 1483. 1484. 1485. 1486. 1487. 1488. 1489. 1490. 1491. 1492. 1493. 1494. 1495. 1496. 1497. 1498. 1499. 1500. 1501. 1502. 1503. 1504. 1505. 1506. 1507. 1508. 1509. 1510. 1511. 1512. 1513. 1514. 1515. 1516. 1517. 1518. 1519. 1520. 1521. 1522. 1523. 1524. 1525. 1526. 1527. 1528. 1529. 1530. 1531. 1532. 1533. 1534. 1535. 1536. 1537. 1538. 1539. 1540. 1541. 1542. 1543. 1544. 1545. 1546. 1547. 1548. 1549. 1550. 1551. 1552. 1553. 1554. 1555. 1556. 1557. 1558. 1559. 1560. 1561. 1562. 1563. 1564. 1565. 1566. 1567. 1568. 1569. 1570. 1571. 1572. 1573. 1574. 1575. 1576. 1577. 1578. 1579. 1580. 1581. 1582. 1583. 1584. 1585. 1586. 1587. 1588. 1589. 1590. 1591. 1592. 1593. 1594. 1595. 1596. 1597. 1598. 1599. 1600. 1601. 1602. 1603. 1604. 1605. 1606. 1607. 1608. 1609. 1610. 1611. 1612. 1613. 1614. 1615. 1616. 1617. 1618. 1619. 1620. 1621. 1622. 1623. 1624. 1625. 1626. 1627. 1628. 1629. 1630. 1631. 1632. 1633. 1634. 1635. 1636. 1637. 1638. 1639. 1640. 1641. 1642. 1643. 1644. 1645. 1646. 1647. 1648. 1649. 1650. 1651. 1652. 1653. 1654. 1655. 1656. 1657. 1658. 1659. 1660. 1661. 1662. 1663. 1664. 1665. 1666. 1667. 1668. 1669. 1670. 1671. 1672. 1673. 1674. 1675. 1676. 1677. 1678. 1679. 1680. 1681. 1682. 1683. 1684. 1685. 1686. 1687. 1688. 1689. 1690. 1691. 1692. 1693. 1694. 1695. 1696. 1697. 1698. 1699. 1700. 1701. 1702. 1703. 1704. 1705. 1706. 1707. 1708. 1709. 1710. 1711. 1712. 1713. 1714. 1715. 1716. 1717. 1718. 1719. 1720. 1721. 1722. 1723. 1724. 1725. 1726. 1727. 1728. 1729. 1730. 1731. 1732. 1733. 1734. 1735. 1736. 1737. 1738. 1739. 1740. 1741. 1742. 1743. 1744. 1745. 1746. 1747. 1748. 1749. 1750. 1751. 1752. 1753. 1754. 1755. 1756. 1757. 1758. 1759. 1760. 1761. 1762. 1763. 1764. 1765. 1766. 1767. 1768. 1769. 1770. 1771. 1772. 1773. 1774. 1775. 1776. 1777. 1778. 1779. 1780. 1781. 1782. 1783. 1784. 1785. 1786. 1787. 1788. 1789. 1790. 1791. 1792. 1793. 1794. 1795. 1796. 1797. 1798. 1799. 1800. 1801. 1802. 1803. 1804. 1805. 1806. 1807. 1808. 1809. 1810. 1811. 1812. 1813. 1814. 1815. 1816. 1817. 1818. 1819. 1820. 1821. 1822. 1823. 1824. 1825. 1826. 1827. 1828. 1829. 1830. 1831. 1832. 1833. 1834. 1835. 1836. 1837. 1838. 1839. 1840. 1841. 1842. 1843. 1844. 1845. 1846. 1847. 1848. 1849. 1850. 1851. 1852. 1853. 1854. 1855. 1856. 1857. 1858. 1859. 1860. 1861. 1862. 1863. 1864. 1865. 1866. 1867. 1868. 1869. 1870. 1871. 1872. 1873. 1874. 1875. 1876. 1877. 1878. 1879. 1880. 1881. 1882. 1883. 1884. 1885. 1886. 1887. 1888. 1889. 1890. 1891. 1892. 1893. 1894. 1895. 1896. 1897. 1898. 1899. 1900. 1901. 1902. 1903. 1904. 1905. 1906. 1907. 1908. 1909. 1910. 1911. 1912. 1913. 1914. 1915. 1916. 1917. 1918. 1919. 1920. 1921. 1922. 1923. 1924. 1925. 1926. 1927. 1928. 1929. 1930. 1931. 1932. 1933. 1934. 1935. 1936. 1937. 1938. 1939. 1940. 1941. 1942. 1943. 1944. 1945. 1946. 1947. 1948. 1949. 1950. 1951. 1952. 1953. 1954. 1955. 1956. 1957. 1958. 1959. 1960. 1961. 1962. 1963. 1964. 1965. 1966. 1967. 1968. 1969. 1970. 1971. 1972. 1973. 1974. 1975. 1976. 1977. 1978. 1979. 1980. 1981. 1982. 1983. 1984. 1985. 1986. 1987. 1988. 1989. 1990. 1991. 1992. 1993. 1994. 1995. 1996. 1997. 1998. 1999. 2000. 2001. 2002. 2003. 2004. 2005. 2006. 2007. 2008. 2009. 2010. 2011. 2012. 2013. 2014. 2015. 2016. 2017. 2018. 2019. 2020. 2021. 2022. 2023. 2024. 2025. 2026. 2027. 2028. 2029. 2030. 2031. 2032. 2033. 2034. 2035. 2036. 2037. 2038. 2039. 2040. 2041. 2042. 2043. 2044. 2045. 2046. 2047. 2048. 2049. 2050. 2051. 2052. 2053. 2054. 2055. 2056. 2057. 2058. 2059. 2060. 2061. 2062. 2063. 2064. 2065. 2066. 2067. 2068. 2069. 2070. 2071. 2072. 2073. 2074. 2075. 2076. 2077. 2078. 2079. 2080. 2081. 2082. 2083. 2084. 2085. 2086. 2087. 2088. 2089. 2090. 2091. 2092. 2093. 2094. 2095. 2096. 2097. 2098. 2099. 2100. 2101. 2102. 2103. 2104. 2105. 2106. 2107. 2108. 2109. 2110. 2111. 2112. 2113. 2114. 2115. 2116. 2117. 2118. 2119. 2120. 2121. 2122. 2123. 2124. 2125. 2126. 21

7/21/92
W. C. W.

Analog [Waveform Diagram] -----INSERT to add traces-----

Sample Period [200 ms] [Time 3]
Magnification [1X] 2.000 s/div
Magnify About [X] 20.00 ms/sample
Cursor Moves [X] 19.98 s o to x



Analog [Waveform Diagram] -----INSERT to add traces-----

Sample Period [20 ms] [Time 3]
Magnification [1X] 2.000 s/div
Magnify About [X] 20.00 ms/sample
Cursor Moves [X] 19.98 s o to x

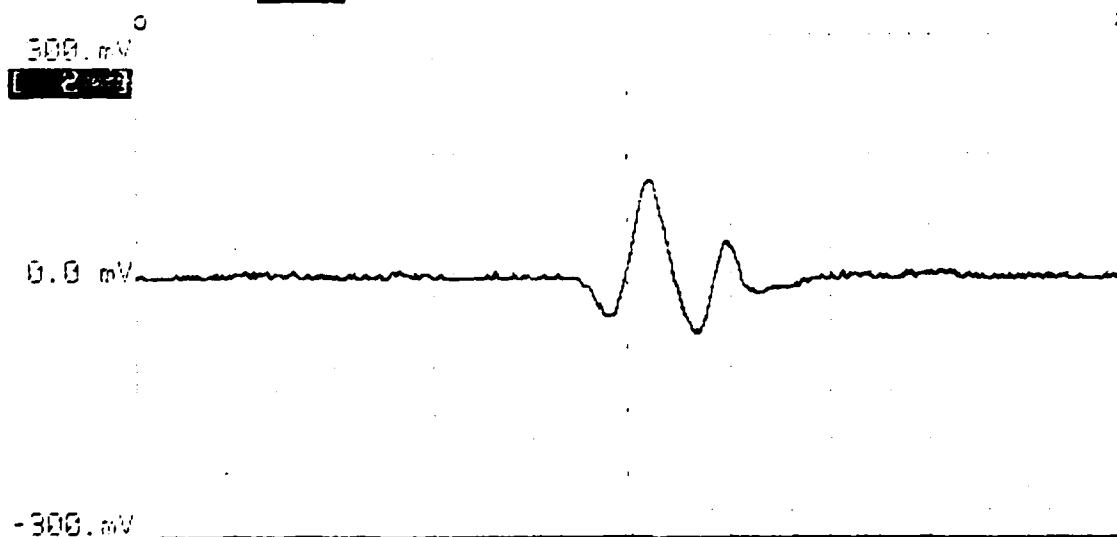
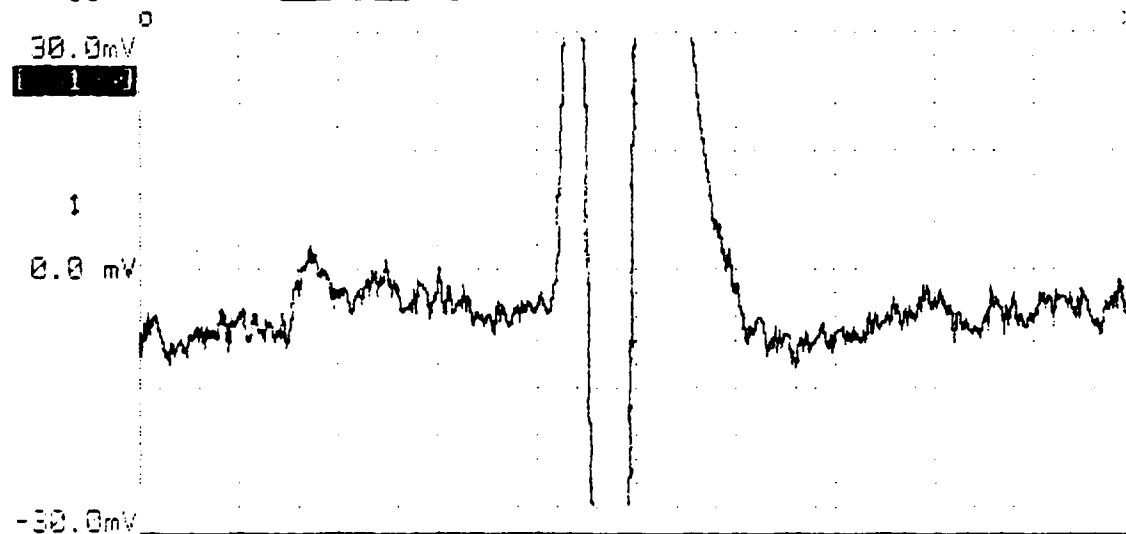


FIGURE 19

Analog [Waveform Trace] -----

Sample Period [20 ms] [Single] Trace Mode
[Center] Trace [000] [ns] After Trigger
Trigger [1] [Rising]
Trigger Level [+] 1.015V



Analog [Waveform Trace] -----INSERT to add traces-----

Sample Period [20 ms] [Single] Trace Mode
[Center] Trace [000] [ns] After Trigger
Trigger [1] [Rising]
Trigger Level [+] 1.015V

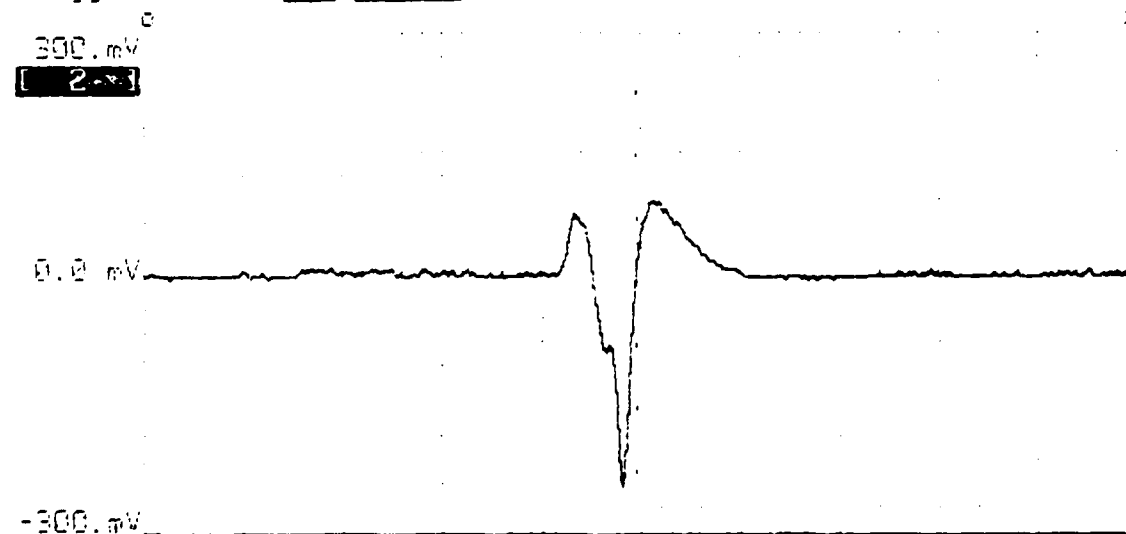


FIGURE 20

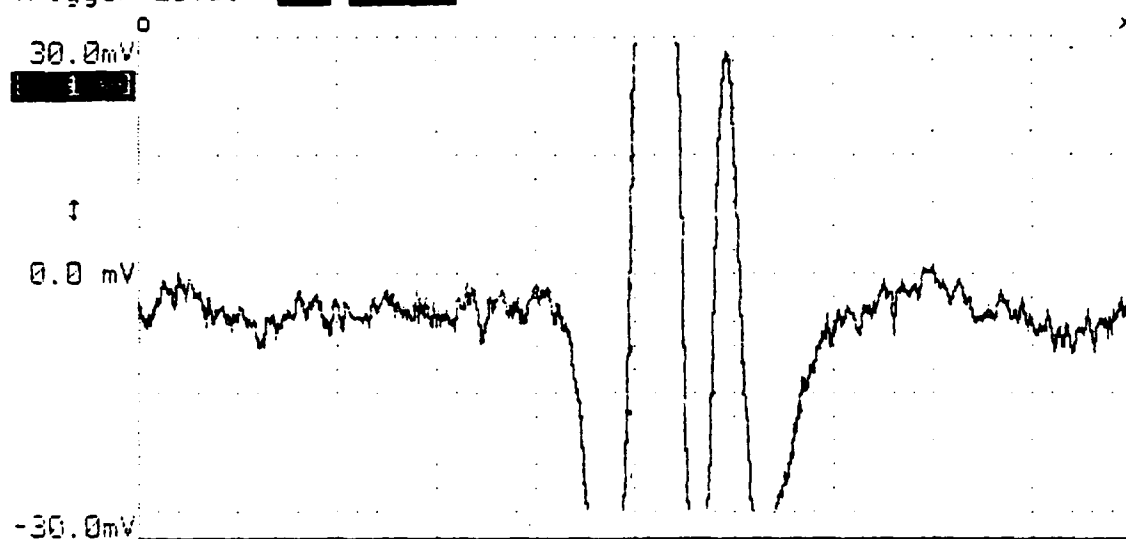
Analogue ☐ Waveform 1 Trace ☐ INSERT to add traces

Sample Period ☐ 20 ms ☐ Single Trace Mode

☐ Center Trace ☐ 1000 ns After Trigger

Trigger ☐ 1.015V ☐ Rising

Trigger Level ☐ 1.015V



Analogue ☐ Waveform 2 Trace ☐ INSERT to add traces

Sample Period ☐ 20 ms ☐ Single Trace Mode

☐ Center Trace ☐ 1000 ns After Trigger

Trigger ☐ 1.015V ☐ Rising

Trigger Level ☐ 1.015V

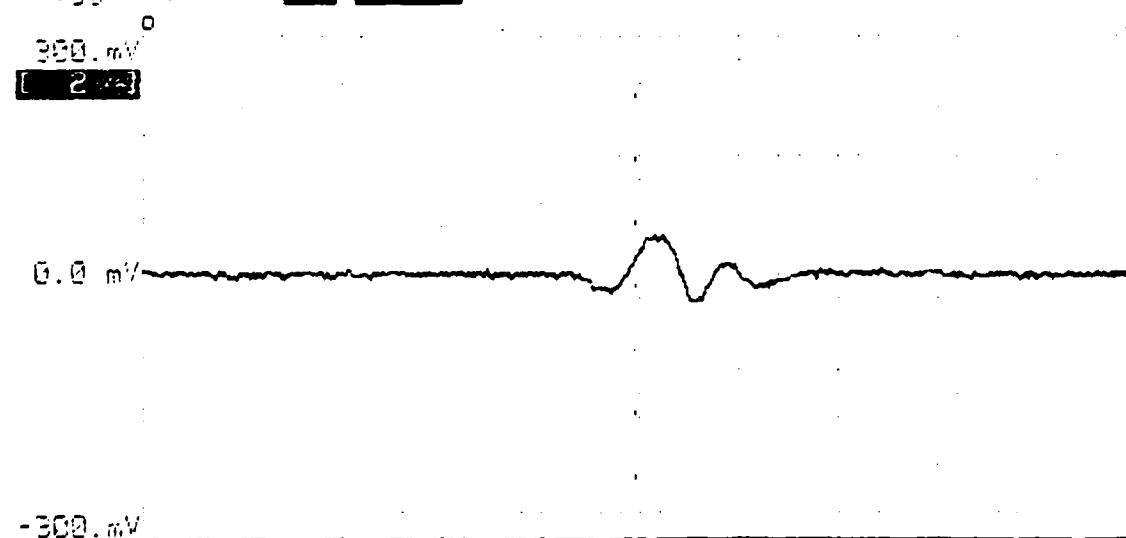


FIGURE 21

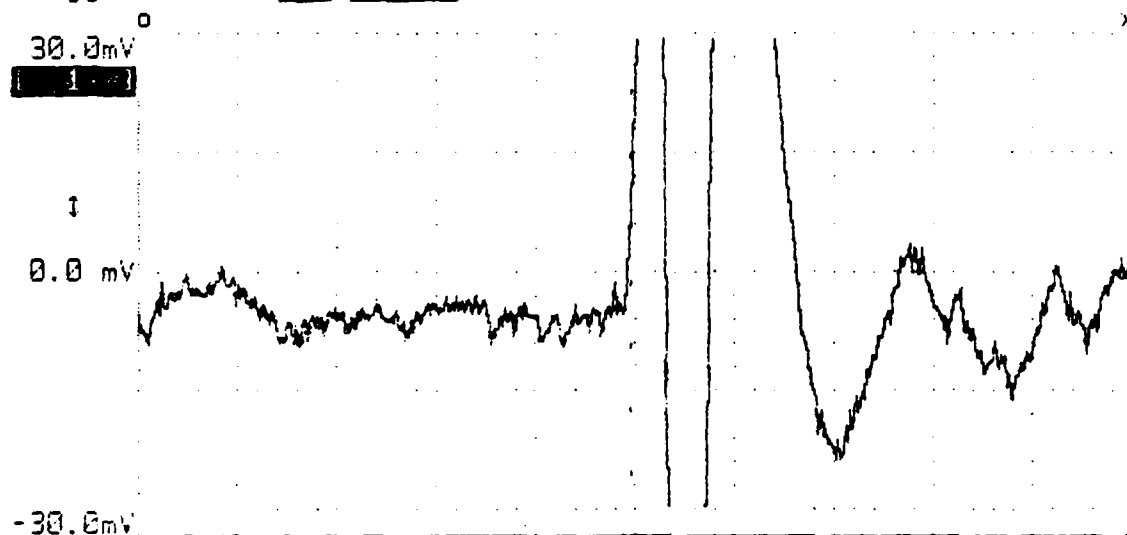
Analog [Waveform / Trace] -----INSERT to add traces-----

Sample Period [20 ms] [Single] Trace Mode

[Center] Trace [0.00] [ns] After Trigger

Trigger [1] [Rising]

Trigger Level [+ 0.015V



Analog [Waveform / Trace] -----INSERT to add traces-----

Sample Period [20 ms] [Single] Trace Mode

[Center] Trace [0.00] [ns] After Trigger

Trigger [1] [Rising]

Trigger Level [+ 0.015V

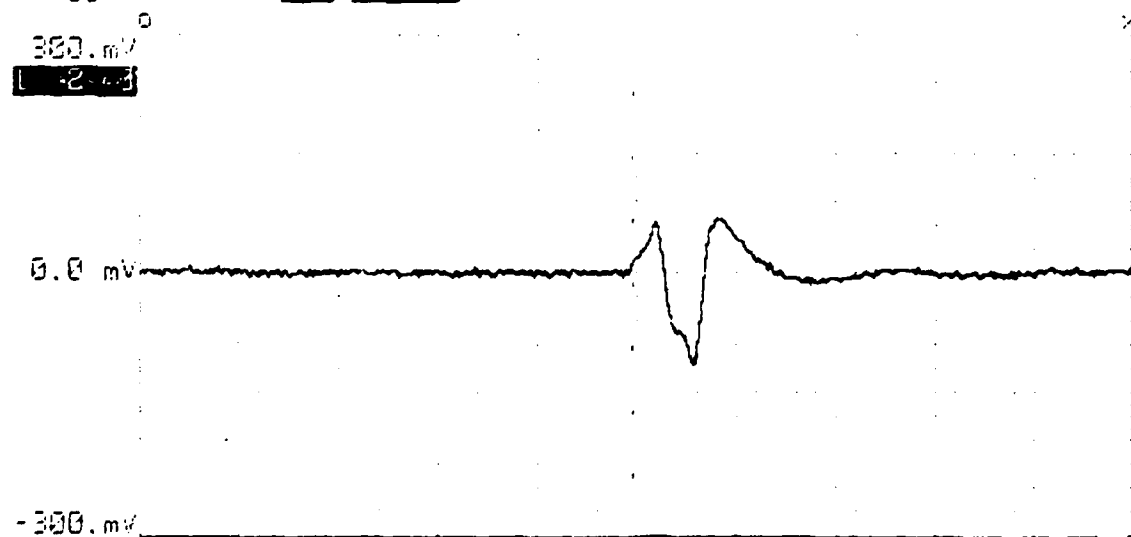


FIGURE 22

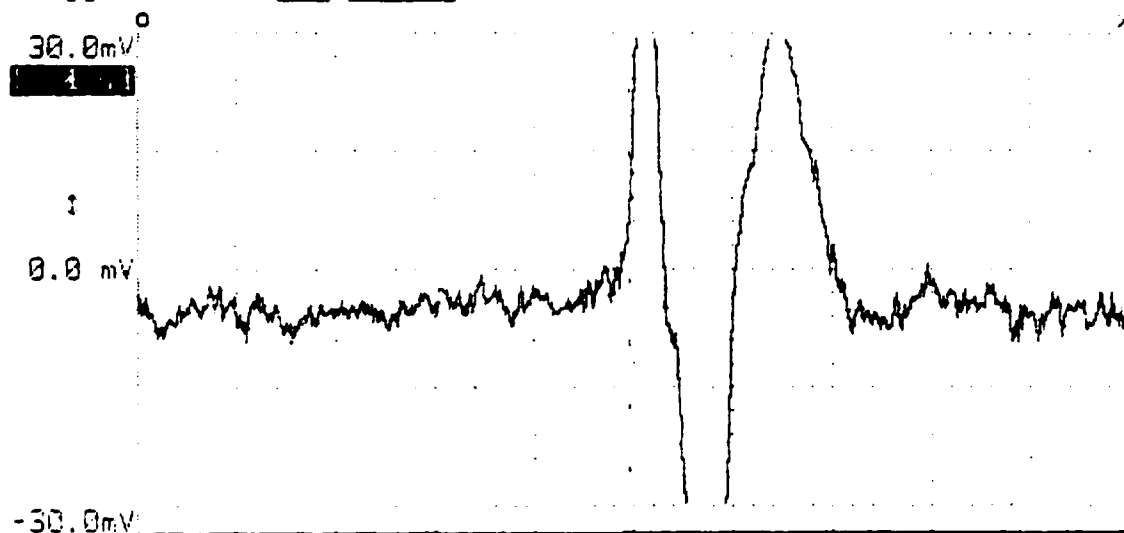
Analog []-----INSERT to add traces-----

Sample Period [20 ms] [Single] Trace Mode

[Center] Trace [000] [ns] After Trigger

Trigger [1] [Rising]

Trigger Level [+] 0.015V



Analog [Waveform / Trace]-----INSERT to add traces-----

Sample Period [20 ms] [Single] Trace Mode

[Center] Trace [000] [ns] After Trigger

Trigger [1] [Rising]

Trigger Level [+] 0.015V

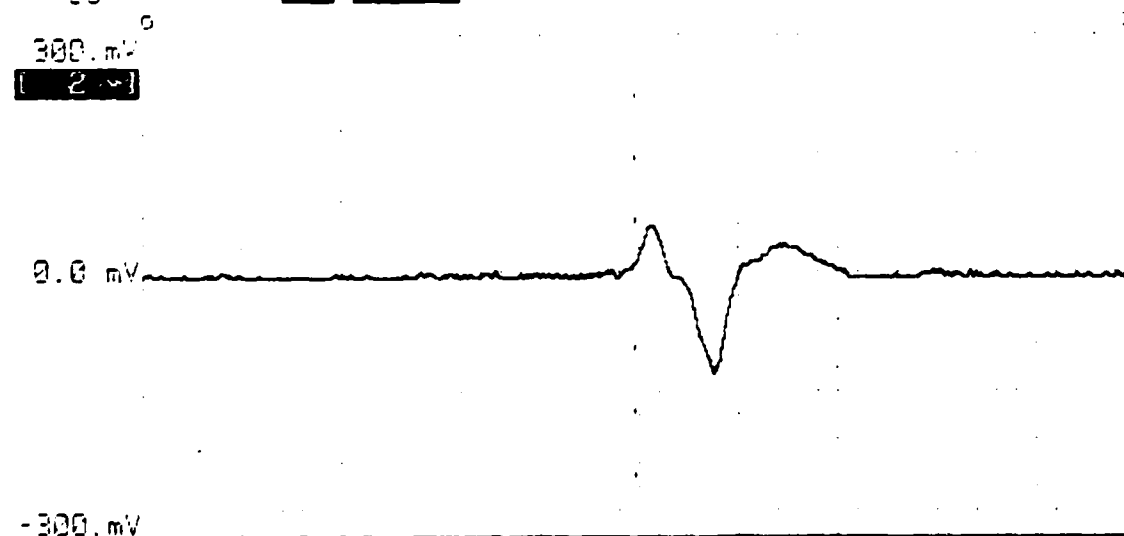


FIGURE 23

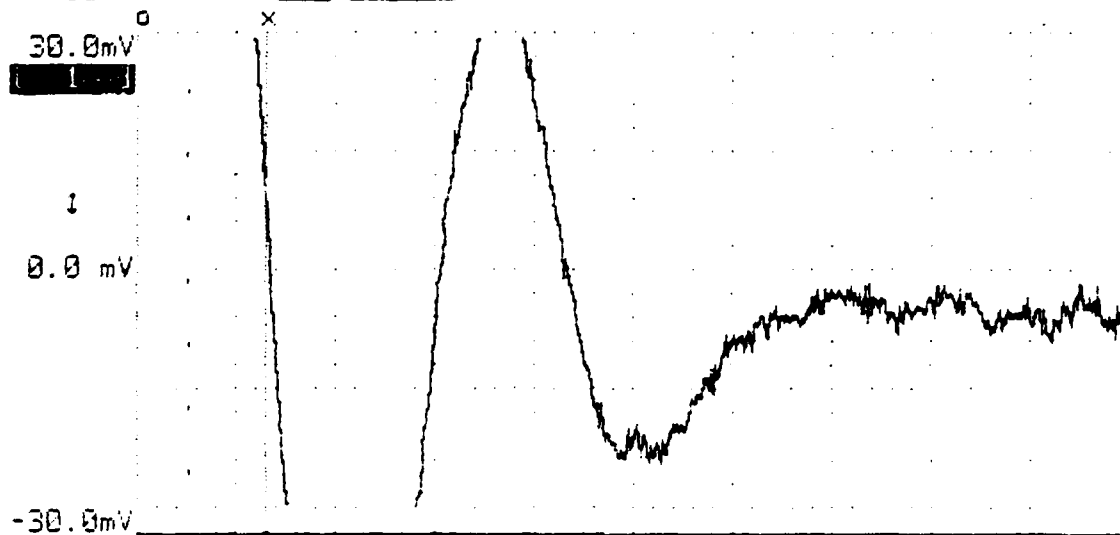
Analog ☐ Waveform ☒ Traces -----INSERT to add traces-----

Sample Period ☐ 5 ms ☒ Single Trace Mode

☒ Start Trace ☐ 500 ms After Trigger

Trigger ☐ 1 ms ☒ Rising

Trigger Level ☒ 0.015V



Analog ☐ Waveform ☒ Traces -----INSERT to add traces-----

Sample Period ☐ 5 ms ☒ Single Trace Mode

☒ Start Trace ☐ 500 ms After Trigger

Trigger ☐ 1 ms ☒ Rising

Trigger Level ☒ 0.015V

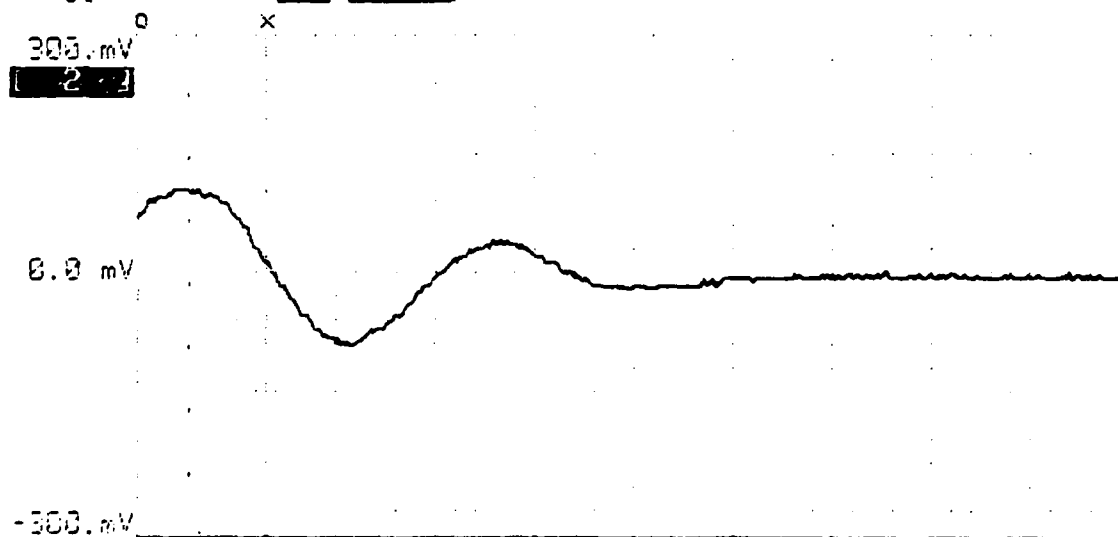


FIGURE 24

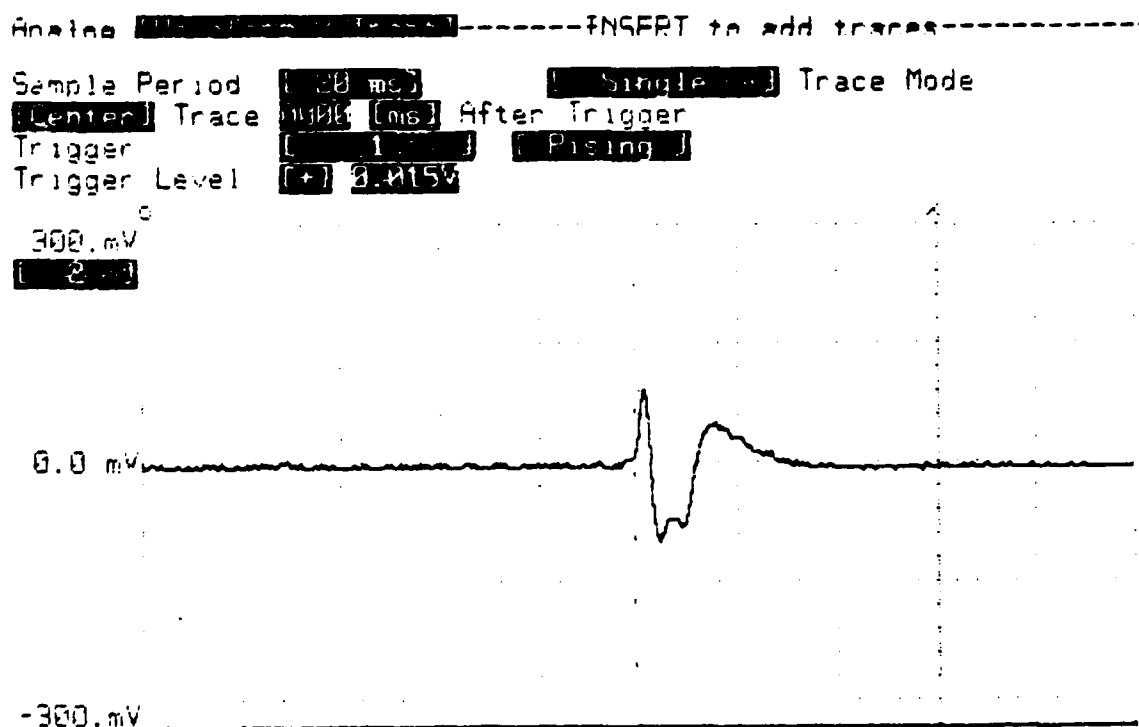
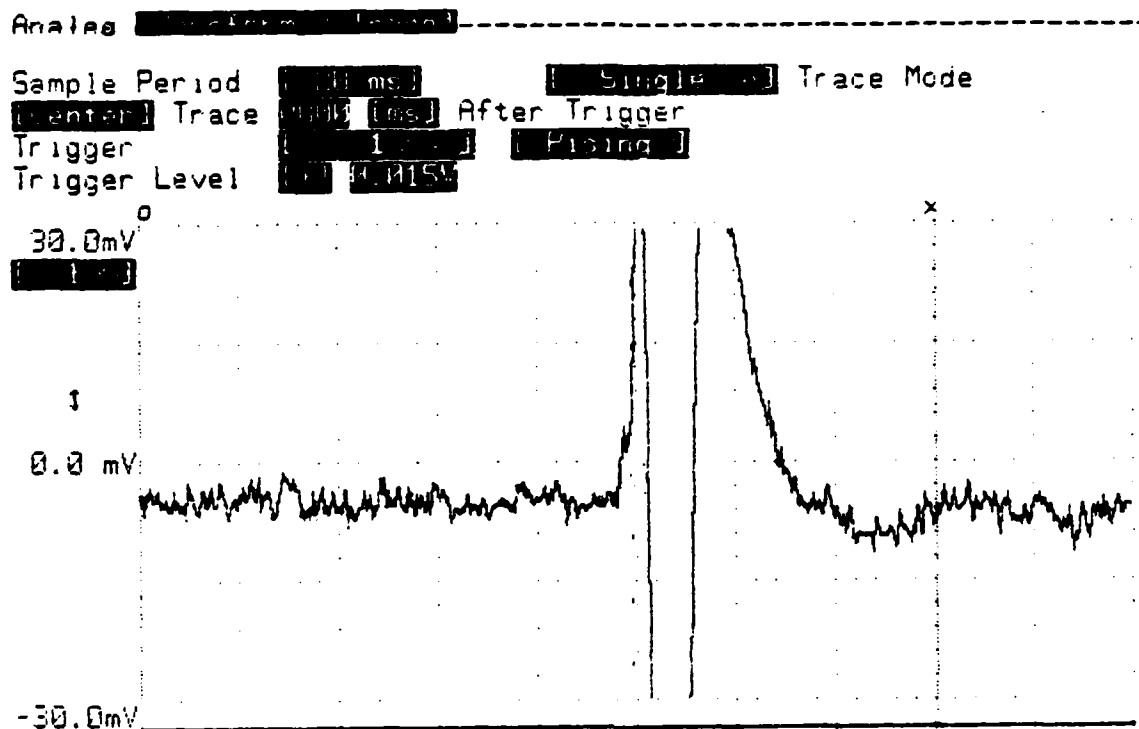
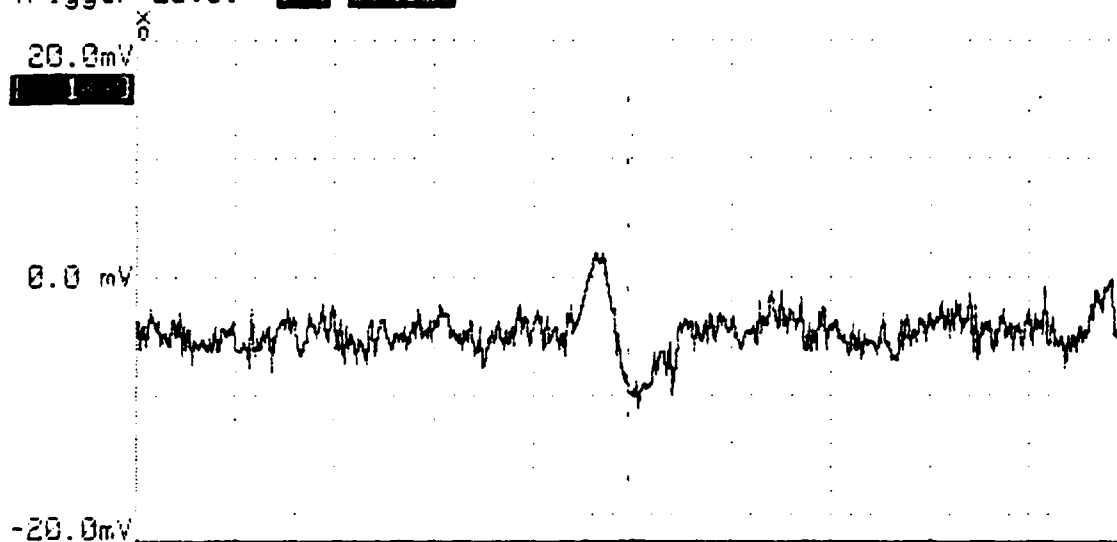


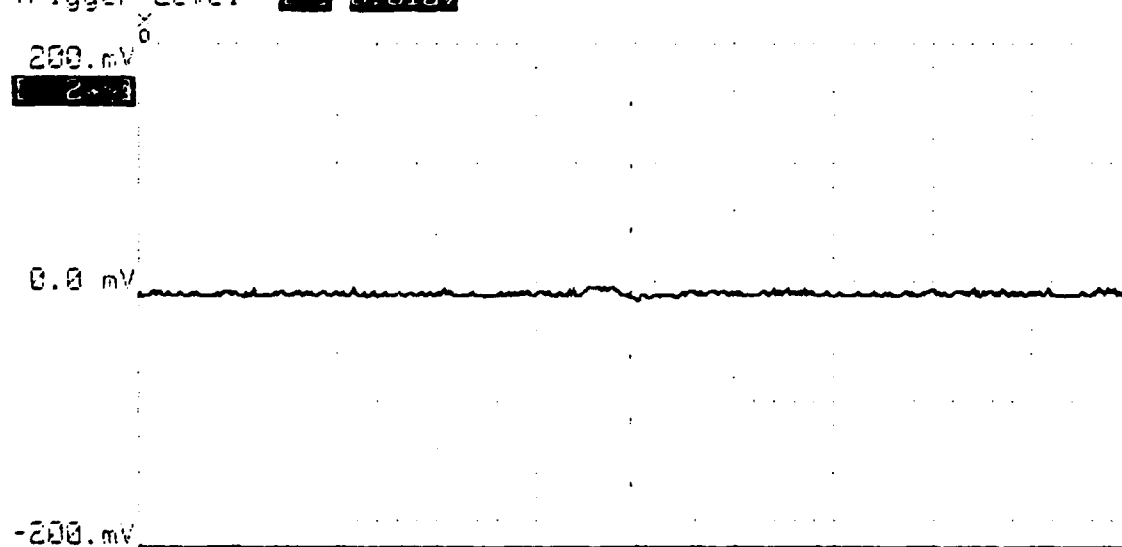
FIGURE 25

Sample Period [10 ms] [Single] Trace Mode
[Enter] Trace [400] [ns] After Trigger
Trigger [1] [Pulse] 1s/div
Trigger Level [0.018V]



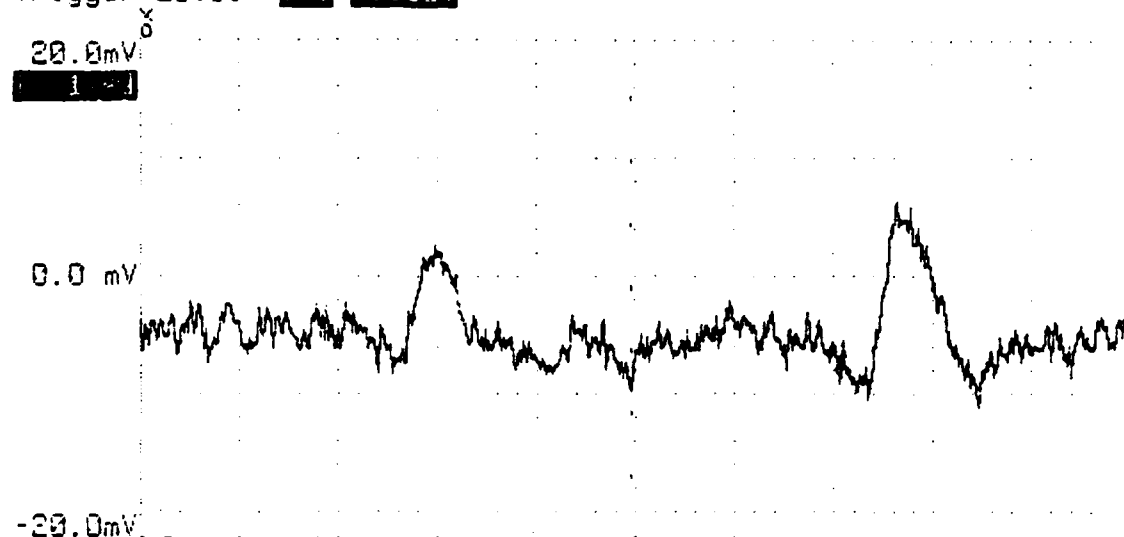
Another ~~XXXXXXXXXXXXXXXXXXXX~~-----INSERT to add trace-----

Sample Period [10 ms] [Single] Trace Mode
[Enter] Trace 0000 [ns] After Trigger
Trigger [1000] [Rising] 1s/div
Trigger Level [-] 0.010V

**FIGURE 26**

Analog ☐ Waveform 1 Trace ☐ INSERT to add traces

Sample Period ☐ 10 ms ☐ Single Trace Mode
☐ Center Trace ☐ 1000 ns After Trigger
Trigger ☐ 1.000V ☐ Rising ☐ 1s/d
Trigger Level ☐ 1.010V



Analog ☐ Waveform 2 Trace ☐ INSERT to add traces

Sample Period ☐ 10 ms ☐ Single Trace Mode
☐ Center Trace ☐ 1000 ns After Trigger
Trigger ☐ 1.000V ☐ Rising ☐ 1s/d
Trigger Level ☐ 1.010V

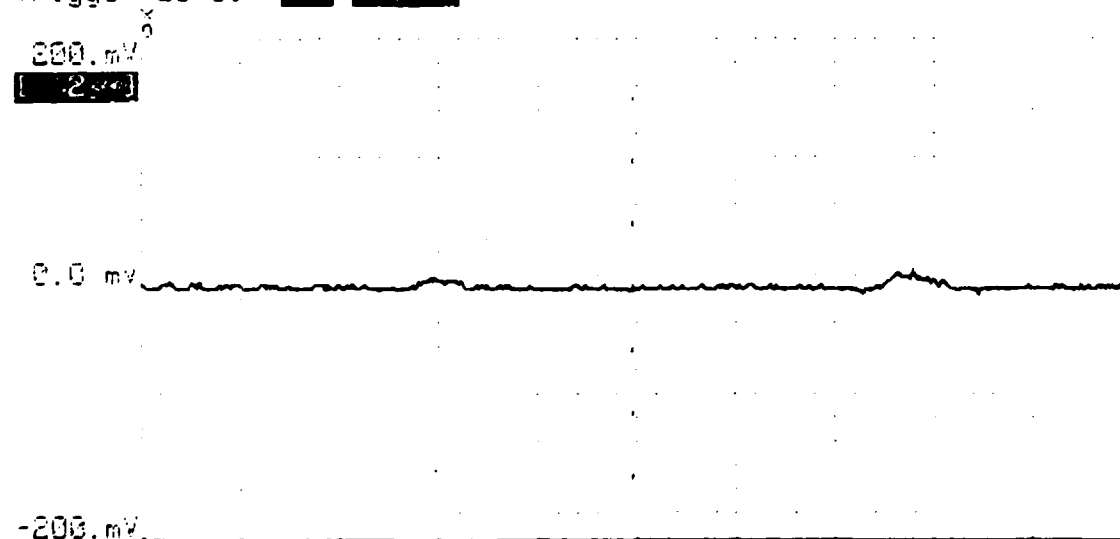


FIGURE 27

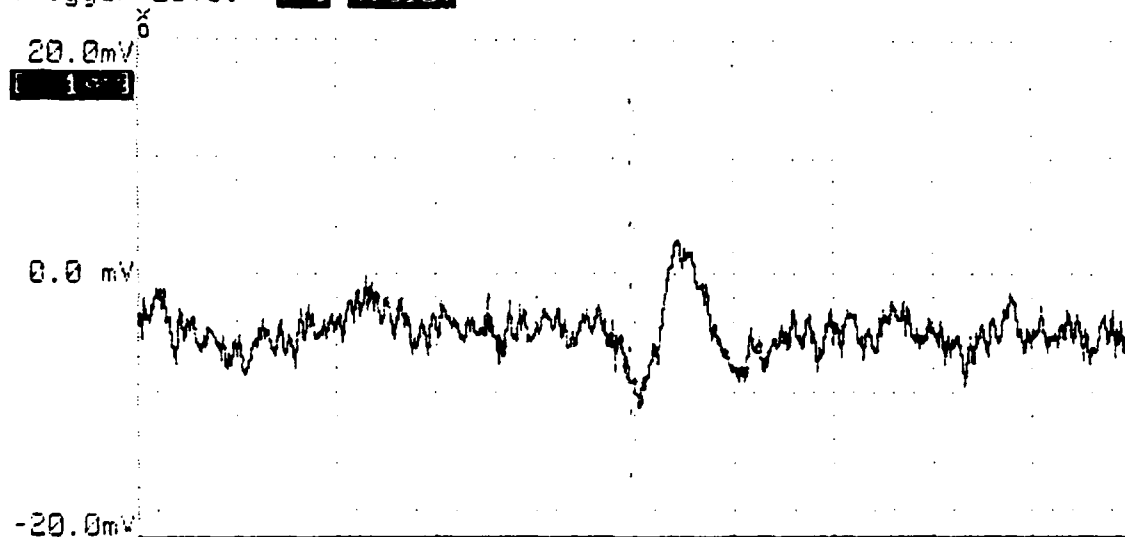
Analog [Waveform 1 Trace] -----INSERT to add traces-----

Sample Period [10 ms] [Single] Trace Mode

[Center] Trace 0000 [ns] After Trigger

Trigger [1.000] [Rising] 1s/2.

Trigger Level [0.010V]



Analog [Waveform 2 Trace] -----INSERT to add traces-----

Sample Period [10 ms] [Single] Trace Mode

[Center] Trace 0000 [ns] After Trigger

Trigger [1.000] [Rising] 1s/2.

Trigger Level [0.010V]

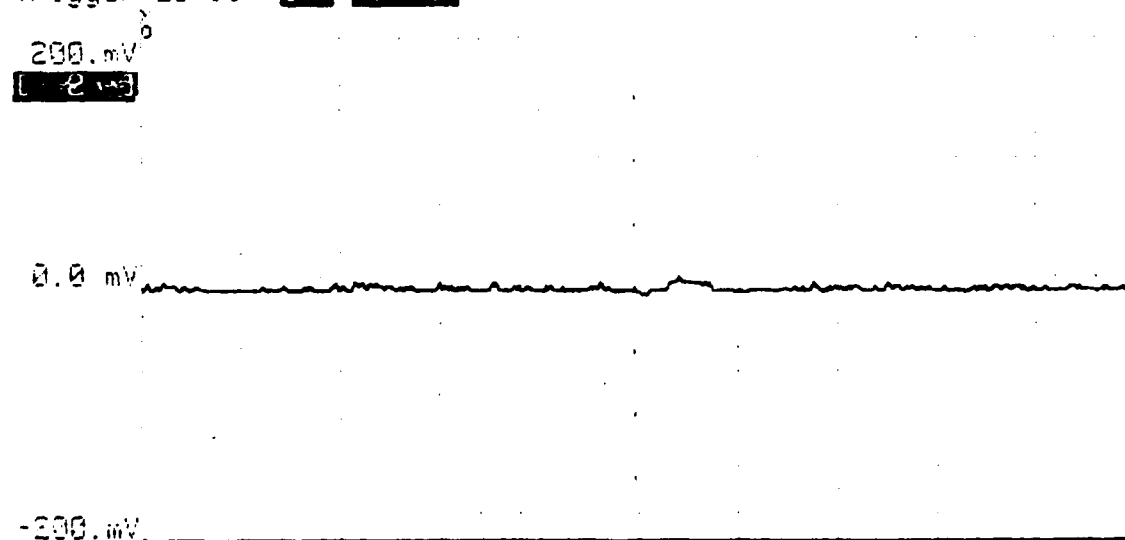
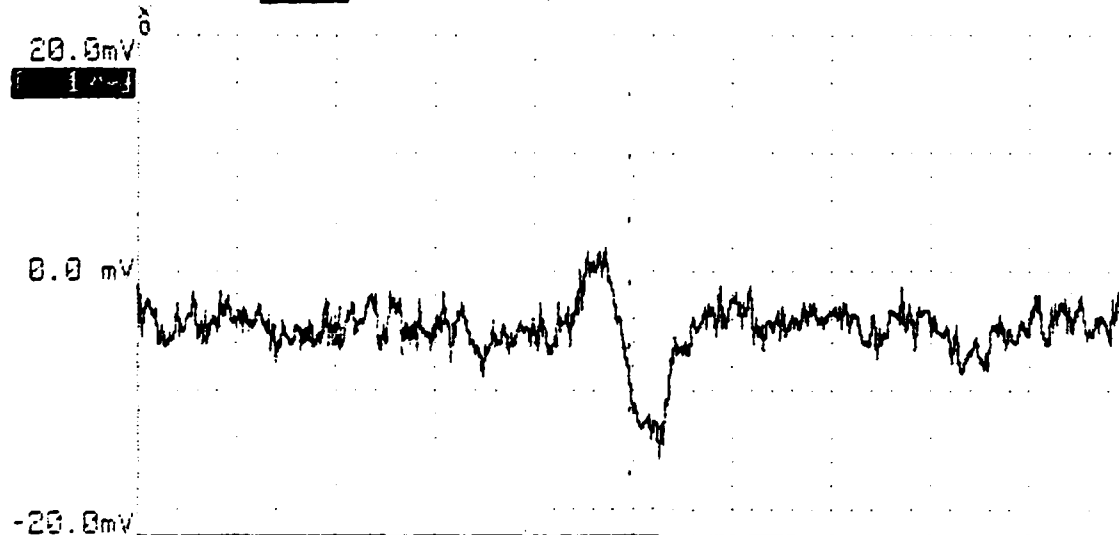


FIGURE 28

Analog **Waveform Diagram**-----

Sample Period **[10 ms]** **[Time]**
Magnification **[1X]** 1.000 s/div
Magnify About **[x]** 10.00 ms/sample
Cursor Moves **[x]** 0.0 μ s 0 to x



Analog **Waveform Diagram**-----INSERT to add traces-----

Sample Period **[10 ms]** **[Time]**
Magnification **[1X]** 1.000 s/div
Magnify About **[x]** 10.00 ms/sample
Cursor Moves **[x]** 0.0 μ s 0 to x

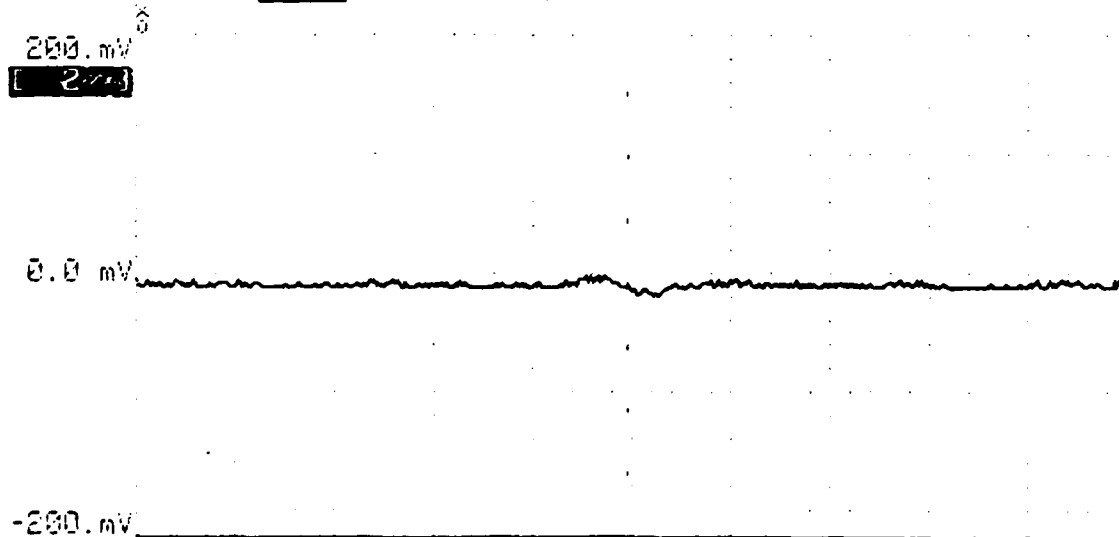
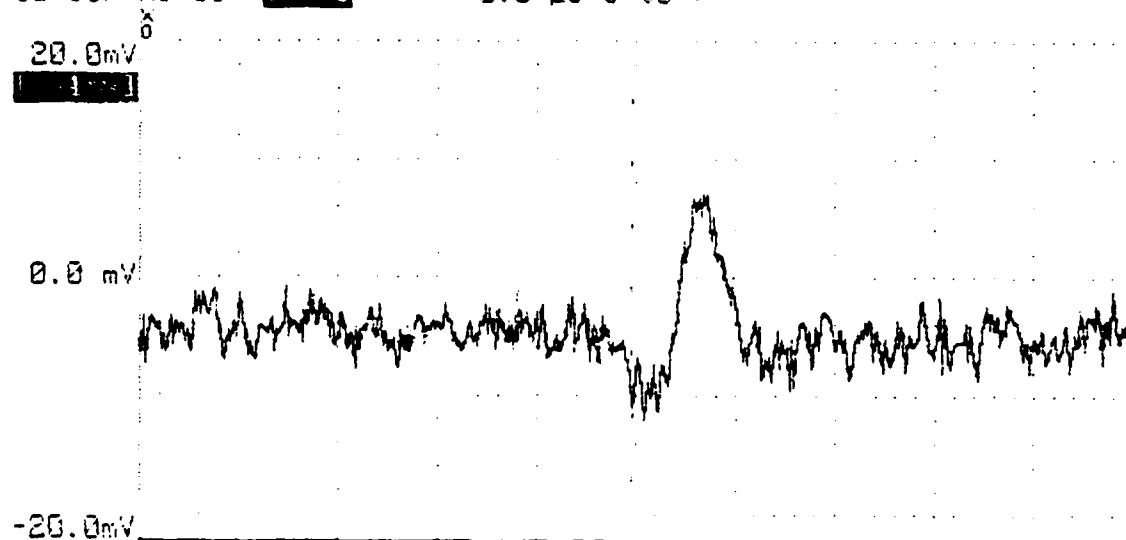
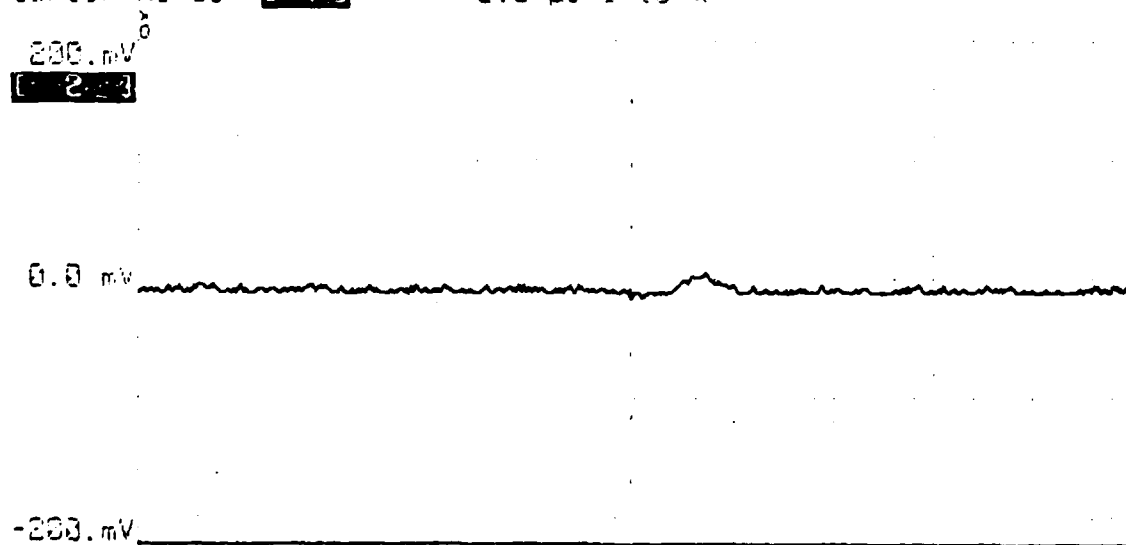


FIGURE 29

| | | |
|---------------|-----------|-----------------|
| Sample Period | [10 ms] | [Time] |
| Magnification | [1X] | 1.000 s /div |
| Magnify About | [X] | 10.00 ms/sample |
| Cursor Moves | [✓] | 0.0 μs o to x |



| | | |
|---------------|---------|-----------------|
| Sample Period | [10 ms] | [Time] |
| Magnification | [1X] | 1.000 s/div |
| Magnify About | [x] | 10.00 ms/sample |
| Cursor Moves | [x] | 0.0 us to x |

**FIGURE 30**

Analog [Waveform Diagram]-----INSERT to add traces-----

Sample Period [10 ms] [Time 1]
Magnification [1X] 1.000 s/div
Magnify About [x] 10.00 ms/sample
Cursor Moves [x] 0.0 μ s to x

20.0mV

[1]

0.0 mV

-20.0mV



Analog [Waveform Diagram]-----INSERT to add traces-----

Sample Period [10 ms] [Time 3]
Magnification [1X] 1.000 s/div
Magnify About [x] 10.00 ms/sample
Cursor Moves [x] 0.0 μ s to x

200.mV

[2]

0.0 mV

-200.mV



FIGURE 31

THIS PAGE INTENTIONALLY BLANK

3D Radar Scatterer Model Derived from Dual Mode Data

William L. Cameron

Boeing Aerospace & Electronics
P.O. Box 3999, Seattle, Washington 98124-2499

ABSTRACT

MMW ISAR imagery and IR images are combined to yield a 3D point scatterer model of an armored vehicle. It is observed that colocated MMW and IR sensors yield orthogonal views of a target. This is due to the fact that the MMW sensor resolves the target along the line-of-sight (LOS) and the IR sensor resolves the target orthogonal to the LOS. Consequently, if MMW scatterers can be identified with points in an IR image taken from the same viewpoint then the 3D coordinates of the scattering centers can be calculated. In this work the correspondence between points in the MMW ISAR and IR images is achieved by using a second IR viewpoint upon which the MMW imagery can be directly overlayed. A 3D point scatterer model of an armored vehicle is calculated using the method outlined above. Figures are presented showing several views of the 3D model obtained.

1. INTRODUCTION

Millimeter wave/infra-red (MMW/IR) sensor fusion addresses the problem of extracting the most useful target identification information from dual mode data. Fusion of information can be attempted at various levels. The MMW and IR information can be processed separately yielding a MMW target identification (ID) and a separate IR target ID. Then the fusion problem is reduced to resolving conflicts between the two ID's. A more challenging approach is to fuse the sensor data, i.e., combine the information from the two sensors to obtain target signature information which cannot be obtained from either sensor independently.

The data to be analyzed in this report is two dimensional imagery derived from turntable measurements. IR imagery and MMW images formed by Inverse Synthetic Aperture Radar (ISAR) processing are studied. The data used to form the images was taken simultaneously with colocated MMW and IR sensors.

Fusion cannot occur without some association or registration of pixels between the images formed from the two sensors. While studying this problem we realized that if this association can be made then the location of the pixels in three dimensions can be determined. In the sections that follow we show how this association is accomplished

for turntable measurement data. Using this information a three dimensional, polarimetric model of target radar scatterers is obtained directly from sensor measurement data. A very simple analysis of the point scatterer model yields geometrical information about the vehicle which is unattainable by a similar analysis of the data from the two sensors done independently and then fusing results.

In section 2 the spatial relationship between IR and MMW ISAR imagery is discussed. A discussion of MMW image formation is presented in section 3. A detailed description of how MMW point scatterers are registered onto IR imagery is presented in section 4 followed by a presentation of results in section 5.

2. INTUITIVE VIEWPOINT

We define the *intuitive viewpoint* of an object represented by an image to be the direction which is orthogonal to the plane in which the object is spatially resolved. This determines the direction of the *intuitive viewpoint* up to a sign. The sign is chosen such that the *intuitive viewpoint* has a positive projection on the LOS or such that it is directed into the ground plane, assuming a ground plane exists.

For visual or IR imagery the *intuitive viewpoint* is the LOS. For ISAR imagery the *intuitive viewpoint* is orthogonal to the LOS. Consequently, colocated MMW and IR sensors, even though they possess the same LOS to an object, have *intuitive viewpoints* which are orthogonal. The transformation required to register IR and MMW images depends on the relationship between their respective *intuitive viewpoints*, not their LOS's. Due to this fact, MMW ISAR and IR imagery taken by colocated sensors (same LOS, orthogonal *intuitive viewpoints*) cannot be registered by simple scaling and translation of the images. The only exception to this rule is the case where the resolution of the target is such that the target geometry can be assumed to be planar.

An interesting consequence of the orthogonality of the MMW ISAR and IR *intuitive viewpoints* is that three dimensional imaging of an object is possible from a single viewpoint. If one can associate scattering centers in a MMW ISAR image with points in an IR image from the same viewpoint then a correspondence is determined between points on images which have orthogonal *intuitive viewpoints*. The three-dimensional coordinates of the points are determined by stereo processing the imagery for the two orthogonal *intuitive viewpoints*. Common to all stereo

processing, the main problem is the determination of the correspondence between points in the two images.

3. MMW POINT SCATTERER IMAGE FORMATION

The MMW data used in this report was obtained from the TABILS15¹ data base. The data is fully polarimetric turntable measurement data taken with a 35 GHz, stepped frequency, pulsed radar. Four transmit/receive states provide fully polarimetric signatures.

MMW point scatterer images are formed in three steps. First, each transmit/receive channel is converted into a two dimensional image by ISAR² processing. Each pixel of the four image planes is complex valued; the relative phase between channels is important for the polarimetric processing which occurs in step three. These ISAR images suffer from artifacts which are a direct result of the Fourier transform processing necessary to achieve high range and cross-range resolution. The effect of these artifacts is to blur point scatterer responses.

The second step of the MMW processing is the removal of the ISAR artifacts. We employ a method introduced by Cameron³ termed Point Scatterer Extraction (PSE). PSE images of armored vehicles exhibit distinct point scatterer responses. The intensity of a point scatterer response in each of the four image planes depends on the scatterer type and its orientation in the plane of the LOS. A discussion of the variability of scatterer response due to scatterer type and orientation is given by Huynen⁴.

The third step in the MMW image formation is to combine the responses from the four complex PSE images into one image and to remove the variability of scatterer intensity due to scatterer type and orientation. To this end, a polarization scattering matrix is calculated for each pixel by combining the responses of corresponding pixels in the four complex PSE images. For each pixel, the scattering matrix is decomposed yielding the intensity of each of eleven basic scatterer types⁵. Each pixel is assigned the intensity and type of the dominant scatterer in its polarimetric

¹ "Target and Background Information Library System (TABILS) Users Manual", Air Force Armament Laboratory, Air Force Systems Command, United States Air Force, Eglin Air Force Base, Florida, August, 1985.

² G.W. Stimson, Introduction to Airborne Radar, pp. 575-576, Hughes Aircraft Co., El Segundo, Cal., (1983).
W.L. Cameron, "Enhancement of Point Scatterer Responses in ISAR Images", Proceedings of the GACIAC Polarimetric

³ Technology Workshop, Redstone Arsenal, Alabama, Aug. 16-18, 1988.

⁴ P.L. Uslenghi (Ed.), J.R. Huynen (Auth.), "Phenomenological Theory of Radar Targets", Electromagnetic Scattering, Academic Press, New York, 1978.

⁵ W.L. Cameron and L. Leung, "Feature Motivated Polarization Scattering Matrix Decomposition", submitted to RADAR 90.

response. The eleven basic scatterer types are: non-reciprocal, left helix, right helix, asymmetric, trihedral, cylinder, dipole, narrow diplane, diplane, quarter-wave device, and symmetric.

The determination of the dominant scatterer type proceeds as follows. Scatterers are divided into three groups based on the regularity of their polarimetric signatures. The three groups are: non-reciprocal, asymmetric and symmetric. Non-reciprocal scatterers are scatterers which violate the reciprocity principle^{6,7}. In general, non-reciprocal responses indicate low signal-to-noise or the presence of special materials. Scatterers which obey the reciprocity principle are either symmetric or asymmetric scatterers. Symmetric scatterers possess an axis of symmetry contained in the plane orthogonal to the LOS. Only symmetric scatterers are assigned an orientation, which is the orientation of their axis of symmetry in the plane orthogonal to the LOS. The most extreme examples of asymmetric scatterers are left and right helices. For this reason left and right helices are distinguished from other asymmetric scatterers. Scatterers which exhibit asymmetric responses are declared to be left or right helices if their helical response is great enough, otherwise they are simply declared to be asymmetric. Symmetric scatterers are declared to be one of the following types: trihedral, cylinder, dipole, narrow diplane, diplane, quarter-wave device, or symmetric (non-specific symmetric scatterer).

The final MMW image has three pieces of information associated with each pixel: scatterer intensity, scatterer type, scatterer orientation. The final images are simple enough that individual scatterers can be matched to features observed in IR images.

4. CORRESPONDENCE FOR STEREO PROCESSING

As we are analyzing turntable measurement data the correspondence problem can be solved simply by using two IR images. The first IR image is chosen such that its LOS is orthogonal to the MMW LOS. This IR image will have an *intuitive viewpoint* equal to that of the MMW image. The other IR image is chosen with the same LOS as the MMW image. In this case the *intuitive viewpoints* will be orthogonal. The IR and MMW images with equal *intuitive viewpoints* can be registered by a simple scaling and translation of the images. Registration of these images establishes

⁶ D.S. Saxon, "Tensor Scattering Matrix for the Electromagnetic Field", Phys. Rev., 100, 1771, (1955).

⁷ J.H. Van Vleck, Theory of Electric and Magnetic Susceptibilities, Oxford University Press, London, (1932).

the correspondence between MMW scatterer positions and IR features. Using this correspondence individual MMW scatterers can be registered onto the IR image which has the *intuitive viewpoint* which is orthogonal to the MMW *intuitive viewpoint*, i.e., the same LOS. Using this procedure the MMW scatterer positions are determined from two orthogonal viewpoints and the three-dimensional coordinates of the MMW scatterers are derived by simple stereo processing.

For the example given (see Fig. 2) we have chosen to use MMW data with an LOS corresponding to a sensor depression angle of 40° and the turntable positioned at 0° (head-on view of target). The MMW *intuitive viewpoint* is orthogonal to this. The IR image which has the same *intuitive viewpoint* as the MMW image has an LOS corresponding to a sensor depression angle of 50° with the turntable rotated 180° .

In order for the IR and MMW images to be aligned by a simple scale change and translation the IR image must be reflected about the horizontal and vertical axes. The reflections would not be necessary if the repositioning of the viewpoint were accomplished by a physical rotation of the sensor by 90° about the z axis (see Fig. 1). Note that repositioning the sensor in this way causes a flip in the vertical direction in the rest frame of the sensor relative to the target vertical. Repositioning the viewpoint using a 180° rotation of the turntable (or sensor about the z axis) does not flip the vertical of the sensor relative to the target, but it does flip the sensor's horizontal orientation relative to the target. For a sensor depression angle of 45° , rotation about the z axis can be simulated by rotating 180° about the z axis and then reflecting the image about the vertical and horizontal axes. In general, if the sensor depression angle is θ , the same process applies except that the 180° rotation data must have a depression angle of $90^\circ - \theta$.

Figure 2 illustrates the fact that MMW PSE and IR images which have the same *intuitive viewpoint* can be registered by a simple scale change and translation of the images. Figure 2a is the PSE image of an armored vehicle which has been scaled to match the dimensions of the IR images, Figs. 2b, 2c. We have sacrificed detail for clarity by displaying only the locations of the major scatterers in the PSE image, omitting their intensity, type and orientation. Figure 2b is an IR image of the vehicle which has the same LOS as the PSE image (40° sensor elevation angle, 0° turntable rotation). Figure 2c is an IR image of the vehicle which has (approximately) the same *intuitive viewpoint* as the PSE image (IR LOS has 40° sensor elevation angle, 180° turntable rotation angle). Figure 2c has been reflected

horizontally and vertically to compensate for axis sign reversal as discussed previously.

The scaling of both the IR and MMW PSE images is known. The only difficulty in registering the images with the same *intuitive viewpoint* is in determining the relative translation. The PSE image can be decomposed into four recognizable sets of points. The first set is composed of the points which lie roughly in two straight lines along either side of the vehicle. The second set of points are the two symmetrically placed returns from the headlights at the front of the vehicle. The remaining two sets of points are two clusters. One cluster lies just above the headlight set and is due to scattering from the roof of the vehicle. The other set of points is approximately in the shape of the letter "V". The apex of this set is due to scattering from the launcher support column and the extremities are due to scattering from the launchers. The far rear of the vehicle is not visible in the PSE image causing the signature to be shorter than the vehicle, even after compensating for aspect angle. The relative translation is determined by aligning the four sets of points with their respective features in the corresponding IR image. This is not possible to accomplish using the MMW and IR images with the same LOS, Figs. 2a and 2b. The result of aligning the MMW and IR images with the same *intuitive viewpoint* is illustrated in Fig. 2d.

The IR image features underlying the MMW scatterer positions in Fig. 2d are identified with IR features from the (nearly) orthogonal IR viewpoint image, Fig. 2b, by direct comparison of the images. The scatterers in the MMW image, Fig. 2a, are indirectly identified with positions on the IR image with the same LOS, Fig. 2b, using the IR image (Fig. 2c) with the same *intuitive viewpoint* as the MMW image as an intermediary.

5. RESULTS

Employing the method described in section 4, two dimensional scatterer positions are determined from two orthogonal viewpoints. Define the primed coordinate system such that y' is directed anti-parallel to the MMW sensor LOS, x' is parallel to the x axis (see Fig. 1) and choose z' such that it completes the right-handed coordinate system. The MMW PSE image, Fig. 2a, yields (x', y') coordinates of scatterers directly. Indirect registration (as described in the previous section) of the MMW scatterer positions onto Fig. 2b yields the (x', z') coordinates of scatterers. Combining these results yields the (x', y', z') coordinates of the MMW scatterers.

Figures 3 and 4 present various views of a 3D scatterer model derived from the image data presented in Fig. 2. Fig. 3a shows scatterer positions obtained directly from the MMW PSE image (Fig. 2a) which corresponds to an *intuitive viewpoint* which is orthogonal to the MMW LOS. Scatterer positions are indicated by cubes. Fig. 3b is the model viewed from the positive y direction (refer to Fig. 1 coordinate system). Fig. 3c is the model viewed from directly overhead. The contraction of the apparent length of the target due to aspect angle can be seen by comparing Figs. 3a and 3c. Figs. 4a and 4b are views of the model from broadside and askew, respectively.

MMW scatterer types, as well as intensity, are displayed in Figure 6. The symbols, defined in Fig. 5, are registered directly and indirectly, as discussed above, onto two IR views. Figure 6a is the (x', y') plane view and Fig. 6b is the (x', z') plane view.

Display of the 3D model with scatterer intensity, orientation and type requires a set of 3D symbols to be defined. This set is defined in Fig. 7. Figure 8 shows two views of the 3D scatterer model using 3D symbols to indicate scatterer type, orientation and intensity. Scatterer intensities are indicated by scaling the scatterer symbols displayed in Fig. 7.

The vehicle length, width and height dimensions, in meters, are $5.8 \times 2.4 \times 2.3$. Vehicle dimensions as measured using the IR and MMW PSE images independently are 5.68×2.4 and 3.46×2.09 , respectively. These measurements do not account for sensor aspect, but are simply boundary measurements of blobs, in the case of IR, and clusters, in the case of MMW. These are measurements one might expect an automatic target recognition algorithm to provide. The vehicle dimensions derived from the 3D model are $4.51 \times 2.09 \times 1.37$.

If the vehicle is modeled as a two dimensional rectangle in the plane of the turntable then one would expect a contraction in the apparent length of the vehicle due to aspect. The vehicle height tends to increase its apparent length. For the case given these two effects cancel each other yielding an IR length estimate which is quite accurate.

The MMW length measurement is shorter than one would expect, even taking into account the effect of aspect. This is due to shadowing of scatterers in the rear of the vehicle as is apparent from Fig. 2d.

The 3D model length, width and height measurements were made along the vehicle axes and thus are not affected

by aspect angle. The main deficiency in the 3D model measurements stems from the shadowing of scatterers in the rear of the vehicle and underneath the lower apron of the vehicle. The height of the vehicle above the lower apron is approximately .89 meters which is somewhat more in agreement with the 3D model measurement than the total vehicle height.

The method presented is useful for unraveling some of the complexities of MMW scattering, as well as understanding the relationship between IR and MMW signatures. A more complete understanding of target geometry is obtained by fusing sensor reports before features are extracted.

ACKNOWLEDGMENT

The author gratefully acknowledges the assistance of Mr. David Froelich in the preparation of the figures appearing in this paper.

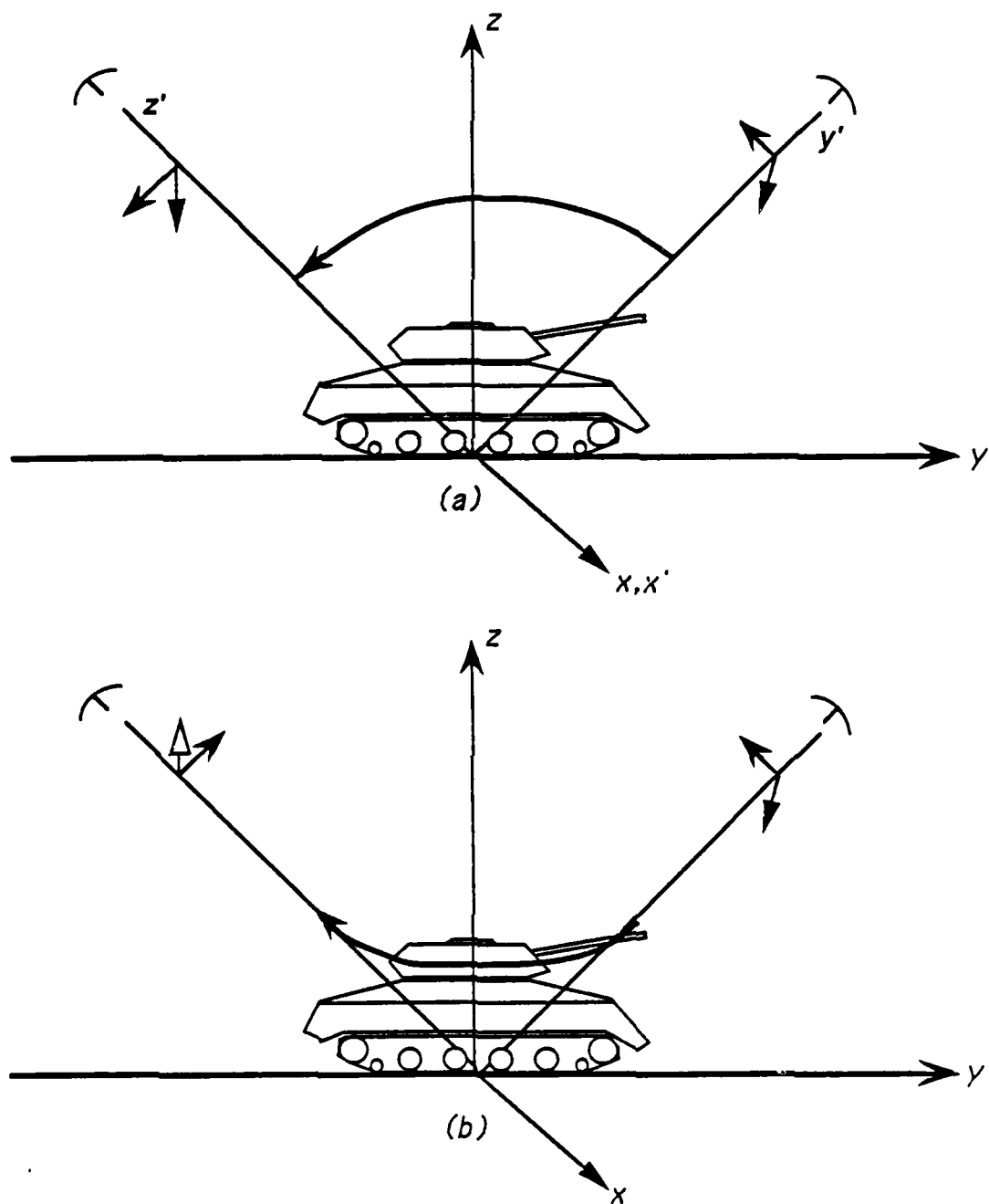
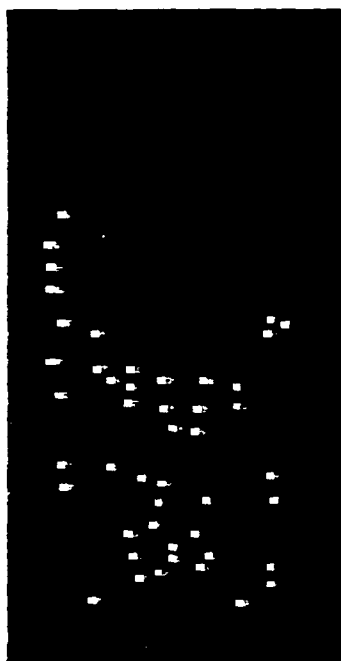


Figure 1. Orientation of coordinate system fixed in sensor relative to target coordinate system for repositioning of the sensor by rotating about: a) the x axis, b) the z axis. Style of arrow indicates vectors in the plane of the page (\rightarrow), out of the page (\rightarrow) or into the page (\rightarrow).



(a)



(b)



(c)



(d)

Figure 2. Images of armored vehicle derived from sensor data: a) PSE image scatterer positions, LOS directed 40° from ground plane and head-on. b) IR image with LOS same as (a), c) IR image with LOS nearly orthogonal to (a) and (b), d) overlay of (c) with (a).

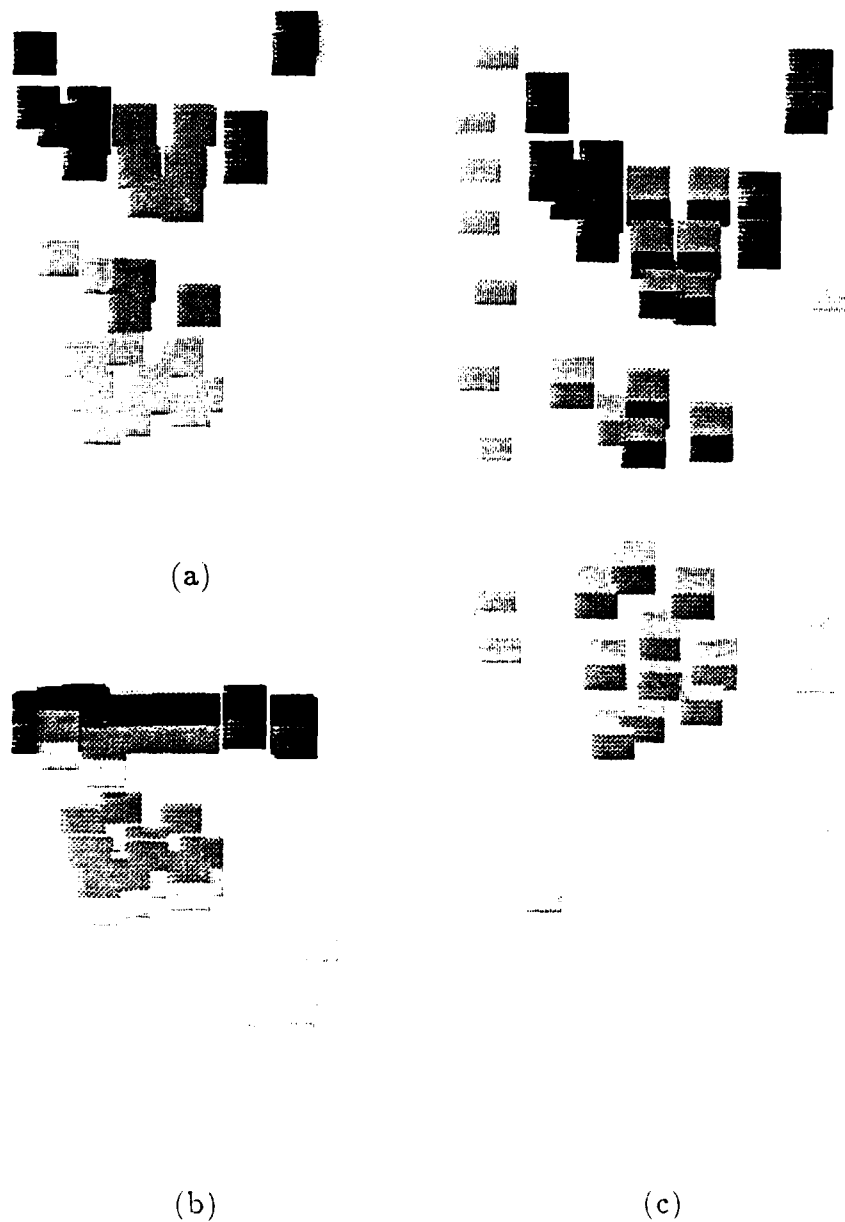
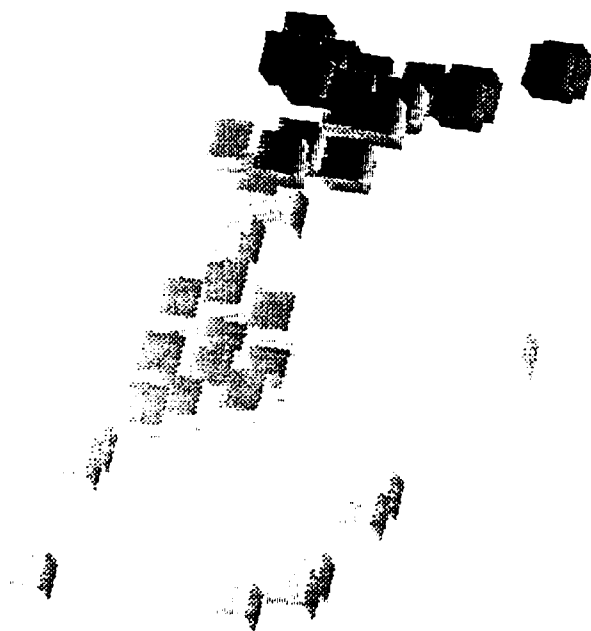


Figure 3. Three views of 3D radar scatterer model generated from dual mode data. Scatterers on the lower apron, mid-level, launcher support column and launchers are shaded light to dark. Views are: a) radar *intuitive view-point*, b) head-on and c) overhead.



(a)



(b)

Figure 4. 3D scatterer model with views: a) broadside, b) skewed.

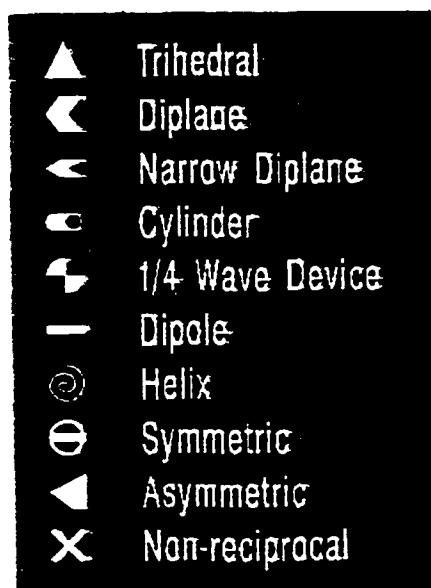


Figure 5. Scatterer type symbols.

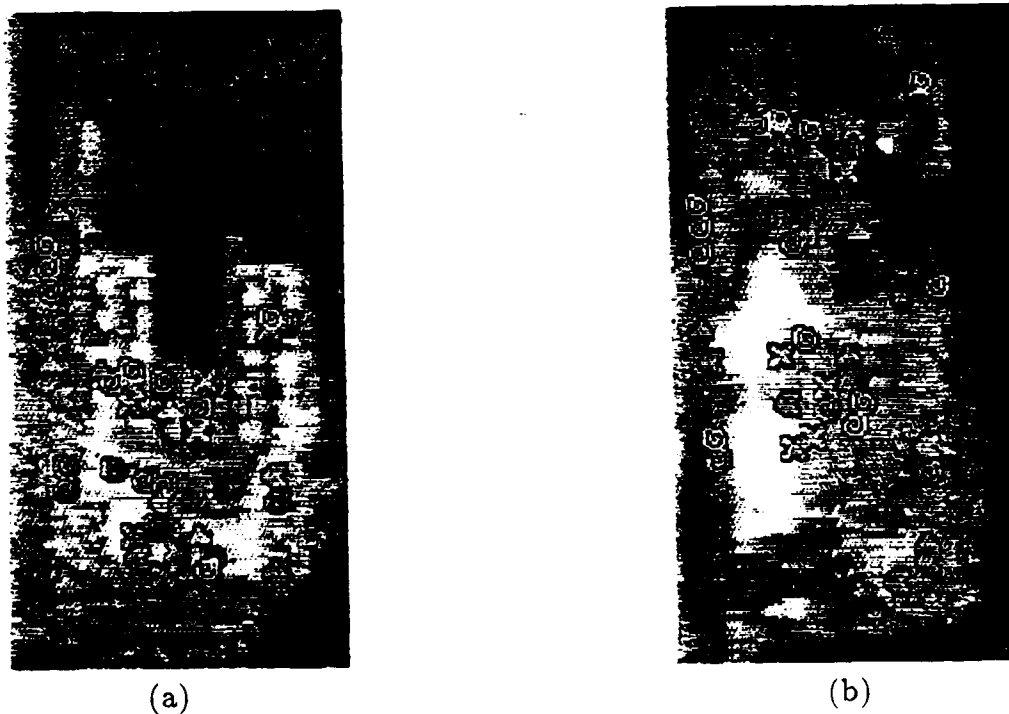


Figure 6. MMW scatterer symbols registered onto IR images: a) direct registration by scaling and translation, b) individual scatterers registered using 3D model position information.

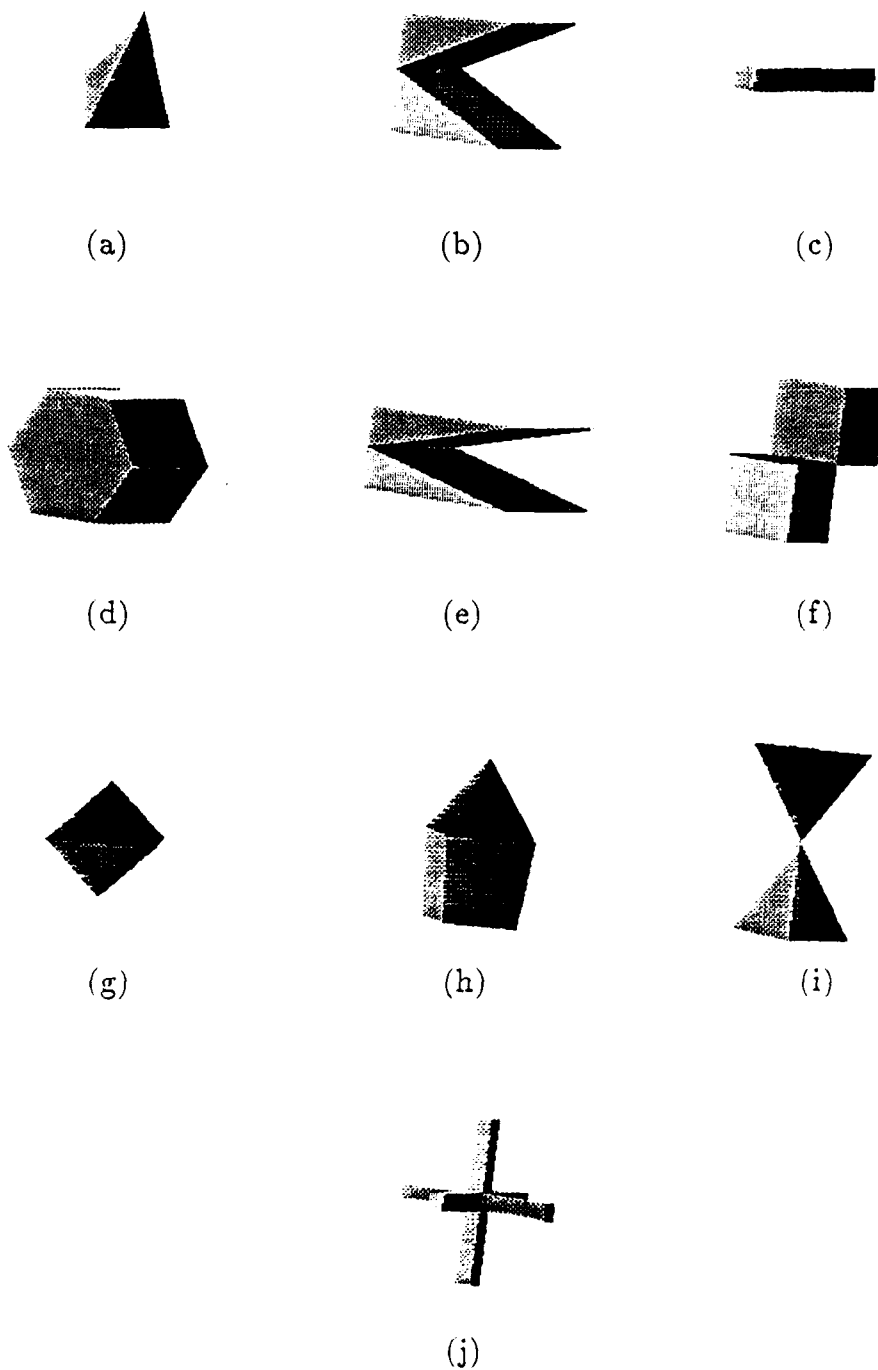


Figure 7. Scatterer symbols for 3D display: a) trihedral, b) diplane, c) dipole, d) cylinder, e) narrow diplane, f) $\frac{1}{4}$ wave device, g) symmetric, h) asymmetric, i) helix, j) non-reciprocal.



(a)



(b)

Figure 8. 3D scatterer model viewed: a) broadside, b) skewed.

THIS PAGE INTENTIONALLY BLANK

SYNTHETIC LASER RADAR IMAGE GENERATION

Jeffrey M. Gillberg, Randy Johnston, Joel T. Lee
Honeywell Systems and Research Center
Minneapolis, Minnesota 55418

and

Richard Peters, Duc Nguyen
CECOM's Center for Night Vision and Electro-Optics
Ft. Belvoir, VA 22060-5667

The data necessary for robust target recognition algorithm development are not always readily available, especially when advanced sensors are being considered. Data collection exercises are almost always plagued by high cost, sensor intermittence, and lack of terrain and target variety. As a result, target recognition algorithms developed to date suffer from homogeneous testing conditions. An example of an advanced sensor under consideration for target recognition systems is an imaging laser radar sensor. Laser radars can provide high resolution range information as well as high resolution reflectance information about the target. These observables are invariant under conditions of varying target temperature, ambient temperature, and lighting. The invariant observables and the 3-D geometric nature of the data make laser radar a good sensor choice for target recognition algorithm development. In order to circumvent the data availability problems that exist, some researchers have been and will continue to utilize synthetic laser radar imagery for recognition algorithm development.

In the Laser Radar ATR Algorithms (LARAA) program, we are currently developing a synthetic laser radar image generation capability that will be somewhat automated, incorporate a laser radar sensor model, and will consist of a variety of targets, clutter, and terrain selections. This capability will utilize currently available geometric target models such as the Ballistic Research Labs CSG models and the ERIM wireframe models, and will integrate the geometric target models with the terrain, clutter, and sensor models developed in the program. The result will be a extensible and modular synthetic image generation capability and a large database of synthetic laser radar range imagery for use in recognition algorithm development.

In this paper we will describe the synthetic laser radar image generation effort in the LARAA program including an overview of the geometric target models, terrain models, sensor model, and the overall integration process. Preliminary synthetic imagery will also be presented.

I. INTRODUCTION

The development of electronic terrain board technology is a rapidly growing area of research. There are several different applications for this technology; some of these applications are listed below:

- battlefield simulation for weapon systems testing
- flight training (man in the loop)
- sensor and target phenomenology modeling
- target recognition algorithm development and testing

There are two major areas of technology development in electronic terrain board research. One area is the development of techniques for data compression/representation and computational expedience to solve problems related to the real time generation/presentation of sequences of data. The other area is the understanding (quantification) of object/sensor phenomenology in order to solve problems related to the generation of accurate and verified imagery for a particular sensor. The work described in this paper fits into the latter area of technology development.

A controlled environment (input data set) is an essential need in the development and testing of target recognition algorithms, especially if algorithm performance understanding is an objective. The data necessary for robust target recognition algorithm development are not always readily available, especially when advanced sensors (i.e. laser radar) are being considered. Data collection exercises are almost always plagued by high cost, sensor intermittence, and lack of terrain and target variety. As a result, target recognition algorithms developed to date suffer from homogeneous testing conditions. The purpose of this paper is to describe on-going efforts in the development of a synthetic laser radar image generation capability that will provide a controlled environment for recognition algorithm development.

The work presented here is currently being performed under the CCNVEO/Honeywell Laser Radar ATR Algorithm (LARAA) program. The objective of the Synthetic Laser Radar Image Generation task in LARAA is to circumvent the data availability problems that exist by developing a data synthesis capability that will augment "real" data in target recognition algorithm development efforts. Section II will present an overview of the technical approach. Section III will present some concluding remarks.

II. TECHNICAL APPROACH

In order to avoid duplication of previous efforts, our technical approach for synthetic laser radar image generation borrows from previously developed "pieces" of modeling technology. The pieces of technology that have not been fully developed will be enhanced as necessary, and the overall capability will be integrated into a flexible and expandable synthetic image generation capability. The six major "pieces" of technology needed for synthetic image generation are as follows:

1. Geometric target models
2. Atmospheric propagation/scattering models
3. Laser radar sensor model
4. Terrain models
5. Clutter models
6. Model integration executive

For this task in the LARAA program, we are "bootstrapping" off of relevant research/development in 4 of the 6 listed technology areas. The clutter model and the model integration executive are the technology areas that will be developed "from scratch" in the LARAA program in order to meet the specific needs of synthetic image generation for future ATR algorithm development.

In the remainder of this section, an overview of the LARAA program technical approach for each of the 6 technology areas listed above is presented.

Geometric Target Models

The Ballistic Research Laboratory (BRL) has developed an extensive CAD solid modeling system and ray-tracing benchmark. Many different targets are available from BRL and the documentation and utility of the software is

excellent. Visible (E-O) target signatures can be rendered with various lighting models with the baseline software; other available software can render thermal signatures or radar signatures of the targets. LARAA will develop software (using the BRL CAD tools where appropriate) to generate high sampling resolution range signatures of the targets.

The Environmental Institute of Michigan (ERIM) has developed wireframe target models for ATR algorithm evaluation in the PAIRSTECH program. These models are much less detailed than the BRL solid models, but may prove to be adequate for some synthetic imagery (particularly low spatial resolution imagery). Under the LARAA program, we will develop range signature rendering software for the wireframe models. A qualitative and quantitative benchmark comparing the ERIM wireframe and the BRL CSG models will be performed in order to aid in the selection of target models for the synthetic imagery.

Atmospheric propagation/scattering models

Several different software packages exist that are complete atmospheric propagation models, handling broadband and/or narrowband electromagnetic energy. Because software packages are available that are directly applicable, the LARAA program has no planned upgrades to this technology. Rather, LARAA will (with lowest priority) integrate atmospheric effects into the synthetic image generation capability using one or more of the available software packages. This is considered to be a low priority item for this phase of the LARAA program so, as a baseline, one set of atmospheric degradations for nominal atmospheric conditions will be used. Software "hooks" will be left the future integration of a complete atmospheric model.

Laser Radar Sensor Model

The laser radar sensor model is one of the most important factors in creating realistic synthetic imagery. The model for an imaging laser radar sensor can be broken up into two parts - the scanning (or imaging) mechanism for the sensor and the physics (phenomenology) associated with the transmission, scattering, and detection of the laser

C and E are arbitrary functions useful for modifying the amplitude and shape of the gaussian surface, and x' and y' are points (x,y) after applying a rotation to them:

$$x' = x \cos(\theta) - y \sin(\theta)$$

$$y' = x \sin(\theta) + y \cos(\theta)$$

θ is the rotation angle of the gaussian surface in the xy plane.

The elevation z of a given (x,y) coordinate is the contribution of all the m gaussian surfaces at that point:

$$z(x,y) = \sum_{i=1}^m G_i(x,y)$$

For a given gaussian surface G , seven parameters control its shape: θ , σ_x , σ_y , μ_x , μ_y , E , and C . Including m , the number of gaussian surfaces that constitute the terrain, these variables can create terrains of arbitrary shape and complexity.

Once the terrain is defined in this fashion, it can be raytraced to acquire the range map. Figure 1 illustrates a terrain map and the resulting relative range, absolute range, and intensity maps.

Since both terrain-generation methods create locally smooth surfaces, fractal perturbations can be incorporated into the terrain model to provide local roughness and add "landscape" features to the terrain (trees, treelines, etc.).

Clutter models

Another issue this program addresses is clutter modeling. For our purposes, a clutter object is defined as an object that shares a certain degree of similarity with a given target that an ATR intends to recognize. This degree of similarity can be parameterized as the difficulty of the clutter object. This clutter parameterization will control the

beam. The scanning model describes the spatial sampling that the laser radar will perform; the phenomenological model describes the target/laser beam interaction, signal-to-noise ratio, range measurement errors and dropouts. We are applying previous work that has developed mathematical models for particular laser radar systems in the creation of an imaging laser radar sensor model that is more accurate than heuristically "adding gaussian noise" to the image or "smoothing" the image.

Terrain models

Two methods for creating elevation data for the terrain model are being exploited; digital elevation data developed by the DMA (Defense Mapping Agency), NCIC (National Cartographic Information Center), and CCNVEO, and by using gaussian surfaces.

The elevation data obtained from the DMA and NCIC represents coarse samples of real terrain. The resolution (distance between samples) of these data varies between approximately 10 and 40 meters. The CCNVEO data provided are the elevation map of CCNVEO's physical terrain board. This fictitious terrain is divided into 1 kilometer square sectors which are subdivided into quadrants and then into rows. Each row consists of five elevation points that are two-hundred meters apart. As a result of the low resolution of these data, the rendered terrain will be quite smooth.

Combinations of gaussian surfaces are suitable for creating more complicated and arbitrary terrains than the digital elevation data. The gaussian surfaces are also well suited to automatic synthetic image generation, since the surfaces can be easily created by using random parameters (perhaps sampled from a given density). The form of the gaussian equation has been modified for this application:

$$G(x,y) = \frac{C(x,y)}{2\pi\sigma_x\sigma_y} e^{-0.5\left[\frac{(x'-\mu_x)^2}{\sigma_x^2} + \frac{(y'-\mu_y)^2}{\sigma_y^2}\right]} + E(x,y)$$

automatic generation of the synthetic laser radar imagery. Each image is created based on the a priori clutter difficulty selected for that image. Thus the performance of a recognition algorithm can be evaluated as a function of clutter difficulty.

Clutter will be modeled as perturbations of targets. For example, a clutter object for an M60 tank could be the tank itself with the turret removed. Since some targets exhibit local similarities, one target can be perturbed to be a clutter object for another target. Other perturbation methods include moving subsets of a target model's vertices, slicing a target model with a given function, adding artifacts to target surfaces, etc. Eventually the types of perturbations formed will be dependent on the level of clutter difficulty desired. For example, clutter formed as a result of perturbing a facet of a target model may cause a recognition algorithm more problems than clutter formed by removing the front half of the target model. The minimum Hausdorff distance¹ between the target model and the clutter object will aid the determination of the relationship between clutter difficulty and perturbation type.

Model Integration

The model integration executive will integrate each piece of technology into an comprehensive synthetic image generation capability. The integration approach will be designed to maintain flexibility so that upgrades and changes to each technology nugget can be easily accommodated.

The overall approach to synthetic laser radar image generation is illustrated in Figure 2. The approach calls for having a database available for each element of the desired synthetic scene (e.g. the targets, terrain, and clutter). The database for each scene element will contain the high resolution range map generated by the ray tracing operation (or any other suitable method) and will contain the reflectance distribution statistics for that particular element. The desired synthetic scene is specified by the scene description files, which can be created and edited interactively using an overlay display tool on the Sun computer, giving visual feedback on what the scene will look like. The clutter

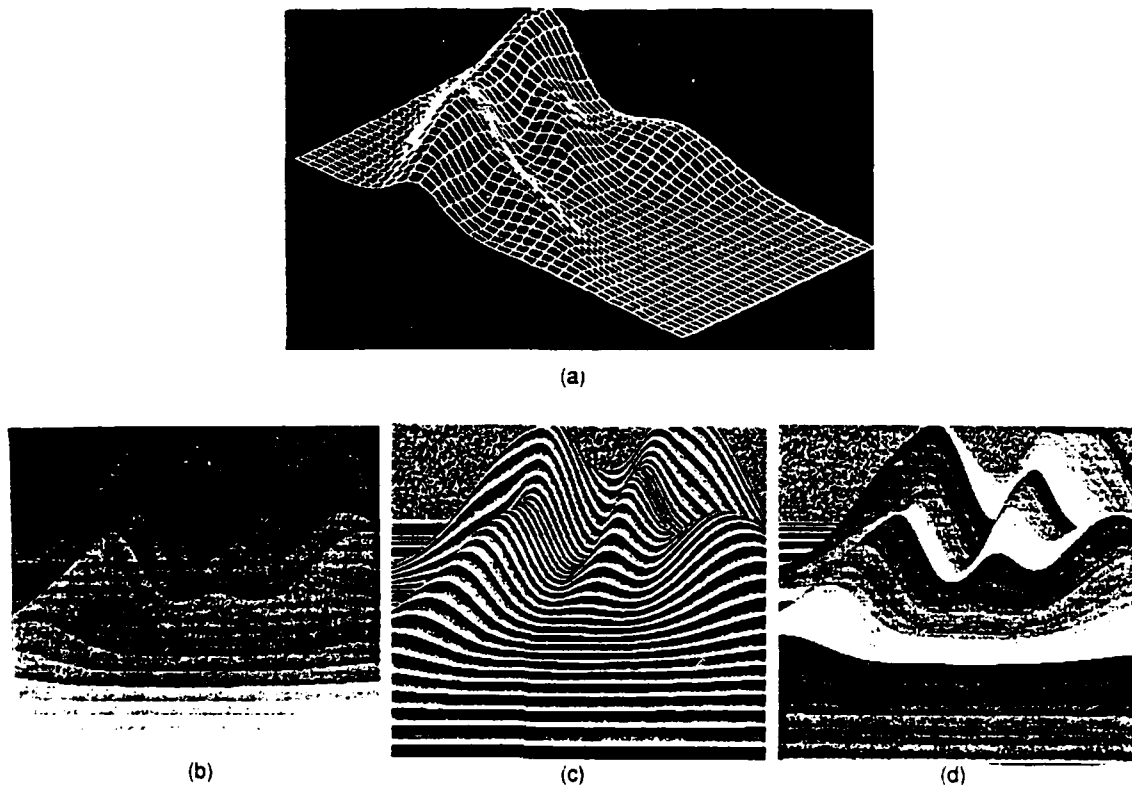
¹ D. Mumford, "The Problem of Robust Shape Description", Center for Intelligent Control Systems, Harvard University, Cambridge, Mass., 1987.

elements may be treated separately in order to randomize its placement and incorporate parameters that describe the difficulty of the clutter; this cannot be determined until the clutter models we will use are developed further.

Some synthetic imagery generated to date will be presented at the symposium. Because of the difficulty of printing color results, the synthetic imagery are not included in the written paper.

III. SUMMARY

In this paper, we have presented our ongoing efforts in the areas of synthetic laser radar image generation. Our approach will provide a means for generating parameterized synthetic laser radar imagery for use in recognition algorithm research. The use of a controlled algorithm development and evaluation environment will result in a better understanding of algorithm performance and ultimately in more robust recognition algorithms.



a. Terrain map, b. Intensity, c. Relative range, d. Absolute Range

Figure 1. Synthetic Terrain Map Results

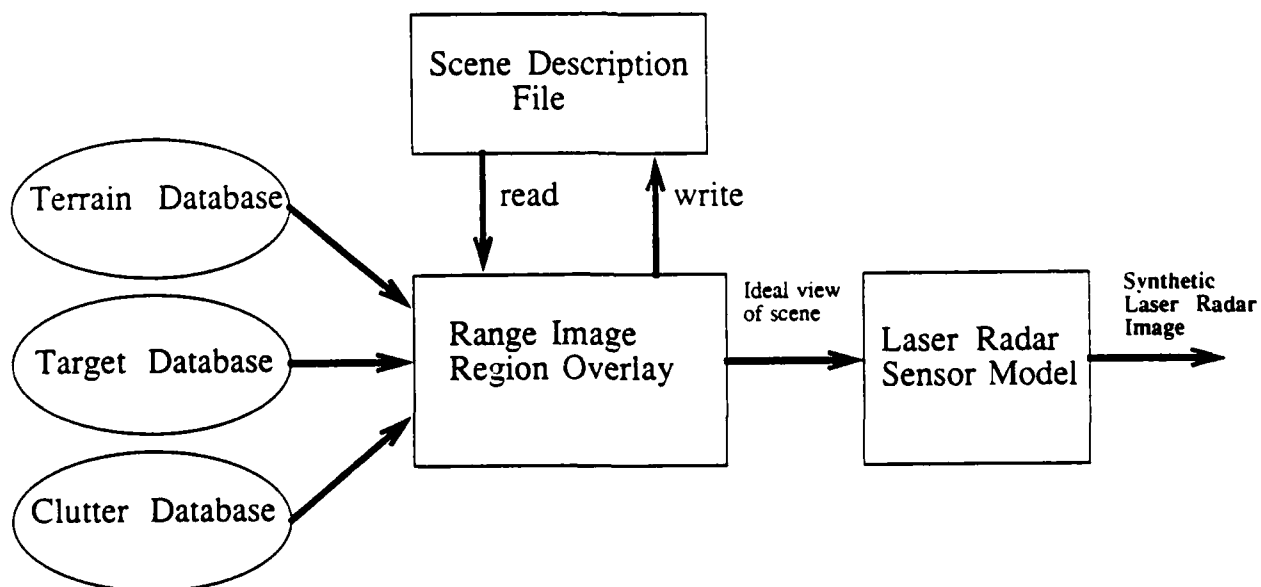


Figure 2. Synthetic Laser Radar Image Generation Approach

THIS PAGE INTENTIONALLY BLANK

Presented at the
DIGITAL/ELECTRONIC TERRAIN BOARD SYMPOSIUM
5-6 October 1989 GACIAC PR 89-07

Effect of Atmospheric Turbulence on Electro-Optical Systems

by

Walter B. Miller
Jennifer C. Ricklin
David H. Marlin

U.S. Army Atmospheric Sciences Laboratory
White Sands Missile Range, New Mexico 88002-5501

ABSTRACT

The IMTURB model characterizes the effects of clear-air optical turbulence on electro-optical (EO) imaging devices and laser transmitters operating in the atmospheric surface boundary layer and is valid for wavelengths from the visible through the far infrared. Similarity theory and the Kolmogorov principle of universal equilibrium are employed to characterize optical turbulence structure over regions typical of applications, based on simple environmental observables. A profile for the refractive index structure parameter is estimated, then used as input to a weak perturbation propagation model. Receiver coherence diameter, log-amplitude variance, scintillation averaging length, isoplanatism effective path length, and related subsidiary propagation statistics are then estimated for a selected propagation path. Outer and inner scale profiles are also estimated for advanced applications. Model results for two sample cases are discussed.

1.0 INTRODUCTION

It is well understood that irregularities in the atmospheric refractive index result in distortion of propagating electromagnetic waveforms. In a landmark analysis based on the work of Kolmogorov,^{1 2 3} it was postulated that a primary source of such irregularities is the turbulent motion of the

This paper was originally presented at the meeting of AGARD, Copenhagen, Denmark (1989).

atmosphere in the presence of temperature and moisture gradients. It was further postulated that these irregularities possess a quantifiable statistical structure.⁴ The validity of these postulates is generally accepted, and the term "optical turbulence" has come into general usage to denote random, turbulence-induced fluctuations in the atmospheric refractive index.

When an electromagnetic wave propagates through an atmosphere where optical turbulence is present, the wave front acquires a progressive degree of distortion. Departure of the phase front from its nominal shape results in a decrease in registered image quality for electro-optical (EO) imaging systems. Images appear distorted and blurred. A laser beam exhibits an increase in beam diameter in excess of that predicted by diffraction theory. In addition, the entire beam is subject to optical turbulence-induced random translations of the beam centroid, a phenomenon called beam wander. The purpose of the IMTURB model is to quantify these and related effects.⁵

IMTURB differs from typical propagation models for optical turbulence in that a profile is calculated for the refractive index structure parameter (often referred to as a C_n^2 profile) from simple meteorological and environmental information. Previous methods often relied on the use of one or more measured point values for the refractive index structure parameter. From these measurements, profiles were extrapolated by a scaling law.⁶ In the region of the atmosphere where terrain surface features play a significant role in determining optical turbulence structure, such an approach may impose severe limitations. This region of the atmosphere, called the surface boundary layer, ranges in height from tens to hundreds of meters depending on atmospheric conditions. Above the surface boundary layer, the degree of statistical consistency over

regions commensurate with propagation path length may be such that point measurements of C_n^2 or even free atmosphere models may be adequate to specify global optical turbulence structure. This is the case with many astronomical applications. However, within the surface boundary layer, a propagation path may cross several differing optical turbulence regimes, each driven by slightly different environmental factors. Point measurements, extended to a profile with a power law and extrapolated over the total propagation path, may give rise to misleading results. In response to the problems inherent in modeling this scenario, IMTURB employs environmental parameters exhibiting statistical consistency over regions consistent with most laser transmitter and imaging applications.

In the complex environment of the atmospheric surface boundary layer, a precise and comprehensive description of surface energy fluxes driving the optical turbulence mechanism is difficult. The number of observations necessary to quantify point-specific behavior of the surface fluxes is greater than available even in well-instrumented field experiments. In addition, spatial and temporal variations in environmental factors along the length of the propagation path challenge the validity of even the most carefully performed site characterizations. To combat these difficulties, the modeling basis for IMTURB combines the micrometeorology of the atmospheric surface boundary layer with the well-understood and documented weak fluctuation theory of electromagnetic propagation through optical turbulence.^{7 8 9 10} To characterize the micrometeorology, Obukhov similarity theory^{11 12 13 14} is used to determine basic flux profile relationships. The Kolmogorov principle of universal equilibrium¹⁵ employs these relationships to define profiles for the turbulent inner and outer scales and the refractive index structure parameter. Both Obukhov similarity theory

and the Kolmogorov principle of universal equilibrium are concerned with modeling the behavior of surface energy fluxes in a statistically consistent environment. Therefore, the shape of the calculated C_n^2 profile reflects the total environmental state more completely than would a profile obtained from a scaling law. A profile for outer scale occurs naturally in the application of the universal equilibrium principle; inner scale is obtained using a method described by Ochs and Hill.¹⁶ Although the version of IMTURB currently available through the Electro-Optical Systems Atmospheric Effects Library (EOSAEL) uses the Kolmogorov spectrum to calculate propagation statistics, planned updates include extension to strong perturbation theory and use of the modified von Karman,¹⁷ Hill,¹⁸ or Andrews spectrums.¹⁹ Profiles for inner and outer turbulence scales are included for advanced applications.

2.0 MODELING OPTICAL TURBULENCE STRUCTURE

Obukhov similarity theory is used to calculate surface energy fluxes and related quantities for a specified geographical location, date, and time. The meteorological observables required are percent cloud cover and a value for temperature, pressure, and windspeed. The earth's aerodynamic features are summarized by specification of a roughness length²⁰ or by calculation of the roughness length from an observed roughness element.²¹ The algorithms used by IMTURB to estimate flux profile relationships were first proposed by Stewart²² for use in determining turbulent velocity spectrums over complex terrain. These algorithms were later refined and extended²³ to calculate C_n^2 and outer scale profiles. The computational flow detailing calculation of these profiles is as follows.

From latitude, longitude, and Greenwich mean time (GMT), solar zenith angle may be calculated. From solar zenith angle, the amount of solar irradiance on the earth's surface in the absence of cloud cover may be estimated for the specified location and time.²⁴ Knowledge of percent cloud cover allows determination of global irradiance and radiation class²⁵ and a first estimate of sensible heat flux.²⁶ Mean horizontal windspeed, atmospheric pressure, and temperature, estimated for a specified height within the surface boundary layer, may be combined with radiation class to estimate the Pasquill fractional stability parameter. When combined with terrain roughness length, the Pasquill fractional stability parameter allows estimation of both the Obukhov length and scaling ratio.²⁷ The scaling ratio appears as the independent variable in the dimensionless wind shear and lapse rate, both basic quantities from the similarity theory. Two forms for dimensionless wind shear and lapse rate are included, one proposed by Businger²⁸ and the other by Hansen.^{29 30} From either of the two forms, the corresponding diabatic influence functions are calculated. An equation deriving from basic similarity relationships involving mean horizontal windspeed and the diabatic influence function for momentum allows calculation of friction velocity.³¹

Knowledge of a value for temperature, used in the similarity equation defining characteristic temperature, allows an independent second estimate of sensible heat flux. To maintain consistency among the similarity parameters, an iterative scheme is employed to adjust friction velocity and Obukhov length so that values for sensible heat flux predicted by similarity theory and solar irradiance are in agreement. From this adjusted set of parameters, profiles are obtained for both potential temperature and potential temperature gradient.³² Sufficient information now exists to estimate profiles for the potential

temperature structure parameter and, ultimately, the refractive index structure parameter.

Rigorous development of the theoretical link between the gradient profile for potential temperature and the profile for the refractive index structure parameter may be found in Tatarski³³ and Ishimaru.³⁴ The refractive index of the atmosphere is a function of wavelength, temperature, pressure, and specific humidity. For optical and infrared wavelengths, humidity over land is negligible, and the refractive index may be expressed as³⁵

$$n = 1 + \frac{77.6P}{K} \left(1 + 7.52 \times 10^{-3} \lambda^{-2} \right) 10^{-6}, \quad (1)$$

where P is pressure in millibars, K is temperature in K and λ is wavelength in micrometers. This expression, when combined with the mean potential temperature gradient, results in the following approximation for the gradient of the mean refractive index³⁶

$$\frac{\partial n}{\partial z} \approx \frac{(-77.6 \times 10^{-6} P)(1 + 7.52 \times 10^{-3} \lambda^{-2})}{kz(\Theta - \alpha z)^2} T_* \Phi_h(\zeta), \quad (2)$$

where n is mean refractive index, Θ is mean potential temperature, z is height above ground in meters, α is the adiabatic lapse rate, k is von Karman's constant, T_* is characteristic temperature, and $\Phi_h(\zeta)$ is dimensionless lapse rate. Used with results from the Kolmogorov principle of universal equilibrium, eq. (2) allows calculation of profiles for the refractive index structure parameter.³⁷

3.0 PROPAGATION STATISTICS DESCRIBING SYSTEM PERFORMANCE

For each propagation path through the atmosphere, a choice of statistics may be estimated describing loss in system performance due to optical turbulence. The statistics chosen for IMTURB derive from a comprehensive and flexible propagation model based on weak fluctuation theory^{3,8} wherein all propagation statistics are weighted integrals of the refractive index structure parameter over the propagation path. The four basic propagation statistics are (1) receiver coherence diameter; (2) log-amplitude variance; (3) scintillation averaging length; and (4) isoplanatism effective path length. Subsidiary statistics include limiting resolution source length, isoplanatism source size, and normalized intensity variance. Other options available to the IMTURB user include (1) choice of plane or spherical wave; (2) spatial power spectrum for log-amplitude and phase variations; (3) fast and slow modulation transfer functions; (4) imaging optics resolution/transmitter beam spread; (5) heterodyne receiver analysis; (6) predetection compensation analysis; and (6) normalized, aperture-averaged intensity receiver analysis. The four basic propagation statistics are described below.

The receiver coherence diameter is the most widely known of the basic propagation statistics. It is a fundamental measure of wave front distortion and is required for estimation of such fundamental forms as the mutual coherence function and modulation transfer function. In an atmosphere free of optical turbulence, an imaging system has the potential for virtually unlimited increases in resolution with corresponding increases in optics diameter. However, when the same system is operated in the presence of optical turbulence, there is a diameter beyond which further size increases produce no significant increase in

resolution. This diameter is reflected in the receiver coherence diameter.³⁹ Reciprocally, the degree of optical turbulence-induced beam spread for focused or collimated laser transmitters may be approximated from the receiver coherence diameter for spherical or plane wave propagation, respectively.

The variance of the log-amplitude ratio is a point statistic relating to optical turbulence-induced random fluctuations in the amplitude of an electromagnetic wave. The log-amplitude ratio is the real part of a complex stochastic integral describing electromagnetic propagation through optical turbulence. Derivation and interpretation of this integral are major concerns of weak perturbation theory. This propagation statistic, commonly called the log-amplitude variance,⁴⁰ is useful in predicting the onset of saturation. Saturation occurs when multiple scattering among optical turbules becomes significant; weak fluctuation theory is then said to "saturate."

The last two basic propagation statistics are scintillation averaging length and isoplanatism effective path length. The scintillation averaging length⁴¹ describes the phenomenon of aperture averaging. As "photon bucket" type photo-receivers increase in area, there is a corresponding decrease in the fluctuations of measured intensity. The scintillation is said to be "averaged" over the area. Apertures with diameters one-tenth the scintillation averaging length exhibit variations in intensity similar to those predicted for a point, while apertures on the order of ten times the scintillation averaging length exhibit little variation in intensity. The isoplanatism effective path length, used with receiver coherence diameter, defines the isoplanatic angle and hence the isoplanatic patch.⁴² Within a region the size of the isoplanatic patch, wave front distortion is nearly constant, and image quality may be improved by the

removal of wave front tilt. Isoplanatic patch size is useful in the design of adaptive devices for partial correction of optical turbulence effects.

In addition to the interpretive value of basic and subsidiary propagation statistics, IMTURB provides path specific fast and slow modulation transfer functions. These may be used in conjunction with an image processing system to allow simulation of specified EO system behavior in a controlled, sterile environment.

4.0 SAMPLE MODEL RESULTS

Two sample scenarios are described here to illustrate typical model results. In the first scenario, Case A, an EO imaging sensor operating at $1.06 \mu\text{m}$ and located 2 m above the ground observes a target 500 m distant and 11 m above the ground. Spherical wave propagation is appropriate with the source at the target. The site is White Sands Missile Range (WSMR), New Mexico (USA), located at latitude 32° north, longitude 106° west. The date is 31 May 1984; the time is 1300 mountain standard time (MST), translating to a GMT of 2000. The day is cloudless; the upwind terrain is a broad region of desert brush and scrub, having a tabulated roughness length of 16 cm. From a nearby observation tower with sensors located 10 m above the ground, air temperature is 35°C ; pressure is 850 mbar (the altitude of the Tularosa Basin where the WSMR is located is 4000 ft above sea level); and the average windspeed is 3 m/s. IMTURB characterizes the atmosphere as strongly unstable, with the height of the surface boundary layer estimated at 11 m. The set of basic and subsidiary propagation statistics for Case A is given in table 1. Note that log-amplitude

variance is 0.206, indicating that Case A is within the limits of weak fluctuation theory.

Table 1. Basic and Subsidiary Propagation Statistics for Case A

| Basic Propagation Statistics | | |
|--------------------------------------|-------|----------------|
| * Receiver Coherence Diameter | 1.54 | centimeters |
| * Log-Amplitude Variance | 0.206 | nepers-squared |
| * Scintillation Averaging Length | 2.78 | centimeters |
| * Isoplanatism Effective Path Length | 117.7 | meters |
| Subsidiary Propagation Statistics | | |
| * Limiting Resolution Source Length | 3.89 | centimeters |
| * Isoplanatism Source Size | 3.26 | centimeters |
| * Normalized Intensity Variance | 1.28 | |

The conditions chosen for Case B illustrate the significant difference in optical turbulence structure arising from relatively minor changes in environmental conditions. The location, terrain, time, temperature, and pressure are identical to Case A. However, cloud cover has increased to 25 percent and windspeed to 5 m/s. IMTURB predicts a moderately unstable atmosphere with the height of the surface boundary layer near 43 m. The basic and subsidiary propagation statistics for Case B are listed in table 2, from which we see that log-amplitude variance is reduced to 0.092, well within the bounds of weak fluctuation theory.

Table 2. Basic and Subsidiary Propagation Statistics for Case B.

| Basic Propagation Statistics | | |
|--------------------------------------|-------|----------------|
| * Receiver Coherence Diameter | 2.65 | centimeters |
| * Log-Amplitude Variance | 0.092 | nepers-squared |
| * Scintillation Averaging Length | 2.93 | centimeters |
| * Isoplanatism Effective Path Length | 126.0 | meters |
| Subsidiary Propagation Statistics | | |
| * Limiting Resolution Source Length | 2.26 | centimeters |
| * Isoplanatism Source Size | 5.25 | centimeters |
| * Normalized Intensity Variance | 0.44 | |

Due to space limitations, the variety of atmospheric stability and similarity parameters descriptive of the micrometeorology have been omitted. However, we have included profiles for the turbulent inner and outer scales and for the refractive index structure parameter. These profiles characterize the optical turbulence structure over the region encompassing the propagation path and are adequate even for advanced applications. The three profiles for Cases A and B are listed in figs. 1, 2, and 3. All profiles are terminated at the maximum extent of the surface boundary layer, by definition the absolute value of the Obukhov length. Note that outer scale follows the rule of thumb for unstable atmospheres, that is, outer scale approximately equals height above ground. Inner scale exhibits the dependence on wind velocity observed by numerous investigators.⁴³ The severity of optical turbulence can be determined from the C_n^2 profiles, as shown in fig. 3. Notice that optical turbulence strength decreases rapidly with height in both cases. For these examples, one would expect significant degradation in performance for EO systems operating in the visible to near infrared (IR), and in the far IR over longer ranges. Values for

the receiver coherence diameter of 1.5 cm and 2.6 cm for Cases A and B, respectively, attest to this fact.

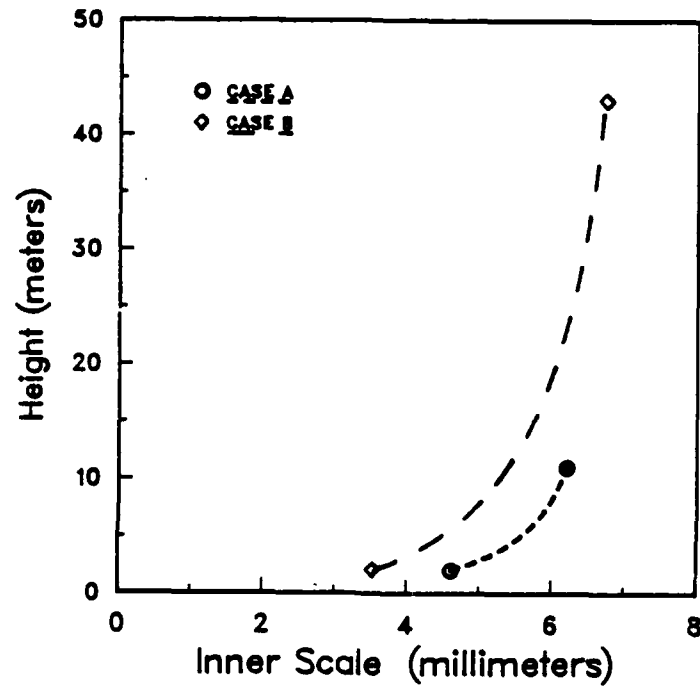


Figure 1. Plot of the Turbulent Inner Scale with Height for Cases A and B

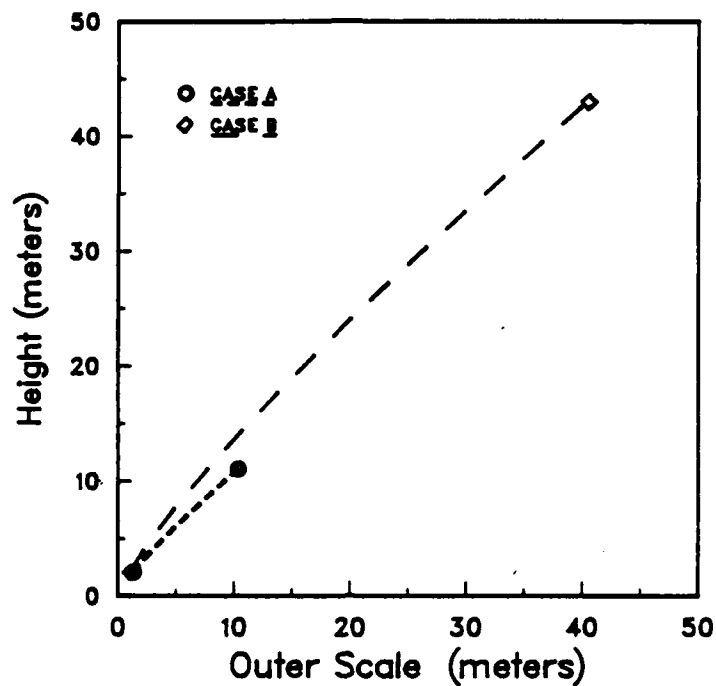


Figure 2. Plot of the Turbulent Outer Scale with Height for Cases A and B

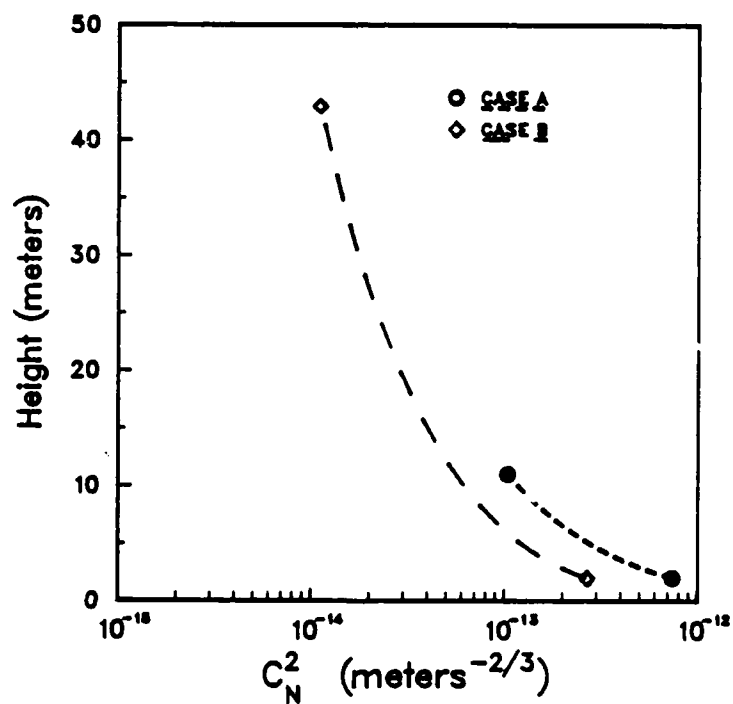


Figure 3. Plot of the Refractive Index Structure Parameter with Height for Cases A and B

Related to the receiver coherence diameter is the subsidiary statistic limiting resolution source size. This is the maximum resolution possible for the propagation path and wavelength regardless of optics size. In terms of laser performance, the limiting resolution source size is the "spot" size of a laser focused to a point. In Case A, the value is 3.9 cm; for Case B, 2.3 cm. In the former case, a sensor would be able to resolve nothing smaller than 3.9 cm on the target at 500 m. In Case B the same system can resolve details as small as 2.3 cm.

Figure 4 provides a comparative plot of log-amplitude variance with range for Cases A and B. The increase in range of validity for weak fluctuation theory in the latter case is noticeable. The relatively short distances to saturation in comparison with normal engagement ranges are a strong incentive to extend model results by use of strong perturbation theory. It is also instructive to plot receiver coherence diameter versus range for Cases A and B. Referring to fig. 5, we see that as range increases, the integrated effect of optical turbulence is evident, as is the consistently superior performance of the system operated under the environmental conditions of Case B.

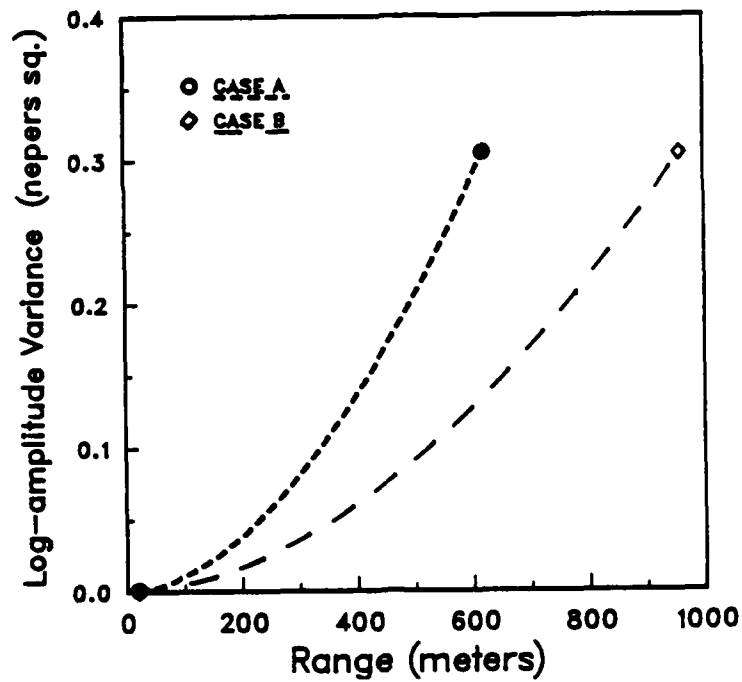


Figure 4. Plot of the Log-Amplitude Variance with Range, Extended to Saturation. The Sensor is at 2 m and Target is at 11 m (Cases A and B)

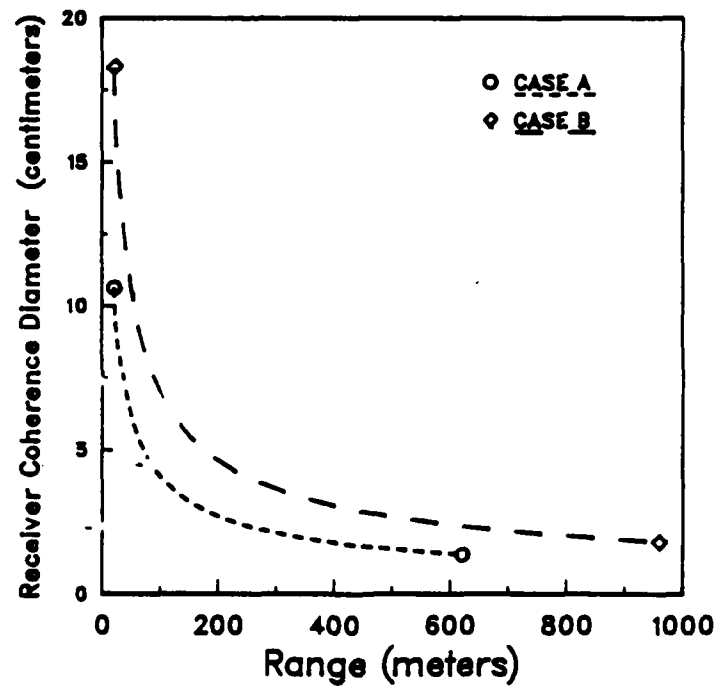


Figure 5. Plot of the Receiver Coherence Diameter with Range for a Sensor at 2 m and Target at 11 m (Cases A and B)

An interesting property of certain propagation statistics that occur as integrals over the propagation path is the phenomenon of path weighting. For spherical wave propagation, receiver coherence diameter exhibits this trait. Consider a scenario identical to Case A except that the sensor and target positions are reversed. The receiver coherence diameter calculated for a sensor at 11 m and target at 2 m, with a path length of 500 m, is 2.6 cm. This represents, coincidentally, the increase in system performance of Case B over Case A. A plot of receiver coherence diameter versus range for the two sensor/target geometries is given in fig. 6.

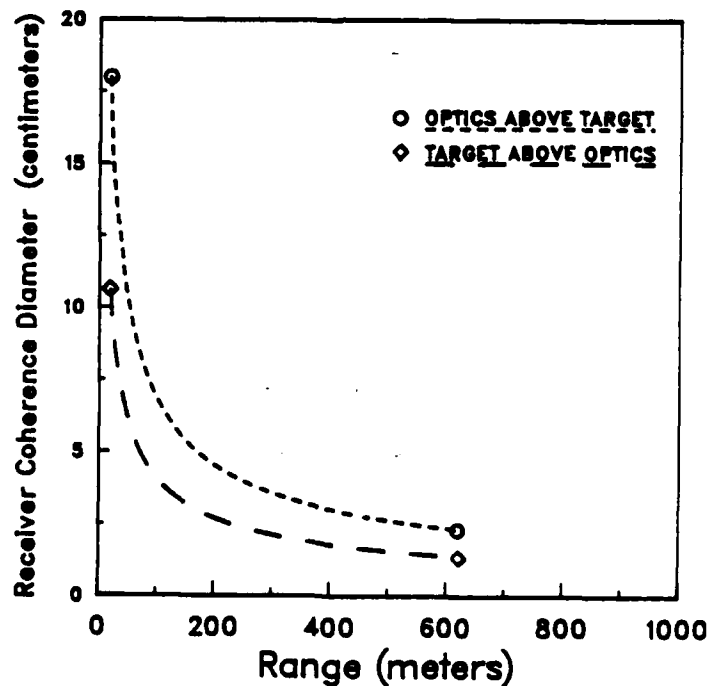


Figure 6. Plot of Receiver Coherence Diameter versus Range for Case A, and with Target and Optics Positions Reversed

Perhaps the most exciting application of the IMTURB model arises from its use in simulating degradation due to optical turbulence using digital image processing techniques.^{44 45} The U.S. Army Atmospheric Sciences Laboratory (ASL) has incorporated an IMTURB clone into ASL's library of models for simulation of atmospheric effects on system performance, called BATL. BATL is currently under development at the ASL Image Processing Laboratory and employs a Gould IP8500 with real time digital disk and VAX 11/780 host computer. Examples of image degradation due to optical turbulence performed in near real-time using a convolution technique are given below. Figure 7 shows an image of a tank taken at a far-IR wavelength over a 2330-m path. Figure 8 is the same image, viewed over a horizontal path through moderate optical turbulence. If the sensor is raised about 10 m above the ground, we see that optical turbulence effects are reduced, as shown in fig. 9. Figure 10 demonstrates the blurring effect severe optical turbulence produces.



Figure 7. Image of a Tank Taken at a Far-IR Wavelength Over a 2330-m Path.

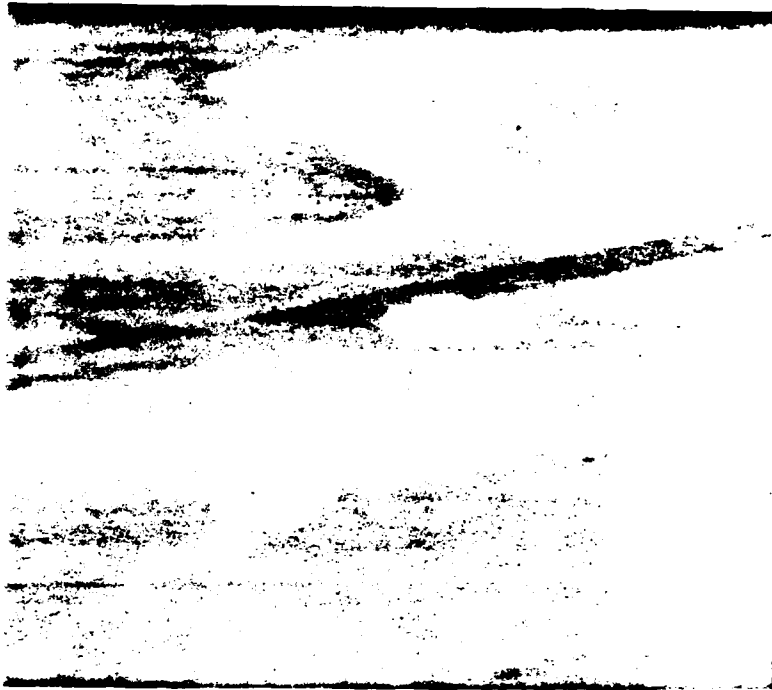


Figure 8. Same Image as Above but Viewed Over a Horizontal Path Through Moderate Optical Turbulence



Figure 9. Optical Turbulence Effects are Reduced When the Sensor is Raised About 10 m Above the Ground



Figure 10. The Blurring Effect Severe Optical Turbulence Produces

LITERATURE CITED

- Andrews, L. C., and R. L. Phillips, 1989: "New temperature spectrum model based on fluctuations in the average dissipation rate," Propagation Engineering, N. S. Kopeika and W. B. Miller, eds, Proceedings SPIE 1115.
- Batchelor, G. K., 1947: "Kolmogoroff's theory of locally isotropic turbulence," Proceedings Camb Phil Soc, 43, 533-559.
- Busch, N. E., 1973: "On the mechanics of atmospheric turbulence," Workshop on Micrometeorology, D. A. Haugen, ed, pp. 1-65, American Meteorological Society.
- Businger, J. A., 1973: "Turbulent transfer in the atmospheric surface layer," Workshop on Micrometeorology, D. A. Haugen, ed, pp. 67-100, American Meteorological Society.
- Clifford, S. F., 1978: "The classical theory of wave propagation in a turbulent medium," Laser Beam Propagation in a Turbulent Atmosphere, J. W. Strohbehn, ed, pp 9-44, Springer-Verlag, New York.
- Durack, D. L., and M. K. Giles, 1988: "Method to compute space-variant image degradation by atmospheric turbulence," Optical, Infrared and Millimeter Wave Propagation Engineering, W. B. Miller and N. S. Kopeika, eds, Proceedings SPIE 926, 286-295.
- Fried, D. L., 1966: "Optical resolution through a randomly inhomogeneous medium for very long and very short exposures," J Opt Soc Am, 56, 1372.
- Fried, D. L., 1967: "Aperature averaging of scintillation," J Opt Soc Am, 57, 169.
- Fried, D. L., 1974: Theoretical Study of Non-Standard Imaging Concepts, Interim Technical Report on RADC Contract No F30602-74-C-0115, RADC Report No TR-74-185 and RADC Report No TR-74-276, Rome Air Development Center, Griffiss Air Force Base, NY.
- Fried, D. L., 1974: Theoretical Study of Non-Standard Imaging Concepts, RADC-TR-76-51 (AD A023627), Rome Air Development Center, Griffiss Air Force Base, NY.
- Fried, D. L., Theoretical Analysis of Aperature Averaging, Optical Science Consultants Report No. DR-015, Final Report of NASA Contract NAS5-23272.
- Giles, M. K., and D. L. Durack, 1988: "A convolution model of long-exposure image blur due to atmospheric turbulence," Optical Infrared and Millimeter Wave Propagation Engineering, W. B. Miller and N. S. Kopeika, eds, Proceedings SPIE 926, 296-304.
- Goodman, J. W., 1985: Statistical Optics, pp 361-457, John Wiley & Sons, New York.
- Hansen, F. V., 1977: The Critical Richardson Number, ECOM-5829, U.S. Army Atmospheric Sciences Laboratory, White Sands Missile Range, NM.

- Hansen, F. V., 1980: Flux Profile Relationships for Development of Standards of Comparison, Internal Report, U.S. Army Atmospheric Sciences Laboratory, White Sands Missile Range, NM.
- Hill, R. J., 1978: "Models of the scalar spectrum for turbulent advection," J Fluid Mech 88(3), 541-562.
- Ishimaru, A., 1978: Wave Propagation and Scattering in Random Media, Vol I and II, Academic Press, New York.
- Kolmogoroff, A. N., 1941: "Dissipation of energy in the locally isotropic turbulence," C R Acad Sci, U.S.S.R., 32(1), 16-18.
- Kolmogoroff, A. N., 1941: "The local structure of turbulence in incompressible viscous fluid for very large Reynolds' numbers," C R Acad Sci, U.S.S.R., 30(4), 301-305.
- Kung, E. C., 1963: "Climatology of aerodynamic roughness parameter and energy dissipation in the planetary boundary layer of the northern hemisphere," Annual Report, Studies of the Effects of Variations in Boundary Conditions on the Atmospheric Boundary Layer, Contract DA-36-039-AMC-00878-0, Department of Meteorology, University of Wisconsin, Madison, WI.
- Liu, M., D. Durran, P. Mundkur, M. Yocke, J. Ames, 1976: The Chemistry, Dispersion and Transport of Air Pollutants Emitted From Fossil Fuel Power Plants in California: Data Analysis and Emission Impact Model, Contract Report No. EF76-18R, Systems Applications, Incorporated, San Rafael, CA.
- Miller, W. B., J. C. Ricklin, and W. J. Stewart, 1987: An Optical Turbulence Code for the Surface Boundary Layer ASL-TR-0220, U.S. Army Atmospheric Sciences Laboratory, White Sands Missile Range, NM.
- Miller, W. B., and J. C. Ricklin, 1988: "Description of optical turbulence effects on propagation in the atmospheric surface boundary layer," Optical, Infrared and Millimeter Wave Propagation Engineering, W. B. Miller and N. S. Kopeika, eds, Proceedings SPIE 926, 268-277.
- Miller, W. B., and J. C. Ricklin, 1989: IMTURB: A Module for Imaging Through Optical Turbulence, ASL-TR-0221-27, U.S. Army Atmospheric Sciences Laboratory, White Sands Missile Range, NM. (in preparation)
- Obukhoff, A., 1941: "On the energy distribution in the spectrum of a turbulent flow," C R Acad Sci, U.S.S.R., 33(1), 19-21.
- Ochs, G. R., 1989: formerly with NOAA/WPL, Privately communicated through D. Tofsted, U.S. Army Atmospheric Sciences Laboratory, White Sands Missile Range, NM.
- Ochs, G. R., and R. J. Hill, 1985: "Optical-scintillation method of measuring turbulence inner scale," Appl Opt, 24(15), 2430-2332.

Note: Articles were translated using the spelling "Kolmogoroff," while modern usage has name spelled "Kolmogorov." Thus, we use "Kolmogorov" in the text, and "Kolmogoroff" in references.

- Paulson, C. A., 1970: "The mathematical representation of wind speed and temperature profiles in an unstable atmospheric surface layer," J Appl Meteorol, 9, 857-861.
- Ricklin, J. C., 1986: The Impact of Optical Turbulence on Target Acquisition, ASL-TR-0209, U.S. Army Atmospheric Sciences Laboratory, White Sands Missile Range, NM.
- Smith, F. B., 1972: "Proceedings of the Third Meeting of the Expert Panel on Air Pollution Modeling," NATO Committee on the Challenges of Modern Society, ch XVII, Paris, France.
- Smith, F. B., 1979: "The relation between Pasquill stability P and Kazanski-Monin stability (in neutral and unstable conditions)," Atmos Environ, Pergamon Press Ltd., United Kingdom 13, 879-881.
- Smith, F. B., and R. M. Blackhall, 1979: "The application of field experiment data to the parameterization of plumes from ground level and elevated sources," Mathematical Modeling of Turbulent Diffusion in the Environment, C. J. Harris, ed, Academic Press, New York.
- Stewart, W. J., 1985: An HP-9825 Computer Model for Turbulent Velocity Spectra, ASL-CR-85-0100-2, U.S. Army Atmospheric Sciences Laboratory, White Sands Missile Range, NM.
- Tatarski, V. I., 1961: Wave Propagation in a Turbulent Medium, trans, R. A. Silverman, McGraw-Hill Book Co., New York.
- Wyngaard, J. C., 1973: "On surface layer turbulence," Workshop on Micrometeorology, ed, D. A. Haugen, pp. 101-149, American Meteorological Society.

ENDNOTES

¹ A. N. Kolmogoroff, "The local structure of turbulence in incompressible viscous fluid for very large Reynolds' numbers," C. R. Acad. Sci., U.S.S.R. 30(4), 301-305 (1941).

² A. N. Kolmogoroff, "Dissipation of energy in the locally isotropic turbulence," C. R. Acad. Sci., U.S.S.R. 32(1), 16-18 (1941).

³ G. K. Batchelor, "Kolmogoroff's theory of locally isotropic turbulence," Proc. Camb. Phil. Soc., 43, 533-559 (1947).

⁴ V. I. Tatarski, Wave Propagation in a Turbulent Medium, trans. R. A. Silverman, McGraw-Hill Book Co., New York (1961).

⁵ W. B. Miller and J. C. Ricklin, U.S. Army Atmospheric Sciences Laboratory, White Sands Missile Range, New Mexico, IMTURB: A Module for Imaging Through Optical Turbulence (1989), ASL-TR-0221-27. (in preparation)

⁶ J. C. Ricklin, U.S. Army Atmospheric Sciences Laboratory, White Sands Missile Range, New Mexico, The Impact of Optical Turbulence on Target Acquisition (1986), ASL-TR-0209.

⁷ Tatarski, V. I., op. cit.

⁸ A. Ishimaru, Wave Propagation and Scattering in Random Media, Vol. I and II, Academic Press, New York (1978).

⁹ S. F. Clifford, "The classical theory of wave propagation in a turbulent medium," Laser Beam Propagation in a Turbulent Atmosphere, J. W. Strohbehn, ed., pp. 9-44, Springer-Verlag, New York (1978).

¹⁰ J. W. Goodman, Statistical Optics, pp. 361-457, John Wiley & Sons, New York (1985).

¹¹ A. Obukhoff, "On the energy distribution in the spectrum of a turbulent flow," C. R. Acad. Sci., U.S.S.R., 33(1), 19-21 (1941).

¹² N. E. Busch, "On the mechanics of atmospheric turbulence," in Workshop on Micrometeorology, D. A. Haugen, ed., pp. 1-65, American Meteorological Society (1973).

¹³ J. A. Businger, "Turbulent transfer in the atmospheric surface layer," in Workshop on Micrometeorology, D. A. Haugen, ed., pp. 67-100, American Meteorological Society (1973).

¹⁴ J. C. Wyngaard, "On surface layer turbulence," in Workshop on Micrometeorology, D. A. Haugen, ed., pp. 101-149, American Meteorological Society (1973).

¹⁵ Ishimaru, A., op. cit., Vol. II, Appendix C.

¹⁶ G. R. Ochs and R. J. Hill, "Optical-scintillation method of measuring turbulence inner scale," Appl. Opt., 24(15), 2430-2332 (1985).

- ¹⁷ Ishimaru, A., op. cit., pp. 420-422.
- ¹⁸ R. J. Hill, "Models of the scalar spectrum for turbulent advection," J. Fluid Mech., 88(3), 541-562 (1978).
- ¹⁹ L. C. Andrews and R. L. Phillips, "New temperature spectrum model based on fluctuations in the average dissipation rates," in Propagation Engineering, N. S. Kopeika and W. B. Miller, eds., Proc. SPIE 1115 (1989).
- ²⁰ Miller, W. B., and J. C. Ricklin, op. cit., Appendix B.
- ²¹ E. C. Kung, Dept. of Meteorology, University of Wisconsin, Madison, WI, "Climatology of aerodynamic roughness parameter and energy dissipation in the planetary boundary layer of the northern hemisphere," in Annual Report Studies of the Effects of Variations in Boundary Conditions on the Atmospheric Boundary Layer (1963), Contract DA-36-039-AMC-00878-0.
- ²² W. J. Stewart, U.S. Army Atmospheric Sciences Laboratory, White Sands Missile Range, New Mexico, An HP-9825 Computer Model for Turbulent Velocity Spectra (1985), ASL-CR-85-0100-2.
- ²³ W. B. Miller, J. C. Ricklin, and W. J. Stewart, U.S. Army Atmospheric Sciences Laboratory, White Sands Missile Range, New Mexico, An Optical Turbulence Code for the Surface Boundary Layer (1987), ASL-TR-0220.
- ²⁴ Miller, W. B., and J. C. Ricklin, op. cit., Appendix C.
- ²⁵ F. B. Smith, "The relation between Pasquill stability P and Kazanski-Monin stability (in neutral and unstable conditions)," in Atmospheric Environment, Pergamon Press Ltd., United Kingdom 13, 879-881 (1979).
- ²⁶ F. B. Smith, "Proceedings of the Third Meeting of the Expert Panel on Air Pollution Modeling," in NATO Committee on the Challenges of Modern Society (Paris, France, 1972), ch. XVII.
- ²⁷ M. Liu et al., National Technical Information Center, The Chemistry, Dispersion and Transport of Air Pollutants Emitted From Fossil Fuel Power Plants in California: Data Analysis and Emission Impact Model, Contract Report No. EF76-18R, (1976).
- ²⁸ Businger, J. A., op. cit.
- ²⁹ F. V. Hansen, U.S. Army Atmospheric Sciences Laboratory, White Sands Missile Range, New Mexico, Flux Profile Relationships for Development of Standards of Comparison (1980), Internal Report.
- ³⁰ F. V. Hansen, U.S. Army Atmospheric Sciences Laboratory, White Sands Missile Range, New Mexico, The Critical Richardson Number (1977), ECOM-5829.
- ³¹ C. A. Paulson, "The mathematical representation of wind speed and temperature profiles in an unstable atmospheric surface layer," J. Appl. Meteorol., 9, 857-861 (1970).

³² F. B. Smith and R. M. Blackhall, "The application of field experiment data to the parameterization of plumes from ground level and elevated sources," in Mathematical Modeling of Turbulent Diffusion in the Environment, C. J. Harris, ed., Academic Press, New York (1979).

³³ Tatarski, V. I., op. cit.

³⁴ Ishimaru, A., op. cit.

³⁵ Clifford, S. F., op. cit.

³⁶ W. B. Miller and J. C. Ricklin, "Description of optical turbulence effects on propagation in the atmospheric surface boundary layer," in Optical, Infrared and Millimeter Wave Propagation Engineering, W. B. Miller and N. S. Kopeika, eds., Proc. SPIE 926, 268-277 (1988).

³⁷ Miller, W. B., and J. C. Ricklin, op. cit.

³⁸ D. L. Fried, Rome Air Development Center, Griffiss Air Force Base, New York, Theoretical Study of Non-Standard Imaging Concepts (1976), RADC-TR-76-51 (AD A023627).

³⁹ D. L. Fried, "Optical resolution through a randomly inhomogeneous medium for very long and very short exposures," J. Opt. Soc. Am., 56, 1372 (1966).

⁴⁰ D. L. Fried, "Aperture averaging of scintillation," J. Opt. Soc. Am., 57, 169 (1967).

⁴¹ D. L. Fried, Theoretical Analysis of Aperture Averaging, Optical Science Consultants Report No. DR-015, Final Report on NASA Contract NAS5-23272.

⁴² D. L. Fried, Rome Air Development Center, Griffiss Air Force Base, New York, Theoretical Study of Non-Standard Imaging Concepts, Interim Tech. Report on RADC Contract No. F30602-74-C-0115, RADC Report No. TR-74-185 (1974) and RADC Report No. TR-74-276 (1974).

⁴³ G. R. Ochs, formerly with NOAA/WPL, Privately communicated through D. Tofsted, U.S. Army Atmospheric Sciences Laboratory, White Sands Missile Range, New Mexico, (1989).

⁴⁴ D. L. Durack and M. K. Giles, "Method to compute space-variant image degradation by atmospheric turbulence," in Optical, Infrared and Millimeter Wave Propagation Engineering, W. B. Miller and N. S. Kopeika, eds., Proc. SPIE 926, 286-295 (1988).

⁴⁵ M. K. Giles and D. L. Durack, "A convolution model of long-exposure image blur due to atmospheric turbulence," in Optical, Infrared and Millimeter Wave Propagation Engineering, W. B. Miller and N. S. Kopeika, eds., Proc. SPIE 926, 296-304 (1988).

THIS PAGE INTENTIONALLY BLANK

ADAPTIVE TERRAIN MODELS
FOR REAL-TIME SIMULATION

Lori L. Scarlatos
Grumman Data Systems, M.S. D12-237
1000 Woodbury Road
Woodbury, NY 11797

ABSTRACT

Flexibility and speed of the digital/electronic terrain board simulations depends on the cartographic data structures used to produce simulations. We have consequently identified three primary requirements for terrain data structures to support maximum flexibility and speed. Specifically, data structures must support (1) multiple levels of detail, (2) fast spatial search, and (3) data compression without loss of accuracy. We present two hierarchical terrain data structures which support these capabilities. The first structure is a quadtree built via pyramidal decomposition. The second structure is a hierarchical arrangement of triangulated irregular networks (TINs). In this paper we describe both structures, discussing the benefits and limitations of both, and presenting implementation results.

1. INTRODUCTION

Designed to simulate the real world in three or more dimensions and in all useful spectrums, the digital/electronic terrain board requires cartographic data structures that will support its proposed capabilities. Cartographic data structures significantly effect the speed and flexibility with which data may be accessed, processed, and displayed. Therefore, careful consideration must be given to these structures. A recent report out of Rome Air Development Center [Tesser88] identified three primary data structure requirements for fast and flexible 3D visualization of cartographic data: (1) multiple levels of detail, (2) fast spatial search, and (3) data compression without loss of accuracy. These requirements are equally applicable to the digital/electronic terrain board.

Of all the cartographic entities used by digital cartographic applications, terrain topology is the most important, providing a foundation upon which all other data sources are based. Most digital simulator systems rely on terrain data stored in a grid format such as the Defense Mapping Agency's Digital Terrain Elevation Data (DMA DTED). Grid formats store elevation

values in a two-dimensional matrix. Row and column positions in the matrix correspond to latitude and longitude on the earth, with a fixed increment between the measured elevation samples (posts). Perspective views of a terrain grid may be generated from a regular triangular mesh produced by connecting the posts with triangle edges.

We have chosen to focus on terrain data structures for the digital/electronic terrain board. In the remainder of this section we discuss the three data structure requirements listed above, showing that the traditional grid structure is inadequate. We then present two alternative data structures that do meet the requirements: quadtrees and refined triangulation hierarchies. The second section describes quadtrees: what quadtrees are, how we build and store quadtrees representing terrain, and our implementation results. The third section similarly describes refined triangulation hierarchies. The section after that explores trade-offs of the two data structures, and the final section draws some conclusions about the work that we have done.

1.1 MULTIPLE LEVELS OF TERRAIN DETAIL

Different points of view, as well as different situations, require different levels of detail in terrain representation. High resolution data provides essential detail to applications in which relatively small surface changes are important in a localized area. Some examples are low-level flight simulation, radar simulation, and trafficability, visibility, and cross country movement analysis. On the other hand, lower resolutions enable faster processing and display of data covering a larger gaming area. Applications with a global scope -- such as C³I mission planning and long distance flight plans -- therefore benefit from the use of lower resolution data. Although low resolutions contain less information, they must accurately retain critical terrain information, losing only insignificant details. Otherwise the resulting representation will be misleading.

Because there are benefits and drawbacks to selecting any level of detail, mixed resolutions will be useful to the digital/electronic terrain board. Combining various levels of detail can increase the scope of a view without significantly increasing the number of polygons. Close-

range or tactically important areas may be represented with high levels of detail, while peripheral areas need only generalized representation with low levels of detail. Such fish-eye views provide fast visualizations with required levels of detail without overloading the display buffer.

Multiple levels of detail in gridded data are commonly achieved by modifying the distance between posts. However, because they do not adaptively conform to the terrain, gridded data are inadequate for applications in which accuracy, processing time, or a smooth transition between resolutions is important. For example, small post increments for high levels of detail result in a very large number of polygons which may or may not be essential to the terrain representation. This is a problem because any unnecessary polygons will unnecessarily increase processing time for 3D display or sensor simulation. On the other hand, low levels of detail with greater distances between posts ignore terrain characteristics. Critical features may therefore appear to move, change size or shape, or even disappear altogether in the lower resolutions. And because there is no smooth transition between resolutions, terrain features can fluctuate or even pop in and out of view, thereby distracting the viewer.

Figures 1 and 2 illustrate some of these problems. We selected a 256x256 grid of DTED-1 elevation posts -- representing less than 15x15 arc minutes over Nevada -- as a test region. Figure 1 shows a perspective view of that area, represented by a mesh of 131,072 triangles. We then subsampled the data three times, producing meshes over the same area but with approximately 10000, 5000, and 2500 triangles respectively. Figure 2 shows perspective renderings of these subsampled grids, using the same perspective view as figure 1. Notice how the square hill in the foreground becomes a cone, and then shifts off of the page. This anomaly becomes even more apparent in dynamic simulations.

1.2 FAST SPATIAL SEARCH

Fast data search and retrieval reduce the time required to produce a single simulated sensor image, and will make dynamic simulations possible in the digital/electronic terrain board. For example, we must rapidly access elevation data at successive points along a route to simu-

late targets moving over the terrain. Point location is also important for querying the data base about a position, and for interactively inserting and removing targets in "what-if" scenarios. Fast range retrieval reduces time spent producing multiple resolution terrain representations and mapping images to terrain surfaces. Fast neighborhood searches are important for retrieving blocks of data in simulated fly-throughs, and for gathering information about neighboring locations. They also simplify line-of-sight and shadow analysis, contour generation and, in some cases, hidden surface calculations.

Both data compaction and clever organization help facilitate fast spatial searches. The regularity of gridded terrain data provides the best structure for fast access with a search time of $O(1)$. The more adaptive structures in relational and vector data bases -- such as Tactical Terrain Data -- have an inherent search time of $O(n)$. This is because each record of a relational structure must be examined sequentially until the desired data are found. Hierarchical structures are a compromise, storing data adaptively while facilitating $O(\log n)$ search time. To see how significant these orders of complexity can be, suppose that a data base has one million elements to search. Searching for data at a given spatial location could take up to one million operations in a relational structure, twenty operations in a hierarchical structure, and one operation in a terrain grid.

1.3 DATA COMPRESSION WITHOUT LOSS OF ACCURACY

Data compression facilitates fast data access, processing, and display, and enables simulations to employ larger gaming areas. The need for data compression is best illustrated by looking at requirements for visualizing flight over a region. At an altitude of 200 feet, a pilot can see up to 30 kilometers ahead. With a 160 degree field of view, the area of visibility covers 1254 square kilometers. Using gridded data with a post spacing of approximately 100 meters, this corresponds to approximately 12,500 posts or 24,200 triangles. At an altitude of 2000 feet, the pilot can see up to 95 kilometers ahead, encompassing 3993 square kilometers of terrain. This corresponds to approximately 40,000 posts or 80,000 triangles.

Commercial graphics systems can currently render approximately 2000 smooth-shaded polygons in real time (1/30th of a second). The two simulations described here would therefore require a compression ratio of 12:1 for the low level flight and 40:1 for flight at the higher altitude. Furthermore, it's important to notice that these numbers do not reflect the additional polygons required to simulate cultural features, or map imagery on the terrain. Such typical additions would further compound the problem. Therefore, although experts in the field generally agree that graphics systems will be able to render more than 30,000 polygons in real time by the year 1991, data compression will still be required.

As shown earlier, subsampling gridded data can produce views which are inaccurate, and therefore inadequate for navigation or mission rehearsal purposes. It is therefore necessary to find a compacting structure which maintains the greatest degree of accuracy possible at each resolution level.

1.4 GRUMMAN APPROACH

Our objective is to develop terrain data structures which meet the above requirements. Specifically, we wish to find a data structure with the following characteristics. First, the data must be adaptive, conforming to the unique characteristics of a piece of terrain. This data will then contain the smallest number of elements possible for the required level of accuracy. Second, multiple levels of detail must be readily available with smooth transitions between the levels. Major features must retain their positions and significant characteristics at all levels of detail. Third, the data must have an underlying structure which facilitates fast spatial searches for point locations, ranges, and neighborhoods. Fourth, the terrain representation must facilitate fast processing and display.

Our approach was to explore two alternative structures for storing multiple resolution terrain: quadtrees and refined triangulation hierarchies. Both structures are adaptive, thereby storing greater detail for more irregular areas and retaining critical features at even the lowest resolutions. We were able to achieve 10:1 compression and better with both structures, resulting

in little or no loss of information [Tesser89] [Scarlato90b]. Both structures are hierarchical, facilitating $O(\log n)$ search time. Hierarchical organization of the levels of detail -- which are derived from one another -- also ensures consistency between resolutions and makes all levels of detail immediately available at all times. This is especially important for dynamic simulation. The following sections describe our approach and results in more depth.

2. QUADTREES

Quadrees have recently attracted much interest as a means for representing image and cartographic data. Part of their appeal is their ability to adaptively represent $2^n \times 2^n$ data arrays in hierarchical levels of detail that conform to a regular grid. Formally, a quadtree is a tree data structure in which the nodes represent square regions covering the original array. The root node covers the entire array. Each non-leaf node has exactly four children representing four quadrants subdividing the region of the parent node. A leaf node represents either a single element in the original array, or a $2^k \times 2^k$ region of the original array which is adequately represented by a single node's elevation or intensity value.

Quadrees and their representations are well documented in the literature [Samet88]. One representation, the linear quadtree [Gargantini82], stores region data as a collection of nodes encoded by a sequence of directional codes also known as quadcodes. Linear quadrees are especially good for spatial search because neighborhood information is intrinsic to the encoding of the nodes [Li87], and the path from the root to a node is contained within that node's quadcode. Quadcodes are concatenations of base 4 digits which specify the location of each leaf node relative to the root of the tree. Every digit in a quadcode corresponds to a quadrant in the subdivision of a region. The position of each digit represents the level of the tree at which that subdivision was made. Thus the length of a quadcode indicates the depth of a tree node, and the quadcode itself provides the path from the root to that node. In addition to the quadcode, each node has an associated value such as elevation or image intensity.

2.1 BUILDING QUADTREES

Quadtree data structures can be built either top-down or bottom-up. We build them top-down by examining the results of a Laplacian pyramid, which is built as follows [Tesser89].

Starting with the actual gridded elevation data we build a pyramid of data levels, each level being one quarter of the size of the level below. A pyramid level is created by smoothing and subsampling the previous level. Smoothing consists of convolving the original elements with a Gaussian kernel which removes high frequencies from the data. The bottom of the resulting pyramid is therefore the original data array, and the top is a single element representing the entire data area. We then build a second pyramid of data which is smoothed only. These two pyramids are used to find the Laplacian pyramid, which is the difference between the other two pyramids.

Finally, we build the quadtree by examining successive levels of the pyramid, starting near the top, and subdividing nodes which need more detail. If a node at the current level adequately represents the region that it covers, then that node becomes a leaf in the tree. We base our subdivision decision on two criteria: the intrinsic roughness of the area, and extrinsic factors which focus on an area of interest. Intrinsic factors simply take into account the fact that large areas can be used to adequately represent slowly varying terrain. Extrinsic factors consider areas which have been defined as being important to an application, such as an area that a pilot may be flying over or the neighborhood of a target.

2.2 IMPLEMENTATION RESULTS

We created a linear quadtree from the same region of DTED used to produce figure 1, as described in section 1.1. Quadtree decomposition took less than 8.5 seconds of CPU time on a VAX 8530, saving 11,396 posts in the linear quadtree. At display time, these points were triangulated in less than 3 CPU seconds producing 22,299 triangles at the highest resolution. This corresponds to 6:1 data compression at the highest level of detail. Visual comparisons and statistical analysis [Tesser89] verified the accuracy of this data set, even at a level producing 10:1

compression.

Figure 2 shows the resulting quadtree at three different levels of detail, corresponding to approximately 10000, 5000, and 2500 triangles respectively. This translates to 13:1, 26:1, and 52:1 compression of the original grid. Notice how well the critical features are retained, as compared to the subsampled DTED grid.

3. REFINED TRIANGULATION HIERARCHIES

Triangulated tessellations have long been recognized as ideal structures for producing fast perspective views. Commonly used by geographic information systems (GIS) and computer image generation systems, triangles are ideal because all points defining a facet are, by definition, co-planar. For this reason, other data forms are often converted into triangles before they are rendered [VonHerzen87] [Snyder87].

Triangulated irregular networks (TINs) are triangulated tessellations used to represent terrain topology. Formally, a TIN is a planar graph consisting of a set of points V and a set of non-intersecting edges E which define triangular regions. These triangular regions completely cover the convex hull containing all elements in V . Irregular triangulations have an advantage of being highly adaptive, allowing smooth areas to be represented by relatively few sample points and triangles; rough or irregular areas may be represented by as many points as are needed to accurately represent the structure. Irregular triangulations may also be made to conform to irregular but important boundaries such as ridge lines, drainage systems, elevation contours, coastlines, and political boundaries. The result is a compact yet precise data representation.

Despite their advantages, TINs do pose several problems. Each TIN represents a single level of detail, providing no guarantee of continuity between two different resolution TINs for the same area. Furthermore, spatial search on a TIN structure takes $O(n)$ time. To overcome these obstacles, we developed the refined triangulation hierarchy.

3.1 BUILDING REFINED TRIANGULATION HIERARCHIES

Refined triangulation hierarchies, first sketched in [Tesser88] and described in full in [Scarlato90b], are TIN levels of detail which are connected by arcs in a hierarchical fashion. Because each level of detail is derived from an earlier level, there is a smooth transition between resolutions, and fast ($O(\log n)$) spatial search is facilitated.

Refined triangulation hierarchies are built bottom-up, starting with a high resolution triangulation. This high resolution triangulation is derived by finding the critical points in a region [Scarlato90a], and then triangulating those points with any number of available algorithms such as those in [Watson84], [Preparata85], [Correc87], [Christensen87] and [Scarlato89]. Every other resolution level is derived from the next higher resolution by selectively removing the least significant points and their associated edges, and then retriangulating resulting holes in the mesh. New triangles in the lower resolution are then linked by arcs to old triangles in the higher resolution, indicating overlaps in the different levels. This process is repeated until the entire area of interest is represented by a minimal number of triangles.

3.2 IMPLEMENTATION RESULTS

We created a triangle reduction data set from the same region of DTED used to produce figure 1, as described in section 1.1. The highest resolution data were created by triangulating ridge and valley lines and elevation contours from the DTED [Scarlato89], producing 5933 points and 11,774 triangles in 7.52 CPU seconds on a VAX 8530. This corresponds to 12:1 data compression at the highest level of detail. Visual comparisons and statistical analysis [Scarlato90b] verified the accuracy of this data set. The final refined triangulation hierarchy was created in 7:42.29 CPU minutes resulting in 27 resolution levels.

Figure 2 shows the resulting refined triangulation hierarchy at three different levels of detail, corresponding to approximately 10000, 5000, and 2500 triangles respectively. This translates to 13:1, 26:1, and 52:1 compression of the original grid. Notice how well the critical features are retained, as compared to the subsampled DTED grid.

4. DATA STRUCTURE TRADE-OFFS

In our analysis of the two selected data structures, we found that both structures address the requirements of the digital/electronic terrain board. Specifically, we found that quadrees and refined triangulation hierarchies have the following advantages.

First, both structures contain related levels of detail in connected hierarchies. This ensures a smooth transition between resolutions, allowing multiple resolution views to be generated with ease.

Second, fast spatial point and range searches are facilitated by the hierarchical structures. Neighborhood searches may also be done on both structures.

Third, both structures are adaptive, ensuring that lower resolutions are missing only the least important data values. This means that critical features will retain their positions and relative shapes at all resolution levels.

Fourth, successively lower resolutions in both structures only eliminate data which are least important to the terrain topology. Thus critical features are retained, and only minimal details are lost.

4.1 QUADTREE ADVANTAGES

Although both structures are good representations for terrain data, we did discover that each has its own advantages over the other. The regular rectangular orientation of quadrees, for example, produces several advantages over TINs. One advantage is that rectangles aligned with the rectangular coordinate system, like partitions in a quadtree, are the simplest shapes to test for intersections. Consequently, the constant factor in the spatial search time complexity is less for quadrees than it is for triangulation hierarchies. Linear quadrees, also by exploiting the regular structure, are able to reduce the search for neighbors to a simple indexing problem by using quadcodes [Li87]. Irregular triangulations must rely on supplemental adjacency information for neighborhood searches.

Another advantage of quadtrees' regular rectangular structure is that they are derived naturally from commonly available gridded sources such as elevation matrixes and digital images. TINs must rely on a separate algorithm to cull critical points from the matrixes to produce points to be triangulated. Therefore the accuracy of a high resolution triangulation, and all related lower resolutions, depends on how critical points and lines are selected.

Finally, quadtrees tend to occupy less disk space than TINs. Quadcodes for a $2^n \times 2^n$ area of interest require $2n$ bits of data each. Each quadcode then needs an additional elevation value. For our 256x256 test region, we therefore stored a 2-byte quadcode and a 2-byte elevation value for each leaf in the quadtree. Thus a 10:1 compression ratio on the points results in a 5:1 compression on disk. TINs, which must store three-dimensional coordinates and adjacency lists, do not compress the data as well on disk.

4.2 REFINED TRIANGULATION HIERARCHY ADVANTAGES

Refined triangulation hierarchies, on the other hand, benefit from the flexibility afforded by irregular triangulations. Triangular facets, for example, are ideal for perspective image generation and sensor simulation. All polygon rendering hardware and software take triangles as input, and frequently require it. TIN data structures may therefore be rendered in real time. Quadtrees are not as flexible as TINs for 3D modelling, requiring a triangulation step before they may be rendered. Although triangulation of our test area takes little more than 3 CPU seconds on a VAX 8530, this is 900 times too slow for real time display.

Another advantage of irregular triangulations is that they have maximum adaptability. This means that points along a ridge or valley line may fall anywhere on the terrain, with any distance between those points, and still appear in the triangulation. It also means that only important points need be saved in the data base. Alternatively, quadtree regions must be split into regular quadrants along lines which have nothing to do with the terrain characteristics. Therefore some of the points in the quadtree are saved in a resolution level because of location within the area, regardless of their topological significance. Furthermore, quadtree structures are

not optimal because all child nodes must be identical in size and orientation.

Finally, TINs may be created from varying data sources, including contour maps and stereo imagery, in addition to the traditional grid formats. Quadtrees may only be built from gridded data.

5. CONCLUSIONS

In this paper we have shown that two adaptive terrain models -- quadtrees and refined triangulation hierarchies -- solve the problems presented by subsampled grid data. These structures retain critical terrain information using minimal amounts of data. This ensures that important features will retain their positions and general shapes at all resolution levels, without bogging the system down with extraneous data. Compression ratios of 10:1 and better have been achieved in our tests with excellent results. These models also store multiple levels of detail hierarchically, providing smooth transitions between data levels and facilitating fast spatial search. Finally, these data structures may be constructed automatically within a reasonable time frame.

Our work with these adaptive structures is not over yet. Currently, we are refining algorithms for building multiple resolution terrain in real time from quadtrees and refined triangulation hierarchies. We are also exploring ways of overcoming the limitations listed above. Finally, we are researching the applicability of these and other hierarchical structures to the storage of multiple resolution cultural data for display and analysis.

6. ACKNOWLEDGEMENTS

My deepest appreciation goes to all the researchers at Grumman Data Systems whose work has been critical to this effort: Herb Tesser, Eric DeMund, and Geoffrey Gardner.

7. REFERENCES

- [Correc87] Correc, Y. and Chapuis, E. (1987). Fast computation of Delaunay triangulations. *Advances in Engineering Software*, 9(2), 77-83.
- [Christensen87] Christensen, A. (1987). Fitting a triangulation to contour lines. *Proceedings of AUTO-CARTO 8*, 57-67.
- [Gargantini82] Gargantini, I (1982). An effective way to represent quadtrees. *Communication of the ACM*. Vol. 25, No. 12. December, 905-910.
- [Li87] Li, S., Loew, M. (1987). The quadcode and its arithmetic. Adjacency detection using quadcodes. *Communications of the ACM*, Vol. 30, No. 7, July, 621-631.
- [Preparata85] Preparata, F.P. (1985). *Computational geometry*. Springer-Verlag.
- [Samet88] Samet, H., Webber, R. (1988). Hierarchical data structures and algorithms for computer graphics. *IEEE Computer Graphics and Applications*, May, 48-68, July, 59-75.
- [Scarlato89] Scarlatos, L.L. (1989). A compact terrain model based on critical topographic features. *Proceedings of AUTO-CARTO 9*, 146-155.
- [Scarlato90a] Scarlatos, L.L. (1989). An automated critical line detector for digital elevation matrixes. To be published.
- [Scarlato90b] Scarlatos, L.L. (1989). A refined triangulation hierarchy for multiple levels of terrain detail. To be presented at IMAGE V, June 1990.
- [Snyder87] Snyder, J.M., and Barr, A.H. (1987). Ray tracing complex models containing surface tessellations. *SIGGRAPH 1987, Computer Graphics*, Vol. 21, No. 4, July, 119-128.
- [Tesser88] Tesser, H., Scarlatos, L.L., DeMund, E., and Beadon, A.D. (1988). *Requirements for the real-time three-dimensional display of digital cartographic data*. Contract No. F30602-87-C-0137, Rome Air Development Center.
- [Tesser89] Tesser, H., and DeMund, E. (1989). Adaptive decomposition of terrain. Presented at AUTO-CARTO 9.
- [VonHerzen87] Von Herzen, B., and Barr, A.H. (1987). Accurate triangulations of deformed, intersecting surfaces. *SIGGRAPH 1987, Computer Graphics*, Vol. 21, No. 4, July, 103-110.
- [Watson84] Watson, D.F. and Philip, G.M. (1984). Survey: systematic triangulations. *Computer Vision, Graphics, and Image Processing*, 26, 217-223.



Figure 1: Full resolution DTED ~ 131,000 polygons



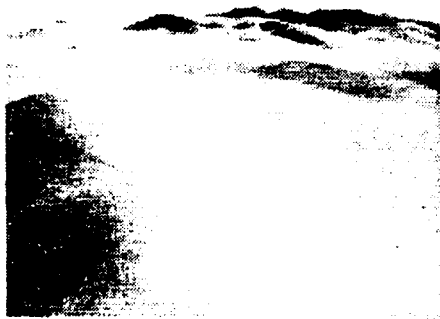
Subsampled DTED ~ 10,000 polygons



Quadtree ~ 10,000 polygons



Refined TIN ~ 10,000 polygons



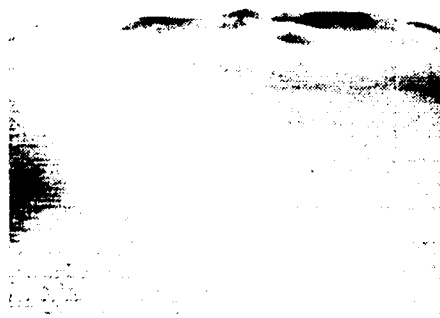
Subsampled DTED ~ 5,000 polygons



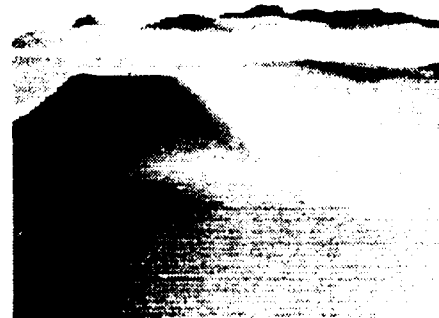
Quadtree ~ 5,000 polygons



Refined TIN ~ 5,000 polygons



Subsampled DTED ~ 2,500 polygons



Quadtree ~ 2,500 polygons



Refined TIN ~ 2,500 polygons

Figure 2: DTED, Quadtree, & Refined Triangulation (TIN) at varying levels of detail

Presented at the
DIGITAL/ELECTRONIC TERRAIN BOARD SYMPOSIUM
5-6 October 1989 GACIAC PR 89-07

Terrain Visualization

Laslo Greczy
US Army Environmental Topographic Laboratory
Attn: CEETL-GL-V
Fort Belvoir, Virginia 22060

ABSTRACT

Functional Area Description. The goal of the Terrain Visualization Functional Area is to provide the Army C3I and training communities with improved capabilities to rapidly combine, effectively visualize, and readily assimilate battlefield terrain, environmental, intelligence and maneuver information. This will be accomplished by developing sophisticated data fusion and 3-D Computer Image Generation (CIG) technologies; and transitioning these capabilities to current and future Army demonstration and development programs.

Principal Developments Scheduled. The following describes the principal hardware/software developments scheduled to provide the Army with this sophisticated terrain visualization capability.

| <u>Principal Development</u> | <u>Completion Date</u> |
|--|------------------------|
| Install and test real time visual system
hardware enhancements to CIG testbed | 3Q FY89 |
| Initiate testbed demonstration tailored to
user scenarios | 4Q FY89 |
| Complete user requirements analysis | FY90 |
| Demonstrate CIG applications for DTSS/ASAS
functionality | FY91 |
| Complete assessment of downsized, low cost
hardware alternatives | FY92 |
| Complete design of modular components for
DTSS/ASAS CIG engine | FY93 |
| Complete design of advanced 3-D mission
planning workstation | FY95 |

Key Technologies. Key technical and developmental issues for this effort fall into five major areas. They are: 1) real time hardware developments and integration; 2) digital terrain data availability and integration; 3) user interface and data fusion capabilities development; 4) applications development, implementation and demonstration; and 5) technology insertion into developmental systems.

Hardware technology barriers in the areas of downsized high throughput computers, high density storage media and high resolution display technology must be overcome to facilitate effective

utilization of CIG technology for tactical applications. Expected advancements in these technologies over the next five years will facilitate the development of fieldable CIG capabilities.

Digital terrain data availability is a key issue for field utilization of CIG technology. Digital Terrain Elevation Data (DTED) is the essential data element for all CIG systems and is gradually becoming available on a world-wide basis. Though Level I Digital Feature Analysis Data (DFAD) is not sufficient to support many tactical CIG applications, plans for Defense Mapping Agency (DMA) Interim Terrain Data (ITD), Tactical Terrain Data (TTD) and Air Force Project 2851 data, as well as the utilization of various imagery sources, will satisfy most CIG data requirements.

Current CIG systems are highly interactive and require extensive operator interaction, particularly in the data base construction and data fusion areas. Significant efforts are required to develop robust data handling and data fusion capabilities that are readily usable by Army analysts and easily implemented on fieldable system architectures.

Though many of the currently available CIG systems operate at real time frame rates (i.e., 30 Hz), the data throughput rates are relatively low and the resultant scenes are not particularly usable for tactical applications. However, many tactical applications do not require real time throughput. Assessments will have to be made to determine field Army scene generation requirements, and applications programs that directly support tactical users will have to be

implemented and demonstrated. A modular, tactical CIG engine will need to be defined in order to hand off the technology to developmental systems.

Development Strategy. In order to meet the objectives of the Terrain Visualization Functional Area, the laboratory CIG capability will be further developed by providing support to other DOD programs. The following objectives will be accomplished through this systematic program support/development process.

- Provide advanced methods for 3-D terrain visualization
- Provide effective simulation techniques for smart weapons
- Provide mission planning/rehearsal capabilities in denied areas
- Support realistic training capabilities in non-lethal environments

Projected Capability (in the period 2000-2010). Rapid effective Terrain Visualization will be accomplished using modular and compact 3-D graphics engines and will be implemented as advanced 3-D mission planning workstations. They will exploit high density storage media and high resolution, large area flat panel displays, VLSI circuitry and parallel processing architectures for real time scene generation. These Terrain Visualization systems will utilize DMA, ITD, TTD, and Air Force Project 2851 data, reconnaissance photography, IR and radar imagery, all source imagery and Image Perspective Transformation (IPT) techniques to produce high quality

3-D perspective scenes. Future CIG systems will provide data throughput rates sufficient to support the detailed data sets required by tactical users. This will facilitate implementation of applications programs that support mission planning/mission rehearsal, command and control, maneuver, IPB and special operations.

THIS PAGE INTENTIONALLY BLANK

Presented at the
DIGITAL/ELECTRONIC TERRAIN BOARD SYMPOSIUM
5-6 October 1989 GACIAC PR 89-07

Multitarget Multisensor Data Fusion:
Radar, ESM, RWR, IFF, and JEM Applications *

Sam P. Chaudhuri
Sensor Data Integration, Inc.
342 Caterina Heights, Concord, MA 01742

ABSTRACT

This paper has focused on the process of combining information from disparate sensors to improve target tracking and classification problems in an automatic target recognition (ATR) system. There are several approaches for handling multitarget multisensor data fusion (MMDF) problem. This paper has also focused on approaches to addressing the problems that would relax the computational and data requirements. This paper, in particular, has considered kinematic as well as attribute data fusion. The kinematic data fusion is accomplished via a Kalman filtering algorithm and the attribute data fusion is performed by three different fusion algorithms:

(1) Voting, (2) Bayesian, and (3) Dempster-Shafer algorithms. A simulator/evaluator has been developed to accomplish a non real-time simulation and evaluation of the MMDF algorithms. The simulation results have demonstrated that target tracking and classification performance is greatly enhanced by using multiple sensors operating in different spectral regions.

* Partially supported by USAF
Contract F19628-87-C-0183

1. INTRODUCTION

To support the mission of the strategic and tactical air control systems, the air surveillance functions must provide a continuous, unambiguous, and current depiction of the airspace situation with respect to friendly, neutral, and hostile aircraft or other enemy threats to the personnel and other resources in the command centers. The following air surveillance capabilities are required to successfully perform the mission:

- (1) detection, and identification of air activity providing position, altitude, heading, and identity information;
- (2) continuous tracking of detected threat objects, selected non-threat, and all friendly objects;
- (3) exchange of air activity information between command centers, tactical air control systems users, other services, and the air defense and command control systems of allied nations;
- (4) correlation or association of sensor tracks within the surveillance system and with inputs from external sources;
- (5) man-machine interaction that will provide an organized presentation of needed information for the decision makers.

The advanced surveillance systems must be capable of providing decision aids for the commanders who must deal with a dense air environment; large quantities of sensor data; multiple dynamic sensors; and a dynamic battle environment. Among the currently fielded surveillance assets that the advanced

surveillance systems must utilize are the radars, ESM sensors, RWR sensors, IFF, and JEM sensors. Potential new surveillance assets that must be planned for include the MMDF system providing better target detection, tracking, and identification capabilities.

The MMDF utilizes a broad range of frequencies which forces an enemy to spread ECM assets over a large portion of the electromagnetic spectrum. A passive detection and tracking capability will support quiet operation when needed, will assist in the location of jamming aircraft as well as other aircraft and cruise missiles, and will provide a capability of identifying non-cooperative aircraft. The resulting fusion of on-board and remote surveillance sensors will fill in gaps in surveillance coverage caused by terrain blockage as well as utilize the low-altitude capabilities of the short range sensors.

This paper has described Sensor Data Integration, Inc.'s approach to the correlation and fusion problems which arise when several sensors carry out surveillance over a certain region. The overall objective is the development of an automated system for detecting, tracking, and identifying targets in a multitarget, multisensor environment. Particularly, this paper has focused on active and passive sensors as previously mentioned. The measurements from these sensor systems/subsystems have varying degrees of uncertainties. The development of the correlation/fusion algorithms accounts for the errors associated with the sensor measurements for the purpose of maintaining an updated combined track file with a high confidence. Thus, the overall accuracy of the combined tracks is improved.

This paper is organized as follows: an introduction to the subject is outlined in section 1. The tracking and ID sensor systems/subsystems are discussed in section 2. In section 3, sensor data correlation techniques are developed; and sensor data fusion techniques are developed in section 4. The simulation results are presented in section 5. A list of references is presented in section 6.

2. ID SENSOR SYSTEMS/SUBSYSTEMS

It is universally recognized that powerful sensors are extremely critical elements of any battle management systems. As the eyes and ears of the battle managers, the sensors must provide necessary information about the target of interest. Since a target may be characterized by many spectral frequencies, a number of dissimilar sensors operating in different spectral regions (for example, MM-Wave radar (1-10 mm) and IR (8-12 microns)) are required for detecting and identifying the targets. Moreover, a number of dissimilar sensors operating in a synergistic manner are required to detect the full variety of targets present in the battle environments.

The sensor systems/subsystems considered in this paper would provide two types of information about the targets:

- (1) kinematic data (position, velocity, and acceleration),
- (2) attribute data (target classification parameters: PRF, PW, Nature (F/H))

There are two approaches to modeling the sensor systems/subsystems:

- (1) analytical approach,
- (2) statistical approach.

This paper has considered statistical modeling of one class of sensors which include IFF, RWR, and JEM sensors. In particular, for simplicity this paper has discussed only the modeling of the IFF sensor.

An IFF sensor consists of two subsystems: an interrogator and a transponder. The output of the IFF is either "response" or "no response". The "response" from the IFF is interpreted as friend (F) and "no response" means either no information or hostile. The statistical approach consists of two steps:

- (1) generation of sensor declarations,
- (2) processing of sensor declarations for computing confidence values.

Generation of IFF Declarations

The IFF system includes two types of errors:

- (1) stochastic errors,
- (2) deterministic errors.

Contributing factors of stochastic errors:

- interference or noise,
- jamming (ECM),
- some trajectory dependent errors.

Contributing factors of fully deterministic errors:

- lack of proper equipment and proper code,
- malfunction of the IFF system,
- hostile spoofer with a knowledge of proper code,
- transponder not turned on for any reason.

The IFF system declaration can be modeled as shown in Figure 1.

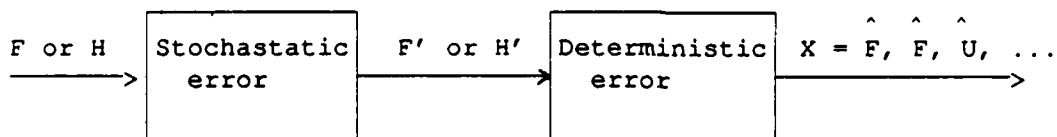


Figure 1.
Modeling of IFF System Declarations

The IFF system parameters are defined as follows:

Stochastic parameters:

$P(F'/F)$ = Probability of a random response given a friend

$P(F'/H)$ = Probability of a random response given a hostile

Deterministic parameters:

$P(F/F')$ = Probability of a consistent response given a friend

$p(F/H')$ = Probability of a consistent response given a hostile

These parameters are used to generate a sequence of IFF declarations.

Now the problem is to compute the IFF system confidence, $P(F/X)$, given a sequence of declarations:

$X = X_1, X_2, \dots, X_n$; and $X_i = \text{either } F \text{ or } u \text{ for all } i\text{'s}$. There are four basic steps to compute the confidence.

Step 1 To compute the likelihood functions

We can compute the likelihood functions $P(X/F)$ and $P(X/H)$ as follows:

$$P(X/F) = P(X/F') P(F'/F) + P(X/H') P(H'/F) \quad (1)$$

Where

$$P(X/F') = \prod_{i=1}^m P(X_i/F')$$

and

$$P(X/H') = \prod_{i=1}^m P(X_i/H')$$

Similarly, $P(X/H)$ is computed as

$$P(X/H) = P(X/F') P(F'/H) + P(X/H') P(H'/H) \quad (2)$$

Step 2 To compute the sum

The sum is calculated as

$$S = P(X/F) P(F) + P(X/H) P(H) \quad (3)$$

where $P(F)$ and $P(H)$ are known a priori probabilities based on the force mix.

Step 3 To compute the a posteriori probability

The a posteriori probabilities (equivalently confidence levels), $P(F/X)$ and $P(U/X)$ are computed as

$$P(F/X) = \{ P(X/F) P(F) \} / S \quad (4)$$

and

$$P(U/X) = \{ P(X/U) P(U) \} / S \quad (5)$$

Step 4 To select the maximum a posteriori probability

The maximum a posteriori probability is selected as the IFF system confidence level for the given sequence of declarations.

Let us explain the concept discussed above through an example.

Example

Assume that the following are the IFF system parameter values:

$$P(F'/F) = 0.96, \quad P(F'/H) = 0.001$$

$$P(F/F') = 0.75, \quad P(F/H') = 0.010$$

It is required to compute the IFF system confidence level as a function of an iteration number when, for example, the sequence of declarations contains all responses. It is also assumed that $P(F) = P(H) = 0.5$.

Solution:

$$(1) \quad X = \hat{F}$$

$$P(X/F) = 0.7204, \quad P(X/H) = 0.0175$$

$$P(F/X) = 0.9763, \quad P(U/X) = 0.0237$$

$$(2) \quad X = \hat{F}, \hat{F}$$

$$P(X/F) = 0.5400, \quad P(X/H) = 0.0057$$

$$P(F/X) = 0.9895, \quad P(U/X) = 0.0105$$

The RWR and JEM sensors have been modeled like the IFF system. For details of the modeling of radar and ESM sensor, the reader is referred to [1].

3. MULTISENSOR DATA CORRELATION TECHNIQUES FOR MULTITARGET ENVIRONMENT

This paper addresses the multisensor report to track correlation and fusion problems which arises when multiple sensors carry out surveillance over a certain region and each sensor has its own data processing unit. The question is how to decide whether two or more reports from different sensor subsystems represent the same target. The correlation refers to the process of associating or grouping together tracks as arising from the same target. The fusion refers to the process of combining the correlated reports from different sensor subsystems for the same target into a single track.

The sensor data correlation and correlated data fusion constitute the heart of the MMDF problem. The process of data correlation and fusion is outlined in Figure 2. Here the correlation module correlates the inputs from all the sensors to the tracks in the master track file. Then the outputs from the correlation module are provided as inputs to the fusion module which uses the correlated track data to update the master track file. This task of correlation and fusion is the subject of the multitarget multisensor data fusion problem.

-
1. Sensor Data Integration, Inc., "Artificial Intelligence Applications to Command, Control, & Communications Systems/Subsystems," Contract No. F19628-87-C-0183, February 1988.

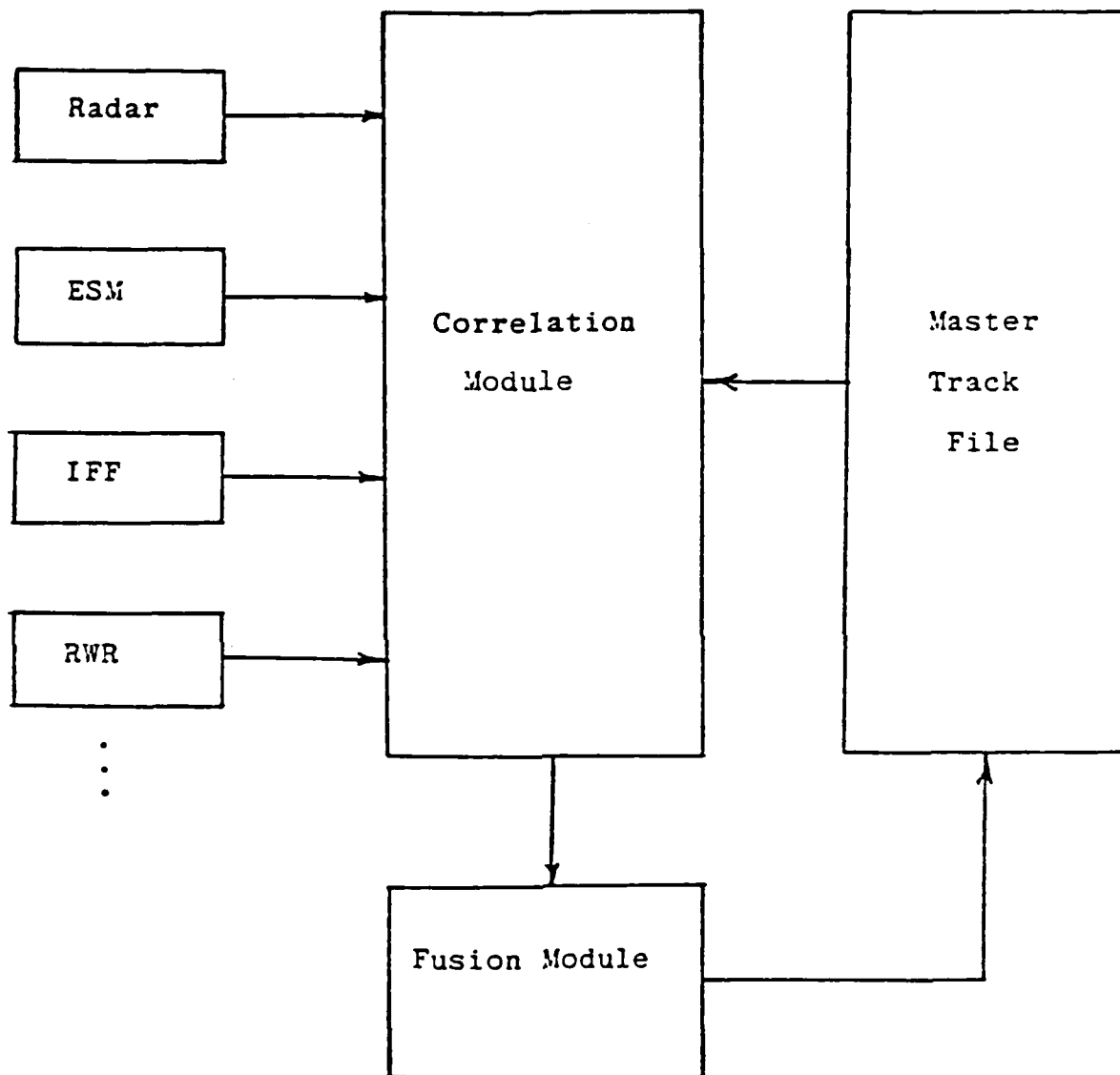


Figure 2.

Measurement to Track Correlation and Fusion Architecture

The key to achieving the goals of real-time C3 systems technology hinges on efficient techniques for real-time multisensor data correlation and fusion. The intent of this study is to develop efficient and effective decision algorithms for proper correlation of multiple sensor data.

3.1 Suboptimal Approach to Multitarget Multisensor Data Correlation

In multitarget multisensor correlation problems, there are two types of uncertainties: (1) uncertainty associated with the sensor measurements, and (2) uncertainty associated with the origin of the measurements. There is always some uncertainties associated with the measurements that are generated by the sensors. Moreover, when there are multiple targets in the same neighborhood, it is difficult to correlate multiple measurements with the multiple targets. Thus the multitarget multisensor correlation problem centers around the measurement origin uncertainty along with the errors imported to the sensor measurements. There are various approaches for handling the multitarget multisensor correlation problem, including optimal decision, maximum likelihood, and track-split filter methods [2].

To overcome the computational problems for real-time applications, suboptimal Bayesian approaches have been investigated in this study. In particular, the following suboptimal approaches have been considered: Probabilistic Data Association (PDA), and Joint Probabilistic Data Association (JPDA) [1].

-
2. R. Carroll, S. Chaudhuri, and M. Mayor, "Multitarget and Multisensor Tracking," A Five-Day Short Course, The George Washington University, D.C., June 5-9, 1989.

4. MULTISENSOR DATA FUSION TECHNIQUE FOR MULTITARGET ENVIRONMENT

The sensor systems considered in this paper provide two types of information about the target:

- (1) kinematic data (position, and velocity),
- (2) attribute data (target nature, type, class, and scattering patterns).

4.1 Kinematic Data Fusion

In the MMDF problem under consideration, several sensors at different locations make measurements of the same targets. These measurements are correlated and then fused at a central location. The sensor measurement errors and times when measurements are available for correlation and fusion greatly influence the performance of the entire tracking and identification system.

The arrival times of sensor measurements at the central location from different sensors may be synchronized or random. Depending upon the modes of sensor measurement arrival times, there are different types of measurement processing schemes [1].

In the synchronized data collection mode, there are three types of sensor measurement processing alternatives:

- Parallel Processing,
- Sequential Processing,

- Compressed Data Processing.

In the parallel processing alternative, the sensor data are correlated in parallel and then the filter is updated with the correlated data in parallel. In the sequential processing alternative, the correlation of measurements is performed sequentially and the filter is updated with the correlated data in a sequential fashion. In the compressed data processing technique, the sensor data are correlated either in parallel or sequentially and then the correlated data are combined to form an integrated data which is then used to update the track filter. For details of these techniques, the reader is referred to [1].

4.2 Attribute Data Fusion

In the attribute data fusion, unlike sensor information are combined to derive high confidence target identification. There are various approaches to fuse unlike sensor information. In particular, this paper has focused on three approaches:

- (1) a voting approach to multitarget multisensor data fusion,
- (2) a Bayesian approach to multitarget multisensor data fusion, and
- (3) a Dempster-Shafer approach to multitarget multisensor data fusion.

4.2.1 Voting Approach to Multitarget Multisensor Data Fusion

The voting approach can be used in making decisions in multisensor data fusion environment. There are two voting approaches considered in this paper:

- (1) simple voting approach,
- (2) weighted voting approach.

In the simple voting approach, the participating sensors are assumed perfect and any declarations made by the sensors are based without any weighting. In this approach, one can assign 1's to those hypotheses that are supported by the measurements and assign 0's to those not supported by the measurements. The fusion consists of the sum of the votes for each target candidate. This approach makes a decision on the basis of which hypothesis gets the most votes. This voting approach is simple to implement. This approach does not require sensor measurement confidence. All that is needed is a database involving all the hypotheses which correlates the measurements with the hypotheses.

The weighted voting approach would require some knowledge about the quality of the sensor declarations. This quality indication could be in the form of confidence value as used in the Bayesian or Dempster-Shafer approach. When sensor declarations have different confidence values, the weighted voting approach would require a weight factor to support a sensor measurement.

4.2.2 Bayesian Approach to Multitarget Multisensor Data Fusion

The Bayesian approach to multitarget multisensor data fusion is based on the maximum a posteriori (MAP) probability concept. Consider that T_i is the target type to be identified in the presence of n number of target types in a

given scenario. Let X be a sequence of measurements derived from the same or different sensors. Let us assume that the measurements have been correlated for the i -th target. Now the problem arises how to combine the multiple measurements that make up the sequence:

$$X = [x_1, x_2, \dots, x_m]$$

where m is the number of measurements to be integrated. The problem, therefore, is to compute the confidence, $P(T_i/X)$, given the sequence of declarations X . There are four basic steps to compute $P(T_i/X)$. These steps are identical with the four steps discussed in section 2. However, Figure 3 shows the Bayesian algorithm flow diagram for sensor data fusion as used in this study.

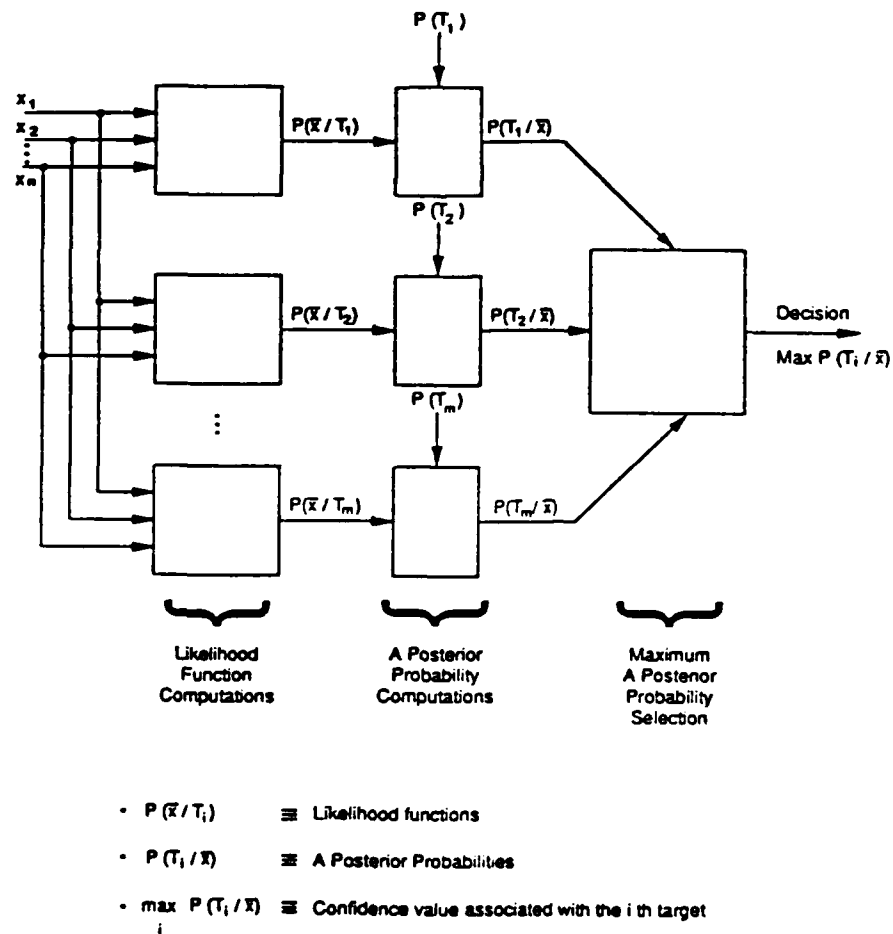


Figure 3.
Bayesian Algorithm Flow Diagram for Sensor Fusion

4.2.3 Dempster-Shafer Approach to Multitarget Multisensor Data Fusion

The Dempster-Shafer theory of evidence yields similar results as Bayesian approach but relaxes some restrictions in the Bayesian approach. The Dempster-Shafer theory is an extension of the Bayesian approach to include uncertainty. The Dempster-Shafer approach uses degrees of belief for representing uncertainty and allows one to assign degrees of belief to subsets of hypotheses. The Bayesian approach requires probability distribution of each element of the subsets which make up the hypotheses.

In the Dempster-Shafer theory, the belief in a proposition is represented by credibility interval (SPT, PLS) where the lower bound SPT indicates the degree to which the evidence supports the hypothesis and the upper bound PLS indicates the degree to which the evidence fails to refute the hypothesis. Each credibility interval (SPT, PLS) is a subinterval of the probability interval (0, 1). The difference between the upper and lower bounds implies the residual ignorance. Complete ignorance is represented by interval (0, 1). Figure 4 outlines the Dempster-Shafer algorithm flow diagram for sensor data fusion.

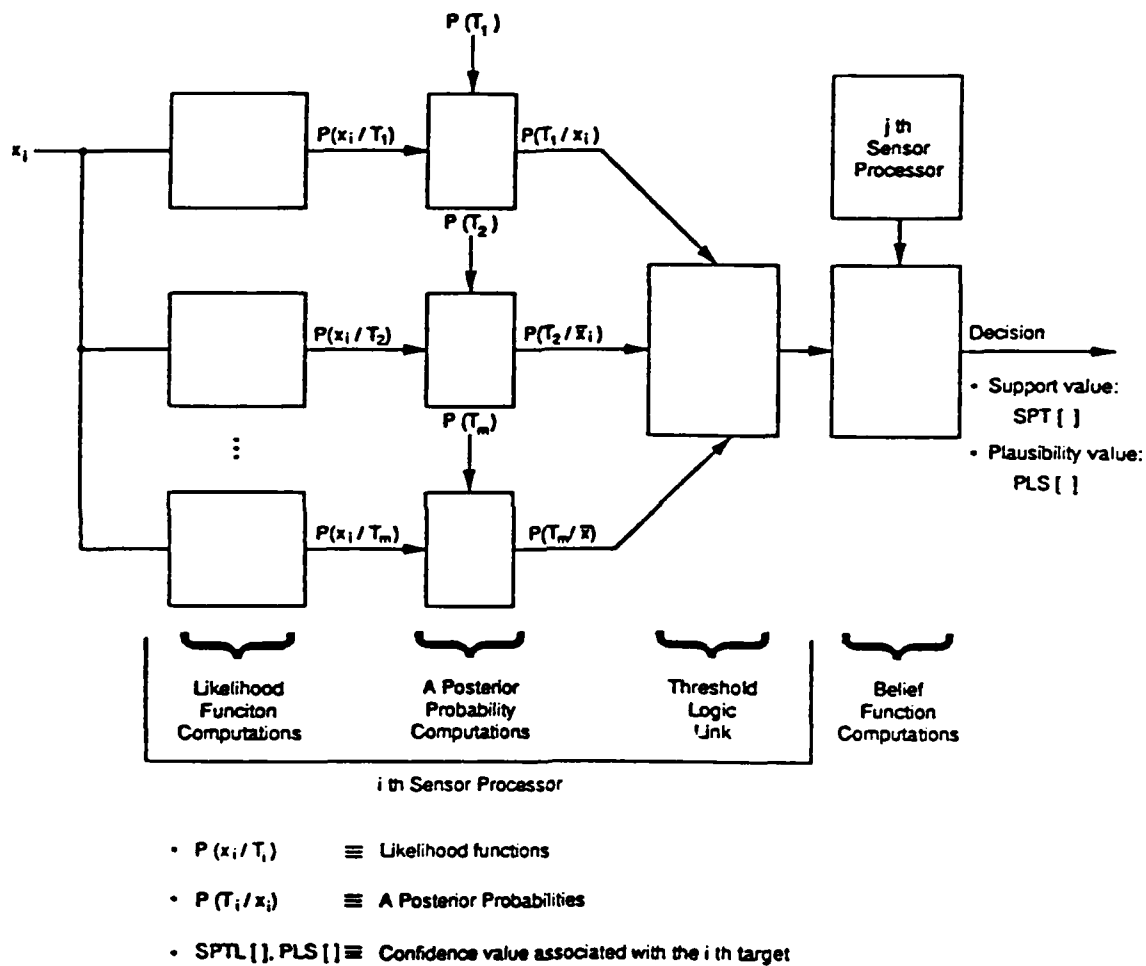


Figure 4.
Dempster - Shafer Algorithm Flow Diagram for Sensor Data Fusion

5. SIMULATION RESULTS

Let us consider an example that demonstrates how target tracking can be improved by using the multisensor fusion. Figure 5 depicts two targets in a horizontal plane starting at 100 nmi from multiple sensors which are colocated at the origin of the assumed coordinate system. The two targets are moving in straight line trajectories with azimuthal angles of 15 and 30 degrees respectively. Both the targets are maintaining a constant speed of 500 knots.

The simulator/evaluator has been used to generate the following:

- (1) target trajectories,
- (2) radar, ESM, IFF, RWR, and JEM measurements and associated variances,
- (3) target state estimation error standard deviations (x and y components),
- (4) confidence levels associated with the target ID's.

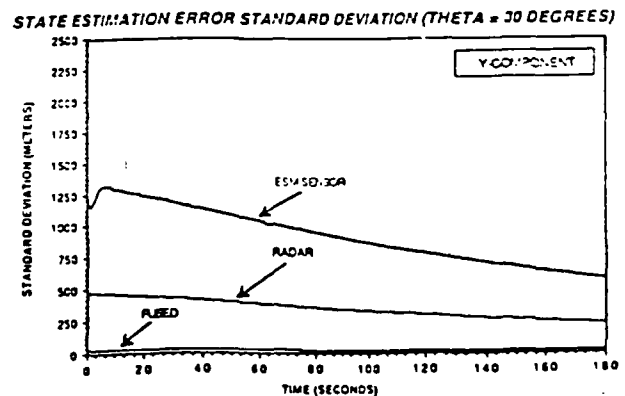
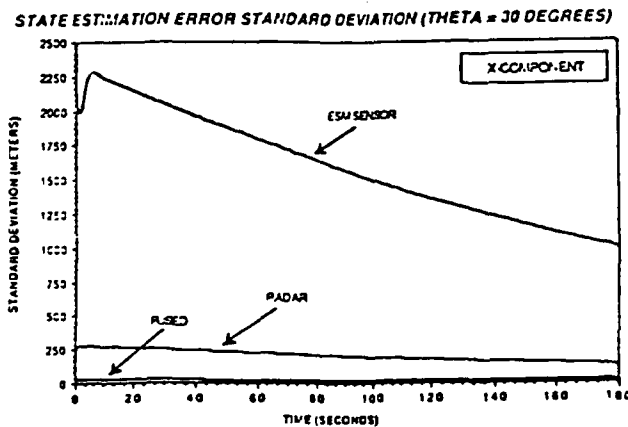


Figure 5.
Trajectories for Two Targets

In the Phase I final report [1], a few test cases are presented to demonstrate the performance of the MMDF algorithms for target tracking and identification. Test cases have been formulated to illustrate the benefit of the MMDF algorithms. Only one test case is outlined in this paper.

The scenario for this analysis includes one friendly and one hostile aircraft. The known key parameters of these targets are given in the following database shown in Table 1.

Table 1.

| Targets | Target Parameters | Nature | JEM | RWR | ²
RCS (m) |
|---------|-------------------|--------|-----|-----|--------------------------|
| F-1 | | F | 3 | 5 | 3 |
| H-1 | | H | 1 | 3 | 2 |

The test case has considered F-1 and H-1 aircraft. The radar and ESM sensors have been deployed for tracking the targets. A host of other sensors are also deployed to accurately identify the targets. For simplicity, the tracking results of only one target are outlined in this report. Figure 6 illustrates tracker performance along x and y axes respectively for the 30 degree target. This figure indicates that the tracking performance is agreeably better when the targets are tracked by both the radar and the EMS sensor combined than when tracked by either radar or EMS sensor. These results demonstrate that tracking performance can be greatly enhanced in the multisensor fusion environments.

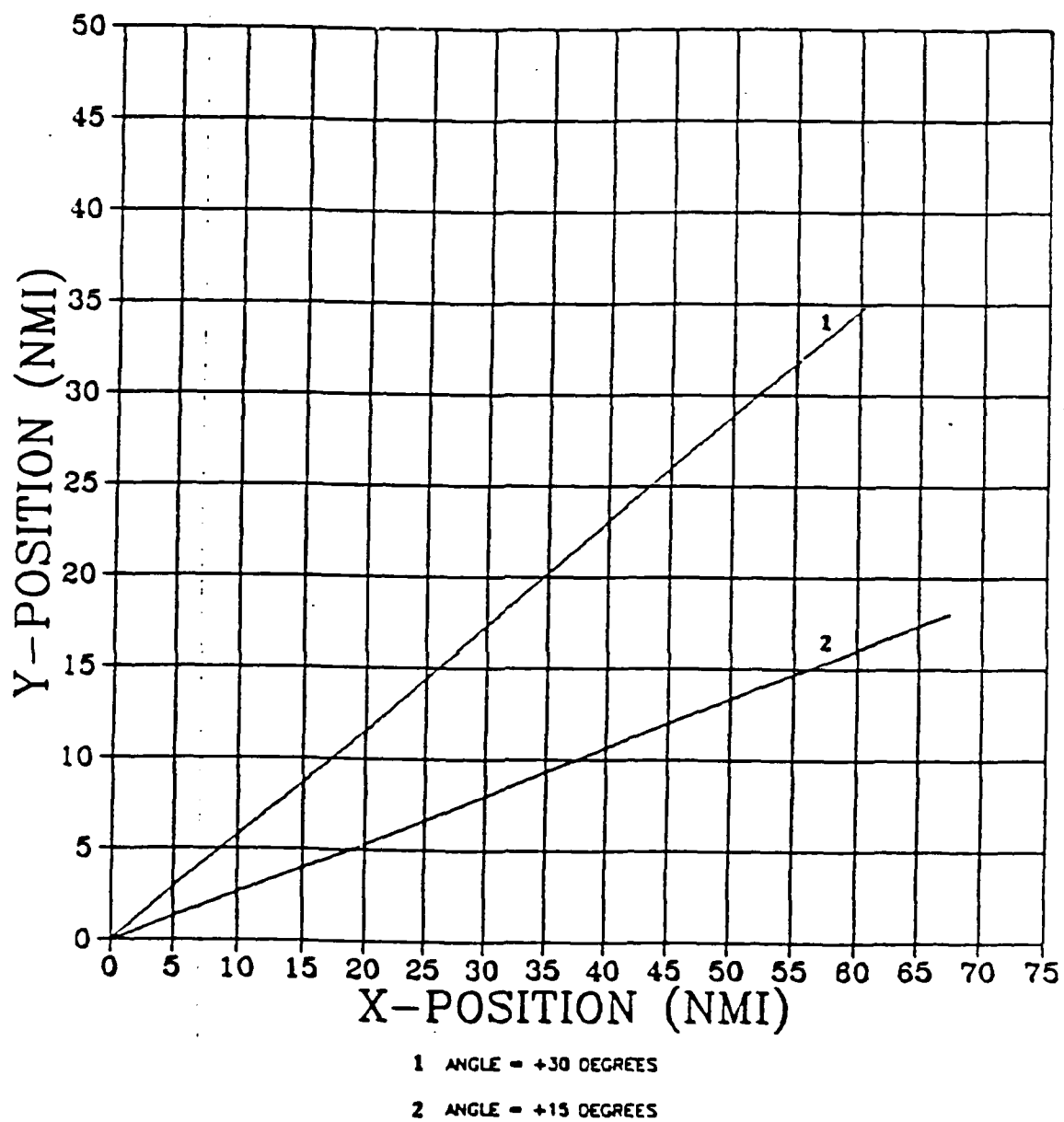


Figure .6
Tracker Performance Results

The following in Table 2 are the correlated sensor declarations associated with the tracked target at a particular time $t-1$ second:

Table 2.

| Sensors | Declaration
Confidence | Declarations | Confidence |
|---------|---------------------------|------------------------|------------|
| IFF | | Not Friend | 0.95 |
| RWR | | R Class 3 | 0.98 |
| JEM | | J Class 1 | 0.98 |
| FPC | | Outside | 0.86 |
| RCS | | ²
2 (m) | 0.80 |

Assuming uniform force mix (that is $P(F) = P(H) = 1/2$), Bayesian approach yields the following confidence values in Table 3.

Table 3.

| Targets (A)
i | Confidence =
$P(A_i / x)$ | Confidences |
|-------------------|------------------------------|-------------|
| F - 1 | | 0.0010 |
| H - 1 | | 0.9997 |

6. REFERENCES

1. Sensor Data Integration, Inc., "Artificial Intelligence Applications to Command, Control, and Communications Systems/Subsystems," Contract No. F19628-87-C-0183, February 1988.
2. R. Carroll, S. Chaudhuri, and M. Mayor, "Multitarget and Multisensor Tracking," A Five-Day Short Course, The George Washington University, D.C., June 5-9, 1989.

Presented at the
DIGITAL/ELECTRONIC TERRAIN BOARD SYMPOSIUM
5-6 October 1989 GACIAC PR 89-07

Multidisplay Multifunction Cockpit Interface
for
The Silicon Graphics IRIS Environment

Dale Robison
Code 3152
Naval Weapons Center
China Lake California 93555

ABSTRACT

This paper describes a multidisplay, multifunction, multiprocessor approach to a cockpit simulation environment that allows for several simultaneous display formats to operate in parallel. The approach produced a state-of-the-art cockpit simulation that is low cost, distributed across several processors, and is readily expandable to new situations. Additional computing capability can be added through the uses of a sophisticated message handling scheme. The system is readily customizable to most display formats that are currently in existing aircraft, and new formats can readily be added as needed.

Approved for public release; distribution unlimited.

Introduction

A single-seat attack aircraft simulation facility that would allow human factors performance evaluations in a real-time, multidisplay, multifunction environment was required as part of the Intelligent Air Attack System (IAAS) development(ref 1). A testing environment was developed around a Silicon Graphics IRIS graphics workstation that allows investigators to evaluate task performance when a pilot is required to perform several simultaneous tasks. The environment simulates a detailed state-of-the-art cockpit that contains an out-of-cockpit view, a heads-up display (HUD), three multipurpose displays with operational push buttons, a multipurpose data entry control panel, a throttle and stick with multifunction control switches, and numerous cockpit switches. After its initial success as the testing facility of the Intelligent Air Attack System, the facility is now being reconfigured to other experiments involving pilot performance, display evaluations, and work load studies.

The cockpit displays supplied on the CRT of a Silicon Graphics IRIS workstation are animated at a refresh rate of 10 Hz. A touchscreen overlays the display to allow interaction with graphically generated push buttons. The simulation supplies the pilot with real-time animated displays which represent the information he

(ref 1) Intelligent Air Attack System (IAAS): Project and Product Definition, by Judith Lind, China Lake, Calif., NWC, April 1988, NWC TM 6161 (Unclassified).

would receive from onboard sensors, system databases and avionics(see Figure 2.). Multiprocessor communication is maintained between the IRIS, two Zenith 80386 computers and an IBM PC through the use of an ethernet network using TCP/IP protocol. Communication to and from the non-IRIS related cockpit controls and switches use the ethernet, the mouse port and an additional RS-232 port.

Description

The physical cockpit environment is designed to give the pilot the sense and feel of a real cockpit. The NWC physical cockpit mockup consists of a 4 x 4 x 12-foot framed shell covered with masonite, an aircraft ejection seat, an F/A-18 throttle and stick with multifunction control switches, a set of fixed-function panel switches, a 19 inch Hitachi monitor interfaced to the IRIS, and foam core mockups of other standard cockpit switches and panels.

The simulation software is categorized into six major components: (1) the main program, (2) the aircraft simulation, (3) the external world models, (4) the avionics models, (5) the message handler and (6) the display control system. Each component is described below.

The NWC simulation is a version of the Silicon Graphics flight program that has been radically modified. The primary program was reduced to one page of function calls, and new functions needed by our requirements were added. The program has grown from the original 170 kilobytes of "C" language source code to over 1.5 megabytes of source code.

The airframe simulation is a six-degree-of-freedom simulation, that can fly several aircraft models simultaneously. The flight characteristics of each aircraft are defined by a set of parameters that are carried internally in the aircraft data record. The primary aircraft has the characteristics of a subsonic, heavily-loaded single-seat attack aircraft.

As the need for other types of dynamic models became apparent, it was noted that many of them could be inserted into the simulation as "aircraft" and manipulated as such. Ships, missiles, as well as tanks and armored personnel carriers were made available, each with its own "flight characteristics" ranging from "very slow and sluggish" to "very fast and maneuverable".

The IRIS graphics world model contains sky, ocean, land, and any other objects such as ships and missiles which are located visually outside of the cockpit. The graphics processors manipulate the imagery and present the pilot with the out-of-cockpit views that result from manipulating the aircraft.

Each ship model derives its identity, speed and location from the scenario files that are loaded at the beginning of the program, and then independently simulates the behavior of that ship for the remainder of the simulation run. Each ship model has radar emissions, and determines the current mode of operation that is compatible with its weapons and sensors. The radar-warning-receiver (RWR) model reads each ship model for emitter information.

When the missile simulation is started as a result of a ship initiating a launch, the missile derives its flight characteristics from the ship's database, and then flies out toward the aircraft using a lead-intercept algorithm. The intercept algorithm is designed to intercept and detonate the missile when it reaches its closest proximity to the target. Missiles can be defeated if: (1) the aircraft drops below the radar horizon, (2) the missile falls into the sea, or (3) an active expendable countermeasure leads it astray. Due to the complexity of the algorithms and the fact that realistic update rates must be maintained, only one missile at a time is currently allowed. Certain display formats are frozen during the later segments of a missile flyout and only those displays essential to flying the mission continue to be updated at the normal update rate.

Models of expendible electronic warfare countermeasures (flares, chaff, jammers, etc) are designed to have a specified life usually measured in seconds, and lose their effectiveness exponentially over time. Only the judicious use of the countermeasures combined with the correct timing of the deployment will result in an effective defense against the missile threats.

The simulation's radar model supplies the positional data necessary for the radarscope. The NWC simulation's radar model has a sea-search mode and a sea-surface-track mode. Track-while-scan capability is not currently implemented. The tracking of a surface target results in the loss of radarscope imagery for any other contact. Figure 2 contains a sample of the radarscope format.

Part of the war-at-sea scenario called for processing of Inverse Synthetic Aperture Radar (ISAR) imagery. The size of the database precluded its existing in the main simulation. Network messages were generated by the radar model, which instructed another processor on the network to process the correct files and return the data to the display processors for pilot evaluation. The display format of the returned data is in Figure 2.

The Stores Management System currently manages Harpoon missiles. Weapon programming parameters are loaded through the simulated keyboard entry device known as the upfront control panel, while other weapon parameters can be downloaded using the bezel buttons on the SMS

display. A hardwired Master Arm switch and stick switches must be activated to "release" the weapons. See Figure 2 for the display format.

The RWR uses the radar emission data from ships, and generates outputs that an actual RWR would present to the pilot. No true emission processing is done. However the model does intentionally introduce azimuth ambiguity and some random spurious signals to make its output more realistic. An RWR display format is displayed in the window area (See Figure 1.).

The Missile Detector System (MDS) simulates a short-range doppler radar system capable of detecting in-the-air missiles. The information is sent to another peripheral program which determines the threat identification and how best to defeat it. The MDS model records only those threats that are closing on the aircraft. An MDS display format is used to present information to the pilot, and is overlayed onto the HUD.

The forward looking infrared (FLIR) model is simulated by creating images of vehicles colored to represent the object as it would look in infrared. The images are then filtered to generate various amounts of noise, and are made available on the FLIR display format.

The systems message handler is an interface between the simulation and the other computers on the ethernet network and performs two major tasks, synchronizing of the startup of the programs on the other processors, and passing messages between the various

processors. Individual messages are passed to and from the various computers on the system using any of the eighty predefined messages. The messages are directly vectored to the receiving computer's processing software by their message number where the data is extracted and processed.

The display control system is a set of functions designed to control and display any of the display formats currently available. This system consists of display management functions, display generation and updating functions, and bezel button functions. Examples of formats are in Figure 2.

The display management software manages two sets of data, one representing the logical displays and the other representing the physical displays. Each logical display represents an active display format available for display, and controls the manipulation of the format. The physical display controls which logical displays are visible and where they are located on the CRT (see Figure 1.).

The logical display management software is centered around logical display structures which contain the information that is pertinent to the operation of a specific logical display. Logical displays contain; the graphics objects identifiers, pointers to the functions associated with the display, and several flag variables.

The physical display functions control the mapping of the logical displays to the physical display zones on the surface of the monitor. There is currently one physical display structure for each of the six

graphics zones on the monitor. Logical displays can be reassigned to any of the three multifunction displays at any time, and in any order. Experience has shown that it is unwise to map a logical display to more than one physical display zone since only one of the physical display zones will be redrawn after an update. Except for the menu display, only one of each avionics display format is allowed.

Different formats have different refresh requirements. Update rates vary from 10 Hz to no update needed. Updates to the CRT are tightly controlled since the graphics refreshes are time consuming. The individual display formats consist of foreground and background images. Writemasking, a graphics process, is used to protect static portions of a display from being erased during an animation sequence.

Each display format has a description file that is in the form of a header file and a format template file. The header file contains arrays of button labels and an array of bezel button functions allowing the programmers to change bezel functions and labels easily without searching through code. The format template file contains functions which perform the following: define the labels, define the foreground object, define the background object, define the update function, and define all bezel button functions that are unique to the display format.

The NWC simulation has nearly unlimited display format capabilities. New display formats are added to the system by generating the model to create the data, defining the display format that meets the template, and then defining what its logical display format parameters are. Once built, the display is made available by activating it from some other existing format, or causing it to be mapped to a display zone when the simulation starts.

Control functions operated via the bezel buttons are executed directly from the logical display structure. A button press executes the function defined in the logical-display-button array. Changing the functionality of the button is as simple as loading another function into that element of the array.

Conclusions

The Intelligent Air Attack System (IAAS) was the first project to fully utilize the cockpit simulation. Decision aids, task management, and display management was supplied by the peripheral programs and presented to the pilots in a war-at-sea scenario. The cockpit allowed pilots to interact with decision aids, and task orientated displays, while attempting to fly the aircraft, launch weapons, and counter hostile missiles. Two sets of simulations were required for the evaluations, a baseline "F/A-18 like" cockpit (ref 2) and the IAAS cockpit(ref 3). Display formats were developed for both . IAAS has proven itself to be a viable technology that could prove itself valuable in the 1990's.

The cockpit simulator is a low cost approach that can meet the needs of many projects. Future expansion of the system will include the addition of other IRIS graphics processors and displays to widen the field of view, and parallel processing capability to increase the fidelity of the models.

(ref 2) McDonnell Douglas Corp. F/A-18 Avionics Display Format Diagrams,
St Louis, Mo., 17 Mar 1980 (Unclassified)

(ref 3) Intelligent Air Attack System: Display Format Diagrams by
Judith Lind, China Lake, Calif., NWC, April 1988, NWC TM6207
(Unclassified)

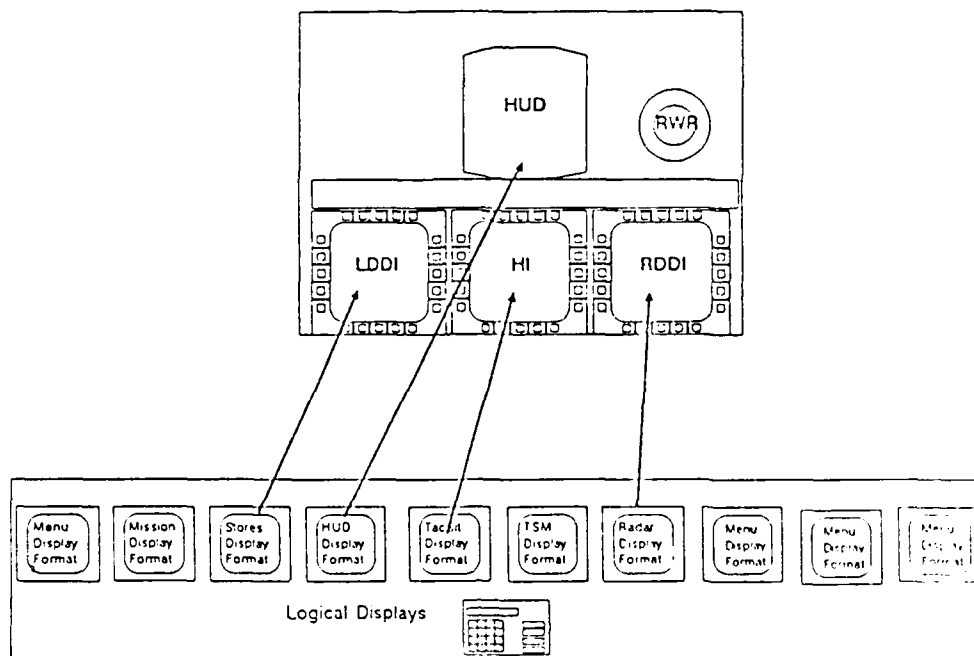


Figure 1 A: Normal Display Configuration

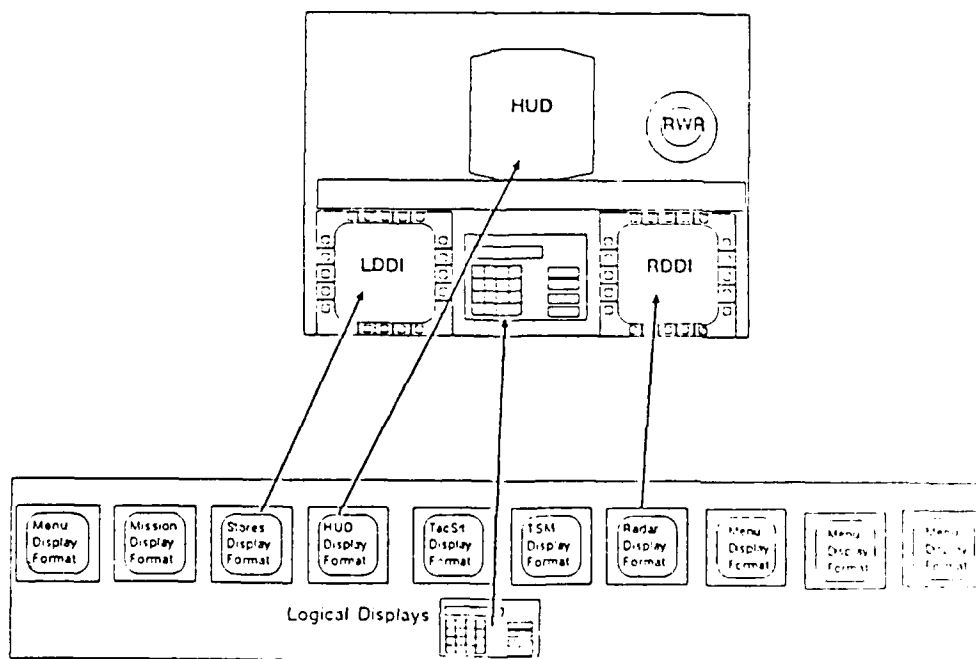
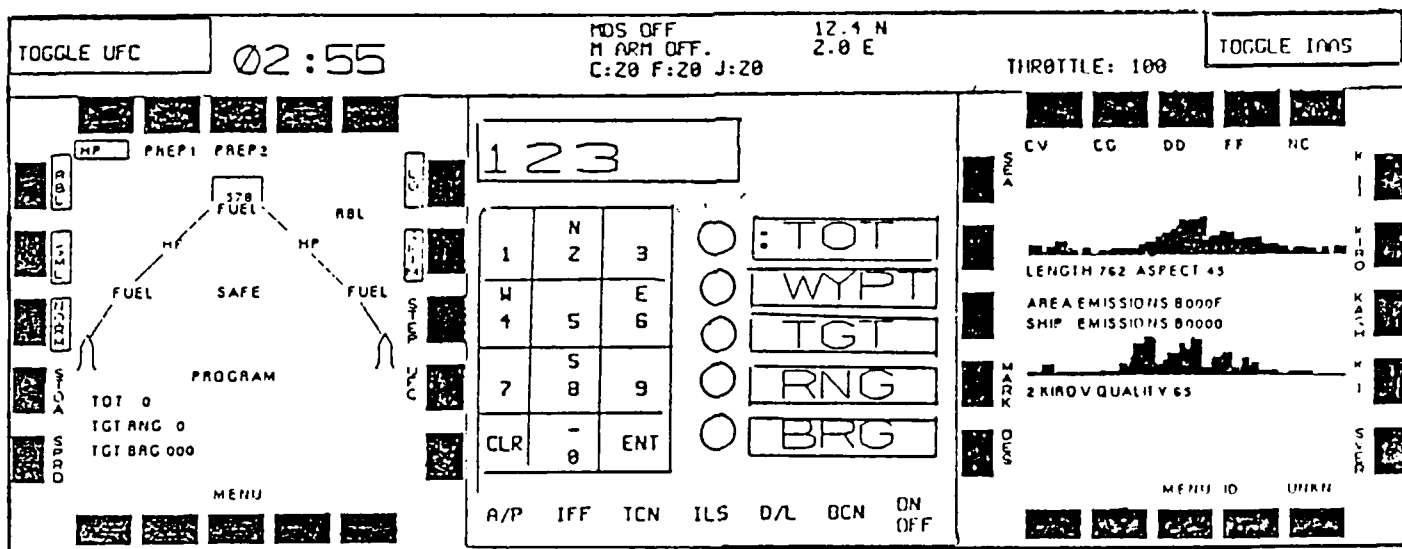


Figure 1B: Keypad Display Option

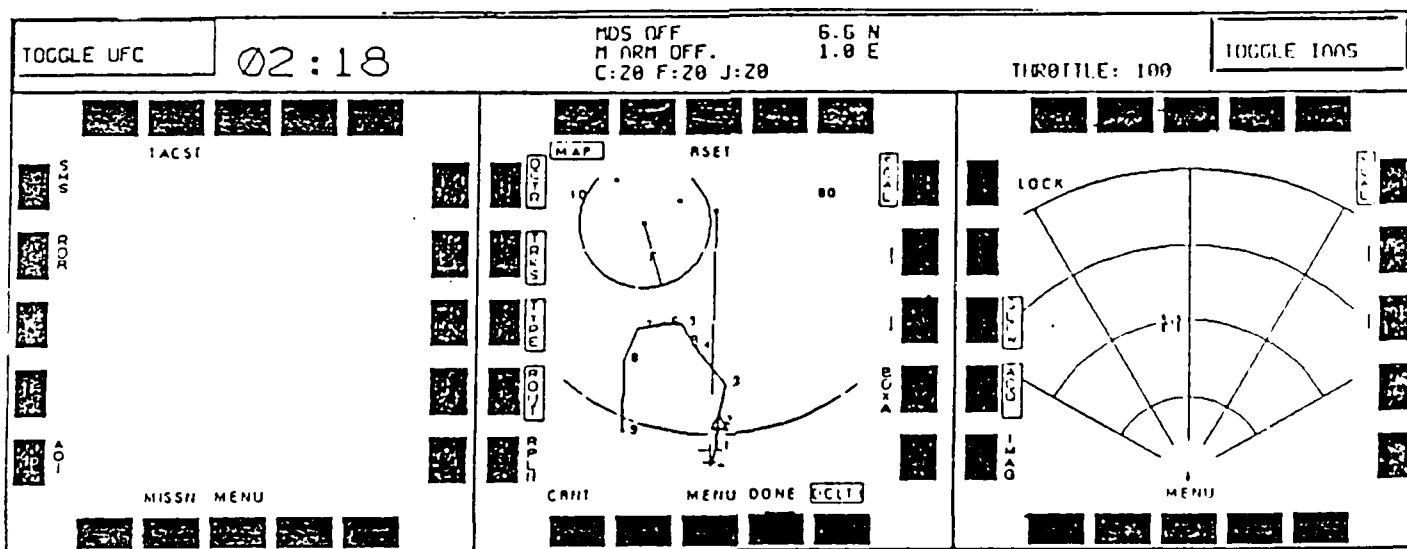
Logical Display to Physical Display Mapping



Store Management Harpoon Format

UpFront Control Panel Format

Classifier Decision Aid Format



Top Menu Format

Tactical Situation Format

Radar Track Mode Format

Figure 2. Example Display Formats used in the IAAS Project.

THIS PAGE INTENTIONALLY BLANK

SANDTABLE, A DISPLAY OF THE ELECTRONIC BATTLEFIELD

Dennis Lui
HQ, US Army CECOM
CECOM Center for EW/RSTA
Fort Monmouth, NJ 07703-5000

ABSTRACT

The SANDTABLE Project was conceived to show how the US Army Communications-Electronics Command (CECOM) sensor systems are used, what they do, where they are employed, what enemy force they detect and how they interface with all command and control systems on the battlefield. SANDTABLE utilizes a computer controlled system to display maps and imagery and to perform analysis of multi-source data. Graphics depicting locations, events, sensors, mission plans and lines of communication can be presented over the maps and imagery on a high resolution color monitor. By utilizing the Digital Terrain Elevation Data (DTED), terrain analysis such as determining the terrain elevation, slope profiles, three dimensional terrain view, terrain masking and radial line of sight can be performed. Engineer Topographic Laboratories' three dimensional video terrain and models of sensors can be integrated into the SANDTABLE computer system and displayed on the color monitor.

1.0 INTRODUCTION

1.1 SANDTABLE Tasking

The SANDTABLE project was originated from the tasking given by CECOM Commanding General, Major General Billy M. Thomas. His tasking was to build a huge SANDTABLE with intelligence/electronic warfare rigs deployed over a Corps sector showing all the present and future sensor systems and lines of communication.

1.2 SANDTABLE Implementation

In order to fulfill the SANDTABLE tasking, an approximately 1000 square feet of SANDTABLE and sensor models have to be built. Due to the physical size of this huge SANDTABLE and small sensor models constraint, a different approach utilizes the computer controlled system has been used. The

computer controlled system is capable of displaying maps and imagery and performing terrain analysis. Thus, by utilizing the computer controlled system, the physical SANDTABLE with sensor systems can be easily simulated. A one hour videotape version which describes the electronic battlefield is being used in lieu of the physical SANDTABLE.

2.0 ELECTRONIC BATTLEFIELD DISPLAY

2.1 Computer Controlled System

The computer controlled system consists of the following hardware components:

- a. Personal computer with 16 bits microprocessor and math co-processor, graphic processor, keyboard, mouse and a high resolution color computer monitor.
- b. Videodisc player
- c. High resolution color TV monitor
- d. CD-ROM player
- e. Optical disc recorder/player
- f. Video camera
- g. Color printer

The computer system is capable of controlling and accessing information from the videodisc player, CD-ROM player and the optical disc recorder/player. It can also perform information management, terrain analysis, measurement and display.

The computer system utilizes the videodisc player to display videodisc maps on the high resolution color TV monitor. Graphical characters, symbols or ICONS can be overlayed on the map background. The computer system can retrieve Digital Terrain Elevation Data (DTED) from the CD-ROM player and perform terrain analysis. By using the optical disc recorder and video camera, still photographs can be recorded. Three dimensional static and dynamic models of sensors and targets placed on terrain images, and a dynamic fly by of models can also be recorded on the optical disc and played back on the TV monitor. Hard copy of text and graphics can be printed out on the color printer.

The hardware components are low cost and commercially available products. Videodisc maps are widely available through the Defense Mapping Agency (DMA), COINS, Joint National Intelligence Dev. Staff (JNIDS), BDM, Computer Corporation of America (CCA), Interactive Television Company (ITC), Routing Technology Services, Inc. (RTSI), Defense Advanced Research Projects Agency (DARPA), Sandia National Laboratory (SNL), System Control Technology (SCT), and Institute for Defense Analysis (IDA). The above list is not all inclusive, there are other agencies not listed above which also produced videodisc maps.

2.2 Electronic Battlefield Display

To generate a battlefield condition, map of Europe is displayed on the monitor. Using the graphical capability of the system, the boundary of 7th Corps is drawn. The Corps area is further broken down into three divisions, and three brigades in a division. Graphical character representation for the CECOM sensor and jammer systems, and the enemy systems are drawn and depicted on the map background. Systems information descriptions, capabilities, drawings and pictures are recorded and stored on the optical disc as collateral data. Communications flow from the sensor systems to the commander is graphically represented on the map background. The description of the Army tactical command and control system architecture is recorded and stored on the optical disc. The optical disc is used as a storage means for the collateral data and retrieved by the computer and displayed on the TV monitor.

The Engineer Topographic Laboratories' three dimensional model of sensors, terrain images and dynamic fly by of sensors are recorded as collateral data on the optical disc. To retrieve these collateral data, mouse cursor is placed on the specific geographic location or sensor systems graphical character on the map background. The computer searches the collateral database for data associated with the coordinates near the cursor location and displays user selectable item menu on the computer display monitor. The collateral data will then be displayed on the TV monitor upon user selection for displays.

The Digital Terrain Elevation Data (DTED) is used to perform terrain analysis such as radar

terrain masking, radial line of sight calculation, oblique terrain view, tinted elevation map display and terrain slope display. The radar terrain masking function provides a graphic display of the radar terrain mask from a marked point by inputting radar's antenna height, range and ray spacing in degrees. The radial line of sight function provides a graphic display of the line of sight in all directions from a marked point by inputting observer's height, viewing range and ray spacing in degrees. The oblique terrain views function provides a three dimensional terrain graphic on the computer display monitor by marking the observer and target locations. The tinted elevation map function overlays the map with colors representing elevation levels. The terrain slope function overlays the map with a pattern of colors representing the slope of terrain.

In order to simulate a battlefield condition and to display the results of battlefield changes, the real time updating function is being used. The graphical representation of the sensor system with geographic location on the map background can be updated from a remote system via the RS 232 port to the computer. The updated file contains changes in movement and speed of the sensor system indicating battlefield changes. The computer system receives the real time updating information and displays position movements on the TV monitor.

3.0 CONCLUSION

The SANDTABLE project utilizes a computer controlled video presentation to describe the extensive use of electronics on the modern battlefield. The SANDTABLE computer system enables the users to perform mission planning, information management, terrain analysis, measurement, information display and real time event updating. The SANDTABLE computer system can be used for different purposes and applications such as presentation, simulation or test bed.

Presented at the
DIGITAL/ELECTRONIC TERRAIN BOARD SYMPOSIUM
5-6 October 1989 GACIAC PR 89-07

Terrain and Target Signature Simulation

Dr. John H. Lewis
Hughes Aircraft Company
P. O. Box 9399
Long Beach, California 90810-0399

ABSTRACT

Just as significant advancements in imaging weapon systems have expanded battlefield tactical concepts, this performance improvement has dictated a need for advancements in test and evaluation techniques. The basis for both expanded weapon system employment and more capable development tools is technology driven. Today in the growing field of terrain, target, and sensor simulation, Computer Image Generation (CIG) is an important tool to improve and hasten design development, test and evaluation, and tactics development.

Simulation of multi-band imaging infrared seekers for the tactical environment is under way at a number of laboratories. A system approach based on photo and sensor image inputs, which is derived from first principals and produces real time ambient condition specifiable infrared imagery, will be described. This

approach has been demonstrated and is being integrated for both tactical and strategic infrared imaging in a hardware-in-the-loop configuration.

Advanced processing techniques, including a number of graphics structures (polygons, fractals, voxels), are incorporated as well as two and three-dimensional image processing.

Presented at the
DIGITAL/ELECTRONIC TERRAIN BOARD SYMPOSIUM
5-6 October 1989 GACIAC PR 89-07

Image Generation - VICAM

Scott Brandt, Michael Miller, Carl Graf
Honeywell, Inc.
3660 Technology Drive
Minneapolis, Minnesota 55418

ABSTRACT

Over a decade ago, Honeywell pioneered the work in photo-based image generation (in the IR and visual domains) for missile evaluation and training systems. This technology is now being applied to mission planner/rehearsal systems and aircraft cockpit instrumentation. Large, accurate, ultra-high resolution photo-quality, multi-spectral displays at high update rates from a common database appear to be requirements for both mission rehearsal and Digital/Electronic Terrain Board (D/ETB) systems.

Creating real-time computer generated images of terrain and man-made objects of sufficient fidelity and accuracy to serve as an ATR test system is the difficult problem for D/ETB. One solution is to geometrically and temperature/emissivity model the terrain/objects. This method has numerous problems, including the verification of the accuracy of the model. Honeywell's approach uses real images manipulated digitally by empirical and model data to yield extremely high quality 3D perspective views. These views may

be manipulated to simulate the desired moving sensor/platform/target situation. Furthermore, the resolution and sensor type are limited only by the input imagery provided. Atmospheric and sensor effects are also simulated digitally..

Honeywell's solution for high fidelity aircraft display, mission rehearsal systems, and perhaps the D/ETB is through the use of a common database for imaging data and the implementation of proven image generation algorithms in VHSIC class ASICs.

Presented at the
DIGITAL/ELECTRONIC TERRAIN BOARD SYMPOSIUM
5-6 October 1989 GACIAC PR 89-07

Smart Weapons Operability Enhancements Program

Dr. Pat Welsh
US Army Cold Regions Environmental & Engineering Laboratory
72 Lyme Road
Hanover, NH 03755

ABSTRACT

Smart weapon systems offer one of the most significant opportunities to offset threat numerical superiority with technology. The Army has planned multi-billion dollar investments in smart munitions over the next several years. A major barrier to advancement of effective smart weapons has been the lack of a systematic incorporation of the complexities of the environment throughout the development process. Smart weapons must be able to discriminate relatively small targets out of large areas dominated by the environment. The utility of high fidelity target characterization is compromised by the current simplistic description of the environment. To address this problem, the DOD is funding a Smart Weapons Operability Enhancement (SWOE) program as one of its Balanced Technology Initiatives (BTI). The purpose of the SWOE program is to provide the basis for extending current smart weapons development strategy to more comprehensively include consideration of dominant environmental conditions in expected areas of conflict.

The SWOE program is a tri-service effort managed by the US Army Cold Regions Research and Engineering Laboratory (CRREL). The objective of the program is to provide the hardware development community with the measurement, modeling, information and simulation tools necessary to effectively consider and exploit the operational environment in smart weapons test and evaluation. Information that defines the background environment in terms significantly relevant to proposed sensor concepts will be developed and demonstrated for two primary users: smart weapons system "testers/evaluators" and "designers". This will provide the ability to plan developmental test programs to answer the most pressing performance questions, maximize the utility of the test data with regard to performance in a wider range of conditions, minimize the testing required to complete proof of principal and influence the design of the system as early as possible. In the longer term, SWOE will provide the ability to project approximate performance prior to building a brass board and to forecast test results prior to testing by means of a simulation capability that will impact design in the earliest stages.

Efforts were initiated during FY89 to demonstrate the SWOE community's collective capabilities to model and simulate the environment based on first principles IR models using real terrain and measured data. This paper will discuss the overall SWOE program goals and objectives and present the results of the demonstration efforts to date.

FROM DATA BASE CREATION TO PERSPECTIVE SCENE
GENERATION IN A SINGLE PARALLEL PLATFORM

Michael P. Battaglia
Image Data Corporation
Pasadena, California

The Problem!

Users of mission planning, rehearsal and simulation systems have been plagued with problems which result largely from overspecialization and incompatibility. They've been faced with the necessity of using one system to create the data base, a second system to process the imagery and a third system to generate the perspective scenes. To further add to the problem, some data exist in pixel (picture element) form, other data as polygons and still other data not even as imagery, at all. As a result, a great deal of their time is spent in learning and understanding these various systems and data forms rather than actually deriving useful benefit from the technology.

Similarly, designers of each of the systems mentioned above have their tasks complicated by the apparent incompatibility of the data forms. They are also usually unwilling to compromise the capability of their technological tools in order to accommodate the various data forms. And with good reason: such compromises usually result in greatly degraded performance. This is especially true in perspective scene generation, where, for example, the reduction of the number of polygons that a system can generate immediately impacts the realism of the scene and the failure to reduce impacts the scene generation time.

The Solution:

Recently, however, technological advances have made it possible to overcome these inherent problems. One approach involves the use of a "voxel" data base. Voxels are volume, or three dimensional, pixels. Such a data base may be built in a pixel processing system and will support both polygon and voxel perspective scene generatic

For example, a comprehensive software package, typified by Image Data's PARA/SERIES Image Exploitation Software, will enable the user to create the data base, process the pixel data and create perspective scenes, in a single platform.

Prior to building the data base it is usually necessary to prepare the source imagery for analysis. This includes the use of various image processing algorithms to remove noise, enhance the scene,

cartographically correct the image, define edges and similar operations. At this point the two dimensional image is ready to be incorporated into a three dimensional data base through the addition of the third dimension, elevation.

Elevation data may be merged with the source imagery or extracted from it. Various techniques are available to accomplish this task. Merging involves the use of external elevation data. Examples of externally supplied elevation data sets are Digital Elevation Models (DEM) from the US Geological Survey and Digital Terrain Elevation Data (DTED) from the Defense Mapping Agency. These are usually provided in non-image form and must first be converted. In doing so, the elevation postings must be arranged in a raster format similar to the image. Then, an intensity assignment is made at each location, proportional to the elevation value of the original posting. This then forms a black and white image, representative of the elevation, where lighter shades of gray indicate higher elevations. If the postings are more coarsely distributed than the pixels in the source image, an interpolative process may be employed to establish a unique elevation value for each pixel location. Conversely, if the postings are denser than the pixel distribution, averaging may be employed. Since the image and elevation data were separately collected, their formats will not be the same, geometrically. Therefore, an additional step is needed when using external elevation sources. This involves geometric transformation of one image to the other, typically through tiepoint selection and polynomial warping.

An alternative means of incorporating elevation information into the data base is through extraction. The extraction of elevation data is usually accomplished through one of two methods, depending on the source imagery available. If the image is monoscopic (i.e. a single image) shadow length and solar elevation angle may be used to calculate the elevation of features within the scene. This process is usually very interactive although morphological algorithms may be used in conjunction with intensity thresholds to define shadow edges in a more automated fashion. Obviously, this process may be employed only for those images where shadows, related to elevation, actually exist. This eliminates certain sensors operating in wavelength bandwidths where shadows are not relevant to elevation. Also, it does not work for those scenes where shadows are not present, such as at night in the visible spectrum. Finally, shadow length can be very complex and difficult to measure, such as in cases where one shadow falls upon others. However, there are times where this is the only means available for obtaining any elevation information about a geographic area.

A much more automated potential exists where stereoscopic imagery is available. Stereo sets (pairs or greater) may be used to provide elevation information if the altitude and the convergence angle of the sensors are known. It is important to note that the stereo

imagery could be collected by a single sensor providing multiple images displaced in time. It is also possible to extract elevation from stereo sets where the sensors may not be temporally displaced but on different platforms, such as satellites and aircraft. Further, the sensors may even generate data in completely different portions of the spectrum, such as thermal and radar imagery. And there may exist different combinations of these variables with which the data base creator must work. However, given the availability of stereo imagery and the use of edge and/or gray level correlation along with the appropriate geometric transformation algorithms, elevation data may be obtained with a high degree of accuracy in an automated fashion.

Neither of the extraction approaches covered above requires geometric transformation to superimpose the image data with the elevation data. This is true since the elevation data was derived directly from the source imagery. Similarly, no interpolation will be required since the elevation data can be extracted for every pixel location in the image.

At this point other feature attributes may be determined to create a more comprehensive data base. Using techniques such as supervised and unsupervised classification of multi-spectral imagery or thermal classification of infrared data will permit spectral attributes to be assigned to each voxel in the data base. Likewise, textural and shape attributes may be derived and assigned. This then creates a surface material classification which may be included in perspective scenes for additional functionality. Knowledge of surface material classes is also extremely useful when the user wishes to simulate the response of sensors elsewhere in the electromagnetic spectrum. If the spectral signature of the feature is known, it is feasible to convert its radiometric response to another portion of the spectrum. As an example, if a metal structure is identified in a visible image, one can simulate its thermal characteristics under differing solar illumination conditions.

Why Parallel?

Up to this point, only a limited advantage could be obtained from a parallel processing platform. Algorithms such as Fourier transforms, multispectral classifications and geometric manipulations derived benefit from parallel implementation.

However, it is in the area of perspective scene generation that dramatic improvement in performance can be achieved through parallelism. The data base which has been created can be used to generate photorealistic perspective scenes for mission planning, mission rehearsal and simulation applications. In order to generate these scenes rapidly and still preserve all of the resolution inherent in the data base, an array of high performance parallel

processors with closely coupled, shared memory becomes indispensable. An architecture of this type running a constant-time, ray trace algorithm will enable the user to achieve real-time scene generation (i.e. 30/60 fps.) Further, when this parallel architecture is married to a polygon generator and Z-buffer memory, dynamic objects may be inserted into the scene under independent control and a truly photorealistic simulation capability results. Further realism may be added to the overall system through the addition of shading and lighting algorithms to the software library. That, however, is the topic of another discussion.

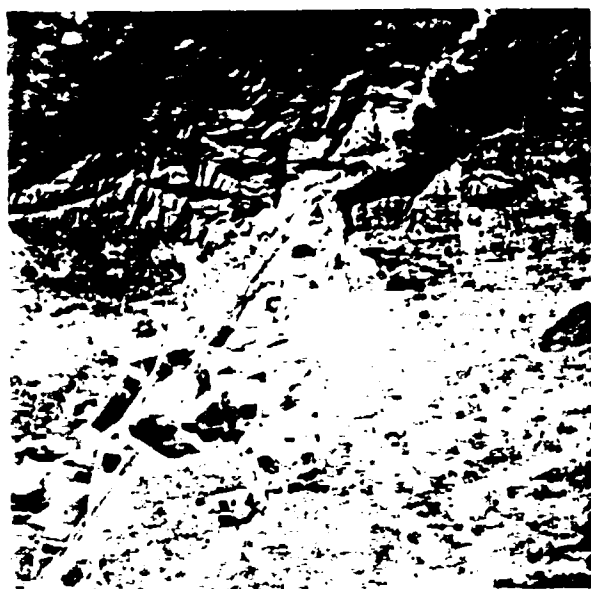
The Conclusion:

Recent developments in parallel architectures, commodity processors and advanced algorithms eliminate the need for multiple systems and data bases in applications involving perspective scene generation. Mission planners may now use a single system to accomplish their goals. Further, this approach has the collateral benefit of device independence. Users have the opportunity to avail themselves of current hardware technology with a minimum amount of cost and delay when transporting their applications software systems to these newer and more powerful platforms. Efficiency is greatly improved since users continue to work with familiar software while benefiting from technology advancements.

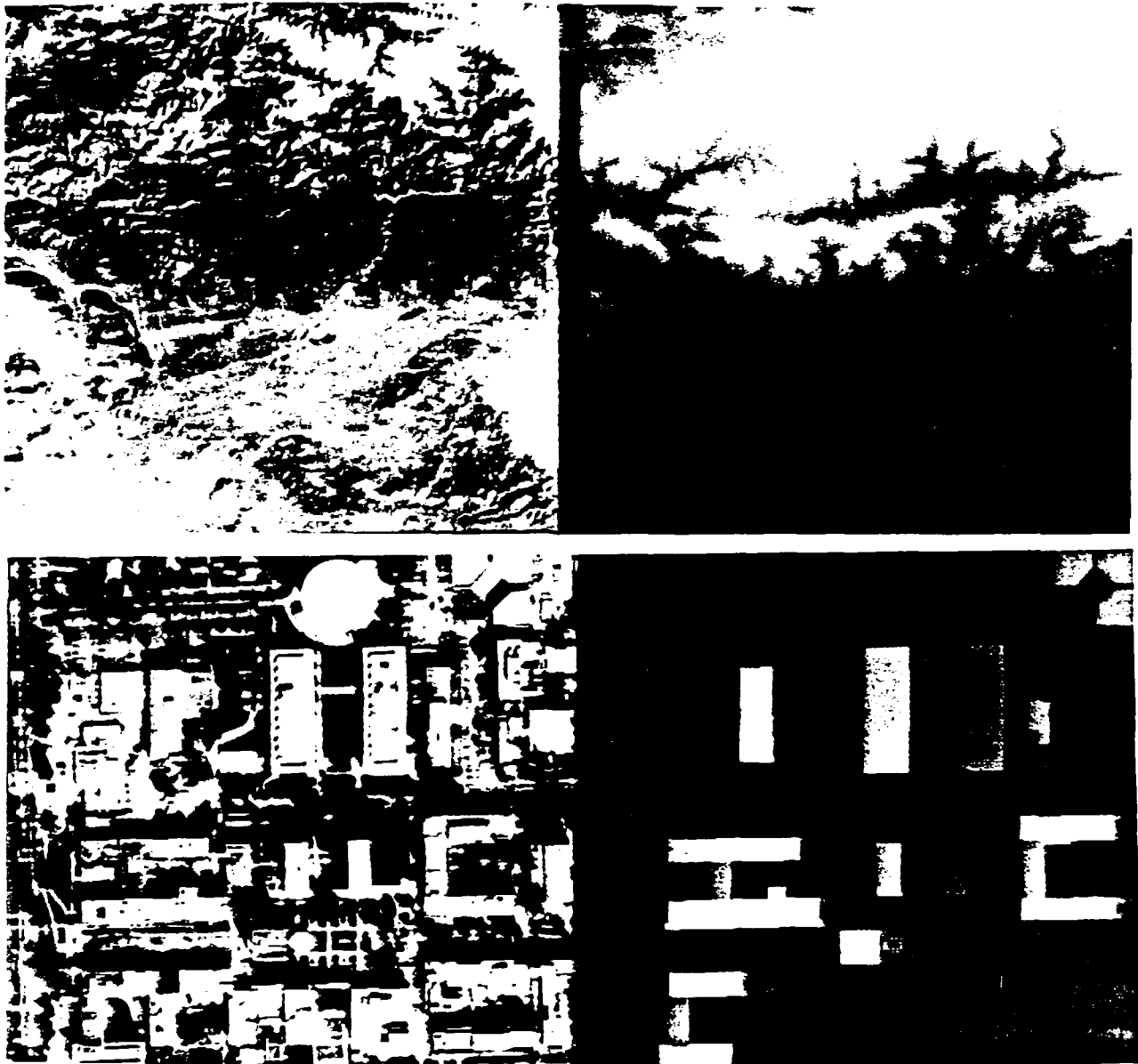
The following series of images were obtained from a single parallel platform utilizing the PARA/SERIES Software System developed by Image Data Corporation. They clearly indicate that it is possible to process imagery, create a 3-D data base and generate photorealistic perspective scenes with a common platform and software.

References:

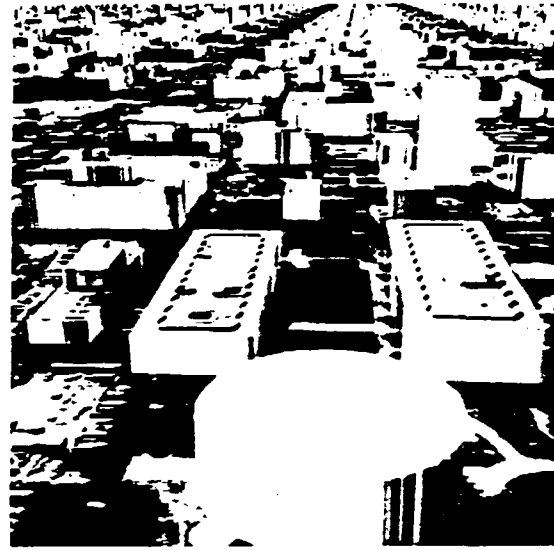
1. M.L.Nack, M.P.Battaglia & A.Nathan
"Real Time Perspective Image Generation"
2. M.L.Nack, A.Nathan & R.Nathan
"Parallel Processing Applied to Image Processing and Perspective Scene Generation"
3. M.P.Battaglia
"Perspective Scene Generation Employing the Use of Real Imagery"



The photo-composite above shows an original LANDSAT image of the San Gabriel Valley in the upper left hand quadrant. To the right of it is a binary edge image for extracting shape information. Below that is the result of an unsupervised multispectral classification showing 22 classes. The final quadrant is one of a sequence of perspective scenes of the area. The "fly through" was accomplished at near-real-time rates.



The photo-composite above shows two techniques for building an elevation data base. The upper pair depicts an original Landsat 3-band multispectral image alongside a US Geological Survey elevation data set converted into a gray scale image and geometrically warped to superimpose on the Landsat scene. The lower pair consists of an aerial photo of the CalTech campus alongside a partial elevation extraction of several of the buildings. The technique used here measures the length of shadows at a known solar elevation angle. It should be noted that many roofs exhibit varying intensities, indicating complex structures such as air conditioning units and dormers, casting independent shadows.



The photo-composite above compares what may be called 2.5-D perspective scene renditions to full 3-D renditions. The upper left quadrant is again the aerial photo of the CalTech campus. The upper right quadrant shows a perspective scene in which the detail of the sides of the buildings was unavailable. The lower right incorporates that missing data through the addition of ground-level photography merged into the data base. This quadrant actually depicts a perspective view of the building with the observer's viewpoint located at ground level. The lower left quadrant further indicates the nature of a true 3-D data base. Here, the observer is placed inside one of the rooms within the building able to look out the window at the outside scene, though no data relative to the inside of the building was in the data base.

THIS PAGE IS INTENTIONALLY BLANK

Attendance List
of the
Digital/Electronic Terrain Board Symposium

Asner, Bernard
Sverdrup Technologies
P. O. Box 1935
Eglin AFB, FL 32542

Ayres, Norman
Rockwell International
3370 Miraloma Avenue
Anaheim, CA 90803

Bello, Martin
Charles Stark Draper Lab
555 Technology Square
Cambridge, MA 02139

Belt, James L.
McDonnell Douglas
Missile Systems Co.
P. O. Box 516
St. Louis, MO 63166

Bergsneider, Peter
US Army Electronic Proving Ground
Attn: STEEP-MO
Fort Huachuca, AZ 85613

Biron, David G.
Massachusetts Institute
of Technology, Lincoln Lab
244 Wood Street
Lexington, MA 02173

Bradford, Lewis
Ford Aerospace Corp.
Ford Road, MS 2119
Newport Beach, CA 92658-8900

Brandt, Scott A.
Honeywell
3660 Technology Drive
Minneapolis, MN 55418

Bui, Khang
US Army CECOM CNVEO
Attn: AMSEL-RD-NV-V
Fort Belvoir, VA 22060-5677

Burrows, Michael K.
General Dynamics
Valley Systems Division
P. O. Box 50-800
Ontario, CA 91761-1085

Cameron, Dr. William L.
Boeing Aerospace & Electronics
P. O. Box 3999, M/S 8H-51
Seattle, WA 98124-2499

Carmer, Dwayne C.
Environmental Research Institute
of Michigan
P. O. Box 8618
Ann Arbor, MI 48107

Cassidy, Tom
Sensci Corporation
1423 Powhatan Street #6
Alexandria, VA 22314

Cathcart, Michael
Georgia Tech Research Institute
Baker Rm. 323-B
Atlanta, GA 30332

Chandler, David
Northrop Corporation
500 East Orangethorpe Avenue
Anaheim, CA 92801

Chaudhuri, Syama P.
Sensor Data Integration, Inc.
342 Caterina Heights
Concord, MA 01742

Chikhani, Rene
AMPEX Corp.
401 Broadway
Redwood City, CA 94063

Clark, Lloyd
US Air Force
WRDC/AARA
Wright Patterson AFB, OH 45433

Cook, Wm. Sidney
Martin Marietta
Box 179, MS DC6374
Denver, CO 80201

Costianes, Pam
USACSTA
Attn: STECS-EN-PH
Aberdeen Proving Ground, MD 21005

Curran, Allen R.
Michigan Technological University
Keweenaw Research Center
College Avenue
Houghton, MI 49931

Delashmit, Walter H.
LTV Missiles & Electronics
P. O. Box 650003
Dallas, TX 75267

Der, Sandor
US Army C2NVEO
Attn: AMSEL-RD-NV-V
Fort Belvoir, VA 22060

Dome, John
US Army C2NVEO
Attn: AMSEL-RD-NV-V
Fort Belvoir, VA 22060

Dudgeon, Dr. Dan E.
MIT Lincoln Laboratory
P. O. Box 73
Lexington, MA 02173-9108

Durham, David R.
Evans & Sutherland
1720 Louisiana Blvd. NE, #306
Albuquerque, NM 87110

Ebersole, John
Creative Optics Inc.
32 Wildwood Drive
Bedford, MA 01730

Ellis, William
TRW, Ballistic Missiles Div.
P. O. Box 1310
San Bernardino, CA 92402

Elrod, Steve
Boeing Aerospace & Electronics
P. O. Box 3999, MS 8H-35
Seattle, WA 98124

Eucker, Bradley
Boeing Military Airplane Co.
P. O. Box 7730
Wichita, KS 67277-7730

Frandsen, Marvin
Sverdrup Technologies Inc.
P. O. Box 1935
Eglin AFB, FL 32542

Frankel, Ronald A.
US Army LABCOM S3TO
Attn: SLCTO
2800 Powder Mill Road
Adelphi, MD 20783

Fulton, Laura O.
US Army CECOM CNVEO
Attn: AMSEL-RD-NV-ISP
Fort Belvoir, VA 22060-5677

Gardner, Geoffrey Y.
Grumman Data Systems
1000 Woodbury Road, MS D12-237
Woodbury, NY 11797

Gillberg, Jeffrey M.
Honeywell
3660 Technology Drive, MN65-2300
Minneapolis, MN 55418

Gleason, James
Environmental Research Institute
of Michigan
P. O. Box 8618
Ann Arbor, MI 48107

Gordon, Daniel
Autometric Inc.
5301 Shawnee Road
Alexandria, VA 22192

Greczy, Laslo
US Army Engineering
Topographic Lab
Attn: CEETL-GL-V
Fort Belvoir, VA 22060

Greenleaf, William G.
Computer Sciences Corporation
200 Sparkman Drive
Huntsville, AL 35805

Gruenzel, Ronald R.
Avionics Laboratory
WRDC/AARI-4
Wright Patterson AFB, OH 45433

Hancock, Gary D.
New Mexico State University
Electrical & Computer Eng. Dept.
P. O. Box 30001, Dept. #3-0
Las Cruces, NM 88003-0001

Harbour, Kenton
Boeing Military Airplane Co.
P. O. Box 7730
Wichita, KS 67277-7730

Hartman, Hollister A.
McDonnell Douglas Space Systems
5301 Bolsa Avenue M/S 14-2
Huntington Beach, CA 92647

Henry, Eugene M.
Martin Marietta Strategic Systems
P. O. Box 179, MS DC6374
Denver, CO 80201

Hoeppepner, Conrad
AAI Corporation
P. O. Box 126
Hunt Valley, MD 21030-0126

Hoover, Carl W.
US Army C2NVEO
Attn: AMSEL-RD-NV-V
Fort Belvoir, VA 22060

Holleman, John E.
Computer Sciences Corporation
200 Sparkman Drive
Huntsville, AL 35806

Jackson, Robert D.
Martin Marietta Aerospace
P. O. Box 5837 E1304
Orlando, FL 32855

Jankovitz, Jack
Naval Air Development Center
Code 4011
Warminster, PA 19874

Jones, Terry
US Army CECOM CNVEO
Attn: AMSEL-RD-NV-ISP
Fort Belvoir, VA 22060-5677

Kadar, Ivan
Grumman
Mail Stop B35-35
Bethpage, NY 11714

Kolodzy, Paul J.
Massachusetts Institute of
Technology, Lincoln Lab
244 Wood Street
Lexington, MA 02173

Knecht, John
Naval Weapons Center
Code 3153
China Lake, CA 93555

Kornfeld, Gertrude
US Army C2NVEO
Attn: AMSEL-RD-NV-V
Fort Belvoir, VA 22060-5677

Kramer, Kimball
DARPA-TTO
1400 Wilson Boulevard
Arlington, VA 22209

Krebaum, Ken
Texas Instruments
P. O. Box 660246
Dallas, TX 75266

Krusinger, Alan E.
US Army Environmental
Topographic Labs
Attn: CEETL-RI-CRS
Fort Belvoir, VA 22060-5546

Lahart, Martin J.
US Army C2NVEO
Attn: AMSEL-RD-NV-ISP
Fort Belvoir, VA 22060-5677

Lander, Michael
US Army C2NVEO
Attn: AMSEL-RD-NV-V
Fort Belvoir, VA 22060-5677

Larson, Rodney M.
Honeywell
3660 Technology Drive
Minneapolis, MN 55428

Lee, Abner W.
Computer Sciences Corporation
200 Sparkman Drive
Huntsville, AL 35805

Lee, Walter
IBM Federal Systems
9500 Godwin Drive
Manassas, VA 22110

Lent, Jerry
Image Data Corporation
600 South Lake Avenue
Pasadena, CA 91106-3955

Leonard, Jim
US Air Force
WRDC/AARA
Wright Patterson AFB, OH 45433

Lin, Phillip P.
Pacific-Sierra Research Corp.
12340 Santa Monica Boulevard
Los Angeles, CA 90025

Lindahl, Charles E.
Texas Instruments
P. O. Box 660246, MS 3603
Dallas, TX 75266

Lindell, Scott D
Martin Marietta
Strategic Systems
P. O. Box 179, MS DC6374
Denver, CO 80201

Lloyd, Elliott
US Army C2NVEO
Attn: AMSEL-RD-NV-AS
Fort Belvoir, VA 22060-5677

Lo, C. M.
Hughes Aircraft Company
P. O. Box 902 E53/E250
El Segundo, CA 90245

Lore, Suzanne
Martin Marietta Electronics
P. O. Box 628007, MS 1304
Orlando, FL 32862-8007

Lorenzo, Maximo
US Army C2NVEO
Attn: AMSEL-RD-NV-V
Fort Belvoir, VA 22060

Lucas, Bob
SAIC
1555 Wilson Boulevard #700
Arlington, VA 22209

Lui, Dennis
US Army CECOM Center for EW/RSTA
Attn: AMSEL-RD-EW-SE
Fort Monmouth, NJ 07703

Marek, Pat
Hughes Aircraft Co.
P. O. Box 902, E53/E250
El Segundo, CA 90245

Martin, Jon
US Army Atmospheric Sciences Lab
Attn: SLCAS-AE-T
White Sands, NM 88002-5501

McEachern, Marc
Boeing Military Airplane Co.
P. O. Box 7730
Wichita, KS 67277-7730

McGrody, Ellen
NAVMAR, Inc.
65 West Street Road #C-206
Warminster, PA 18974

Meggs, Glen
Texas Instruments
P. O. Box 655012
Dallas, TX 75265

Mendelsohn, Jay
Grumman Corporate
Research Center
MS A02-26
Bethpage, NY 11714

Miller, Michael
Honeywell
3660 Technology Drive
Minneapolis, MN 55418

Miller, Scott F.
MRJ, Inc.
10455 White Granite Drive
Oakton, VA 22104

Mills, Lt. Col. James P.
US Air Force
ASD/ENAM
Wright Patterson AFB, OH 45433

Mitzel, James
Rockwell International
3370 Miraloma Avenue, MC DB61
Anaheim, CA 92803

Morgenthaler, David
Martin Marietta
1755 Telestar Drive #220
Colorado Springs, CO 80920

Moore, Charles
DCS Corporation
1330 Braddock Place
Alexandria, VA 22314

Nachbor, John W.
Optical Sensor Modeling &
Analysis
300 Sparkman Avenue
Huntsville, AL 35807

Newsome, Thomas C.
US Army CECOM Center for EW/RSTA
Attn: AMSEL-RD-EW-SE
Fort Monmouth, NJ 07703

Nicoll, Jeff
Institute for Defense Analyses
1801 North Beauregard Street
Alexandria, VA 22311-1772

Norman, Robert H.
General Dynamics, Convair Div.
P. O. Box 85357, MZ 41-6590
San Diego, CA 92138

Novoseller, Daniel E.
TRW Space & Defense
One Space Park Drive MS R1/2044
Redondo Beach, CA 90278

Nguyen, Hung
US Army C2NVEO
Attn: AMSEL-RD-NV-V
Fort Belvoir, VA 22060

Nguyen, Steve
US Army C2NVEO
Attn: AMSEL-RD-NV-V
Fort Belvoir, VA 22060

Olds, Steve
Boeing Advanced Systems
P. O. Box 3707
Seattle, WA 98031

Oyster, John
Hughes Aircraft Company
P. O. Box 902, E53/E250
El Segundo, CA 90245

Peters, Richard J.
US Army CECOM CNVEO
Attn: AMSEL-RD-NV-ISP
Fort Belvoir, VA 22060

Ploysongsang, Avudh
Texas Instruments
P. O. Box 660246
Dallas, TX 75266

Poggio, Enrico C.
Nichols Research Corporation
251 Edgewater Drive
Wakefield, MA 01880

Politopoulos, Anastasios S.
Ford Aerospace & Communications
Ford Road
Newport Beach, CA 92663

Ramroth, Richard R.
Northrop Electronics
Systems Division
500 East Orangethorpe Avenue
Anaheim, CA 98201

Reis, James
Northrop
Research & Technology Center
One Research Park
Palos Verdes, CA 90274

Robbins, John
Technical Solutions
P. O. Box 1148
Mesilla Park, NM 88847

Robison, Dale R.
US Naval Weapons Center
Human Factors Branch, Code 3152
China Lake, CA 93555-6001

Rogers, Eldon C.
Boeing Aerospace & Electronics
P. O. Box 3999, MS 8H-37
Seattle, WA 98124

Rogne, Timothy J.
OptiMetrics Inc.
2008 Hogback Road #6
Ann Arbor, MI 48105

Sabol, Bruce M.
US Army Waterways
Experiment Station
P. O. Box 631
Vicksburg, MS 39181

Savitt, Steve
Honeywell
3660 Technology Drive
Minneapolis, MN 55418

Scalf, Warren D.
Computer Sciences Corporation
200 Sparkman Drive
Huntsville, AL 35805

Scarlatos, Lori L.
Grumman Data Systems
1000 Woodbury Road, MS D12-237
Woodbury, NY 11797

Sengvieng, Amphay
MSD/AFATL/AGS
Bldg. 13A, Rom 287
Eglin AFB, FL 32542-5434

Shazeer, Dov J.
Charles Stark Draper Labs
555 Technology Square
Cambridge, MA 02139

Shea, John
Technical Solutions
P. O. Box 1148
Mesilla Park, NM 88847

Shen, Chyau N.
Naval Air Development Center
Code 5013
Warminster, PA 18974

Shirkey, Dr. Richard C.
US Army Atmospheric Sciences Lab
Attn: SLCAS-AR-I
White Sands, NM 88002-5501

Simon, Wayne E.
Martin Marietta
P. O. Box 179
Denver, CO 80201

Simonds, Robert
Boeing Aerospace
P. O. Box 3999
Seattle, WA 98006

Singer, David
US Army C2NVEO
Attn: AMSEL-RD-NV-ISP
Fort Belvoir, VA 22060-5677

Sjolander, Gary W.
Martin Marietta Strategic Systems
P. O. Box 179
Denver, CO 80201

Smith, Frederick G.
OptiMetrics Inc.
2008 Hogback Road #6
Ann Arbor, MI 48139

Snapp, Kenneth M.
Litton Data Systems
8000 Woodley Avenue
Van Nuys, CA 91302

Stephen, Brian G.
Science & Engineering Associates
1508 JFK Drive
Bellevue, NE 68005

Sundstrom, Bryce M.
MSD/AFATL/AGS
Bldg. 13A
Eglin AFB, FL 32542-5434

Tatum, Wm. Frank
Texas Instruments
P. O. Box 405 MS 3473
Lewisville, TX 70567

Thompson, Wiley E.
New Mexico State University
Electrical & Computer Eng. Dept.
P. O. Box 30001, Dept. #3-0
Las Cruces, NM 88003-0001

Thornloe, Keith
MRJ Inc.
10455 White Granite Drive
Oakton, VA 22124

Velten, Vince
US Air Force
WRDC/AARA-2
Wright Patterson AFB, OH 45433

Wabler, Ray
Merit Technology
4035 Col. Glenn Highway #315
Beavercreek, OH 45431-1601

Waeber, Bruce
Naval Air Development Center
Code 5013
Warminster, PA 18974

Winter, Charles
Hughes Aircraft Co.
8433 Fallbrook Avenue
Canoga Park, CA 91304

Wolfe, 2LT Christopher W.
MSD/AFATL/AGS
Bldg. 13A, Room 287
Eglin AFB, FL 32542-5434

Wood, Rhonde P.
General Dynamics
P. O. Box 748, MS 1761
Fort Worth, TX 76101

Yandow, Craig
Hughes Aircraft Company
P. O. Box 9399
Bldg. A01, M/S 3C920
Long Beach, CA 90820-0399

Zachar, William P.
McDonnell Douglas
Missile Systems Co.
P. O. Box 516
St. Louis, MO 63166

Zelnio, Ed
US Air Force
WRDC/AARA-2
Wright Patterson AFB, OH 45433

Zembower, Andy
IIT Research Institute
4140 Linden Avenue #201
Dayton, OH 45432

THIS PAGE INTENTIONALLY BLANK

THE TACTICAL WEAPON GUIDANCE AND CONTROL INFORMATION ANALYSIS CENTER (GACIAC)

GACIAC is a DoD Information Analysis Center operated by IIT Research Institute under the technical sponsorship of the Joint Service Guidance and Control Committee with members for OUSDRE, Army, Navy, Air Force, and DARPA. The U.S. Army Missile Command provides the Contracting Officer's Technical Representative. Its mission is to assist the tactical weapon guidance and control community by encouraging and facilitating the exchange and dissemination of technical data and information for the purpose of effecting coordination of research, exploratory development, and advanced technology demonstrations. To accomplish this, GACIAC's functions are to:

1. Develop a machine-readable bibliographic data base -- currently containing over 36,000 entries;
2. Collect, review, and store pertinent documents in its field of interest -- the library contains over 11,000 reports;
3. Analyze, appraise and summarize information and data on selected subjects;
4. Disseminate information through the GACIAC Bulletin, bibliographies, state-of-art summaries, technology assessments, handbooks, special reports, and conferences;
5. Respond to technical inquiries related to tactical weapon guidance and control; and
6. Provide technical and administrative support to the Joint Service Guidance and Control Committee (JSGCC).

The products and services of GACIAC are available to qualified industrial users through a subscription plan or individual sales. Government personnel are eligible for products and services under block funding provided by the Army, Navy, Air Force and DARPA. A written request on government stationery is required to receive all the products as a government subscriber.

Further information regarding GACIAC services, products, participation plan, or additional copies of these Proceedings may be obtained by writing or calling: GACIAC, IIT Research Institute, 10 West 35th Street, Chicago, Illinois 60616-3799, Area Code 312, 567-4519 or 567-4526.